Te···O CHALCOGEN BONDING

Te···O CHALCOGEN BONDING IN SUPRAMOLECULAR CHEMISTRY

By PETER CHENG-WEI HO, B.SC.

A Thesis Submitted to the School of Graduate Studies in Partial Fulfilment of the Requirements for the Degree Doctor of Philosophy

McMaster University DOCTOR OF PHILOSOPHY (2021) Hamilton, Ontario

(Chemistry)

TITLE: Te···O CHALCOGEN BONDING IN SUPRAMOLECULAR CHEMISTRY

AUTHOR: Peter Cheng-Wei Ho

SUPERVISOR: Professor Ignacio Vargas-Baca

NUMBER OF PAGES: pages i-xxii, pages 1-85

Lay Abstract

Supramolecular chemistry is a rapidly growing field of research that uses non-covalent interactions to spontaneously build well-organized structures. Among such interactions, hydrogen bonds are the most investigated and highly utilized in chemical and biological systems such as in DNA self-assembly, protein folding, cellulose, synthetic polymers and more. In recent years, much attention has been given to other *non-covalent interactions*, in particular bonding interactions that occur between electron-rich centres with electron-poor covalently bonded atoms of elements in groups 14 to 17 on the periodic table. These bonding interactions are named according to the group of the electron-deficient elements such as halogen bonds (XBs, group 17), chalcogen bonds (ChBs, group 16), "tetrel bonds" (group 14) and "pnictogen bonds" (group 15), as alternatives to hydrogen bonding. The purpose of this thesis is to augment our knowledge of ChBs by investigating the supramolecular chemistry of iso-chalcogenazole *N*-oxides and related compounds. Such molecules spontaneously assemble robust supramolecular structures, like infinite chains (polymers), and macrocyclic tetramers hexamers through Te···O ChB interactions that are strong and yet reversible. The macrocyclic aggregates coordinate to transition metal ions, form adducts with fullerene and host small molecules. The unusual stability of these tellurium-containing supramolecular building blocks, in addition to their strong ChBs, facilitated these investigations. The solubility of these compounds was improved by installing non-polar bulky groups. The macrocyclic cavity can be enlarged by replacing the oxygen atom with phenoxides groups, creating a new family of supramolecular building blocks.

Abstract

Noncovalent interactions have attracted significant attention in the recent decades, both seeking a fundamental understanding and pursuing a wide range of applications. One particular case that has been studied in great detail is *halogen bonding* (XBs). The use of *chalcogen bonding* (ChBs) is only beginning to thrive but already has made a mark in the chemical community. In this thesis, we intended to augment the study of ChBs by examining 1,2-chalcogenazole 2-oxides. These *N*-oxides of C_3NCh (Ch = Se, Te) heterocycles spontaneously assemble supramolecular structures through reversible Te···O ChB interactions. In solution, their macrocyclic tetramers and hexamers exist in equilibrium. These rings as well as supramolecular polymers (infinite chains in crystalline phase) have been authenticated by single-crystal X-ray diffraction. Despite the reversibility of the Te···O link, the macrocycles display properties typical of covalent macrocycles, including ability to coordinate metal ions, host small molecules, and form adducts with fullerenes. The compounds are stable to tellurium halogenation and unreactive to Lewis bases. However, they are readily cleaved by Brønsted and Lewis acids. Transformation of the structure of iso-tellurazole *N*-oxides by formal insertion of an aromatic bridge between the nitrogen and oxygen atoms led to a new family of supramolecular building blocks. A disubstituted benzene bridge yielded three isomers, all of which display signs of aggregation in solution and crystallize in either polymeric or macrocyclic aggregates. Among the latter, the *ortho* compound assembled a calixarene-like trimer while the *para* derivative built a macrocyclic tetramer akin to a molecular square.

Acknowledgements

It is a genuine pleasure to express my profound appreciation and gratefulness to my graduate supervisor and mentor Professor Ignacio Vargas-Baca. His dedication and patience for his students is one important factor helping me complete this work.

I profusely thank the members of my supervisory committee, Professors David Emslie and Yurij Mozharivskyj for their interest on my research and their helpful suggestions enabled me to advance my thesis.

I am thankful for the help from the staff of the mass-spec facility (Dr. Kirk Green), NMR facility (Drs. Bob Berno, Hilary Jenkins), and X-ray diffraction laboratory (Dr. James Britten). Their expert advice was essential to obtain high-quality results.

I am grateful to my funding sources: McMaster University and its Department of Chemistry & Chemical Biology, the Natural Science Engineering Research Council of Canada (NSERC), the Ontario Graduate Scholarship (OGS program, and Mitacs Globalink).

I am thankful for my past and present group members: Valerie Tomassetti, Jin Wang, Justin Lomax, Alberto Cevallos, Phillip MacDougall, Matthew Craig, Jiwon Lee, Robert Bui, Shanel Sequeira, Francesca Meloni, Derek Morim and Lucia Lee.

I want to acknowledge my friend Sam Ros for suffering through grad school with me.

I am extremely grateful for my mother, father and my sister for their constant encouragement and support in my life.

Table of Contents

Lay Abstract iii

Abstract iv

Acknowledgements v

Table of Contents vi

List of Schemes viii

List of Abbreviations and Symbols ix

List Compounds xi

Declaration of Academic Achievement xviii

Chapter 1. Introduction. Chalcogen bonding in Materials Chemistry 1

1.1 Preamble 1

1.2 Thesis organization 3

1.3 Chalcogen bonding in Materials Chemistry 4

Chapter 2. Influence of acidic media on the supramolecular aggregation 17

of iso-tellurazole *N*-oxides 17

2.1 Preamble 17

Chapter 3. Synthesis and structural characterisation of the aggregates of benzo-1,2-

chalcogenazole 2-oxides 24

3.1 Preamble 24

Chapter 4. Building New Discrete Supramolecular Assemblies through the Interaction of Iso-Tellurazole *N*-Oxides with Lewis Acids and Bases 35

4.1 Preamble 35

Chapter 5. Macrocyclic Complexes of Pt(II) and Rh(III) with Iso-Tellurazole: *N*-Oxides 49

5.1 Preamble 49

Chapter 6. Competing Effects of Chlorination on the Strength of Te···O Chalcogen Bonds Select the Structure of Mixed Supramolecular Macrocyclic Aggregates of Iso-Tellurazole *N*-Oxides 58

6.1 Preamble 58

Chapter 7. Iso-Tellurazolium-*N*-Phenoxides: a Family of Te···O Chalcogen-Bonding Supramolecular Building Blocks 64

7.1 Preamble 64

Chapter 8. Conclusions and Outlook 73

8.1 Conclusions 73

8.2 Suggestions of Future Work 78

References cited in the foreword section of each chapter 80

List of Schemes

Scheme 1.1. Supramolecular species formed by auto-association of **1b**, alone or in combination with a Pd(II) salt or C_{60}. Reproduced with permission from reference 18. 3

Scheme 2.1. Synthesis of iso-tellurazole *N*-oxides **1a** (R = ^{t}Bu) and **1b** (R = Ph). Reproduced with permission from reference 18. 18

Scheme 8.1. Summary of the supramolecular aggregates and chemistry of **1**.……..74

Scheme 8.2. Summary of the supramolecular aggregates and chemistry of **2**.……..…..75

Scheme 8.3. Summary of the supramolecular aggregates and chemistry of **3^{o,m,p}**…..…..…77

List of Abbreviations and Symbols

Å	Angstrom (1Å = 10^{-10} m)
a, b, c, α, β, γ	unit cell parameters (in crystallography)
a.u.	atomic units
ACN	acetonitrile
ADF	Amsterdam Density Functional software
ChB	chalcogen bonding or chalcogen bond
cm^{-1}	wavenumber
DCM	dichloromethane
DFT	density functional theory
DMF	dimethyl formamide
DMSO	dimethyl sulfoxide
E	energy
EA	elemental analysis
ESI	electrospray ionization
ETS-NOCV	extended-transition-state method from the natural orbitals for chemical valence
GUI	graphical user interface
HMBC	heteronuclear multiple-bond coherence (pulse sequence)
HOMO	highest occupied molecular orbital
IR	infrared
IUPAC	International Union of Pure and Applied Chemistry
K	Kelvin
LUMO	lowest unoccupied molecular orbital
Me	methyl, functional group
MO	molecular orbital
MS	mass spectrometry
nm	nanometer
NMR	nuclear magnetic resonance (spectroscopy)
ppm	parts per million
r_{vdW}	van der Waals radii
SBI	secondary bonding interaction

T	temperature
^{t}Bu	*tert*-butyl
THF	tetrahydrofuran
TMS	tetramethylsilane
UV-Vis	ultraviolet-visible (spectroscopy)
VT	variable temperature (in NMR)
δ	chemical shift, ppm (parts per million)
λ	wavelength
μ	linear absorption coefficient (in crystallography)
ρ	density of a material (in crystallography)

List of Numbered Compounds

Unless otherwise indicated, the same numbering scheme is used in all chapters.

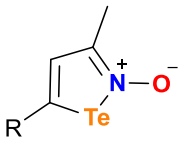

1a R = ^{t}Bu

1b R = Ph

1c R = 3,5-$^{t}Bu_2C_6H_3$

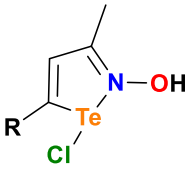

1aHCl R = ^{t}Bu

1bHCl R = Ph

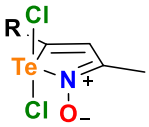

1aCl_2 R = ^{t}Bu

1bCl_2 R = Ph

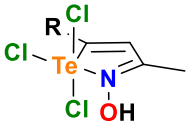

1aHCl_3 R = ^{t}Bu

1bHCl_3 R = Ph

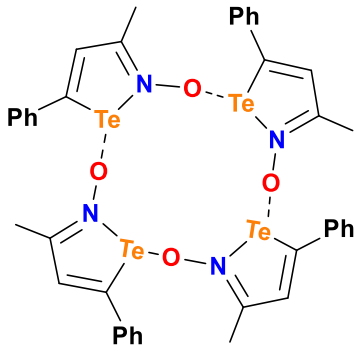

1b$_4$

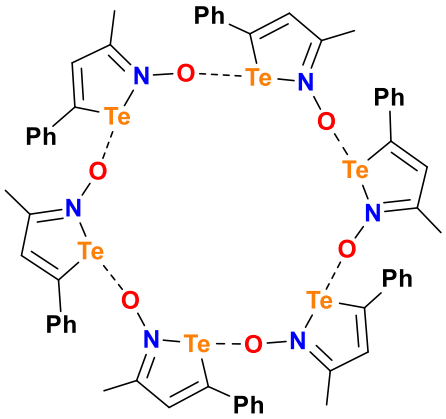

1b$_6$

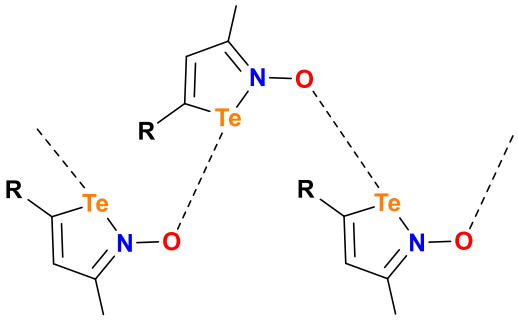

1b$_\infty$

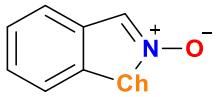

2a Ch = Te

2b Ch = Se

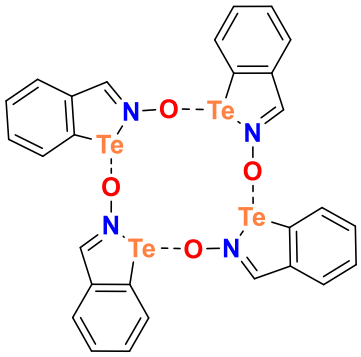

2a$_4$

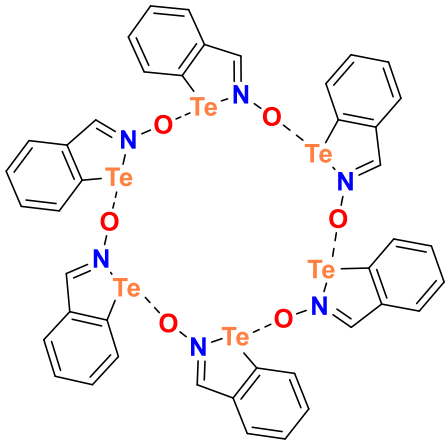

2a$_6$

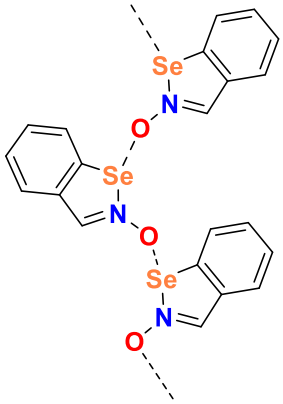
Se
N
O
Se
N
O
Se
N
O

2b∞

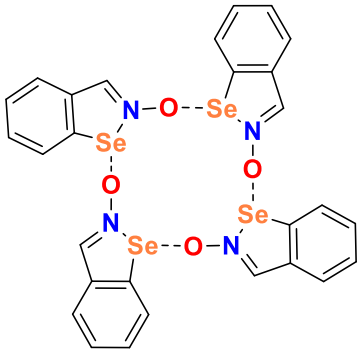
N
O
Se
Se
N
O
O
N
Se
Se
O
N

2b4

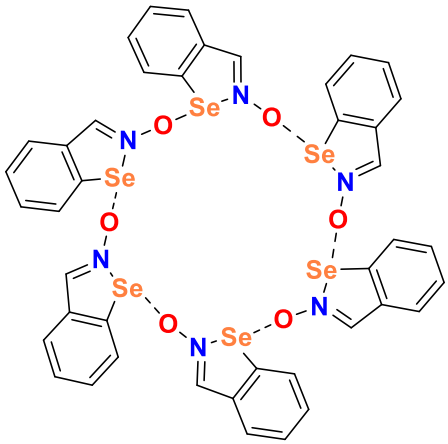
Se
N
O
O
N
Se
Se
N
O
O
N
Se
Se
O
N
Se
O
N

2b6

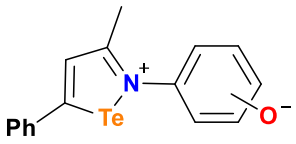
N+
Ph
Te
O−

3$^{o, m, p}$

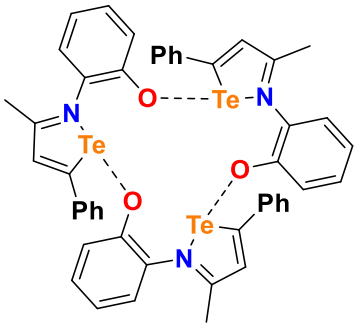
Ph
O
Te
N
N
Te
O
Ph
O
Ph
Te
N

3$^{o}_{3}$

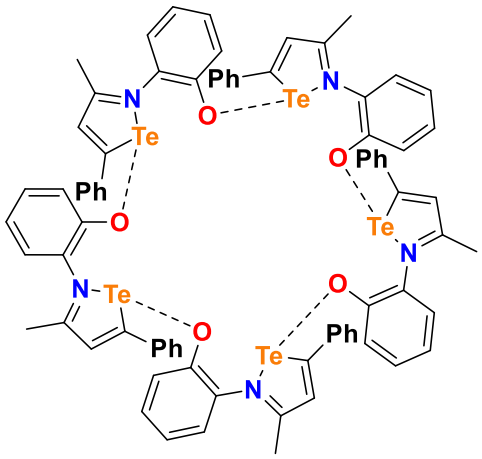
Ph
Te
N
N
Te
O
O
Ph
Ph
O
Te
N
N
Te
O
Ph
O
Te
N

3$^{o}_{5}$

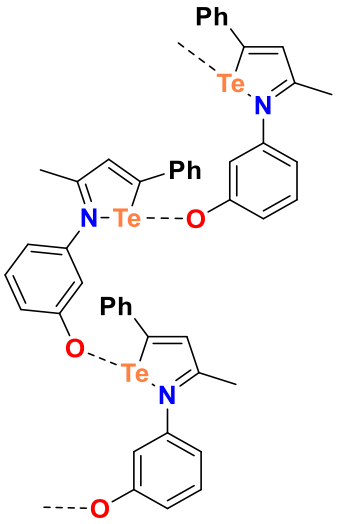

3^{m}_{∞}

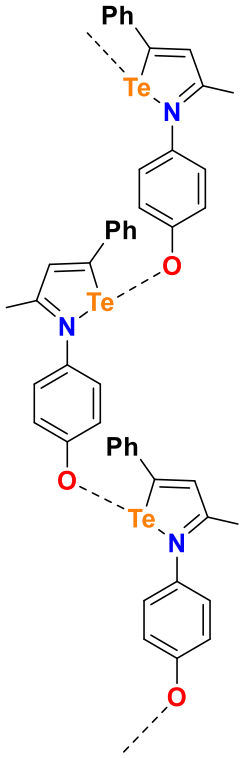

3^{p}_{∞}

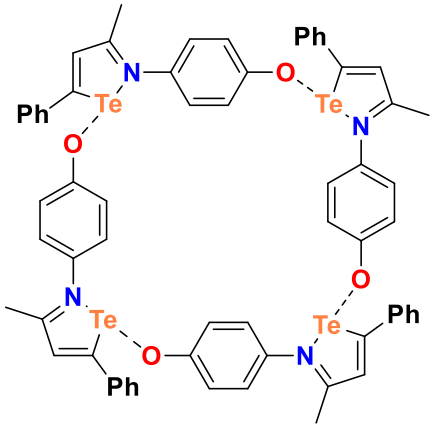

3^{p}_{4}

Declaration of Academic Achievement

The research described in the publication compiled in this thesis is the result of the collaborative effort of students in the Vargas group and McMaster staff. The contributions of the following coworkers are described:

AC - Alberto Cevallos, undergraduate student.

ALB - Antonio L. Braga, Professor at Universidade Federal de Santa Catarina, Brazil.

FM - Francesca Meloni, graduate student.

HAJ - Hilary A. Jenkins, Research Scientist of the McMaster X-ray diffraction and NMR facility.

IVB - Ignacio Vargas-Baca, supervisor.

JFB - James F. Britten, Manager of the McMaster X-ray diffraction facility.

JL - Jiwon Lee, undergraduate student.

JL - Justin Lomax, undergraduate student.

JR – Jamal Rafique, postdoctoral fellow.

JW - Jin Zhao Wang, graduate student.

LML - Lucia M. Lee, graduate student.

PCH - Peter C. Ho, graduate student author of this thesis.

RB - Robert Bui, undergraduate student.

SS - Shanel Sequeira, undergraduate student.

VT - Valerie Tomassetti, undergraduate student.

Chapter 1.

The work was conducted between April 2020 to October 2020.

PCH and JW did the literature search.

PCH, JW, FM and IVB organized the content.

PCH, JW and IVB analyzed the literature reports and wrote the manuscript.

Chapter 2.

The work was conducted between May 2015 to August 2015.

PCH performed the experimental work.

LML assisted with the crystallography refinement.

HAJ, JFB oversaw the crystallography characterization.

PCH and IVB designed the experiments, interpreted the results and wrote the manuscript.

Chapter 3.

The work was conducted between September 2016 to February 2017.

PCH and JL performed all the synthesis.

PCH performed the characterization.

HAJ, JFB oversaw the crystallography characterization.

LML assisted with partial crystallography refinement.

JR and ALB were collaborators for the development of the syntheses.

PCH and IVB designed the experiments, interpreted the results and wrote the manuscript.

The synthetic component of this work was done in collaboration with Antonio Luiz Braga in the Federal University of Santa Catarina, Brazil (Universidade Federal de Santa Catarina) with the financial support of a Mitacs Globalink Research Award.

Chapter 4.

The work was conducted between October 2016 to February 2017

PCH performed the experimental work.

HAJ, JFB oversaw the crystallography characterization.

PCH and IVB designed the experiments, interpreted the results and wrote the manuscript.

Chapter 5.

The work was conducted between September 2016 to January 2019

PCH, RB, AC, SS performed the syntheses.

PCH performed the characterization.

JFB oversaw the crystallography characterization.

PCH and IVB designed the experiments, interpreted the results and wrote the manuscript.

Chapter 6.

The work was conducted between May 2017 to April 2021

PCH, JL, VT performed the syntheses.

PCH performed the characterization.

JFB oversaw the crystallography characterization.

PCH and IVB designed the experiments, interpreted the results and wrote the manuscript.

Chapter 7.

The work was conducted between September 2018 to July 2021

PCH, VT performed the syntheses.

PCH performed the characterization.

JFB oversaw the crystallography characterization.

PCH and IVB designed the experiments, interpreted the results and wrote the manuscript.

Chapter 1. Introduction. Chalcogen bonding in Materials Chemistry

1.1 Preamble

In recent decades, there has been increasing interest in supramolecular interactions in which atoms of heavy p-block elements act as electrophilic centres. The most prominent example is the *halogen bond* (XBs) which was defined by IUPAC in 2013.[1] Recently, considerable attention has been given to the *chalcogen bond* (ChB), formally defined by IUPAC in 2019 as a "net attractive interaction between an electrophilic region associated with a chalcogen atom in a molecular entity and a nucleophilic region in another, or the same, molecular entity".[2] In the typical representation of a chalcogen bond, R-Ch···A, Ch denotes the ChB donor being a chalcogen atom (S, Se, Te) containing an electron-deficient region. R-Ch is the molecular entity featuring the ChB donor and A is the ChB acceptor, which commonly is an electron-rich region of a molecular entity such as a lone pair, a π-system, or an anion. The interatomic distance of a ChB typically is in between the sum of van der Waals radii and the sum of covalent radii. Given the same A, the strength of a ChB typically is the strongest with heavier, less electronegative Ch atoms and more electron-withdrawing R. Other factors such as the Lewis basicity of A, and the interaction angle between the Ch and the Lewis base are also crucial as typically the ChB axis is oriented along the extension of a covalent bond opposite to the ChB.

The growth of interest in ChB is reflected in the increasing number of recent publications in this area with focus on a wide range of fields spanning from crystal engineering,[3,4] and catalysis[5–8] to functional materials,[9–14] and anion transport and binding.[15–17] Currently,

most of the work done on ChB is concerned with the solid state and the characterization is mostly based on structural determinations by single-crystal X-ray diffraction.

Less frequent is work done in solution and with systems that undergo structural changes. An important development in this area was the observation of reversible auto-association of molecules of 3-methyl-5-phenyl-1,2-tellurazole 2-oxide, which assemble through Te···O ChBs interactions into helical polymer, annular tetrameric and hexametric structures (**1b**$_4$, **1b**$_6$).[18,19] Nuclear magnetic resonance spectroscopic experiments showed that the cyclic tetramers and hexamers are persistent in solution.[18,19] These annular aggregates display chemical properties of covalently bonded macrocycles (Scheme 1.1) such as ability to bind transition metal ions, forming fullerene adducts, and hosting small molecules in a crystal.[18,19] The work was carried out during my undergraduate research and the corresponding publication is not included in this thesis. That article, however, served as the foundation of my graduate research. This Ph.D. thesis is presented in the "sandwich" format compiling my graduate research published to date.

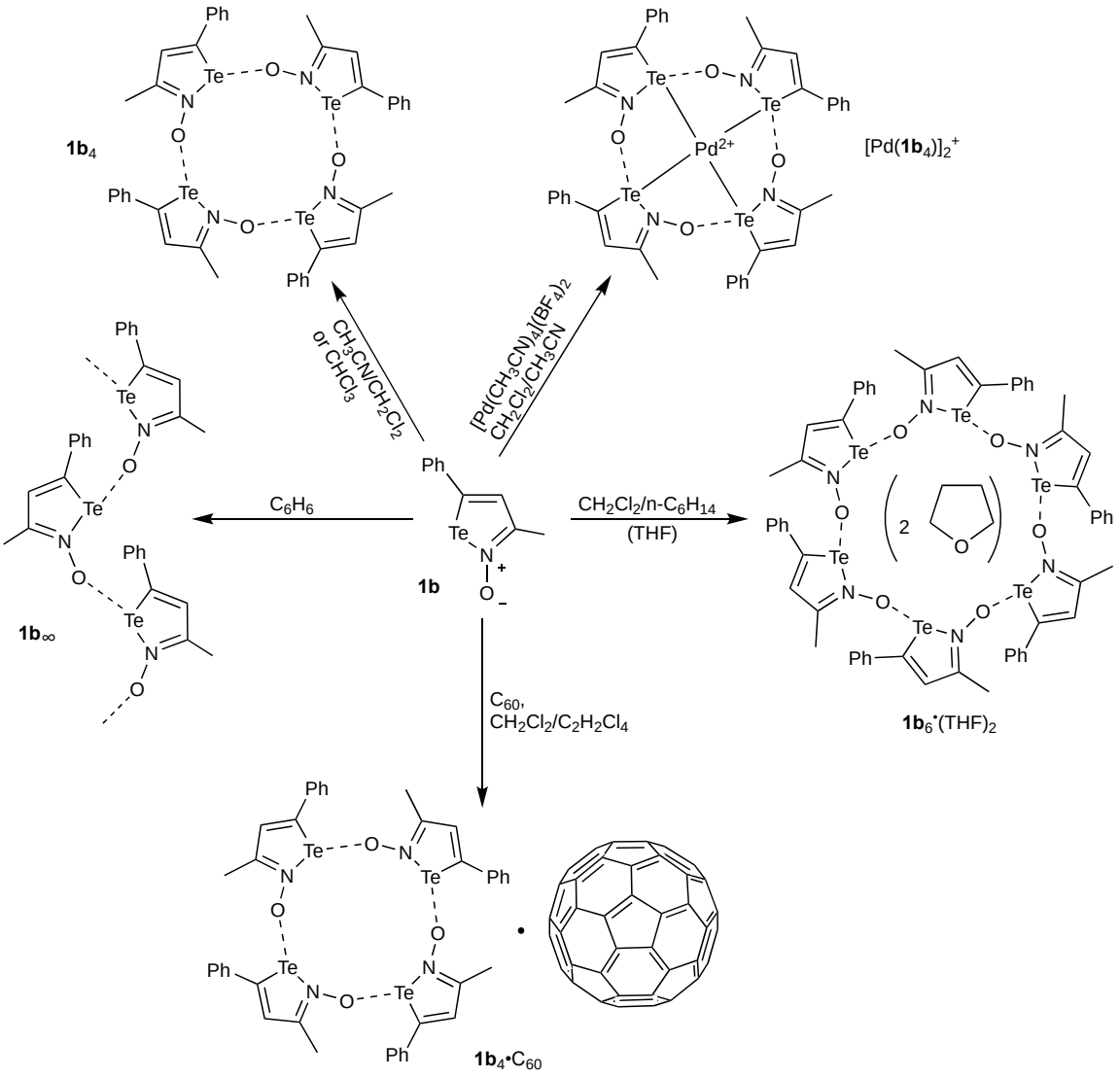

Scheme 1.1. Supramolecular species formed by auto-association of **1b**, alone or in combination with a Pd(II) salt or C_{60}. Reproduced with permission from reference 18.

1.2 Thesis organization

This thesis comprises eight chapters. Chapter 1 serves as an introduction to the field of chalcogen bonding with a review that explores the influence that this interaction has or

might have on the structure and properties of functional materials. Chapter 2 presents the Brønsted acid-base properties on iso-tellurazole *N*-oxides **1a**, and **1b**. Chapter 3 presents the synthesis and chemistry of benzo-1,2-chalcogenazole 2-oxides (**2**). Chapter 4 describes the preparation of borane adduct of iso-tellurazole *N*-oxides and their use to build supramolecular assemblies with Lewis bases. The coordination chemistry of a new supramolecular macrocycle with enhanced solubility (**1c**$_4$) is presented in chapter 5. Chapter 6 discusses the effect of tellurium chlorination on the Te···O ChBs. In chapter 7, the basic structure of the iso-tellurazole *N*-oxide is modified yielding three iso-tellurazolium-*N*-phenoxides (**3^{o,m,p}**) which retain the ability to assemble supramolecular aggregates. Chapter 8 summarizes the major findings of this thesis and discusses possible avenues for future work.

1.3 Chalcogen bonding in Materials Chemistry

This chapter highlights literature cases in which the structures and properties of functional materials are likely influenced by ChB interactions. Most of the examples predate the definition of ChB and systematic work in this area. In some instances, there is a discernible effect of ChB on the macroscopic properties; in others, ChB might have been overlooked and further examination of this materials would be worthwhile.

Original citation: Ho, P. C.; Wang, J. Z.; Meloni, F.; Vargas-Baca, I. Chalcogen Bonding in Materials Chemistry. *Coord. Chem. Rev.* **2020**, *422*, 213464.

This scholarly work is reprinted with permission.

Coordination Chemistry Reviews 422 (2020) 213464

Contents lists available at ScienceDirect

Coordination Chemistry Reviews

journal homepage: www.elsevier.com/locate/ccr

Review

Chalcogen bonding in materials chemistry

Peter C. Ho, Jin Z. Wang, Francesca Meloni, Ignacio Vargas-Baca *

Department of Chemistry and Chemical Biology, McMaster University, 1280 Main Street West, Hamilton, Ontario L8S4M1, Canada

ARTICLE INFO

Article history:
Received 17 November 2019
Received in revised form 20 May 2020
Accepted 18 June 2020

Keywords:
Supramolecular chemistry
Molecular materials
Chalcogen bonding
Crystal structure

ABSTRACT

This review examines recent literature in search for evidence of the influence that *chalcogen bonding* has on the structure and properties of functional materials. Key examples from research on charge transfer salts, neutral heterocyclic free radicals, and paramagnetic coordination compounds are highlighted as intermolecular interactions are critical to properties such as conductivity and magnetic response. Other cases reviewed include the influence of chalcogen bonding on optical properties such as the electronic absorption spectra and the nonlinear optical response of non-centrosymmetric crystal structures. There is also evidence that this type of interaction between molecules translates into macroscopic mechanical properties such as the bulk modulus.

Contents

1. Introduction . . . 1
2. Frequent ChB supramolecular synthons . . . 2
3. Charge transfer salts . . . 3
4. Heterocyclic neutral radicals . . . 6
5. Paramagnetic coordination compounds . . . 9
6. Optical properties . . . 9
7. Mechanical properties . . . 10
8. Outlook . . . 10
Declaration of Competing Interest . . . 11
Acknowledgement . . . 11
References . . . 11

1. Introduction

Recently defined by the IUPAC [1], *chalcogen bonding* (ChB) is a supramolecular interaction between an electrophilic region on a group-16 atom and electron-rich centers with typical interatomic distances that are intermediate between those of typical single bonds and the sum of van der Waals radii (see Table 1 for typical ranges). Early observations were made as early as X-ray crystallographic structural determinations became available. For instance, the methyl ester of the *o*-nitro sulfenic acid (Fig. 1) is remarkably flat and the S···O distance is just 2.457 Å [2,3]. At first, some cases were regarded as unusual packing features while others were just ignored. However, this is a fairly common feature in the crystal structures of molecular compounds of sulfur, selenium and tellurium. Following the surge of interest in *halogen bonding*, research in ChB is undergoing fast expansion; several recent reviews [4–11] have covered fundamental aspects and applications of this type of interaction and highlighted examples from literature. Here we identify notable cases in which ChB is present in the structures of functional materials. In some instances, the influence of this interaction on the macroscopic properties is clear; in others, it is not yet established or it is not straightforward to quantify and distinguish it from the effect of other interactions. On occasion, we present cases in which ChB might have been overlooked in the original structural report and discussion.

* Corresponding author.
E-mail address: vargas@chemistry.mcmaster.ca (I. Vargas-Baca).

https://doi.org/10.1016/j.ccr.2020.213464
0010-8545/

Table 1
Distance ranges (Å) from the sum of covalent radii (Σr_{cov}, top) to the sum of van der Waals radii (Σr_{vdW}, bottom) for selected pairs of main group elements.

	C	N	P	O	S	Se	Te	F	Cl	Br	I
C	1.54	1.52	1.83	1.50	1.79	1.93	2.12	1.48	1.76	1.91	2.10
	3.40	3.25	3.50	3.22	3.50	3.60	3.76	3.17	3.45	3.55	3.68
N		1.50	1.81	1.48	1.77	1.91	2.10	1.46	1.74	1.89	2.08
		3.10	3.35	3.07	3.35	3.45	3.61	3.02	3.30	3.40	3.53
P			2.12	1.79	2.08	2.22	2.41	1.77	2.05	2.20	2.39
			3.60	3.32	3.60	3.70	3.86	3.27	3.55	3.65	3.78
O				1.46	1.75	1.89	2.08	1.44	1.72	1.87	2.06
				3.04	3.32	3.42	3.58	2.99	3.27	3.37	3.50
S					2.04	2.18	2.37	1.73	2.01	2.16	2.35
					3.60	3.70	3.86	3.27	3.55	3.65	3.78
Se						2.32	2.51	1.87	2.15	2.30	2.49
						3.80	3.96	3.37	3.65	3.75	3.88
Te							2.70	2.06	2.34	2.49	2.68
							4.12	3.53	3.81	3.91	4.04
F								1.42	1.70	1.85	2.04
								2.94	3.22	3.32	3.45
Cl									1.98	2.13	2.32
									3.50	3.60	3.73
Br										2.28	2.47
										3.70	3.83
I											2.66
											3.96

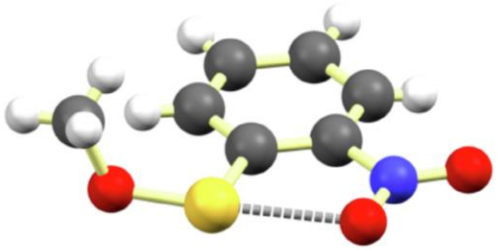

Fig. 1. Molecular structure in the crystal of methyl *o*-nitrobenzenesulfenate; d(S···O) = 2.457 Å (74%), ∡(O-S···O) = 176.4°.

2. Frequent ChB supramolecular synthons

Although a wide variety of molecules can participate in ChB, either as donors or acceptors, most of the structures of their aggregates can be described in terms of the recurrent geometric motifs or supramolecular synthons [12] formed. We have reviewed the wide variety of supramolecular synthons assembled by tellurium molecular compounds and proposed a classification notation elsewhere [10]. The supramolecular synthons most common in the present review areshown in Scheme 1. The simplest, [Ch Nu], is formed by one nucleophile attached to one chalcogen atom; λ^2 and λ^4 chalcogen centers can form up to two of these synthons

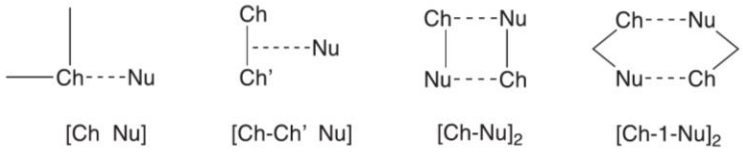

Scheme 1. Chalcogen bonding supramolecular synthons. Ch is a chalcogen element (S, Se, Te); Nu is a nucleophilic center, i.e. the ChB acceptor.

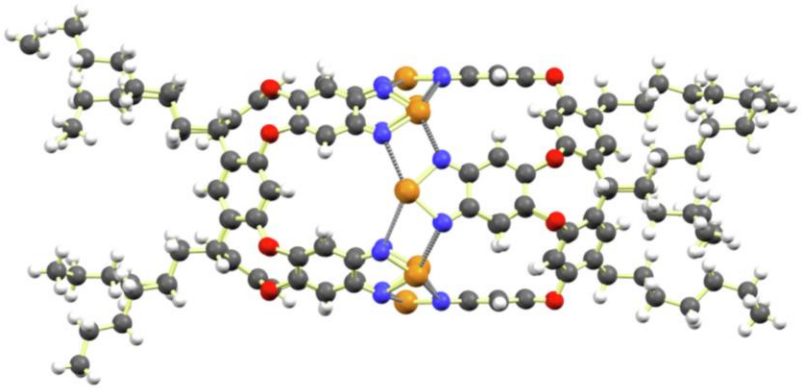

Fig. 2. Crystal structure of a supramolecular capsule based on telluradiazoles and the $[Te\text{-}N]_2$ supramolecular synthon; d(Te···N) = 2.674–2.87 Å (74–80%), ∡(N-Te···N) = 150.3–153.2°.

while λ^3 centers can form up to three ChB's. In addition to that structural element, two chalcogens in a hetero- or homoatomic bond can participate in a three-center interaction, [Ch-Ch′ Nu], when a maximum of electrostatic potential is located between the Ch and Ch′ atoms. Molecules that contain a combination of ChB donor and acceptor centers can link into chains or rings. A special case of the latter is the formation of a supramolecular four-membered ring by two antiparallel ChB's between the atoms of two Ch–Nu bonds. Such supramolecular synthon, $[Ch\text{-}Nu]_2$ is a recurrent structural motif in chalcogen bonding, especially with heterocycles that contain Ch-N bonds. 1,2,5-chalcogenadiazoles are well known for their ability to form $[Ch\text{-}N]_2$ in dimers and ribbons in crystals [13–22], the flexibility of this supramolecular synthon was recently exploited in the construction of supramolecular capsules [23] (Fig. 2). However, formation of $[Ch\text{-}Nu]_2$ can be in competition with other structural motifs;[24] benzothia- and benzoselenadiazole form spiral $[Ch\text{-}N]_\infty$ chains instead of ribbons [25–27], a unique case of the $[S\text{-}N]_3$ supramolecular synthon is observed in the adducts of triptycenetris(thiadiazole) with fullerenes [28] (Fig. 3). A virtual six-membered ring, $[Ch\text{-}Nu]_2$, can be formed by the dimerization of molecules in which Ch and Nu are covalently connected by a 1 atom bridge [29–31]. The macrocycles spontaneously assembled by *iso*-tellurazole *N*-oxides [32–38] are in effect examples of large supramolecular synthons: $[Te\text{-}1\text{-}O]_4$ and $[Te\text{-}1\text{-}O]_6$.

Most frequently, a ChB would be approximately antipodal to the most electronegative element bonded to the chalcogen, but it is also possible that a ChB forms opposite to the less electronegative substituent [39]. For this reason, in the structures highlighted in this review we quote the widest relevant bond angle in addition to the ChB distance in Ångstroms and the corresponding percentage of the sum of van der Waals radii.

3. Charge transfer salts

There is a vast family of crystalline molecular materials prepared by the combination of an electron donor and an electron acceptor. Whether complete or partial, electron transfer between the building blocks generates paramagnetic centers and charge carriers. Many charge-transfer salts have been prepared from electron donors that contain chalcogen atoms, most prominently tetrathiafulvalenes and their heavy analogues. These are good ChB donors, especially in their oxidized states. Anions and electron-acceptor molecules such as tetracyanoquinodimethane and quinones can act as ChB acceptors in the crystal. This effect can be beneficial to the arrangement of the molecules in the lattice, as electron mobility along molecular stacks is a desirable feature. Halide salts of *o*-DMTTF with 2:1 stoichiometry are isostructural, contain stacks of the electron donor connected by S···X (3.492, 3.553, 3.6771 Å for X = Cl, Br, I, respectively) ChB's and C–H···X hydrogen bonds (Fig. 4). The bromide salt is metallic down to 50 K with σ_{RT} ca. 150 S cm^{-1}[40].

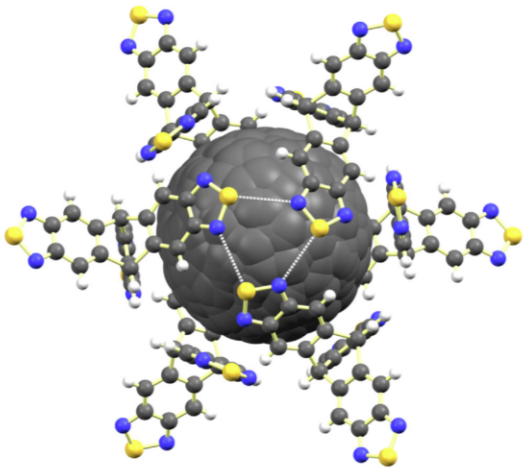

Fig. 3. Organization of molecules with the $[S\text{-}N]_3$ supramolecular synthon in the crystal structure of 2(triptycenetris(thiadiazole))·2C_{60}·1,3,5-$(CH_3)_3C_6H_3$; d(S···N) = 3.41 Å (98%), ∡(N-S···N) = 138.4°.

Similarly, the nitrate mixed-valence salt of o-Me_2TTF contains stacks of the donor molecules piled up along the *a*-axis. Although the anions are disordered, S···O (2.964 Å, 250 K) ChB's are distinguishable and hydrogen bonds further stabilize this arrangement (Fig. 4). The material has σ_{RT} = 3–5 S cm^{-1}, E_{act} = 0.12–0.14 eV, and χ_s ca. 4x 10^{-4} cm^3 mol^{-1} at 300 K, the susceptibility decays progressively to a non-magnetic ground state at around 96 K [41].

In spite of their low basicity, the terminal O atom of polyoxometallates form C-H···O hydrogen bonds and act as ChB acceptors in the crystals of (o-Me_2TTF)$_2$[W_6O_{19}] (S···O = 2.824, 3.129 Å) [42] and (BPDT-TTF)$_2$[W_6O_{19}] (S···O = 3.111, 3.15, 3.22 Å) [43] (Fig. 5).

Additional heteroatoms can turn TTF derivatives into ChB acceptors, which can promote the organization of molecules in ribbons, as observed in the crystals of δ-(BEDT-TTF)$_4$[2,6-naphthalene-bis-(sulfonate)]·4H_2O (S···S 3.341–3.521 Å and δ-(BEDT-TTF)$_4$[2,6-anthracene-bis(sulfonate)]·(H_2O)$_4$ (S···S 3.327–3.385 Å) (Fig. 6). The former is a semiconductor with σ_{RT} = 10^{-2} S cm^{-1}, the latter is a metal at room temperature metal–insulator transition at 85 K; its room temperature conductivity increases with pressure from 100 S cm^{-1} at 1 atm to 250 S cm^{-1} at 1.1 GPa without a change to the transition temperature [44].

The crystal structure of τ-(EDT-TTF-CONMe$_2$)($AuBr_2$)·($C_2H_2Cl_4$)$_{0.5}$ features coplanar pairs of molecules connected by ChB (d(S···O) = 3.269 Å, Fig. 7); multiple S···S short contacts and C-H···O hydrogen bonds are also present; the material's σ_{RT} = 0.025 S cm^{-1} [45]. Flat ribbons are assembled in the crystal of [EDT-TTF-I_2]$_4$[Cd_3(NCS)$_8$]·CH_3CN·H_2O (Fig. 7) by a combination of S···I (3.654, 3.740 Å) and S···S (3.587 Å) ChB's, in addition to S···S and C-H···I hydrogen bonding. The ribbons are stacked and connected to flanking $[Cd_3(NCS)_8]^{2-}$ polymers by I···S (3.248 Å) halogen bonds; the conductivity is σ_{RT} = 0.67 S cm^{-1} [46]. Similar patterns are observed in (tTTF-I)$_2$$ClO_4$ (d(S···I) 3.719 (98%) Å, ∡(C-S···I) = 177.3°) at room temperature, σ_{RT} = 5 S cm^{-1}, $\chi_0 = 2 \times 10^{-5}$ cm^3 mol^{-1}) [47], (EDT-TTF-I_2)$_2$(DDQ)·(CH_3CN) (d(S···I) 3.665, 3.729 Å ∡(C-S···I) = 160.3, 166.7°), σ_{RT} = 0.043 S cm^{-1}) [48] and (EDT-TTF-I_2)$_2$(*D*-camphorsulfonate)·H_2O (d(S···I) = 3.689 (98%), 3.751 Å (99%)) $\sigma_{RT} \approx$ 3–5 S cm^{-1}) [49].

Nitrile groups can act as ChB acceptors in electron acceptors such as TCNQ. In the 1:1 salt (EDT-TTF-I)(TCNQ) (σ_{RT} = 5–8 × 10^{-2} S cm^{-1}, E_{act} = 0.043 eV), EDT-TTF-I molecules stack along *c* and form layers via S···S (3.407, 3.499 Å) and S···I (3.683 Å) ChB's (Fig. 7). And TCNQ stacks along *b* and connect with the electron acceptors through I···N halogen bonding and C-H···N hydrogen bonding. In the 2:1 salt (EDT-TTF-I)$_2$(TCNQ) (σ_{RT} is 10^{-5} S cm^{-1}, E_{act} = 0.31 eV), molecules are organized into alternating DDADDA chains connected by S···N (3.303 Å) ChB and I···N halogen bonds (Fig. 8).

The fluorine atoms of $TCNQF_4$ are also able to act as ChB acceptors as shown by the structure of (EDT-TTF-I)($TCNQF_4$) (σ_{RT} = 10^{-4} S cm^{-1} E_{act} = 0.19 eV) with S···F (3.158 to 3.256 Å) and S···N (3.272 Å) ChB in addition to I···N and C-H···N contacts (Fig. 9) [50]. The use of 1,2,5-C_2N_2S rings in charge transfer salts often leads to the formation of the $[S\text{-}N]_2$ supramolecular synthon. Crystalliza-

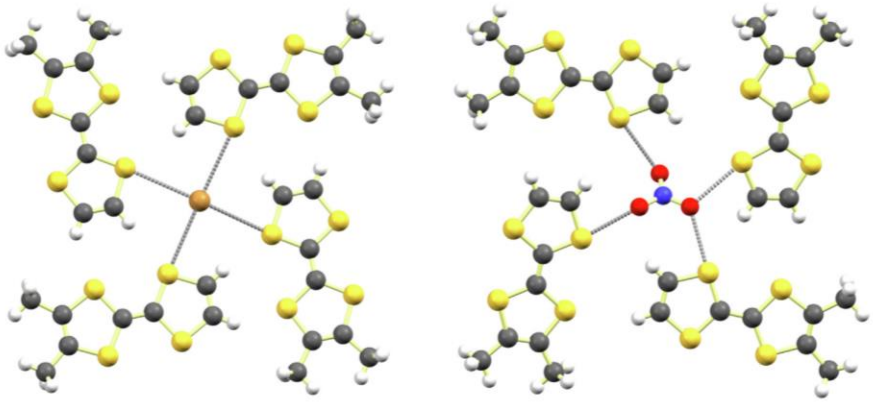

Fig. 4. Organization of the molecular units and halide anions in the crystals of [*o*-DMTTF]$_2$Br (left); d(S···Br) = 3.553 Å (97%), ∡(C-S···Br) = 168.5°; and [*o*-Me$_2$TTF]$_2$NO$_3$ (right); d(S···O) = 2.964 Å (89%), ∡(C-S···O) = 167.3° at 250 K.

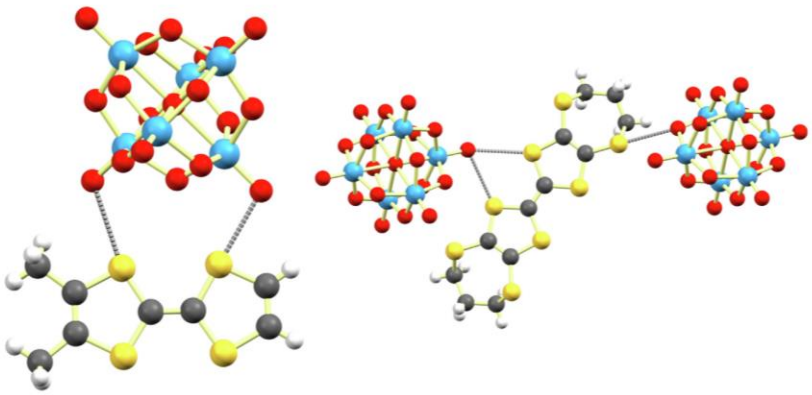

Fig. 5. Two examples of a polyoxotungstate as a ChB acceptor in charge transfer salts of tetrathiofulvalenes: (*o*-Me$_2$TTF)$_2$[W$_6$O$_{19}$] (left); d(S···O) = 2.824 (85%), 3.129 Å (94%), ∡(C-S···O) = 159.4, 169.4°; and (BPDT-TTF)$_2$[W$_6$O$_{19}$] (right); d(S···O) = 3.111 (94%), 3.15 (95%), 3.22 Å (97%), ∡(C-S···O) = 177.2, 142.5, 146.5°.

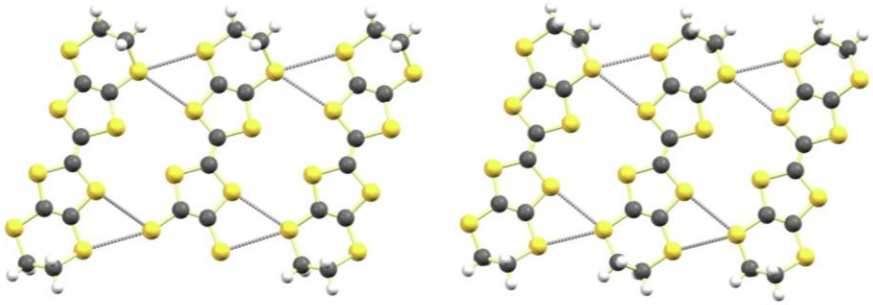

Fig. 6. Ribbons of electron donors in the crystal structures of δ-(BEDT-TTF)$_4$[2,6-naphthalene-bis-(sulfonate)]·4H$_2$O (left); d(S···S) = 3.341–3.521 Å (93–97%), ∡(C-S···S) = 157.6–164.8°; and δ-(BEDT-TTF)$_4$[2,6-anthracene-bis(sulfonate)]·(H$_2$O)$_4$ (right) ; d(S···S) = 3.327–3.385 Å (92–94%), ∡(C-S···S) = 158.2–168.4.

tion of 4,6-dinitro-2,1,3-benzothiadiazole with 4-amino-2,1,3-benzothiadiazole leads to donor–acceptor π-stacked structures. The acceptor molecules are arranged in pairs connected by pairs of antiparallel, S···N (2.993 Å) and S···O (3.276 Å) ChB's (Fig. 9). The charge transfer salt of [1,2,5]thiadiazolo[3,4-c][1,2,5]thiadiazole with 4-amino-2,1,3-benzothiadiazole features an eight-membered ring with four S···N (d(S···N) = 3.046 to 3.303 Å, ∡(N-S···N) = 154.06 to 168.68°) ChB's. Two N-H···N hydrogen bonds likely enhance the stability of the structure (Fig. 10). The crystal of [1,2,5]thiadiazolo[3,4-c][1,2,5]thiadiazole and phenoxatellurine with

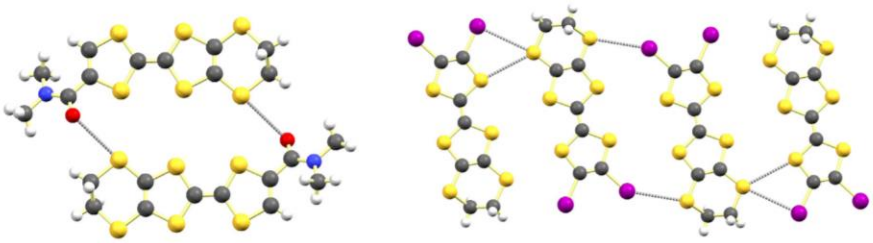

Fig. 7. Intermolecular ChB in the structures of two TTF charge transfer salts τ-(EDT-TTF-$CONMe_2$)($AuBr_2$)·($C_2H_2Cl_4$)$_{0.5}$ (left); d(S···O) = 3.269 Å (98%), ∡(C-S···O) = 171.8° and [EDT-TTF-I_2]$_4$[$Cd_3(NCS)_8$]·CH_3CN·H_2O (right); d(S···I) = 3.654 (97%), 3.740 Å (99%), ∡(C-S···I) = 138.4,167.6° and d(S···S) = 3.587 Å (99%), ∡(C-S···S) = 162.7°.

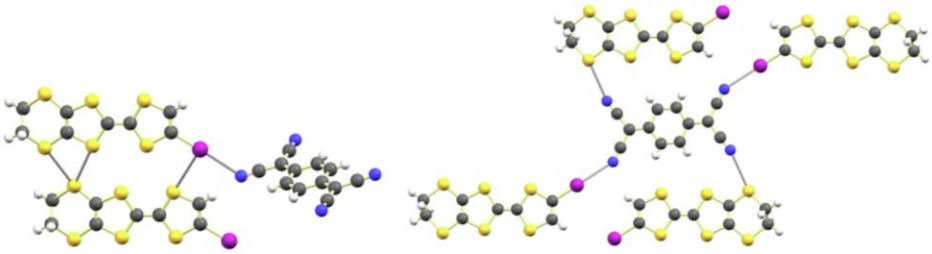

Fig. 8. Supramolecular interactions in the crystals of (EDT-TTF-I)(TCNQ) (left); d(S···S) = 3.407 Å (95%), ∡(C-S···S) = 154.0, 161.8°), d(S···S) = 3.499 Å (97%), ∡(C-S···S) = 151.1°) and d(S···I) = (3.683 Å (97%), ∡(C-S···I) = 168.0°); and (EDT-TTF-I)$_2$(TCNQ) (right); d(S···N) = 3.303 Å (99%), ∡(C-S···N) = 161.6° [50].

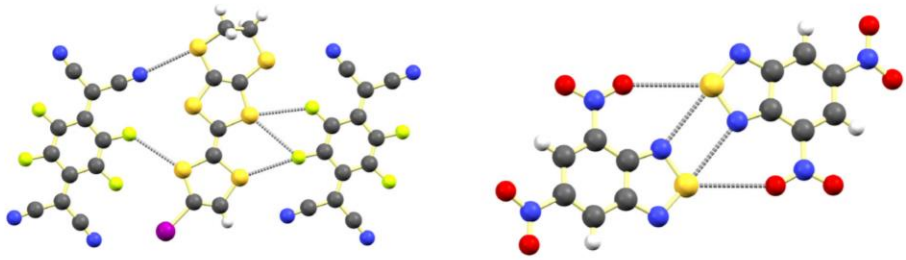

Fig. 9. Intermolecular interactions in the structure of (EDT-TTF-I)($TCNQF_4$) (left); d(S···F) = 3.158–3.256 Å (97–98%), ∡(C-S···F) = 144.3–163.7° and d(S···N) = 3.272 Å (98%), ∡(C-S···N) = 166.4°; and 4,6-dinitro-2,1,3-benzothiadiazole in its co-crystal with 4-amino-2,1,3-benzothiadiazole; d(S···N) = 2.993 Å (89%), ∡(N-S···N) = 165.56° and d(S···O) = 3.276 Å (99%), ∡(N-S···O) = 131.24.

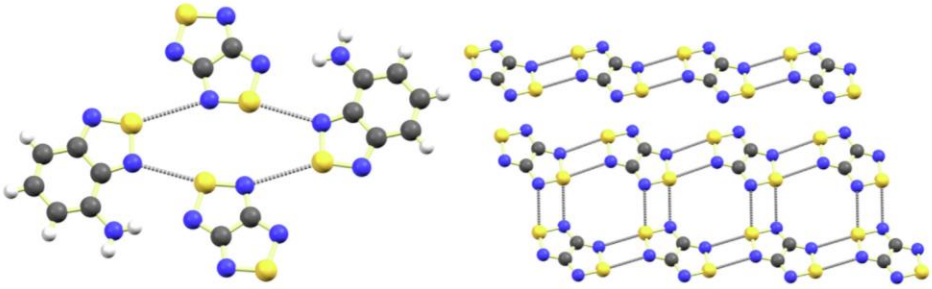

Fig. 10. Supramolecular interactions of $C_2N_4S_2$ in its cocrystals with 4-amino-2,1,3-benzothiadiazole (left); d(S···N) = 3.046–3.303 Å (91–99%), ∡(N-S···N) = 154.06–168.68°); and phenoxatellurine (right); d(S···N) = 3.119–3.1515 Å (93–94%), ∡(N-S···N) = 170.78–176.78°.

a 3:1 ratio has the acceptor molecules organized through the [S-N]$_2$ supramolecular synthon (d(S···N) = 3.119 to 3.1515 Å) along *a* in two chains. One is simple sequence, the other is built by molecules participating in 4 [S-N]$_2$ supramolecular synthons, resulting the periodic repetition of rings formed by four molecules (Fig. 10) [51]. The chains are connected by S···C π contacts.

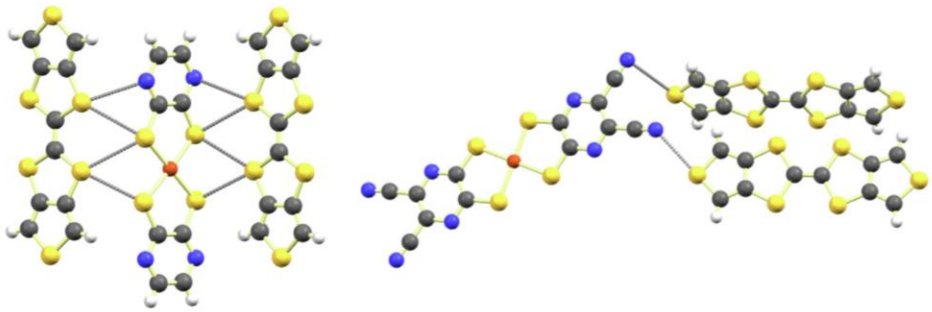

Fig. 11. Intermolecular interactions in the structure of $[DT\text{-}TTF]_4[Cu(pdt)_2]_3$ (left); d(S···S) = 3.366–3.543 Å (94–98%), ∡(C-S···S) = 142.6–169.1°, d(S···N) = 3.176, 3.305 Å (95–99%), ∡(C-S···N) = 159.3–161.5°; and $(DT\text{-}TTF)_2[Cu(dcdmp)_2]$ (right); d(S···N) = 3.091–3.324 Å (92–99%), ∡(C-S···N) = 171.5–179.1°.

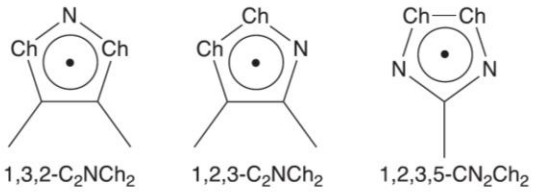

Scheme 2. Structures of dichalcogenazolyl and dichalcogenadiazolyl radical heterocycles.

Anionic $[M^{III}L_2]^-$ (M = Cu, Au, L = a dithiolate) coordination complexes in combination with tetrathiafulvalenes yield semiconductors with significant Seebeck coefficiens. The structure of $[DT\text{-}TTF]_4[Cu(pdt)_2]_3$ (pdt = pyrazine-1,2-dithiolate) features π-stacked dimers of DT-TTF linked by the anion via multiple S···S (3.366–3.543 Å), Nπ ···S (3.176–3.305 Å) ChB's in addition to C-H···N hydrogen bonds (Fig. 11) This material has σ_{RT} = 0.5 S cm^{-1} and S_{RT} = 190 μV K^{-1}; a first order transition with hysteretic loop was observed in the range 125–260 K. The selenium analogue, $[DT\text{-}TTF]_4[Cu(pds)_2]_3$ with S···Se (3.458–3.683 Å (93–99%), ∡(C-S···Se) = 141.9(4)- 171.5(5)°) ChB has σ_{RT} = 0.1 S cm^{-1} and S_{RT} = 180 μV/K) [52]. The crystal of $(DT\text{-}TTF)_2[Cu(dcdmp)_2]$ (dcdmp = 2,3-dicyano- pyrazine-5,6-dithiolate) features N···S (3.091–3.324 Å) ChB's and C-H···N hydrogen bonds, in addition to interstack S···S (3.3652–3.5963 Å) contacts; σ_{RT} = 30 S cm^{-1}, E_{act} = 0.045 eV, S_{RT} = 60 μV/K [53]. The spin-ladder compound $(DT\text{-}TTF)_2[Au(mnt)_2]$ (mnt = maleonitrile dithiolato) displays N···S (3.224 Å (96%), ∡(C-S···N) = 166.0°) ChB's, σ_{RT} = 9 S cm^{-1} and S_{RT} = 38 μV/K [54]. Related compounds have been prepared with M^{II} d^8 ions such as $(DT\text{-}TTF)_2[Ni(mnt)_2]$ (d(N···S) = 3.27 Å (98%), ∡(C-S···N) = 165.6°, σ_{RT} = 40 S cm^{-1}, S_{RT} = 50 μV/K) and $(DT\text{-}TTF)_2[Pt(mnt)_2]$ (d(N···S) = 3.224 Å (96%), ∡(C-S···N) = 166.0 (2)°, σ_{RT} = 40 S cm^{-1}, S_{RT} = 55 μV/K) [55].

4. Heterocyclic neutral radicals

Stable open-shell molecules offer a convenient alternative to charge transfer salts. In particular, organo-chalcogen heterocycles have been central to the development of a variety of molecular materials with a wide range of magnetic and conductive properties. The majority of these materials include within their molecular structure one or two conjugated five-membered rings with seven π electrons. The three most common of those cyclic radicals are shown in Scheme 2. In principle, Ch could be any of the chalcogens. However, most work has been carried out with sulfur and selenium as the tellurium analogues are unstable. Intermolecular interactions, in particular π stacking are favorable to electron mobility to a point, dimerization and Peierls distortions are detrimental to the electrical conductivity.

One of the most interesting and complicated systems in this category is the trithiatriazapentalenyl radical, $C_2S_3N_3$, which exhibits a phase transition from $P2_1/c$ to P-1 on cooling with magnetic bistability and thermal hysteresis (Tc↓=234 K, Tc↑=317 K). The crystal structures display a complex network of intermolecular S···N and S···S contacts and π stacking. The S···N ChB's, which are recognizable by their geometric arrangement (Fig. 12), are 2.918–3.056 Å at 150 K and 3.052–3.252 Å at 310 K [56,57]. Significant hysteresis (Tc↓=297 K, Tc↑=343 K) has been observed in the

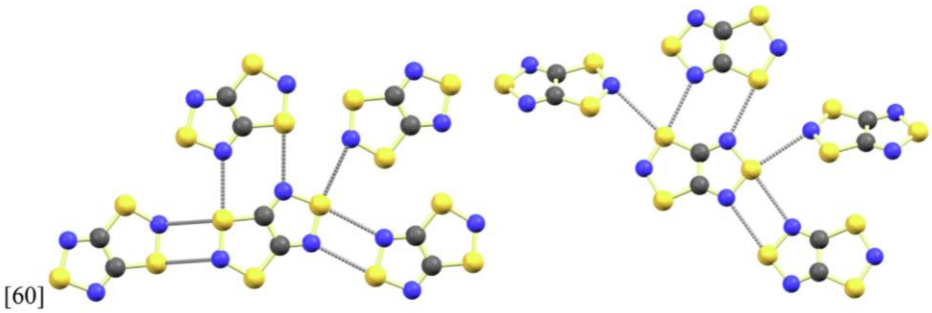

Fig. 12. Detail of packing in the crystal structures of the trithiatriazapentalenyl radical measured at 150 K (left); d(S···N) = 2.918–3.056 Å (87–91%), ∡(N-S···N) = 173.45–176.31°; and 310 K (right); d(S···N) = 3.052–3.252 Å (91–97%), ∡(N-S···N) = 157.9–175.98° [60].

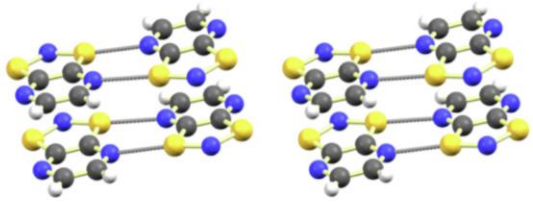

Fig. 13. Detail of the low-temperature structure of PDTA d(S···N) = 2.841–2.875 Å (85–86%), ∡(N-S···N) = 170.84–172.13°.

crystal of [1,3,2]pyrazinodithiazol-2-yl (PDTA, Fig. 13) and linked to changes in the S···N ChB's of the $[S\text{-}1\text{-}N]_2$ supramolecular synthon and S···S contacts [58,59].

The chloride salt of the benzo[1,2-d:4,5-d′]bis[1,3,2]dithiazolyl radical cation crystallizes in diamagnetic and paramagnetic phases at low and high temperature. Both polymorphs consist of layers built by the $[S\text{-}N]_2$ ($d(S\cdots N)_{LT,HT}$ = 3.175, 3.153 Å (95, 94%); ∡(C-S···N) = 176.1, 174.4°), [S N] ($d(S\cdots N)_{LT,HT}$ = 3.089, 3.115 Å (92, 93%); ∡(C-S···N) = 163.9, 164.5°) and [S Cl] ($d(S\cdots Cl)_{LT,HT}$ = 3.124, 3.118 Å (88.0, 87.8%); ∡(N-S···Cl) = 168.7, 167.8°) ChB supramolecular synthons. The phase transition occurs at ca. 150 K without hysteresis and mostly involves changes in the stacking of the layers [60].

The crystal structures of 1,2,3,5-dichalcogenadiazolyl radicals most frequently feature π-stacked dimers. Pyridines and nitriles attached at position 4 lead to the formation of chains thanks to the [Ch-Ch N] supramolecular synthon [61–64] (Fig. 14). Halogen atoms can function in an analogous way [65]. When no other nucleophile is available, the nitrogen atom of the heterocycle can act as ChB acceptor [66–68] (Fig. 15). One of the most interesting structures built by this supramolecular synthon is a spiral column of dithiadiazolyl radicals in a hexagonal phase dopped with iodine

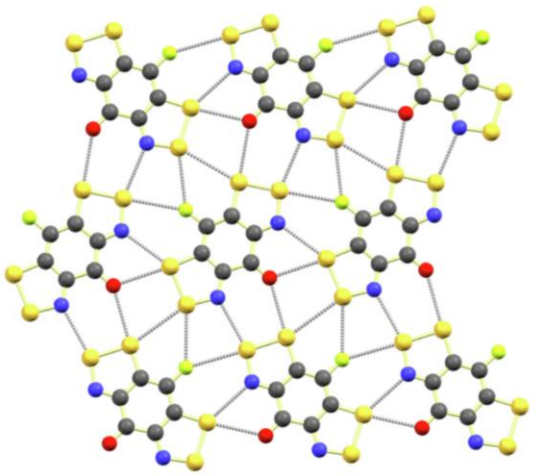

Fig. 16. Packing of molecules and intermolecular interactions in the crystal of FBBO at ambient pressure; d(S···O) = 3.042 Å (92%), ∡(C-S···O) = 175.9°, d(S···O) = 3.132 Å (94%), ∡(C-S···O) = 178.0°), d(S···N) = 3.044 Å (91%), ∡(N-S···N) = 159.9°, d(S···N) = 3.053 Å (91%), ∡(S-S···N) = 149.2°) and d(S···F) = 3.174 Å (97%), ∡(S-S···F) = 156.33°, d(S···F) = 3.218 Å (98%), ∡(S-S···F) = 178.63°. At 10 GPA, d(S···O) = 2.588 Å (78%), ∡(C-S···O) = 177.53°, d(S···O) = 2.670 Å (80%), ∡(C-S···O) = 171.75°, d(S···N) = 2.471 Å (74%), ∡(N-S···N) = 163.64°, d(S···N) = 2.763 Å (82%), ∡(S-S···N) = 156.49°, S···F d(S···F) = 2.761 Å (84%), ∡(S-S···F) = 156.13°, d(S···F) = 2.795 Å (85%), ∡(S-S···F) = 177.90°.

(d(S···N) = 2.90–3.12 Å (87–93%), ∡(N-S···N) = 158.8–166.9°); σ_{RT} = 15 S cm^{-1} χ_M -10×10^{-6} emu $mole^{-1}$ at 360 K) [69].

One of the best illustrations of the impact of ChB on the properties of the neutral radical conductors is provided by the study of the fluoro-oxo-benzene-bridged bisdithiazolyl radical (FBBO). Its

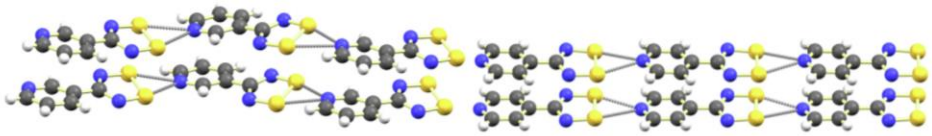

Fig. 14. Linear chains in the crystal structure of the 3- and 4-pyridyl-dithiazolyl radicals; d(S···N) = 2.846(4)-2.970(3) Å (85–89%), ∡(N-S···N) = 159.9–165.8° and d(S···N) = 2.717–2.952 Å (81–88%), ∡(N-S···N) = 155.1–164.4° [62] (left and right, respectively).

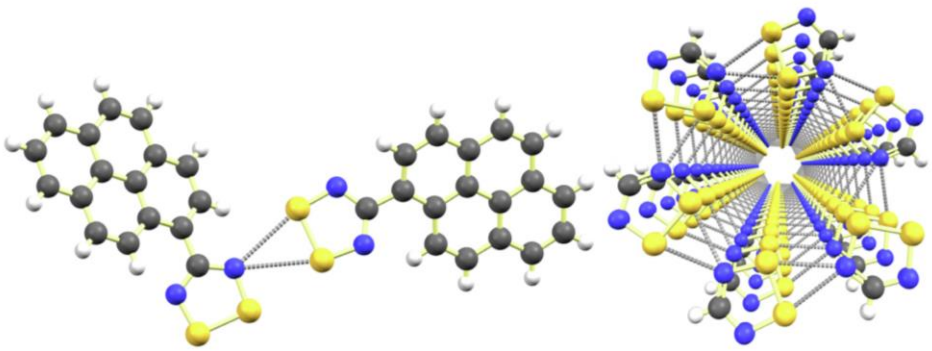

Fig. 15. Intermolecular ChB in the crystal structure of the pyren-1-yldithiadiazolyl radical (left); (d(S···N) = 3.189–3.236 Å (95–97%), ∡(N-S···N) = 161.9–163.2°) [67]. Spiral arrangement of the dithiadiazolyl radicals in the crystal of $[HCN_2S_2]_6I_{1.1}$ (right); (d(S···N) = 2.90(1)-3.12(1) Å (87–93%), ∡(N-S···N) = 158.8–166.9°; iodine atoms are located along the center but are omitted here for clarity.

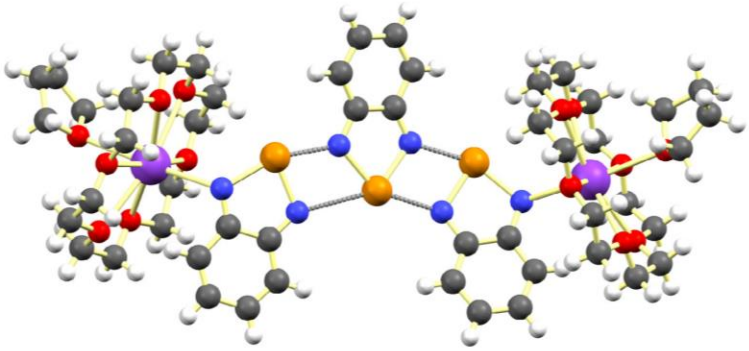

Fig. 17. Molecular unit in the crystal of $[K(18\text{-}C\text{-}6)(THF)]_2[(C_6H_4N_2Te)_3]$; d(Te···N) = 2.250–2.904 Å (62–80%), ∡(N-Te···N) = 141.4–159.4°.

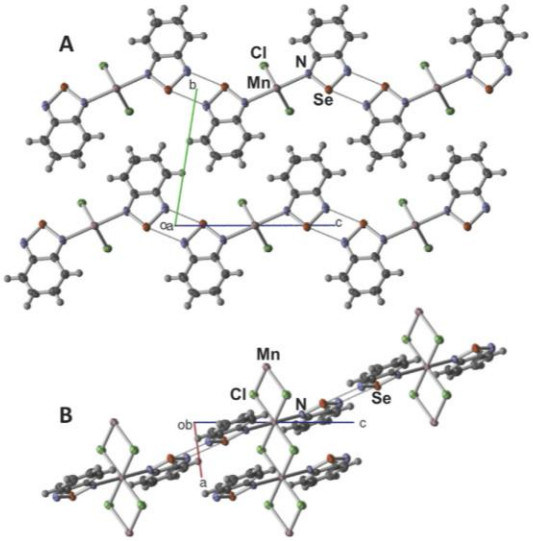

Fig. 18. Two views of the crystal structure of $[MnCl_2(C_6H_4N_2Se)_2]$; d(Se···N) = 2.865 Å (83%), ∡(N-Se···N) = 165.07(9)°. **A**: along *a*; **B**: along *b*. Reproduced from reference [75] with permission from The Royal Society of Chemistry.

crystal structure (Fig. 16) consists of layers of molecules linked by S···O (3.042 Å, 3.132 Å), S···N (3.044 Å, 3.053 Å) and S···F (3.174 Å, 3.218 Å) ChB's. Compression to 10 GPa causes a contraction of 13% along the π-stacking direction and 5 percent along each direction in the plane of the layers. This translates in a decrease of the distances of the ChB's. Simultaneously, the room temperature conductivity increases from 10^{-2} at ambient pressure to 10^2 S cm^{-1} over 6 GPa [70,71]. Similarly, the R3c phase of benzoquino-bis-1,2,3-thia selenazole displays a network of Se···N (d(Se···N) = 2.791 Å (81%), ∡(S-Se···N) = 169.10°, d(Se···N) = 3.231 Å (94%), ∡(S-Se···N) = 162.72°), Se···O (d(Se···O) = 2.654 Å (78%), ∡(N-Se···O) = 155.91°), and S···O (d(S···O) = 2.624 Å (79%), ∡(N-S···O) = 156.41°, d(S···O) = 2.984 Å (90%), ∡(N-S···O) = 174.88°) ChB's which at 6 GPa compresses the Se···N (d(Se···N) = 2.352 Å (68%), ∡(S-Se···N) = 172.31°, d(Se···N) = 2.821 Å (82%), ∡(S-Se···N) = 161.46°), Se···O (d(Se···O) = 2.518 Å (74%), ∡(N-Se···O) = 152.15°), and S···O (d(S···O) = 2.370 Å (71%), ∡(N-S···O) = 157.63°, d(S···O) = 2.656 Å (80%), ∡(N-S···O) = 171.14°) ChB's, while the conductivity increases from 10^{-3} to 10^2S cm^{-1} [72].

Noticeably absent from the examples of materials described above are tellurium compounds, in spite of their propensity to engage in ChB. Challenging syntheses and high reactivity are often the cause. Albeit not a neutral species, the radical anion from the reduction of benzo-2,1,3-telluradiazole was spectroscopically observed in solution for a brief period of time [73]. Very recently, it was isolated and characterized in the solid-state in a trimeric structure (Fig. 17) in which three benzotelluradiazole molecules are connected by two $[Te\text{-}N]_2$ supramolecular synthons. The

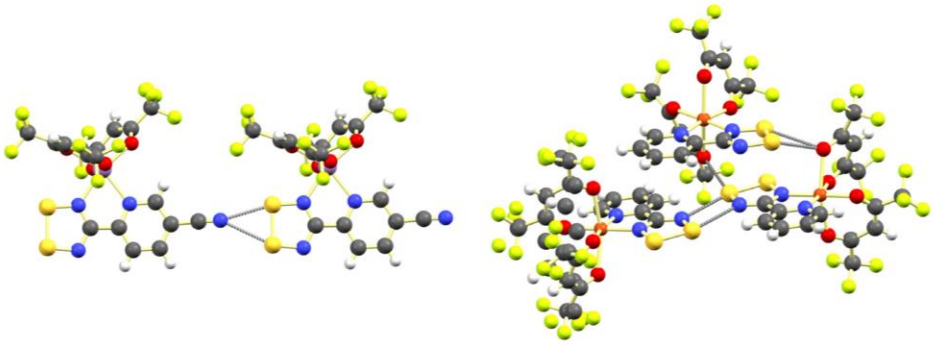

Fig. 19. Supramolecular synthons in the crystal structures of transition metal complexes of 1,2,3,5-dithiadiazolyl radicals. [S-S N] in $[Mn(k\mathrm{N}^2\text{-}4CNpyDTDA)(hfac)_2]$ (left); d(S···N) = 2.869, 3.038 Å (86, 91%), ∡(N-S···N) = 160.3, 167.1°; $[S\text{-}N]_2$ and [S-S O] in $Cu^{II}(\kappa\mathrm{N}^2\text{-}pyDTDA)(hfac)_2]$ (right); d(S···N) = 3.013 Å (90%), ∡(N-S···N) = 166.4° d(S···O) = 2.794, 3.296 Å (86, 92%), ∡(N-S···O) = 162.7, 147.2°.

stoichiometry of the compound and coordination of the terminal heterocycles to potassium suggests these are two benzotelluradiazolidyl radical anions bridged by a neutral molecule of benzotelluradiazole. Unusually, the trimer is not planar and the Te···N ChB's are not symmetrical. However, the material is diamagnetic and computational modeling indicates that the charge is delocalized over the π-orbital manifold of the three benzotelluradiazoles and that a more symmetrical structure would be prone to distortion and easily deformed by packing in the lattice [74].

5. Paramagnetic coordination compounds

ChB interactions provide a pathway for spin–spin coupling through the ligands of transition metal complexes. The crystal structure of $[MnCl_2(C_6H_4N_2Se)_2]$ consists of $[Mn(\mu\text{-}Cl)_2]_\infty$ chains flanked on each side by benzoselenadiazole molecules (Fig. 18), which in turn form the $[Se\text{-}N]_2$ supramolecular synthon (Se···N 2.865(2) Å) with neighboring molecules. DFT calculations indicate there is significant spin polarization throughout the heterocycle, which enables antiferromagnetic coupling between the metal centers [75].

A number of coordination complexes of neutral organo-chalcogen-nitrogen free radicals have been developed in recent years to combine the magnetic properties of the metal ion and the ligands [76]. The crystal structures of many of the complexes readily form ChB's with the most common supramolecular synthons The 4-(4-cyano-2-pyridyl)-1,2,3,5-dithiadiazolyl radical (4CNpyDTDA) chelates Ni^{II} or Mn^{II} in $[M^{II}(\kappa N^2\text{-}4CNpyDTDA)(hfac)_2]$ ($hfac^-$= hexafluoroacetylacetonato) complexes that form isostructural crystals. The [S-S N] supramolecular synthon (d(S···N) = 2.869, 3.038 Å) guides the formation of infinite chains Fig. 19. However, the chains pack in antiparallel directions and the heterocycles form antarafacial dimers that couple their spins [77]. A similar situation is observed in the complex $[Cu^{II}(\kappa N^2\text{-}pyDTDA)(hfac)_2]$ (pyDTDA = 4-(2-pyridyl)-1,2,3,5-dithiadiazolyl), which forms twisted-cofacial dimers, in turn these are connected by the $[S\text{-}N]_2$ (d(S···N) = 3.013 Å) and [S-S O] (d(S···O) = 2.794, 3.296 Å) supramolecular synthons (Fig. 19) [78]

6. Optical properties

ChB can have a significant effect on the spectrum of absorption of conjugated organo-chalcogen compounds. The 1,8-dichalcogena-2,4,5,7-tetraza-2,4,6-octatrienes have been characterized in three distinct structural types (Fig. 20). The *Z,E,Z* geometries feature virtual five- and four-membered rings with S···N ChB's 2.607 Å and 2.835 Å, respectively. There is also a striking difference of color between these compounds. Examples with the shortest S···N ChB's are purple (λ_{max} = 550 nm); the compounds with the other two geometries have red-brown color (λ_{max} = 470 nm). DFT calculations showed that the *Z,E,Z* structure is more stable than the *E,E,E* conformer and suggested that the color difference is the

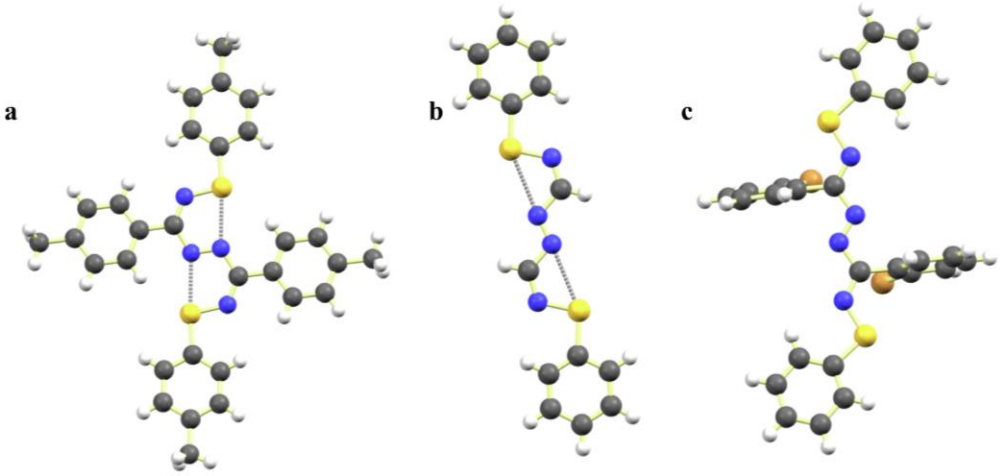

Fig. 20. Examples of structures of R-S-N = C(R′)-N = N-C(R′) = N-S-R. a) *Z,E,Z* R = R′ = 4-$CH_3C_6H_4$; d(S···N) = 2.607 Å (78%), ∡(C-S···N) = 170.5°; b) *Z,E,Z* R = C_6H_5, R′ = H (d(S···N) = 2.835 Å (85%), ∡(C-S···N) = 156.3°); c) *E,E,E* R = C_6H_5, R′ = 2-BrC_6H_4.

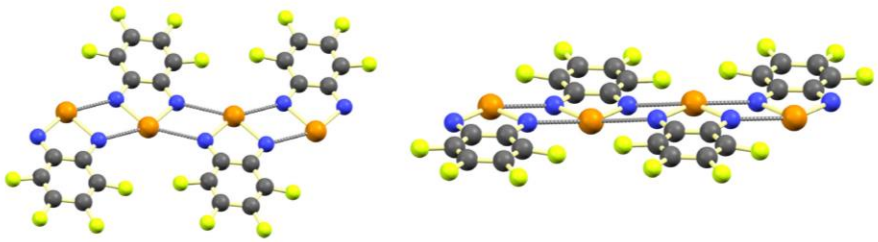

Fig. 21. Detail of intermolecular interactions in the crystal structures of the two phases of 4,5,6,7-tetrafluorobenzo-2,1,3-telluradiazole. Yellow phase (β, left); d(Te···N) = 2.75–2.88 Å (76–80%), ∡(N-Te···N) = 153.3–156.9°. Red phase (α, right); d(Te···N) = 2.63–2.96 Å (73–82%), ∡(N-Te···N) = 149.0–157.7°.

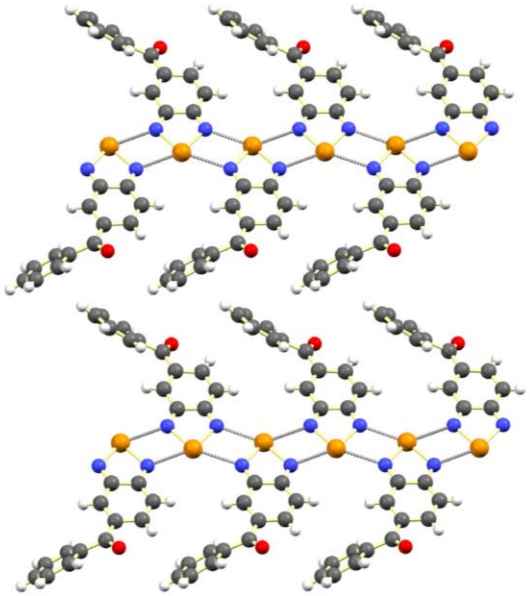

Fig. 22. Detail of packing and intermolecular interactions in the NLO crystal of 5-benzoylbenzo2,1,3-telluradiazole, d(Te···N) = 2.69–2.79 Å (74–77%), ∡(N-Te···N) = 151-154°.

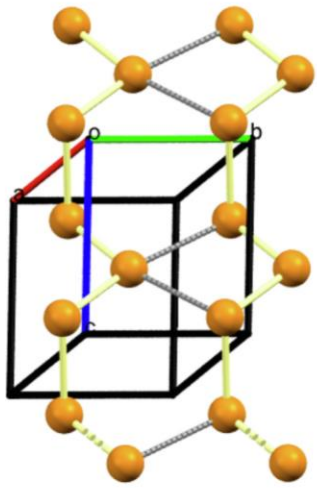

Fig. 23. Detail of the interatomic ChB in the structure of elemental tellurium; d(Te···Te) = 3.501 Å (85%), ∡(Te-Te···Te) = 164.3°. Crystal data from reference [83].

result of orbital mixing enabled by the short S···N ChB's in the five membered rings with a concomitant perturbation of the $\pi_{LUMO} \leftarrow \pi_{HOMO}$ excitation [79,80]. The selenium analogues are only known in the *Z,E,Z* conformer with the two five-membered rings and Se···N (2.648 Å (77%), ∡(C-Se···N) = 163.7°) ChB's [81].

A different effect leads to chromotropism in crystalline tetrafluoro-benzotelluradiazole. Compared to the supramolecular ribbons formed by benzotelluradiazole, the chains of the fluorinated compound are destabilized by steric repulsion between fluorine atoms. The repulsion can be attenuated by a geometric distortion, either by an elongation of every other pair of antiparallel ChB's or by a twist of the $[Te\text{-}N]_2$ supramolecular synthon. Both distortions have been experimentally observed. The first yields a metastable yellow phase (β), the second produces a stable red solid (α, Fig. 21). Heating readily induces the transition to the stable phase. DFT computational analysis did suggest that the color difference is an effect of loss of the inversion center at the $[Te\text{-}N]_2$ supramolecular synthon with the consequent relaxation of the parity selection rule for the first electron excitations [17]. The spontaneous generation of a non-centrosymmetric feature in a ribbon of a telluradiazole due to moderate steric repulsion was employed to promote the growth of molecular crystals capable of second harmonic generation (SHG) from 3,4-dicyano-1,2,5-telluradiazole, 5,6-dichlorobenzo-2,1,3-telluradiazole and 5-benzoylbenzo2,1,3-telluradiazole. Their SHG efficiencies, however, are just about one tenth of the activity of a KDP standard [18].Fig. 22. Fig. 23.

7. Mechanical properties

Under ambient pressure, the trigonal $P3_121$ crystalline form of elemental tellurium consists of helical chains arranged along *c*. The packing has long been regarded as the result of typical van der Waals interactions between chains and the Pauli repulsion between lone pairs of electrons on each atom. However, a detailed computational analysis of electron density revealed an important ChB contribution leading to interchain binding energies (0.173–0.255 eV/atom) significantly larger than the interlayer binding energy of graphite (0.031–0.052 eV/atom) [82]. Such findings are important to understand mechanical properties such as the bulk, Young and shear moduli and the near isotropy of electrical transport properties; all of which are relevant to recent efforts to employ elemental tellurium as a low-dimensional material for optical and electronic applications.

8. Outlook

Applications of chalcogen bonding in crystal engineering, anion binding and transport, and host–guest chemistry are by now familiar. Because chalcogen bonding can be used to influence the solid-state arrangement of molecules, there is significant potential in exploiting this type of supramolecular interaction to manipulate macroscopic properties. This survey has highlighted prominent cases in which ChB's are present in the structures of functional materials, even if such interactions were not explicitly identified or discussed in the original sources. These findings should motivate the re-examination of other materials and suggest new lines of research. In particular, charge transport and magnetic properties are strongly influenced by intermolecular interactions. However, parsing the effects of individual types of intermolecular interactions is very challenging in materials that combine π stacking, multicenter bonding and hydrogen bonding. There is a need for systematic investigations in this area. However, it would be very difficult to achieve this with a purely experimental approach as seemingly small changes in a molecular structure easily lead to differences in supramolecular synthons and packing, and solvatomorphism. Such challenges are exemplified by the structures observed in a recent study of thiophenes grafted to 1,3-chalcogenazole heterocycles [30]. Computational approaches might expedite such investigations but even those would be subject to the limitations of currently available methods to calculate the electronic structure and properties of solids as well as our ability to predict packing in a crystal.

Declaration of Competing Interest

The authors declare that they have no known competing financial interests or personal relationships that could have appeared to influence the work reported in this paper.

Acknowledgement

This work has been supported by the Natural Sciences and Engineering Research Council of Canada (NSERC; IVB-DGI RGPIN-2016-06452, PCH-PGSD), the province of Ontario (JZW-OGF), and the Globus Student Exchange Program (FM).

References

[1] C.B. Aakeroy, D.L. Bryce, G.R. Desiraju, A. Frontera, A.C. Legon, F. Nicotra, K. Rissanen, S. Scheiner, G. Terraneo, P. Metrangolo, G. Resnati, Definition of the chalcogen bond (IUPAC Recommendations 2019), Pure Appl Chem. 91 (2019) (2019) 1889–1892, https://doi.org/10.1515/pac-2018-0713.
[2] W.C. Hamilton, S.J. LaPlaca, The Molecular Structure of the Methyl Ester of o-Nitrobenzenesulfenic Acid, J. Am. Chem. Soc. 86 (1964) 2289–2290, https://doi.org/10.1021/ja01065a040.
[3] Á. Kucsman, I. Kapovits, M. Czugler, L. Párkányi, A. Kálmán, Intramolecular sulphur—oxygen interaction in organosulphur compounds with different sulphur valence state: an X-ray study of methyl-2-nitrobenzene-sulphenate, -sulphinate, -sulphonate and 2-nitrobenzenesulphenyl chloride, J. Mol. Struct. 198 (1989) 339–353, https://doi.org/10.1016/0022-2860(89)80048-1.
[4] M. Fourmigué, A. Dhaka, Chalcogen bonding in crystalline diselenides and selenocyanates: From molecules of pharmaceutical interest to conducting materials, Coord. Chem. Rev. 403 (2020), https://doi.org/10.1016/j.ccr.2019.213084 213084.
[5] N. Biot, D. Bonifazi, Chalcogen-bond driven molecular recognition at work, Coord. Chem. Rev. 413 (2020), https://doi.org/10.1016/j.ccr.2020.213243 213243.
[6] P. Scilabra, G. Terraneo, G. Resnati, The Chalcogen Bond in Crystalline Solids: A World Parallel to Halogen Bond, Acc. Chem. Res. 52 (2019) 1313–1324, https://doi.org/10.1021/acs.accounts.9b00037.
[7] L. Vogel, P. Wonner, S.M. Huber, Chalcogen Bonding: An Overview, Angew. Chem., Int. Ed. 58 (2018) 1880–1891, https://doi.org/10.1002/anie.201809432.
[8] R. Gleiter, G. Haberhauer, D.B. Werz, F. Rominger, C. Bleiholder, From Noncovalent Chalcogen-Chalcogen Interactions to Supramolecular Aggregates: Experiments and Calculations, Chem. Rev. 118 (2018) 2010–2041, https://doi.org/10.1021/acs.chemrev.7b00449.
[9] K.T. Mahmudov, M.N. Kopylovich, M.F.C.G. da Silva, A.J.L. Pombeiro, Chalcogen bonding in synthesis, catalysis and design of materials, Dalton Trans. 46 (2017) 10121–10138, https://doi.org/10.1039/c7dt01685a.
[10] A.F. Cozzolino, P.J.W. Elder, I. Vargas-Baca, A survey of tellurium-centered secondary-bonding supramolecular synthons, Coord. Chem. Rev. 255 (2011) 1426–1438, https://doi.org/10.1016/j.ccr.2010.12.015.
[11] I. Vargas-Baca, T. Chivers, Weakly bonding interactions in organochalcogen chemistry, Phosphorus, Sulfur Silicon Relat. Elem. 164 (2000) 207–227.
[12] G.R. Desiraju, Supramolecular Synthons in Crystal Engineering—A New Organic Synthesis, Angew. Chem., Int. Ed. Engl. 34 (1995) 2311–2327, https://doi.org/10.1002/anie.199523111.
[13] A.F. Cozzolino, I. Vargas-Baca, S. Mansour, A.H. Mahmoudkhani, The Nature of the Supramolecular Association of 1,2,5-Chalcogenadiazoles, J. Am. Chem. Soc. 127 (2005) 3184–3190.
[14] A.F. Cozzolino, J.F. Britten, I. Vargas-Baca, The Effect of Steric Hindrance on the Association of Telluradiazoles through Te−N Secondary Bonding Interactions, Cryst. Growth Des. 6 (2005) 181–186, https://doi.org/10.1021/cg050260y.
[15] A.F. Cozzolino, I. Vargas-Baca, The supramolecular chemistry of 1,2,5-chalcogenadiazoles, J. Organomet. Chem. 692 (2007) 2654–2657, https://doi.org/10.1016/j.jorganchem.2007.02.033.
[16] A.F. Cozzolino, A.D. Bain, S. Hanhan, I. Vargas-Baca, N-Triphenylboryl- and N, N'-bis(triphenylboryl)benzo-2,1,3-telluradiazole, Chem. Commun. (2009) 4043–4045, https://doi.org/10.1039/b904713a.
[17] A.F. Cozzolino, P.S. Whitfield, I. Vargas-Baca, Supramolecular Chromotropism of the Crystalline Phases of 4,5,6,7-Tetrafluorobenzo-2,1,3-telluradiazole, J. Am. Chem. Soc. 132 (2010) 17265–17270, https://doi.org/10.1021/ja107252f.
[18] Anthony F. Cozzolino, Qin Yang, Ignacio Vargas-Baca, Engineering Second-Order Nonlinear Optical Activity by Means of a Noncentrosymmetric Distortion of the [Te−N] 2 Supramolecular Synthon, Crystal Growth & Design 10 (11) (2010) 4959–4964, https://doi.org/10.1021/cg101060s.
[19] L.M. Lee, P.J.W. Elder, A.F. Cozzolino, Q. Yang, I. Vargas-Baca, An experimental and computational investigation of the formation and structures of N-hydro and N, N'-dihydro-benzo-2,1,3-chalcogenadiazolium chlorides, Main Group Chem. 9 (2010) 117–133, https://doi.org/10.3233/mgc-2010-0016.
[20] A.F. Cozzolino, I. Vargas-Baca, Parametrization of a Force Field for Te−N Secondary Bonding Interactions and Its Application in the Design of Supramolecular Structures Based on Heterocyclic Building Blocks, Cryst. Growth Des. 11 (2011) 668–677, https://doi.org/10.1021/cg100951y.
[21] A.F. Cozzolino, P.J.W. Elder, L.M. Lee, I. Vargas-Baca, The role of the Lewis acid−base properties in the supramolecular association of 1,2,5-chalcogenadiazoles, Can. J. Chem. 91 (2013) 338–347, https://doi.org/10.1139/cjc-2012-0323.
[22] L.M. Lee, V.B. Corless, M. Tran, H. Jenkins, J.F. Britten, I. Vargas-Baca, Synthetic, structural, and computational investigations of N-alkyl benzo-2,1,3-selenadiazolium iodides and their supramolecular aggregates, Dalton Trans. 45 (2016) 3285–3293, https://doi.org/10.1039/c5dt04314j.
[23] L.-J. Riwar, N. Trapp, K. Root, R. Zenobi, F. Diederich, Supramolecular Capsules: Strong versus Weak Chalcogen Bonding, Angew. Chem. Int. Ed. 57 (2018) 17259–17264, https://doi.org/10.1002/anie.201812095.
[24] M.R. Ams, N. Trapp, A. Schwab, J.V. Milić, F. Diederich, Chalcogen Bonding "2S–2N Squares" versus Competing Interactions: Exploring the Recognition Properties of Sulfur, Chem.-Eur. J. 25 (2018) 323–333, https://doi.org/10.1002/chem.201804261.
[25] T. Suzuki, T. Tsuji, T. Okubo, A. Okada, Y. Obana, T. Fukushima, T. Miyashi, Y. Yamashita, Preparation, Structure, and Amphoteric Redox Properties of p -Phenylenediamine-Type Dyes Fused with a Chalcogenadiazole Unit, J Org. Chem. 66 (2001) 8954–8960, https://doi.org/10.1021/jo010808h.
[26] A.C. Gomes, G. Biswas, A. Banerjee, W.L. Duax, Structure of a planar organic compound: 2,1,3-benzoselenadiazole (piaselenole), Acta Crystallogr, Sect. C: Cryst. Struct. Commun. C 45 (1989) 73–75, https://doi.org/10.1107/S0108270188008376.
[27] V. Luzzati, Structure cristalline de piasélénol, piazthiol et benzofurazane, Acta Crystallogr. 4 (1951) 193–200, https://doi.org/10.1107/s0365110x51000702.
[28] S. Langis-Barsetti, T. Maris, J.D. Wuest, Molecular Organization of 2,1,3-Benzothiadiazoles in the Solid State, J. Org. Chem. 82 (2017) 5034–5045, https://doi.org/10.1021/acs.joc.6b02778.
[29] Y. Lu, W. Li, W. Yang, Z. Zhu, Z. Xu, H. Liu, 2Ch–2N square and hexagon interactions: a combined crystallographic data analysis and computational study, Phys. Chem. Chem. Phys. 21 (2019) 21568–21576, https://doi.org/10.1039/c9cp04562g.
[30] D. Romito, N. Biot, F. Babudri, D. Bonifazi, Non-covalent bridging of bithiophenes through chalcogen bonding grips, New J. Chem. 44 (2020) 6732–6738, https://doi.org/10.1039/c9nj06202e.
[31] N. Biot, D. Bonifazi, Programming Recognition Arrays through Double Chalcogen-Bonding Interactions, Chem.-Eur. J. 24 (2018) 5439–5443, https://doi.org/10.1002/chem.201705428.
[32] P.C. Ho, R. Bui, A. Cevallos, S. Sequeira, J.F. Britten, I. Vargas-Baca, Macrocyclic complexes of Pt(II) and Rh(III) with iso-tellurazole N-oxides, Dalton Trans. 48 (2019) 4879–4886, https://doi.org/10.1039/c9dt00500e.
[33] J. Wang, P.C. Ho, J.F. Britten, V. Tomassetti, I. Vargas-Baca, Structural diversity of the complexes of monovalent metal d^{10} ions with macrocyclic aggregates of iso-tellurazole N-oxides, New J. Chem. 43 (2019) 12601–12608, https://doi.org/10.1039/c9nj02217a.
[34] P.C. Ho, H.A. Jenkins, J.F. Britten, I. Vargas-Baca, Building new discrete supramolecular assemblies through the interaction of iso-tellurazole N-oxides with Lewis acids and bases, Faraday Discuss. 203 (2017) 187–199, https://doi.org/10.1039/c7fd00075h.
[35] P.C. Ho, J. Rafique, J. Lee, L.M. Lee, H.A. Jenkins, J.F. Britten, A.L. Braga, I. Vargas-Baca, Synthesis and structural characterization of the aggregates of benzo-1,2-chalcogenazole 2-oxides, Dalton Trans. 46 (2017) 6570–6579, https://doi.org/10.1039/c7dt00612h.
[36] P.C. Ho, L.M. Lee, H. Jenkins, J.F. Britten, I. Vargas-Baca, Influence of acidic media on the supramolecular aggregation of iso-tellurazole N-oxides, Can. J. Chem. 94 (2016) 453–457, https://doi.org/10.1139/cjc-2015-0389.
[37] P.C. Ho, P. Szydlowski, J. Sinclair, P.J.W. Elder, J. Kübel, C. Gendy, L.M. Lee, H. Jenkins, J.F. Britten, D.R. Morim, I. Vargas-Baca, Supramolecular macrocycles reversibly assembled by Te−O chalcogen bonding, Nat. Commun. 7 (2016) 11299, https://doi.org/10.1038/ncomms11299.
[38] J. Kübel, P.J.W. Elder, H.A. Jenkins, I. Vargas-Baca, Structure and formation of the first (–O–Te–N–) 4 ring, Dalton Trans. 39 (2010) 11126–11128, https://doi.org/10.1039/c0dt01102a.
[39] A. Franconetti, D. Quiñonero, A. Frontera, G. Resnati, Unexpected chalcogen bonds in tetravalent sulfur compounds, Phys. Chem. Chem. Phys. 21 (2019) 11313–11319, https://doi.org/10.1039/c9cp01033e.
[40] M. Fourmigué, E.W. Reinheimer, K.R. Dunbar, P. Auban-Senzier, C. Pasquier, C. Coulon, A series of strongly one-dimensional organic metals with strictly uniform stacks: (o-DMTTF)$_2$ X (X = Cl, Br, I), Dalton Trans. (2008) 4652–4658, https://doi.org/10.1039/b805511d.
[41] O. Jeannin, E.W. Reinheimer, P. Foury-Leylekian, J.-P. Pouget, P. Auban-Senzier, E. Trzop, E. Collet, M. Fourmigué, Decoupling anion-ordering and spin-Peierls transitions in a strongly one-dimensional organic conductor with a chessboard structure, (o-Me$_2$TTF)$_2$NO$_3$, Iucrj. 5 (2018) 361–372, https://doi.org/10.1107/s2052252518004967.
[42] E.W. Reinheimer, D. Jankowski, R. Świetlik, M. Fourmigué, Hybrid Material Based on the Lindquist Polyoxometalate $[W_6O_{19}]^{2-}$ and the organosulfur donor o-Me$_2$TTF: A Combined Structural and Spectroscopic Study, J. Chem. Crystallogr. 43 (2013) 178–186, https://doi.org/10.1007/s10870-013-0403-4.
[43] E.W. Reinheimer, M. Fourmigué, K.R. Dunbar, Hydrogen Bonding and Sulfur-Sulfur Interactions in the Crystal Structure of the Radical-Cation Salt (BPDT-TTF)$_2$[W_6O_{19}], J. Chem. Crystallogr. 39 (2009) 723–729, https://doi.org/10.1007/s10870-009-9521-4.
[44] F. Camerel, G.L. Helloco, T. Guizouarn, O. Jeannin, M. Fourmigué, A. Frąckowiak, I. Olejniczak, R. Świetlik, A. Marino, E. Collet, L. Toupet, P. Auban-Senzier, E.

Canadell, Correlation between Metal-Insulator Transition and Hydrogen-Bonding Network in the Organic Metal δ-(BEDT-TTF)$_4$[2,6-Anthracene-bis(sulfonate)]·(H_2O)$_4$, Cryst. Growth Des. 13 (2013) 5135–5145, https://doi.org/10.1021/cg401416h.

[45] P. Cauliez, C. Mézière, P. Auban-Senzier, R. Clérac, M. Fourmigué, Square-lattice hybrid organic–inorganic conducting layers in the τ phase of a TTF tertiary amide derivative, New J. Chem. 32 (2008) 1561–1566, https://doi.org/10.1039/b801464g.

[46] M. Fourmigué, P. Auban-Senzier, Anionic Layered Networks Reconstructed from $[Cd(SCN)_3]^-_\infty$ Chains in Pseudo One-Dimensional Conducting Salts of Halogenated Tetrathiafulvalenes, Inorg. Chem. 47 (2008) 9979–9986, https://doi.org/10.1021/ic801207v.

[47] K.-S. Shin, O. Jeannin, M. Brezgunova, S. Dahaoui, E. Aubert, E. Espinosa, P. Auban-Senzier, R. Świetlik, A. Frąckowiak, M. Fourmigué, Inter-layer charge disproportionation in the dual-layer organic metal (tTTF-I)$_2ClO_4$ with unsymmetrical I···O halogen bond interactions, Dalton Trans. 43 (2013) 5280–5291, https://doi.org/10.1039/c3dt52801d.

[48] J. Lieffrig, O. Jeannin, K.-S. Shin, P. Auban-Senzier, M. Fourmigué, Halogen Bonding Interactions in DDQ Charge Transfer Salts with Iodinated TTFs, Crystals 2 (2012) 327–337, https://doi.org/10.3390/cryst2020327.

[49] M. Brezgunova, K.-S. Shin, P. Auban-Senzier, O. Jeannin, M. Fourmigué, Combining halogen bonding and chirality in a two-dimensional organic metal (EDT-TTF-I$_2$)$_2$(D -camphorsulfonate)·H_2O, Chem. Commun. 46 (2010) 3926–3928, https://doi.org/10.1039/c0cc00175a.

[50] J. Lieffrig, O. Jeannin, T. Guizouarn, P. Auban-Senzier, M. Fourmigué, Competition between the C-H···N Hydrogen Bond and C–I···N Halogen Bond in $TCNQF_n$ (n = 0, 2, 4) Salts with Variable Charge Transfer, Cryst. Growth Des. 12 (2012) 4248–4257, https://doi.org/10.1021/cg3007519.

[51] E.A. Chulanova, E.A. Pritchina, L.A. Malaspina, S. Grabowsky, F. Mostaghimi, J. Beckmann, I.Yu. Bagryanskaya, M.V. Shakhova, L.S. Konstantinova, O.A. Rakitin, N.P. Gritsan, A.V. Zibarev, New Charge-Transfer Complexes with 1,2,5-Thiadiazoles as Both Electron Acceptors and Donors Featuring an Unprecedented Addition Reaction, Chem.-Eur. J. 23 (2017) 852–864, https://doi.org/10.1002/chem.201604121.

[52] J.C. Dias, X. Ribas, J. Morgado, J. Seiça, E.B. Lopes, I.C. Santos, R.T. Henriques, M. Almeida, K. Wurst, P. Foury-Leylekian, E. Canadell, J. Vidal-Gancedo, J. Veciana, C. Rovira, Multistability in a family of DT–TTF organic radical based compounds (DT–TTF)$_4$[M(L)$_2$]$_3$ (M = Au, Cu; L = pds, pdt, bdt), J. Mater. Chem. 15 (2005) 3187–3199, https://doi.org/10.1039/b505724h.

[53] R.A.L. Silva, I.C. Santos, E.B. Lopes, S. Rabaça, J. Vidal-Gancedo, C. Rovira, M. Almeida, D. Belo, DT-TTF Salts with [Cu(dcdmp)$_2$]$^-$: The Richness of Different Stoichiometries, Cryst. Growth Des. 16 (2016) 3924–3931, https://doi.org/10.1021/acs.cgd.6b00484.

[54] C. Rovira, J. Veciana, E. Ribera, J. Tarrés, E. Canadell, R. Rousseau, M. Mas, E. Molins, M. Almeida, R.T. Henriques, J. Morgado, J.-P. Schoeffel, J.-P. Pouget, An Organic Spin-Ladder Molecular Material, Angew. Chem., Int. Ed. 36 (1997) 2324–2326, https://doi.org/10.1002/anie.199723241.

[55] E. Ribera, C. Rovira, J. Veciana, J. Tarrés, E. Canadell, R. Rousseau, E. Molins, M. Mas, J.-P. Schoeffel, J.-P. Pouget, J. Morgado, R.T. Henriques, M. Almeida, The [(DT-TTF)$_2$M(mnt)$_2$] Family of Radical Ion Salts: From a Spin Ladder to Delocalised Conduction Electrons That Interact with Localised Magnetic Moments, Chem.-Eur. J. 5 (1999) 2025–2039, https://doi.org/10.1002/(sici)1521-3765(19990702)5:7<2025::aid-chem2025>3.0.co;2-f.

[56] G.D. McManus, J.M. Rawson, N. Feeder, J. van Duijn, E.J.L. McInnes, J.J. Novoa, R. Burriel, F. Palacio, P. Oliete, Synthesis, crystal structures, electronic structure and magnetic behaviour of the trithiatriazapentalenyl radical, $C_2S_3N_3$, J. Mater. Chem. 11 (2001) 1992–2003, https://doi.org/10.1039/b103303b.

[57] W. Fujita, K. Awaga, Room-Temperature Magnetic Bistability in Organic Radical Crystals, Science 286 (1999) 261–262, https://doi.org/10.1126/science.286.5438.261.

[58] J.L. Brusso, O.P. Clements, R.C. Haddon, M.E. Itkis, A.A. Leitch, R.T. Oakley, R.W. Reed, J.F. Richardson, Bistabilities in 1,3,2-Dithiazolyl Radicals, J. Am. Chem. Soc. 126 (2004) 8256–8265, https://doi.org/10.1021/ja048618m.

[59] J.L. Brusso, O.P. Clements, R.C. Haddon, M.E. Itkis, A.A. Leitch, R.T. Oakley, R.W. Reed, J.F. Richardson, Bistability and the Phase Transition in 1,3,2-Dithiazolo[4,5-*b*]pyrazin-2-yl, J. Am. Chem. Soc. 126 (2004) 14692–14693, https://doi.org/10.1021/ja044979q.

[60] W. Fujita, K. Kikuchi, Study of Crystal Structure and Magnetic Properties of a 1,3,2-Dithiazolyl Radical Crystal, BBDTA·Cl, Eur. J. Inorg. Chem. 2013 (2014) 93–100, https://doi.org/10.1002/ejic.201300811.

[61] A.W. Cordes, C.M. Chamchoumis, R.G. Hicks, R.T. Oakley, K.M. Young, R.C. Haddon, Mono- and difunctional furan-based 1,2,3,5-dithiadiazolyl radicals; preparation and solid state structures of 2,5-[(S_2N_2C)OC_4H_2(CN_2S_2)] and 2,5-[(S_2N_2C)OC_4H_2(CN)], Can. J. Chem. 70 (1992) 919–925, https://doi.org/10.1139/v92-123.

[62] A.I. Taponen, J.W.L. Wong, K. Lekin, A. Assoud, C.M. Robertson, M. Lahtinen, R. Clérac, H.M. Tuononen, A. Mailman, R.T. Oakley, Non-Innocent Base Properties of 3- and 4-Pyridyl-dithia- and Diselenadiazolyl Radicals: The Effect of N -Methylation, Inorg. Chem. 57 (2018) 13901–13911, https://doi.org/10.1021/acs.inorgchem.8b02416.

[63] J.F. Britten, O.P. Clements, A.W. Cordes, R.C. Haddon, R.T. Oakley, J.F. Richardson, Stacking Efficiency of Diselenadiazolyl π-Dimers. Consequences for Electronic Structure and Transport Properties, Inorg. Chem. 40 (2001) 6820–6824, https://doi.org/10.1021/ic010678v.

[64] A.W. Cordes, R.C. Haddon, R.G. Hicks, R.T. Oakley, T.T.M. Palstra, Preparation and solid-state structures of (cyanophenyl)dithia- and (cyanophenyl) diselenadiazolyl radicals, Inorg. Chem. 31 (1992) 1802–1808, https://doi.org/10.1021/ic00036a016.

[65] C.P. Constantinides, E. Carter, D. Eisler, Y. Beldjoudi, D.M. Murphy, J.M. Rawson, Effects of Halo-Substitution on 2'-Chloro-5'-halo-phenyl-1,2,3,5-dithiadiazolyl Radicals: A Crystallographic, Magnetic, and Electron Paramagnetic Resonance Case Study, Cryst. Growth Des. 17 (2017) 3017–3029, https://doi.org/10.1021/acs.cgd.6b01700.

[66] Y. Beldjoudi, I. Osorio-Román, M.A. Nascimento, J.M. Rawson, A fluorescent dithiadiazolyl radical: structure and optical properties of phenanthrenyl dithiadiazolyl in solution and polymer composites, J. Mater. Chem. C 5 (2017) 2794–2799, https://doi.org/10.1039/c6tc05576a.

[67] Y. Beldjoudi, M.A. Nascimento, Y.J. Cho, H. Yu, H. Aziz, D. Tonouchi, K. Eguchi, M.M. Matsushita, K. Awaga, I. Osorio-Roman, C.P. Constantinides, J.M. Rawson, Multifunctional Dithiadiazolyl Radicals: Fluorescence, Electroluminescence, and Photoconducting Behavior in Pyren-1'-yl-dithiadiazolyl, J. Am. Chem. Soc. 140 (2018) 6260–6270, https://doi.org/10.1021/jacs.7b12592.

[68] Y. Beldjoudi, A. Arauzo, J. Campo, E.L. Gavey, M. Pilkington, M.A. Nascimento, J. M. Rawson, Structural, Magnetic, and Optical Studies of the Polymorphic 9'-Anthracenyl Dithiadiazolyl Radical, J. Am. Chem. Soc. 141 (2019) 6875–6889, https://doi.org/10.1021/jacs.8b11528.

[69] C.D. Bryan, A.W. Cordes, R.C. Haddon, R.G. Hicks, D.K. Kennepohl, C.D. MacKinnon, R.T. Oakley, T.T.M. Palstra, A.S. Perel, Molecular conductors from neutral-radical charge-transfer salts: preparation and characterization of an I doped hexagonal phase of 1,2,3,5-dithiadiazolyl ([HCN_2S_2]$^•$), J. Am. Chem. Soc. 116 (1994) 1205–1210, https://doi.org/10.1021/ja00083a005.

[70] A. Mailman, S.M. Winter, X. Yu, C.M. Robertson, W. Yong, J.S. Tse, R.A. Secco, Z. Liu, P.A. Dube, J.A.K. Howard, R.T. Oakley, Crossing the insulator-to-metal barrier with a thiazyl radical conductor, J. Am. Chem. Soc. 134 (2012) 9886–9889, https://doi.org/10.1021/ja303169y.

[71] D. Tian, S.M. Winter, A. Mailman, J.W.L. Wong, W. Yong, H. Yamaguchi, Y. Jia, J. S. Tse, S. Desgreniers, R.A. Secco, S.R. Julian, C. Jin, M. Mito, Y. Ohishi, R.T. Oakley, The Metallic State in Neutral Radical Conductors: Dimensionality, Pressure and Multiple Orbital Effects, J. Am. Chem. Soc. 137 (2015) 14136–14148, https://doi.org/10.1021/jacs.5b08254.

[72] K. Lekin, A.A. Leitch, A. Assoud, W. Yong, J. Desmarais, J.S. Tse, S. Desgreniers, R. A. Secco, R.T. Oakley, Benzoquinone-Bridged Heterocyclic Zwitterions as Building Blocks for Molecular Semiconductors and Metals, Inorg. Chem. 57 (2018) 4757–4770, https://doi.org/10.1021/acs.inorgchem.8b00485.

[73] N.A. Pushkarevsky, E.A. Chulanova, L.A. Shundrin, A.I. Smolentsev, G.E. Salnikov, E.A. Pritchina, A.M. Genaev, I.G. Irtegova, I.Yu. Bagryanskaya, S.N. Konchenko, N.P. Gritsan, J. Beckmann, A.V. Zibarev, Radical Anions, Radical-Anion Salts, and Anionic Complexes of 2,1,3-Benzochalcogenadiazoles, Chem.-Eur. J. 25 (2019) 806–816, https://doi.org/10.1002/chem.201803465.

[74] A.A. Dmitriev, N. Pushkarevsky, A.I. Smolentsev, I. Vargas-Baca, N.P. Gritsan, J. Beckmann, A.V. Zibarev, Bis(2,1,3-Benzotelluradiazolidyl) 2,1,3-Benzotelluradiazole: a Pair of Radical Anions Coupled by Te···N Chalcogen Bonding, Chem. Commun. 56 (2020) 1113–1116, https://doi.org/10.1039/c9cc08110k.

[75] L.M. Lee, P.J.W. Elder, P.A. Dube, J.E. Greedan, H.A. Jenkins, J.F. Britten, I. Vargas-Baca, The size of the metal ion controls the structures of the coordination polymers of benzo-2,1,3-selenadiazole, CrystEngComm 15 (2013) 7434–7437, https://doi.org/10.1039/c3ce40752g.

[76] K.E. Preuss, Metal-radical coordination complexes of thiazyl and selenazyl ligands, Coord. Chem. Rev. 289 (2015) 49–61, https://doi.org/10.1016/j.ccr.2014.09.016.

[77] N.G.R. Hearns, R. Clérac, M. Jennings, K.E. Preuss, Manipulating the crystal packing of pyDTDA radical ligand coordination complexes with Mn(II) and Ni (II), Dalton Trans. (2009) 3193–3203, https://doi.org/10.1039/b817214e.

[78] J. Britten, N.G.R. Hearns, K.E. Preuss, J.F. Richardson, S. Bin-Salamon, Mn(II) and Cu(II) Complexes of a Dithiadiazolyl Radical Ligand: Monomer/Dimer Equilibria in Solution, Inorg. Chem. 46 (2007) 3934–3945, https://doi.org/10.1021/ic0619456.

[79] T. Chivers, I. Krouse, M. Parvez, I. Vargas-Baca, T. Ziegler, P. Zoricak, Intramolecular Chalcogen−Nitrogen Interactions: Molecular and Electronic Structures of Geometrical Isomers of the Diazenes RSN=C(R')N=NC(R')=NSR, Inorg. Chem. 35 (1996) 5836–5842, https://doi.org/10.1021/ic960465j.

[80] T. Chivers, B. McGarvey, M. Parvez, I. Vargas-Baca, T. Ziegler, Experimental and Theoretical Investigations of the Formation of the Diazene PhSN=C(H)N=NC(H)=NSPh from $HCN_2(SPh)_3$ by a Thiyl-Radical-Catalyzed Mechanism: Identification of the HC(NSPh)$_2$·Radical and X-ray Structures of $HCN_2(SPh)_3$ and PhSN=C(H)N=NC(H)=NSPh, Inorg. Chem. 35 (1996) 3839–3847, https://doi.org/10.1021/ic960317t.

[81] V. Chandrasekhar, T. Chivers, J.F. Fait, S.S. Kumaravel, Synthesis and structure of azo dyes with short, intramolecular selenium-nitrogen contacts, J. Am. Chem. Soc. 112 (1990) 5373–5374, https://doi.org/10.1021/ja00169a068.

[82] S. Yi, Z. Zhu, X. Cai, Y. Jia, J.-H. Cho, The Nature of Bonding in Bulk Tellurium Composed of One-Dimensional Helical Chains, Inorg. Chem. 57 (2018) 5083–5088, https://doi.org/10.1021/acs.inorgchem.7b03244.

[83] C.E.M. Campos, K. Ersching, J.C. de Lima, T.A. Grandi, H. Höhn, P.S. Pizani, Influence of minor oxidation of the precursor powders to form nanocrystalline CdTe by mechanical alloying, J. Alloys Compd. 466 (2008) 80–86, https://doi.org/10.1016/j.jallcom.2007.11.016.

Chapter 2. Influence of acidic media on the supramolecular aggregation of iso-tellurazole *N*-oxides

Original citation: Ho, P. C.; Lee, L. M.; Jenkins, H.; Britten, J. F.; Vargas-Baca, I. Influence of Acidic Media on the Supramolecular Aggregation of Iso-Tellurazole N -Oxides. *Can. J. Chem.* **2016**, *94*, 453–457.

This scholarly work is reprinted with permission.

2.1 Preamble

The array of properties unveiled in our initial investigations of the aggregates of the iso-tellurazole *N*-oxides **1a** and **1b** strongly suggested that these would be very useful as supramolecular building blocks.[18] In addition to the strength and reversibility of their Te···O ChBs, these compounds are stable in air and moisture. In fact, their synthesis includes and aqueous work up to neutralize H_2SO_4, generated as a by-product of hydrolysis of the last intermediate (Scheme 2.1).

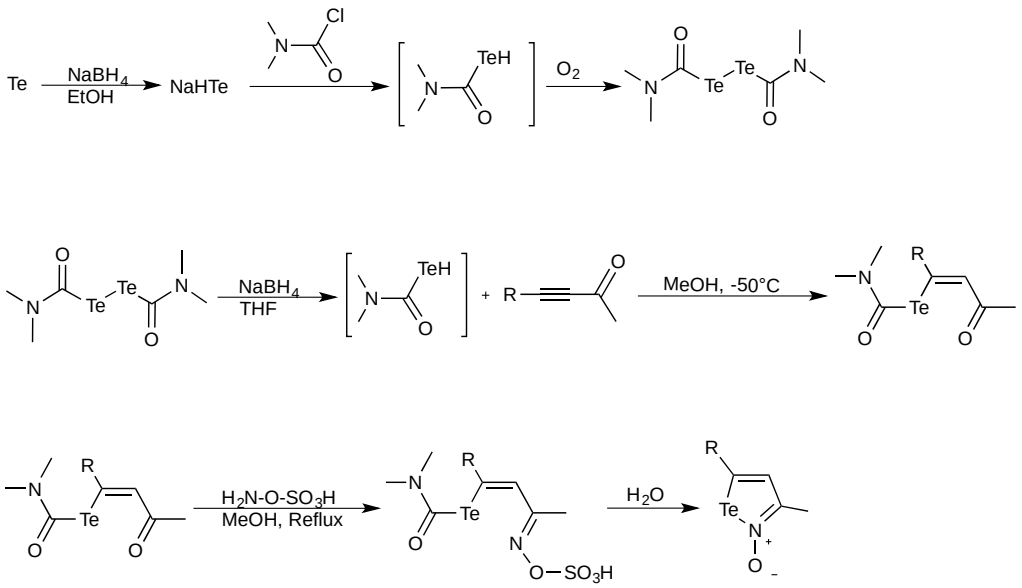

Scheme 2.1. Synthesis of iso-tellurazole *N*-oxides **1a** (R = ^{t}Bu) and **1b** (R = Ph). Reproduced with permission from reference 18.

It was also possible to isolate the protonated forms of the iso-tellurazole *N*-oxides (**1a,b**HCl) when the neutralization was incomplete. Therefore, it became of interest to investigate in detail the acid-base properties of these compounds; the results are presented in this chapter. We found that the self-assembly of **1a**,**b** is disrupted by protonation of the oxygen. The process is reversible, which provides a mean to selectively switch on and off the self-assembly process. The basicity of the oxygen atom has important implications for the coordination chemistry of these compounds with transition metal ions. Being a soft metal ion, Pd(II) does prefer binding the tellurium atoms in the macrocyclic tetramers,[18] but harder metal ions would possible bind instead the oxygen atom and dissociate the Te···O ChBs.

NRC Research Press

ARTICLE

Influence of acidic media on the supramolecular aggregation of iso-tellurazole *N*-oxides

Peter C. Ho, Lucia Myongwon Lee, Hilary Jenkins, James F. Britten, and Ignacio Vargas-Baca

Abstract: Iso-tellurazole *N*-oxides are promising supramolecular building blocks. While in neutral solutions, they form tetra- and hexameric macrocyclic aggregates linked by Te···O secondary bonding (σ hole interactions or *chalcogen bonds*), protonation of the oxygen atom in acidic media disrupts such supramolecular association. The process is reversible and, consequently, can be used to switch on and off the self-assembly process. Hammett acidity measurements gave pK_a values of –3.2 for the protonated molecules. Adducts with HCl and HBr were isolated and structurally characterized. Protonation in solution led to the crystallization of a new polymorph of 3-methyl-5-phenyl-1,2-tellurazole *N*-oxide, which features a unique polymeric arrangement.

Key words: sigma-hole interactions, secondary bonding, chalcogens, supramolecular chemistry, main-group chemistry.

Résumé : Les isotellurazoles *N*-oxydes sont des synthons supramoléculaires prometteurs. Bien qu'en solution neutre, ils forment des agrégats macrocycliques tétramériques et hexamériques retenus par des liaisons secondaires Te···O (interactions de trous σ ou liaisons chalcogène), en milieu acide, la protonation des atomes d'oxygène perturbe une association supramoléculaire de ce type. Ce processus d'association est réversible et peut donc être utilisé pour provoquer ou inhiber le processus d'autoassamblage. Nous avons calculé, pour les molécules protonées, une valeur de pK_a de –3,2 dérivée des mesures de l'acidité en utilisant l'équation de Hammett. En outre, nous avons isolé des adduits de HCl et de HBr et en avons caractérisé les structures. La protonation en solution a entraîné la cristallisation d'un nouveau polymorphe du 3-méthyl-5-phényl-1,2-tellurazole *N*-oxyde présentant une structure polymérique unique. [Traduit par la Rédaction]

Mots-clés : interactions de trous sigma, liaison secondaire, chalcogènes, chimie supramoléculaire, chimie du groupement principal.

Introduction

The remarkable success of halogen bonding[1–4] in areas as diverse as crystal engineering,[2,5–14] supramolecular catalysis,[15] anion recognition,[16] optical materials,[17] and biomimetic chemistry[18–20] has reinvigorated the study of the analogous supramolecular interactions that are centred on other p-block elements. These links ensue when a combination of electrostatic, covalent, and dispersion attractive interactions successfully counters the effect of Pauli's (steric) repulsion.

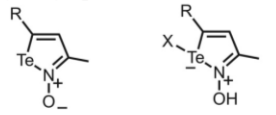

1 **X-1-H**

a R = Ph
b R = ^{t}Bu
X = a halogen

Such interactions often result in auto-association in the crystal structures of molecular compounds that contain heavy chalcogen atoms such as selenium and tellurium. Iso-tellurazole *N*-oxides (**1**) have shown a remarkable ability to form aggregates through Te···O interactions.[21,22] A helical polymer and cyclic tetra- and hexamers (Scheme 1) — respectively examples of the $[Te\text{-}1\text{-}O]_\infty$, $[Te\text{-}1\text{-}O]_4$, and $[Te\text{-}1\text{-}O]_6$ supramolecular synthons[23] — can be selectively obtained by modifying the crystallization conditions. NMR experiments have demonstrated that the cyclic oligomers are persistent in solution and exist in equilibrium. The tetramers act as macrocyclic ligands towards transition metal ions and form adducts with fullerenes, while the hexamer is capable of hosting small molecules in the solid state.[22] In addition to such unique properties, iso-tellurazole oxides are remarkably tolerant of water and oxygen and, therefore, hold great promise for widespread application as supramolecular building blocks.

However, it would be desirable to identify a method to switch on and off the auto-association of these molecules. Because the Te–O *chalcogen bonds* are to a great extent Lewis donor–acceptor interactions, the iso-tellurazole N-oxides are ambiphilic molecules and it may be possible to prevent their association by capping the donor (oxygen) and acceptor (tellurium) centres with acids and (or) bases, respectively.

In this report, we demonstrate that this approach indeed prevents the association of the molecules and can be switched reversibly. We also characterize the basicity of two isotellurazole *N*-oxides by means of the Hammett acidity function and show that the presence of acid in the medium impacts the supramolecular structures assembled in the solid state by the neutral molecules.

Experimental

Materials

The iso-tellurazole *N*-oxides **1a** and **1b** were prepared as described elsewhere.[22] Methanol (Caledon), dichloromethane (Caledon),

Received 7 August 2015. Accepted 22 November 2015.

P.C. Ho, L.M. Lee, H. Jenkins, J.F. Britten, and I. Vargas-Baca. Department of Chemistry and Chemical Biology, McMaster University, 1280 Main Street West, Hamilton, ON L8S 4M1, Canada.

Corresponding author: Ignacio Vargas-Baca (email: vargas@chemistry.mcmaster.ca).

This article is dedicated to celebrating the 50th Anniversary of the Department of Chemistry at the University of Calgary and to highlighting the chemical research being performed by faculty and alumni.

Can. J. Chem. **94**: 453–457 (2016) dx.doi.org/10.1139/cjc-2015-0389

Published at www.nrcresearchpress.com/cjc on 22 April 2016.

Scheme 1. Structurally characterized aggregates of **1a**.

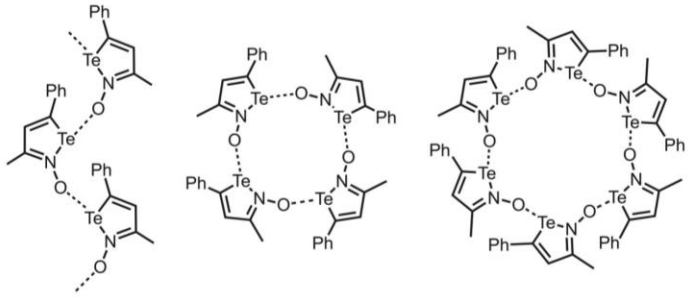

hydrochloric acid (Caledon), hydrobromic acid (Caledon), sulfuric acid (Caledon), trifluoroacetic acid (Aldrich), dichloromethane-d_2 (Aldrich), and methanol-d_4 were used as received. HF was generated in situ by the reaction of CaF_2 with sulfuric acid.

Nuclear magnetic resonance

All spectra were acquired in solution with a deuterated solvent. Spectra were obtained using Bruker AVANCE 500 MHz (Bruker 5-mm Broad Band Inverse probe) or Bruker AVANCE 600 MHz (Bruker 5-mm BROAD BAND OBSERVE probe) spectrometers at 287.5 K unless otherwise indicated. The ^{1}H, ^{13}C, and ^{125}Te spectra were processed using Bruker TopSpin 2.1 or 3.2 software packages. The ^{1}H and ^{13}C spectra were referenced to tetramethyl silane using the deuterated solvent signal as a secondary reference. The ^{125}Te chemical shifts are reported with respect to the room temperature resonance of $TeMe_2$ (δ = 0.00 ppm) but were measured using a secondary reference of diphenyl ditelluride in CD_2Cl_2 (δ = 420.36 ppm).

Ultraviolet-visible absorption spectroscopy

Solution spectra were measured in quartz cuvettes at room temperature in Varian Cary 50 spectrometers operating in dual-beam mode.

Electrospray ionization mass spectrometry

Mass spectra were obtained in positive ion mode on a Waters/Micromass Quattro Ultima Global ToF mass spectrometer operating in W Mode. Pure samples were dissolved and diluted in methanol or acetonitrile. Waters Global and Ultima (ES Q-TOF) mass spectrometers were used to obtain high-resolution mass spectra. (capillary = 4.00 kV, cone = 80 V, RF lens1 energy = 80 V, desolvation temperature = 200 °C, cone gas flow = 100 L/h, desolvation gas flow = 200 L/h, mass range = 50–2200 *m*/*z*, mass resolution = 6000).

Other instrumental methods

Melting points were determined with a Uni-Melt Thomas Hoover capillary melting point apparatus and are reported uncorrected. Infrared spectra were acquired in a Bruker Tensor 27 spectrometer with a MVP-Pro Single Reflection ATR microsampler using a hemispherical germanium crystal. Vibrational spectra were processed using OPUS version 4.2. Elemental analyses were performed by the Science Centre of London Metropolitan University, 29 Hornsey Road, London, UK N7 7DD.

X–1a–H (X = Cl, Br)

Compound **1a** (0.031 mmol) was suspended in methanol (0.5 mL). Concentrated HX was added dropwise until the solid dissolved completely. At that point, 5 mL of distilled water was added and the mixture was extracted with CH_2Cl_2. The organic layer was dehydrated with Na_2SO_4 and evaporated to dryness yielding a microcrystalline sample of X–**1a**–H. E.A. Calcd. for $C_{10}H_{10}ClNOTe$: C 37.16%, H 3.12%, N 4.33%; found: C 37.02%, H 3.15%, N 4.29%.

Cl–1a–H

Yield 97%, melting point 155 °C (d). ^{1}H NMR (600 MHz, CD_3OD, δ ppm): 7.36–7.28 (m, 5H), 7.10 (s, 1H), 2.66 (s, 3H). ^{13}C NMR (600 MHz, CD_3OD, δ ppm): 159.97 (s, 1C), 159.26 (s, 1C), 141.03 (s, 1C), 130.74 (s, 2C), 129.27 (s, 1C), 128.56 (s, 2C), 127.59 (s, 1C), 15.39 (s, 1C). IR (ATR, $\tilde{\nu}$): 3080, 1618, 1557, 1519, 1483, 1442, 1402, 1342, 1218, 1104, 1030, 867, 836, 822, 755, 695, 617. HR-ESMS (*m*/*z*): 289.9825, calcd. for $C_{10}H_{10}NOTe$: 289.7961.

Br–1a–H

Yield 92%, melting point 164 °C (d). ^{1}H NMR (600 MHz, CD_3OD, δ ppm): 7.36–7.28 (m, 5H), 7.04 (s, 1H), 2.25 (s, 3H). ^{13}C NMR (600 MHz, CD_3OD, δ ppm): 161.10 (s, 1C), 156.27 (s, 1C), 141.72 (s, 1C), 130.83 (s, 2C), 129.23 (s, 1C), 128.51 (s, 2C), 127.56 (s, 1C), 15.37 (s, 1C). IR (ATR, $\tilde{\nu}$): 3142, 1589, 1519, 1481, 1441, 1402, 1342, 1222, 1104, 1085, 1030, 867, 836, 821, 753, 694, 615. HR-ESMS (*m*/*z*): 289.9825, calcd. for $C_{10}H_{10}NOTe$ 289.7961. Calcd. for $C_{10}H_{10}BrNOTe$: C 32.66%, H 2.74%, N 3.81%; found: C 32.50%, H 2.61%, N 3.76%.

pK_a evaluation

The pK_a values of the protonated iso-tellurazole *N*-oxides, **1a**–H$^+$ and **1b**–H$^+$, were determined following literature spectrophotometric methods.[24,25] Given the markedly different solubilities of the free bases and their conjugate acids, the equilibria protonation could only be monitored in CH_2Cl_2–ethanol (1:1) mixtures. In the absence of published data, the Hammett acidity function for H_2SO_4 solutions in the mixtures was measured with diphenylamine (pK_a(Ph_2NH^+) = 0.78) as the reference base.

Single-crystal X-ray diffraction

All crystals were mounted on a MiTeGen micromounts with Paratone-N oil. Nylon loops (Hampton, California) or MiTeGen micromounts (Ithica, New York) and Paratone-N oil were used to mount the crystals. Data were collected at 100 K with Mo-Kα radiation (λ = 0.71073 Å) with a Bruker APEX2 diffractometer. A CCD area detector equipped with a low-temperature accessory Oxford cryostream was used. A minimum of 50 frames from three different orientations were used for the determination of the precursory unit cell parameters and final cell advancement after integration in SAINT.[26] The absorption was corrected for each data set in SADABS.[27] Direct methods were used to solve all structures[28] and then refined by the full-matrix least-squares techniques on F^2 using SHELXL.[29] All nonhydrogen atoms were assigned anisotropic thermal parameters. Appropriate riding models were used to place hydrogen atoms in idealized positions.

Results and discussion

Isotellurazole *N*-oxides are prepared by a method (Scheme 2) that includes the *trans* addition of an in situ generated tellurocarbamic acid to an ynone. The resulting enone undergoes condensation with hydroxylamine-*O*-sulfonic acid to introduce the nitrogen atom and the heterocycle is closed by hydrolysis of the

Scheme 2. Sequence of reactions used for the syntheses of **1a** (R = Ph) and **1b** (R = ^{t}Bu).

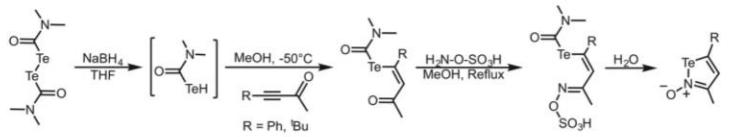

Table 1. Crystallographic data.

Crystal	Cl–**1a**–H	Br–**1a**–H	**1a**$_\infty$
Empirical formula	$C_{10}H_{10}ClNOTe$	$C_{10}H_{10}BrNOTe$	$C_{10}H_9NOTe$
Formula mass	323.24	367.70	286.78
Colour, habit	Yellow, needle	Yellow, needle	Yellow, plate
Crystal dimensions (mm)	0.400×0.360×0.360	0.346×0.224×0.123	0.052×0.158×0.324
Crystal system	Monoclinic	Monoclinic	Orthorhombic
Space group	$P2_1/n$	$P2_1/n$	$Pna21$
Z	8	8	4
a (Å)	11.1348(7)	11.2501(4)	11.6434(5)
b (Å)	10.4989(7)	10.6368(4)	9.7062(4)
c (Å)	18.7386(12)	18.8387(6)	8.5386(3)
α (°)	90	90	90
β (°)	91.1499(10)	91.642(2)	90
γ (°)	90	90	90
Collection ranges	$-14 \le h \le 14$, $-13 \le k \le 13$, $-24 \le l \le 24$	$-17 \le h \le 17$, $-16 \le k \le 16$, $-28 \le l \le 28$	$-19 \le h \le 16$, $-12 \le k \le 16$, $-13 \le l \le 14$
Temperature (K)	100(2)	100(2)	100(2)
Volume (Å^3)	2190.2(2)	2253.41(14)	964.97(7)
D_{calcd} (g cm^{-3})	1.961	2.168	1.974
Radiation type/wavelength (nm)	Mo Kα (λ = 0.71073 Å)	Mo Kα (λ = 0.71073 Å)	Mo Kα (λ = 0.71073 Å)
Absorption coefficient (μ) (mm^{-1})	2.926	6.154	3.040
Absorption correction	Numerical	Numerical	Numerical
F(000)	1232	1376	544
θ range for data collection (°)	2.109–27.494	2.083–33.166	2.73–36.34
Observed reflections	44761	84623	16934
Independent reflections	5028	8609	4597
Data/restraints/parameters	5028/0/259	8609/0/261	4597/1/118
Maximum shift/error	0.002	0.003	0.000
Goodness-of-fit on F^2	1.146	1.010	1.012
Final R indices ($I > 2\sigma(I)$)	$R_1 = 0.0171$, $wR_2 = 0.0394$	$R_1 = 0.0177$, $wR_2 = 0.0377$	$R_1 = 0.0212$, $wR_2 = 0.0431$
R indices (all data)	$R_1 = 0.0178$, $wR_2 = 0.0397$	$R_1 = 0.0227$, $wR_2 = 0.0391$	$R_1 = 0.0242$, $wR_2 = 0.0441$
Absolute structure parameter	na	na	0.0(0)
Extinction coefficient	na	na	na
Largest difference peak and hole (Å^{-3})	0.521, –0.464	0.912, –0.566	0.847, –0.523

Table 2. Selected bond distances and angles.

Crystal	Cl–**1a**–H	Br–**1a**–H	**1a**$_\infty$
Bond distances (Å)			
Te–N	2.173(2), 2.177(2)	2.183(1), 2.185(1)	2.196(2)
N–C3	1.301(3), 1.301(3)	1.299(2), 1.300(2)	1.310(3)
N–O	1.374(2), 1.383(2)	1.381(2), 1.383(2)	1.355(3)
C1–C2	1.356(3), 1.361(3)	1.352(2), 1.360(2)	1.360(4)
C2–C3	1.433(3), 1.436(3)	1.430(2), 1.434(2)	1.432(5)
C1–Te	2.097(2), 2.101(2)	2.100(2), 2.101(1)	2.097(2)
Te–X	2.6816(5), 2.6605(5)	2.7911(2), 2.8125(2)	
Bond angles (°)			
C1–Te–N	76.32(7), 76.46(7)	76.12(5), 76.29(5)	76.74(9)
Te–N–O	127.3(1), 127.8(1)	126.96(9), 127.6(1)	124.9(2)
N–C3–C2	113.4(2), 113.4(2)	113.5(1), 113.6(1)	114.3(2)
C1–C2–C3	120.5(2), 120.7(2)	120.7(1), 120.8(1)	120.7(2)
C2–C1–Te	112.8(1), 113.3(1)	112.9(1), 113.3(1)	113.1(2)

intermediate product. The process yields DMF and sulfuric acid as by-products that are separated in an aqueous workup. In attempts to improve the preparation method for **1a**, the use of brine instead of pure water led to the growth of a new crystalline material from the organic layer. Spectroscopic and structural characterization

Fig. 1. ORTEP detail of the crystal structure of Br–**1a**–H. Displacement ellipsoids are shown at 75% probability.

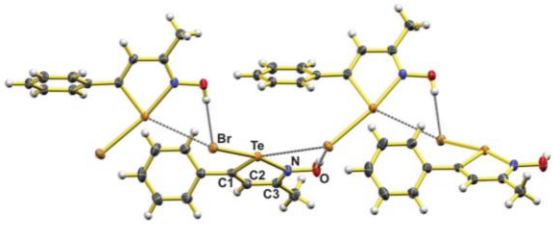

showed that these crystals consist of Cl–**1a**–H. It is remarkable that the C_3NTe heterocycle can tolerate conditions that would easily hydrolyze the Te–N bond of other compounds. For example, 2,1,3-benzotelluradiazoles are easily hydrolyzed and their HCl adducts are even more sensitive to moisture.[30]

Further investigation demonstrated that Cl–**1a**–H can be prepared by treatment of **1a** with hydrochloric acid. Br–**1a**–H was obtained by an entirely analogous procedure using hydrobromic acid. Similarly, hydroiodic acid yielded a microcrystalline product

but this was too unstable for proper characterization; the product would turn yellow–brown on standing, presumably by formation of I_2 and (or) I_3^-. Attempts to obtain an HF adduct failed, resulting in the isolation of starting material only.

X-ray diffraction confirmed the identity of the HCl and HBr adducts of **1a**. Selected crystallographic information is provided in Table 1 and relevant bond distances and angles are presented in Table 2. The two crystals are isostructural; their asymmetric units consist of two independent molecules and thus their internal dimensions are duplicated in Table 2. There are no intermolecular Te···O interactions; instead, the oxygen atoms are protonated (Fig. 1). All bond lengths and angles within the tellurazole heterocycles fall within the ranges previously measured in the crystal structures of the aggregates of **1a** and **1b**; only the exocyclic N–O bonds are slightly longer in X–**1a**–H. The halides are located opposite to the Te–N bond. It is noteworthy to compare the Te–X distances to those observed in sterically protected aryl tellurenyl halides, 2.7048(6) for the bromide[31] and 2.384(1) Å for the chloride.[32] In X–**1a**–H, the Te–Br distances are slightly longer but the Te–Cl distances are much larger and fall at the long end of the range observed in cases in which the tellurium atom is engaged in intramolecular secondary bonding.[26–29,33–36] Each X–**1a**–H molecule is connected to a neighbor by hydrogen bonding to the halogen atom, which in turn is engaged in an interaction with the tellurium atom of the first molecule to a distance (d(Te···Cl) = 3.570, 3.656 Å, d(Te···Br) = 3.602, 3.693 Å) that is shorter than the Te-X sum of van der Waals radii (X = Cl: 3.81 Å, X = Br: 3.91 Å) but much longer than the corresponding single bond. These interactions propagate through the crystal forming infinite chains.

The ^{1}H NMR spectra of X–**1a**–H in MeOD or CD_2Cl_2 solutions feature resonances at higher frequencies than those of **1a**. Treatment of the CD_2Cl_2 solution with DCl–D_2O showed that the position of the resonances of Cl–**1a**–H is sensitive to the addition of an excess of acid. This observation suggests that the HX adducts are partly dissociated and in equilibrium in solution. Likely for this reason, it was not possible to locate the ^{125}Te NMR resonance in simple solutions of X–**1a**–H. However, the ^{125}Te resonance was observed at 1768 ppm when an excess of CF_3CO_2D was added to a solution of **1a** in CD_2Cl_2 (cf. 1595 ppm in the absence of acid). Further confirmation of the reversibility of protonation was obtained by treating X–**1a**–H with bases such as sodium hydroxide or sodium carbonate, which quantitatively regenerated free **1a** in solution. The dissociation constants of the conjugate acids (**1a**–H$^+$ and **1b**–H$^+$) were then evaluated in CH_2Cl_2–EtOH–H_2SO_4 mixtures by monitoring the dependency of the degree of protonation on the Hammett acidity function (eq. 1; Fig. 2). For simplicity, this analysis neglected the aggregation equilibria that **1a** and **1b** undergo in solution. Nevertheless, the pK_a values for the two compounds were consistently –3.2332, which place these iso-tellurazole *N*-oxides close to dialkyl ethers in the basicity scale:

$$(1) \qquad H_0 = pK_a(BH^+) + \log(|BH^+|/|B|)$$

The protonation of iso-tellurazole oxides could also be used to introduce these compounds into polar liquids. For example, **1a** is practically insoluble in methanol but readily dissolves upon addition of a small amount of trifluoroacetic acid. Interestingly, slow evaporation of such solution crystallized the pure iso-tellurazole *N*-oxide in a new polymorph with a unique structure. Relevant crystallographic information and molecular dimensions are provided in Tables 1 and 2, respectively. In this lattice (Fig. 3), the molecules of **1a** form an infinite polymer along the 001 two-fold screw axis. The arrangement features, therefore, two orientations of the tellurazole heterocycles with interplanar angles of 61.6°. This is in contrast with the previously identified[22] polymeric phase in which the **1a** molecules assemble a spiral polymer with three molecular units per turn. All bond distances and angles in

Fig. 2. Hammett acidity plots for **1a** (open circles) and **1b** (solid circles) in CH_2Cl_2–EtOH–H_2SO_4 mixtures. The ratios of protonated and free base were determined by measurement of absorbance at 390 and 370 nm for **1a** and **1b**, respectively.

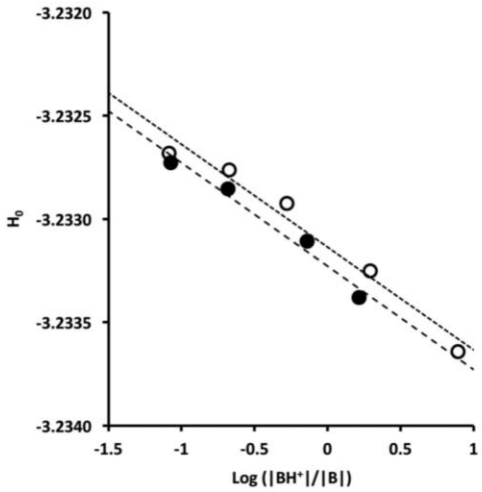

Fig. 3. ORTEP detail of the crystal structure of the **1a** polymorph obtained from CF_3CO_2H–CH_3OH mixtures. The short distance between tellurium and a C–C bond in the phenyl group of a neighboring molecule is shown with a broken line. The displacement ellipsoids are shown at 75% probability.

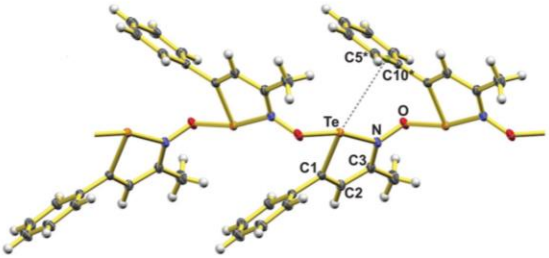

the new structure are consistent with the values observed in all other polymorphs of **1a**. However, one unique feature of this structure is an apparent interaction between tellurium and the phenyl ring of an adjacent molecule. The distance between the chalcogen and the centroid of the C5–C10 bond is just 3.592 Å (cf. the sum of van der Waals radii 3.76). Short contacts between tellurium and aromatic rings have been identified in other organotellurium compounds.[37]

Outlook

The ability of iso-tellurazole oxides to reversibly undergo protonation increases their appeal as supramolecular building blocks because it confirms that they are very robust molecules. In addition, it provides a means to selectively switch on and off their auto-association. This property also has implications for the coordination chemistry of these molecules and their aggregates. Tellurium-bonded macrocyclic complexes of the tetramer have been obtained with soft ions such as Pd(II)[22] but harder ions are likely to prefer coordination by the oxygen atom; current investigations are intended to locate the boundary between these extremes.

Published by NRC Research Press

Supplementary material

Supplementary material is available with the article through the journal Web site at http://nrcresearchpress.com/doi/suppl/10.1139/cjc-2015-0389. The X-ray crystallographic coordinates for all structures reported in this article have been deposited at the Cambridge Crystallographic Data Centre under deposition Nos. CCDC 1415156, 1415157, and 1417405. These data can be obtained free of charge from The Cambridge Crystallographic Data Centre (www.ccdc.cam.ac.uk/data_request/cif).

Acknowledgements

The support of the Natural Sciences and Engineering Research Council of Canada (IVB-DG, LML-PSD) and McMaster University (PCH-Summer Work Program) is gratefully acknowledged. Portions of this work were made possible by the facilities of the Shared Hierarchical Academic Research Computing Network (SHARCNET: www.sharcnet.ca) and Compute/Calcul Canada.

References

(1) Pedireddi, V. R.; Reddy, D. S.; Goud, B. S.; Craig, D. C.; Rae, A. D.; Desiraju, G. R. *J. Chem. Soc., Perkin Trans. 2* **1994**, 2353. doi:10.1039/P29940002353.
(2) Desiraju, G. R.; Ho, P. S.; Kloo, L.; Legon, A. C.; Marquardt, R.; Metrangolo, P.; Politzer, P.; Resnati, G.; Rissanen, K. *Pure Appl. Chem.* **2013**, *85*, 1711. doi:10.1351/PAC-REC-12-05-10.
(3) Metrangolo, P.; Resnati, G. *Cryst. Growth Des.* **2012**, *12*, 5835. doi:10.1021/cg301427a.
(4) Priimagi, A.; Cavallo, G.; Metrangolo, P.; Resnati, G. *Acc. Chem. Res.* **2013**, *46*, 2686. doi:10.1021/ar400103r.
(5) Metrangolo, P.; Resnati, G. *Halogen Bonding*; Springer Berlin Heidelberg: Berlin and Heidelberg, 2008; Vol. 126.
(6) Metrangolo, P.; Pilati, T.; Resnati, G.; Stevenazzi, A. Curr. Opin. Colloid Interface Sci. **2003**, *8*, 215. doi:10.1016/S1359-0294(03)00055-4.
(7) Metrangolo, P.; Neukirch, H.; Pilati, T.; Resnati, G. *Science* **2008**, *321*, 918. doi:10.1126/science.1162215.
(8) Fourmigué, M. *Curr. Opin. Solid State Mater. Sci.* **2009**, *13*, 36. doi:10.1016/j.cossms.2009.05.001.
(9) Rissanen, K. *CrystEngComm* **2008**, *10*, 1107. doi:10.1039/B803329N.
(10) Metrangolo, P.; Meyer, F.; Pilati, T.; Resnati, G.; Terraneo, G. *Angew. Chem. Int. Ed.* **2008**, *47*, 6114. doi:10.1002/anie.200800128.
(11) Erdelyi, M. *Chem. Soc. Rev.* **2012**, *41*, 3547. doi:10.1039/c2cs15292d.
(12) Bertani, R.; Sgarbossa, P.; Venzo, A.; Lelj, F.; Amati, M.; Resnati, G.; Pilati, T.; Metrangolo, P.; Terraneo, G. *Coord. Chem. Rev.* **2010**, *254*, 677. doi:10.1016/j.ccr.2009.09.035.
(13) Raatikainen, K.; Rissanen, K. *Chem. Sci.* **2012**, *3*, 1235. doi:10.1039/c2sc00997h.
(14) Metrangolo, P.; Resnati, G.; Pilati, T.; Liantonio, R.; Meyer, F. *J. Polym. Sci. A Polym. Chem.* **2007**, *45*, 1. doi:10.1002/pola.21725.
(15) Kniep, F.; Jungbauer, S. H.; Zhang, Q.; Walter, S. M.; Schindler, S.; Schnapperelle, I.; Herdtweck, E.; Huber, S. M. *Angew. Chem. Int. Ed.* **2013**, *52*, 7028. doi:10.1002/anie.201301351.
(16) Langton, M. J.; Robinson, S. W.; Marques, I.; Félix, V.; Beer, P. D. *Nat. Chem.* **2014**, *6*, 1039. doi:10.1038/nchem.2111.
(17) Virkki, M.; Tuominen, O.; Forni, A.; Saccone, M.; Metrangolo, P.; Resnati, G.; Kauranen, M.; Priimagi, A. *J. Mater. Chem. C* **2015**, *3*, 3003. doi:10.1039/C5TC00484E.
(18) Jentzsch, A. V.; Emery, D.; Mareda, J.; Nayak, S. K.; Metrangolo, P.; Resnati, G.; Sakai, N.; Matile, S. *Nat. Commun.* **2012**, *3*, 905. doi:10.1038/ncomms1902.
(19) Manna, D.; Mugesh, G. *J. Am. Chem. Soc.* **2012**, *134*, 4269. doi:10.1021/ja210478k.
(20) Jentzsch, A. V.; Matile, S. *J. Am. Chem. Soc.* **2013**, *135*, 5302. doi:10.1021/ja4013276.
(21) Kübel, J.; Elder, P. J. W.; Jenkins, H. A.; Vargas, Baca, I. *Dalton Trans.* **2010**, *39*, 11126. doi:10.1039/c0dt01102a.
(22) Ho, P. C.; Szydlowski, P.; Sinclair, J.; Elder, P. J. W.; Kübel, J.; Gendy, C.; Lee, L. M.; Jenkins, H. A.; Britten, J. F.; Morim, D. R.; Vargas Baca, I. *Nat. Commun.* **2016**, *7*, 11299.
(23) Cozzolino, A. F.; Elder, P. J. W.; Vargas, Baca, I. *Coord. Chem. Rev.* **2011**, *255*, 1426. doi:10.1016/j.ccr.2010.12.015.
(24) Dolman, D.; Stewart, R. *Can. J. Chem.* **1967**, *45* (9), 903. doi:10.1139/v67-154.
(25) Paul, M. A. *J. Am. Chem. Soc.* **1954**, *76*, 3236. doi:10.1021/ja01641a049.
(26) Engman, L.; Wojtoń, A.; Oleksyn, B. J.; Śliwiński, J. *Phosphorus Sulfur Silicon Relat. Elem.* **2004**, *179*, 285. doi:10.1080/10426500490262289.
(27) Singh, H. B.; Apte, S. D.; Zade, S. S.; Butcher, R. J. *Organometallics* **2003**, *22*, 5473. doi:10.1021/om034222s.
(28) Kumar, S.; Singh, H. B.; Wolmershäuser, G.; Kandasamy, K. *Organometallics* **2003**, *22*, 5069. doi:10.1021/om0340948.
(29) Hamor, T. A.; Chen, H.; McWhinnie, W. R.; McWhinnie, S. L. W.; Majeed, Z. *J. Organomet. Chem.* **1996**, *523*, 53. doi:10.1016/0022-328X(96)06375-9.
(30) Lee, L. M.; Elder, P.; Cozzolino, A. F.; Yang, Q.; Vargas-Baca, I. *Main Group Chem.* **2010**, *9*, 117. doi:10.3233/MGC-2010-0016.
(31) Sasamori, T.; Sugamata, K.; Tokitoh, N. *Heteroat. Chem* **2011**, *22*, 405. doi:10.1002/hc.20698.
(32) Heitz, S.; Hesse, M.; Beckmann, J. *Inorg. Chem.* **2007**, *46*, 3275. doi:10.1021/ic062469m.
(33) Rakesh, P.; Singh, H. B.; Butcher, R. J. *Acta Crystallogr. Sect. E: Struct. Rep. Online* **2012**, *68*, 0214. doi:10.1107/S1600536811054328.
(34) Menon, S. C.; Singh, H. B.; Patel, R. P.; Kulshreshtha, S. K. *J. Chem. Soc. Dalton Trans.* **1996**, 1203. doi:10.1039/DT9960001203.
(35) Kumar, S.; Singh, H. B.; Wolmershäuser, G. *J. Organomet. Chem.* **2005**, *690*, 3149. doi:10.1016/j.jorganchem.2005.04.006.
(36) Srivastava, K.; Shah, P.; Singh, H. B.; Butcher, R. J. *Organometallics* **2011**, *30*, 534. doi:10.1021/om1009022.
(37) Zukerman-Schpector, J.; Haiduc, I. *CrystEngComm* **2002**, *4*, 178. doi:10.1039/B201969H.

Chapter 3. Synthesis and structural characterisation of the aggregates of benzo-1,2-chalcogenazole 2-oxides

Original citation: Ho, P. C.; Rafique, J.; Lee, J.; Lee, L. M.; Jenkins, H. A.; Britten, J. F.; Braga, A. L.; Vargas-Baca, I. Synthesis and Structural Characterisation of the Aggregates of Benzo-1,2-Chalcogenazole 2-Oxides. *Dalton Trans.* **2017**, *46*, 6570–6579.

This scholarly work is reprinted with permission.

3.1 Preamble

While iso-tellurazole 2-oxides (**1**) have a very interesting chemistry and are air stable, their synthesis is laborious, involving several intermediates that are sensitive to air, moisture, temperature and light (Scheme 2.1).[18] The process initiates with the synthesis *in situ* of NaTeH from tellurium powder and sodium borohydride. Bis-(*N*,*N*-dimethylcarbamoyl)-ditelluride is added to generate the corresponding tellurocarbamic acid. This is not isolated, instead it is oxidized to the bis-(*N*,*N*-dimethylcarbamoyl)-ditelluride, which is photosensitive but can be stored for a long time. Reduction of the ditelluride regenerates the *N*,*N*-dimethyltellurocarbamic acid, which reacts with an ynone to form the (Z)-4-[(dimethylamino)carbonyltelluro]-4-phenyl/t-butyl-3-buten-2-one. The five-membered ring is closed by the reaction with hydroxyamine-*o*-sulfonic acid, followed by and aqueous workup. The challenges in this method motivated the search for a more efficient method.

This chapter presents a synthetic method for a benzo-annulated iso-tellurazole *N*-oxide (**2**), which is less labor-intensive. The syntheses is indeed simpler. Only one lithiation step requires a moisture free environment and can be performed without Schlenk techniques.

Dalton Transactions

PAPER

View Article Online
View Journal

Check for updates

Cite this: DOI: 10.1039/c7dt00612h

Synthesis and structural characterisation of the aggregates of benzo-1,2-chalcogenazole 2-oxides†

Peter C. Ho,[a] Jamal Rafique,[b] Jiwon Lee,[a] Lucia M. Lee,[a] Hilary A. Jenkins,[a] James F. Britten,[a] Antonio L. Braga *[b] and Ignacio Vargas-Baca *[a]

Received 18th February 2017,
Accepted 31st March 2017

DOI: 10.1039/c7dt00612h

rsc.li/dalton

Iodine oxidation of bis[2-(hydroxyiminomethyl)phenyl] dichalcogenides yields benzo-1,2-chalcogenazole 2-oxides. Annulated derivatives of iso-tellurazole *N*-oxides spontaneously aggregate into cyclic tetra- and hexamers through Te···O chalcogen bonding; the structures of the co-crystals with benzene and CH_2Cl_2 illustrate the ability of these macrocycles to interact with small guest molecules. The selenium congener crystallizes forming a supramolecular polymer. VT NMR indicates that both compounds aggregate in solution but only at low temperature in the selenium case. The different abilities of these molecules to engage in supramolecular interactions are interpreted on the basis of their electronic properties evaluated with DFT-D3 calculations.

Introduction

The remarkable success of halogen bonding[1,2] in supramolecular chemistry has sparked great interest in analogous secondary bonds[3] formed by other heavy main-group elements. Organic derivatives of chalcogens (sulfur, selenium and tellurium) form molecules that often engage in this type of interaction. For instance, dichalcogena alkynes form tubular structures in crystalline lattices,[4–6] and telluradiazoles are well-known for their abilities to bind Lewis bases[7–11] and to form infinite ribbons in the solid state.[7,12] These concepts have recently been extended to the construction of benzo-tellurazole chains,[13] the development of tellurophenes capable of anion recognition in solution[14] and catalysis of the reduction of quinolines and imines by dithienothiophenes.[15]

A unique development in this area, with no equivalent in halogen bonding, is the reversible autoassociation of 1,2-tellurazole 2-oxides (Scheme 1, **1**) through Te···O interactions forming annular structures ($\mathbf{1}_4$ and $\mathbf{1}_6$) that are persistent in solution and display chemical properties of actual macrocycles such as binding transition metal ions, forming fullerene adducts, and hosting small molecules.[16] Although the preparation of these compounds requires several steps that must be carried out under an inert atmosphere, the heterocycles and their aggregates are remarkably stable under ambient conditions and are tolerant of water. Mineral acids such as HCl and HBr protonate the oxygen atom while the halide binds the chalcogen; the process is reversible providing a means to switch on and off the self-assembly of these molecular building blocks.[17]

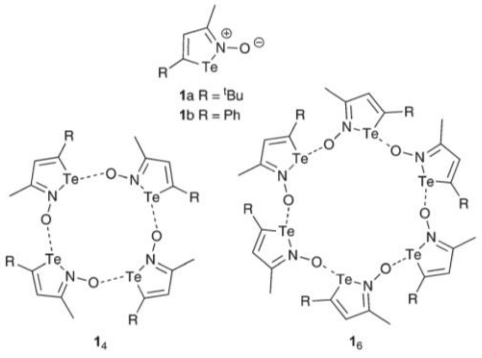

Scheme 1 Iso-tellurazole oxides and their macrocyclic aggregates.

In search of a synthetic method which could grant easier access to this type of compounds, we considered annulated derivatives such as benzo-1,2-tellurazole 2-oxide (Scheme 2, **2a**). As long as the autoassociation of heterocycles is preserved, annulation of the 1,2-tellurazole 2-oxide to a benzo ring would confer advantages such as increased stability, four positions that in principle are available for functionalization and an increased van der Waals surface that would likely enhance the interaction

[a]Department of Chemistry and Chemical Biology, McMaster University, 1280 Main Street West, Hamilton, Ontario, Canada L8S 4M1. E-mail: vargas@chemistry.mcmaster.ca
[b]Department of Chemistry, Federal University of Santa Catarina, Florianópolis, Santa Catarina, 88040-900, Brazil. E-mail: braga.antonio@ufsc.br

†Electronic supplementary information (ESI) available: Details of crystallographic data and DFT optimized structures. CCDC 1507753–1507755 and 1530647. For ESI and crystallographic data in CIF or other electronic format see DOI: 10.1039/c7dt00612h

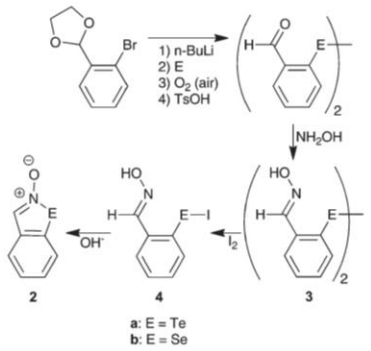

Scheme 2 Synthesis of benzo-1,2-chalcogenazole 2-oxides **2a,b**.

of macrocycles with aromatic molecules. Here we report the preparation of such a compound, demonstrate its ability to form supramolecular aggregates, and show that the synthetic method is readily applicable to the selenium congener **2b**.

Results and discussion

Synthesis

As shown in Scheme 2, the proposed approach for the synthesis of **2a** consists of the lithiation of ketal-protected 2-bromo benzaldehyde followed by reaction with elemental tellurium. Aerobic oxidation yields a ditelluride which is deprotected and condensed with hydroxyl amine to produce bis[2-(hydroxyiminomethyl)phenyl]ditelluride (**3a**). We reasoned that its reaction with I_2 would give in the first instance **4a**, an analogue of the products of the reaction of **1a,b** with HCl and HBr, thus addition of a base would generate **2a**.

The steps along this route proceed with good yields and an inert atmosphere is only required for the initial lithiation and subsequent reaction with elemental tellurium. The pure dioxime **3a** or its bis(2-formylphenyl)ditelluride precursor can be conveniently stored as a stable intermediate product. However, **4** is unstable, it is best prepared *in situ* and should be promptly transformed into the target compound **2a**. The equivalent sequence of steps led to the 1,2-selenazole 2-oxide **2b**. Analytically pure benzotellurazole *N*-oxide, (**2a**) can be obtained from the crude product by recrystallization from a 1 : 1 mixture of dichloromethane and pyridine.

Crystal structures

Pure **2a** forms plate-like crystals that belong to the $P\bar{1}$ space group (Table 1). They contain $\mathbf{2a}_4$ in a chair conformation (Fig. 1) analogous to the structure previously observed for $\mathbf{1b}_4$.[16,18] Given the C_i symmetry, the tetramer is generated from two crystallographically independent units of **2a**. Adjacent heterocycles subtend an interplanar angle of 72.34° (*cf.* 60.16° in $\mathbf{1b}_4$). The two trans-annular Te–Te distances, 3.6990(2) and 4.3638(4) Å, are much shorter than the distances 5.5895(2) and 5.3043(2) Å of $\mathbf{1b}_4$. Packing (Fig. 2) of the $\mathbf{2a}_4$ macrocycles along the *a* and *b* axes is driven by π-stacking. Additional Te···O short contacts (3.151(2) Å, *cf.* Σ_{rvdW} = 3.58 Å) are formed between neighbouring macrocycles; but the C–Te···O angle (145.2°) strongly deviates from the ideal linear geometry of σ-hole interactions.

Table 1 Crystallographic and refinement parameters for all characterized polymorphs of **2a** and **2b**

Crystal composition	6(**2a**)·1.78(CH_2Cl_2)·0.22(H_2O)	4(**2a**)	4(**2a**)·C_6H_6	$\mathbf{2b}_{\infty}$
CCDC	1507753	1507754	1507755	1530647
Empirical formula	$C_{43.78}H_{34}Cl_{3.56}N_6O_{6.22}Te_6$	$C_{28}H_{20}N_4O_4Te_4$	$C_{34}H_{26}N_4O_4Te_4$	C_7H_5NOSe
Crystal system	Trigonal	Triclinic	Monoclinic	Orthorhombic
Space group	$P3_1$	$P\bar{1}$	$C2/c$	$P2_12_12_1$
a [Å]	14.4246(7)	7.2250(2)	18.646(3)	7.3324(9)
b [Å]	14.4246(7)	8.7915(3)	17.433(2)	8.0016(10)
c [Å]	21.3472(12)	12.1257(4)	10.6572(15)	11.8324(15)
α [°]	90	106.411(2)	90	90
β [°]	90	102.489(2)	95.384(2)	90
γ [°]	120	90.001(2)	90	90
V [Å^3]	3846.6(4)	719.81(4)	3448.9(8)	694.22(15)
Z, ρ (calc.) [g cm^{-3}]	3, 2.118	1, 2.277	4, 2.051	4, 1.895
T [K]	100.15	100.15	296.15	100.15
μ [mm^{-1}]	3.604	4.054	3.393	5.327
2θ range [°]	5.02 to 67.072	5.788 to 66.262	6.412 to 56.598	6.146 to 56.782
Limiting indices	$-22 \le h \le 22$	$-11 \le h \le 11$	$-24 \le h \le 24$	$-9 \le h \le 9$
	$-22 \le k \le 22$	$-13 \le k \le 13$	$-22 \le k \le 23$	$-10 \le k \le 10$
	$-33 \le l \le 33$	$-18 \le l \le 18$	$-14 \le l \le 14$	$-15 \le l \le 15$
Refl. collected/unique	131 669/20 091	23 510/5456	13 318/4255	7086/7086
R(int.)	0.0477	0.0239	0.0276	0.1164
No. of parameters	602	181	208	93
$R_1{}^a$/w$R_2{}^a$ ($I > 2\sigma(I)$)	0.0330/0.0709	0.0238/0.0637	0.0410/0.0820	0.0351/0.0859
$R_1{}^a$/w$R_2{}^a$ for all data	0.0435/0.0759	0.0299/0.0677	0.0697/0.0917	0.0400/0.0876
Goodness-of-fit on F^2	1.005	1.009	1.036	1.059
Largest difference peak/hole [e Å^{-3}]	1.76/−0.68	1.42/−0.55	0.97/−1.51	1.62/−0.49

^{a} $R_1 = \Sigma||F_o| - |F_c||/\Sigma|F_o|$, $wR_2 = \{\Sigma[w(F_o^2 - F_c^2)^2]/\Sigma w(F_o^2)^2\}^{1/2}$.

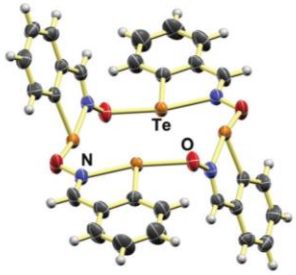

Fig. 1 ORTEP (75%) plot of the tetrameric aggregate of benzotellurazole *N*-oxide (**2a**) as observed in a crystal of the pure compound. Te···O 2.235(2), 2.245(2) Å; Te–N 2.235(2), 2.197(2) Å; N–O 1.357(3), 1.355(3) Å; N–Te–O 162.37(7), 164.45(7)°; Te–N–O 126.3(1), 122.7(1)°; Te–O–N, 111.6(1), 115.5(1)°; Te–O–N–Te 89.4(1), 19.0(2)°.

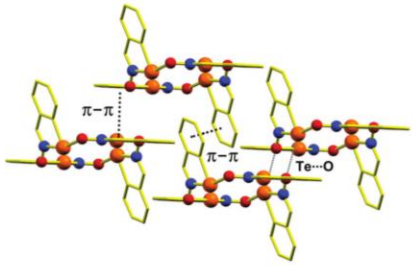

Fig. 2 Detail of packing in the crystal of $\mathbf{2a}_4$ highlighting the interactions between macrocyclic tetramers.

A second polymorph was isolated when the solvent mixture used for crystallization contained a small amount (15% v/v) of pyridine. This hexagonal $R\bar{3}c$ phase is built from $\mathbf{2a}_6$ macrocycles (Fig. 3) arranged in layers, similar to those observed in the crystal of $\mathbf{1b}_6$·2THF. However, in this case the layers pack in an ABC pattern, not AB, and the macrocycle cavities conform isolated pockets instead of pores (Fig. 4). The voids are occupied by water and dichloromethane molecules, the relative occupations of which were determined from the structural refinement affording a composition $\mathbf{2a}_6(CH_2Cl_2)_{1.78}(H_2O)_{0.22}$ which is consistent with the results of combustion analysis. In addition, the 3 vibrational modes of the water molecule are well resolved in the infrared spectrum (Fig. S2†). All the heterocycles in the structure of $\mathbf{2a}_6$ are crystallographically distinct and, of all the tellurazole *N*-oxide aggregates characterized until now, they are the closest to be truly orthogonal to each other (interplanar angles range from 80.03 to 88.79°). In these macrocycles the trans-annular Te–Te distances (7.1297(8), 7.3407(8) and 7.3589(5) Å) are slightly shorter than 7.638(2) Å observed in $\mathbf{1b}_6$·2THF.[15] As in the case of $\mathbf{2a}_4$, π-stacking is the predominant interaction between the macrocycles in each layer. Crystallographic refinement of the CH_2Cl_2 population showed a loss of only 3% in a sample held at 0.3 Torr for 12 hours.

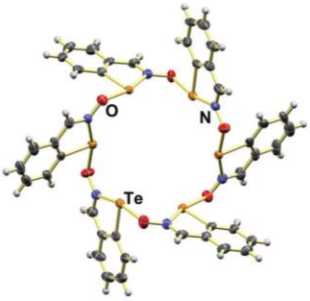

Fig. 3 ORTEP (75%) plot of the hexameric aggregate of benzotellurazole *N*-oxide as observed in the crystal of composition $\mathbf{2a}_6(CH_2Cl_2)_{1.78}(H_2O)_{0.22}$. Te···O 2.201(6), 2.178(5), 2.187(4), 2.188(6), 2.188(5), 2.189(4) Å; Te–N 2.262(5), 2.268(4), 2.261(6), 2.262(5), 2.268(5), 2.267(6) Å; N–O 1.374(6), 1.365(9), 1.370(7), 1.361(6), 1.369(7), 1.361(9) Å; N–Te–O 164.6(2), 164.7(2), 163.6(2), 163.9(2), 164.0(2), 164.5(2); Te–N–O 127.1(4), 126.8(4), 127.1(4), 127.1(4), 126.6(4), 127.2(4); Te–O–N 114.4(4), 114.5(4), 115.2(4), 115.3(4), 116.1(4), 116.4(4)°; Te–O–N–Te 11.2(6), 12.5(6), 2.2(7), 6.4(6), 15.1(7), 5.4(6)°.

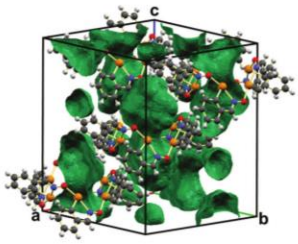

Fig. 4 Detail of packing in the crystal of $\mathbf{2a}_6(CH_2Cl_2)_{1.78}(H_2O)_{0.22}$. Void surfaces are calculated with a 1 Å probe.

Acicular crystals grown from benzene belong to the *C*2/*c* space group and feature the tetramer $\mathbf{2a}_4$ in a hitherto not observed twist-boat conformation (Fig. 5) which sits on a two-fold axis. There are two distinct trans-annular Te–Te distances (5.2164(8) and 5.2172(8) Å) in this ring. The macrocycles align along the *c*-axis forming tubular channels which are occupied

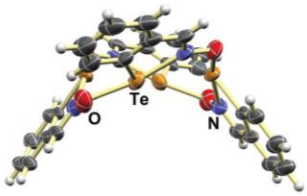

Fig. 5 ORTEP (50%) plot of the tetrameric aggregate of benzotellurazole *N*-oxide as observed in a crystal of composition $\mathbf{2a}_4$·C_6H_6. Te···O, 2.201(4), 2.213(4) Å; Te–N 2.244(5), 2.250(4) Å; N–O 1.361(7), 1.368(5) Å; N–Te–O 161.3(2), 164.6(1)°; Te–N–O 125.4(3), 127.2(3)°; Te–O–N 110.0(3), 115.7(3)°; Te–O–N–Te 1.4(5), 42.6(4)°.

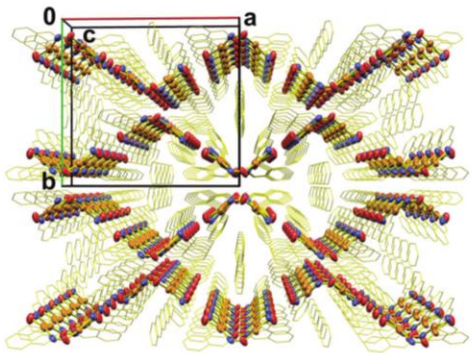

Fig. 6 Detail of the crystalline structure of $\mathbf{2a}_4 \cdot C_6H_6$ highlighting the channels occupied by benzene molecules.

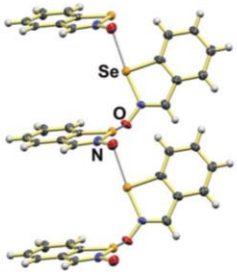

Fig. 7 ORTEP (75%) depicting the organization of the molecules in the crystal of **2b**. Se···O 2.412(5) Å; Se–N 1.938(5) Å; N–O 1.315(6) Å; N–Se–O 172.3(2)°; Se–N–O 118.8(4)°; Se–O–N, 108.1(3)°; Se–O–N–Se 86.3(4)°.

by benzene molecules (Fig. 6) giving an overall stoichiometry $\mathbf{2a}_4 \cdot C_6H_6$. Combustion analysis was satisfactory for freshly grown crystals, but the loss of benzene became apparent after a few days of dry storage.

The observed ranges of Te···O (2.178(5) to 2.245(2) Å), and Te–N (2.198(2) to 2.274(7) Å) distances as well as the average N–Te–O (163.4°), N–Te–C (75.8°) and O–N–Te (126.4°) angle values are comparable to those measured in the crystal structures of **1a** and **1b**,[18] suggesting that they are equally stable.

While all the polymorphs of **2a** that could be identified contained macrocyclic aggregates, attempts to grow crystals of **2b** under different conditions yielded only one crystalline phase that belongs to the $P2_12_12_1$ space group. In this case the molecules are linked by 2.412(5) Å (*cf.* Σ_{rvdW} = 3.42 Å) Se···O chalcogen bonds (Fig. 7) forming infinite chains that lay along the *b* axis of the unit cell. This arrangement is reminiscent of the packing in the crystals of **1b** grown in the presence of trifluoroacetic acid.[17]

Solution NMR spectroscopy

As in the case of **1a** and **1b**,[16] the ^{1}H NMR spectrum of **2a** in solution (Fig. 8) is indicative of aggregation. For a 2 mM solution in CD_2Cl_2, significant broadening of the resonances is observed at room temperature. Upon cooling, the peak width increases and new resonances appear creating an intricate pattern that is not completely resolved at 190 K using the 500 MHz instrument. The 8.86 ppm singlet at 298 K that arises from the hydrogen atom on the heterocycle (H3) splits into at least 7 separate resonances that spread from 8.7 to 9.1 ppm and have different intensities. The low solubility of **2a** precludes a thorough study but the ratio of intensities of the singlets at 8.87 and 8.93 ppm at 190 K is dependent on the concentration (2 mM: 1 : 1.3; 0.4 mM: 1 : 0.9), which indicates that these resonances arise from two structures related by aggregation. Such a behaviour is observed in the spectrum of **1b** at 190 K due to the equilibrium between tetramers and hexamers.

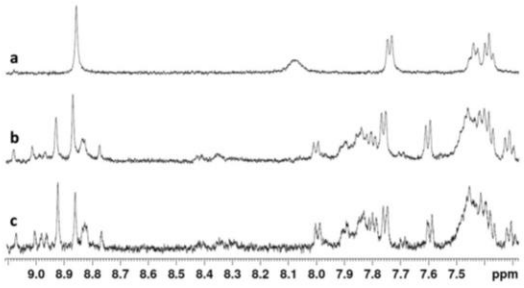

Fig. 8 VT ^{1}H NMR spectrum of **2a** in CD_2Cl_2. (a) 2 mM, 298 K; (b) 2 mM, 190 K; and (c) 0.4 mM, 190 K.

The complex VT ^{1}H NMR spectra of **2a** are in sharp contrast with those of **2b** (Fig. 9). No significant broadening is observed between 190 and 298 K, however, the frequencies of two resonances (H3 and H7) strongly depend on temperature, following a sigmoidal trajectory. A third resonance (from H4) displays the same behaviour, albeit within a much narrower range. Such profiles are characteristic of fast supramolecular aggregation equilibria, thus the observed frequencies are averaged. The data were analysed assuming that all aggregation steps have the same equilibrium constant (K), with an isodesmic model.[19] The temperature dependency of δ(H3) served as the basis to model the degree of aggregation (α) with eqn (1) where T_m is the melting temperature, *i.e.* T for which $\alpha = 0.5$, and ΔH is the molar change of enthalpy:

$$\alpha = \frac{1}{1 + e^{-0.908\Delta H \frac{T - T_m}{RT_m^2}}} \quad (1)$$

The fitted model (Fig. 10) was then used to estimate the aggregation number (AN, Fig. 11). At 190 K, the AN value of 4.8 at 190 K suggests that hexamers and tetramers are present in solution. In fact, the most NMR sensitive hydrogen atoms would be brought close to each other by the assembly of annular aggregates. The structures of the crystals that contain $\mathbf{2a}_4$ and $\mathbf{2a}_6$ are useful examples in this regard, since they feature 2.9–3.2 Å distances between the H3 and H7 of neigh-

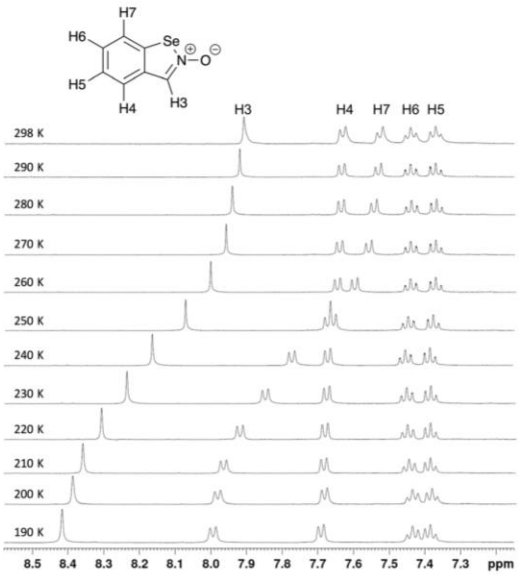

Fig. 9 VT ^{1}H NMR of **2b** in CD_2Cl_2 (15 mM). ^{1}H–^{13}C HMBC assignments are labelled using standard IUPAC numbering.

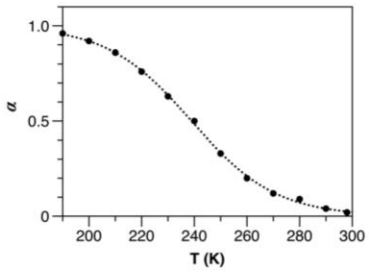

Fig. 10 Degree of aggregation (a) of **2b** as a function of temperature modelled for the resonance of H3. The dotted line corresponds to the model with fitted parameters T_m = 239 K and ΔH = −33 kJ mol^{-1}.

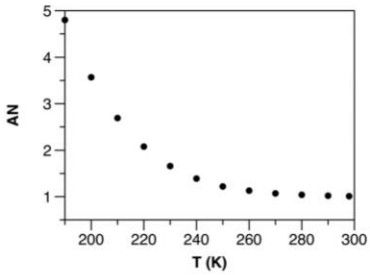

Fig. 11 Aggregation number (AN) of **2b** as a function of temperature, calculated from the resonance of H3.

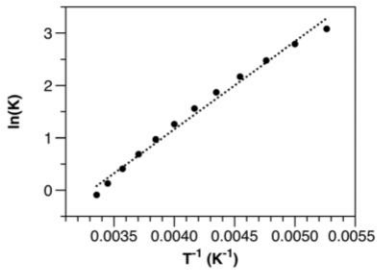

Fig. 12 Van't Hoff plot for the autoassociation equilibrium of **2b** in CD_2Cl_2. Fitting parameters: ΔH = −14.0 ± 0.4 kJ mol^{-1}, ΔS = −46 ± 2 J mol^{-1} K^{-1}, and r^2 = 0.999.

bouring molecules. Similar distances would be obtained in the selenium case.

At each measured temperature, the equilibrium constant was evaluated with eqn (2), all points were used to extract the thermodynamic parameters with a Van't Hoff analysis (Fig. 12).

$$\mathrm{AN} = \frac{1}{(1-\alpha(T))^{1/2}} = \frac{1}{2} + \frac{1}{2}(4KC_{\mathrm{T}} + 1)^{1/2} \qquad (2)$$

The negative entropy change is consistent with aggregation. Although the fitted enthalpy change confirms the exothermic character of the process, its magnitude is different from the value obtained from the degree of the aggregation plot. Such disagreements are not uncommon[19] as the model contains approximations, therefore these values must be used with caution.

DFT calculations

GGA (PBE-D3, ZORA, TZ2P) calculations were performed to assess the relative strengths of the Se···O and Te···O chalcogen bonds formed by the benzo-1,2-chalcogenazole 2-oxides. Because previous investigations[16] have shown that the energies of such interactions are approximately additive, modelling was based on the individual molecules and dimers of **2a** and **2b**. Consistent with the crystallographic observations, the minimized dimers are not planar, and the optimized angles between the molecular planes are 71.2° and 66.3° in $\mathbf{2a}_2$ and $\mathbf{2b}_2$, respectively. The optimized intramolecular distances in the dimers differ by less than 0.11 Å with respect to the crystallographic determinations and by less than 0.07 Å from the optimized individual molecules. The deviations in the E···O (E = Te, Se) distances are 0.165(4) Å for $\mathbf{2a}_2$ and 0.206(5) Å for $\mathbf{2b}_2$.

The binding energy of the chalcogen bonds ($E_{\mathrm{E\cdots O}}$, E = Te, Se) was evaluated and analysed using the Ziegler–Rauk transition-state approach,[20–22] which assumes a hypothetical stepwise process. In the first stage, the individual molecules are calculated using the geometries optimized for the dimers but without orbital mixing. Calculation of this transition-state yields the electrostatic interaction (E_{elstat}) and Pauli

Table 2 Energy decomposition analysis for dimerization of **2a** and **2b**. All DFT calculations were done with GGA (PBE-D3, ZORA, TZ2P). All values are given in kJ mol^{-1} unless otherwise noted

	2a$_2$, E = Te	**2b**$_2$, E = Se
E_{elstat}	−269.54	−81.55
E_{Pauli}	418.08	118.94
E_{Steric}	148.54	37.38
$E_{Orbital}$	−229.83	−62.11
$E_{Dispersion}$	−11.68	−9.85
$E_{E\cdots O}$	−92.97	−34.58
$E_{Preparation}$	17.98	3.04
E_{Total}	−74.99	−31.54
$\Delta ZPE \times 10^{-2}$ [eV]	2.14	1.81
ΔH	−72.68	−29.21
ΔS [J mol^{-1} K^{-1}]	−186.74	−171.85
$\Delta G_{273.15\ K}$	−17.01	22.03

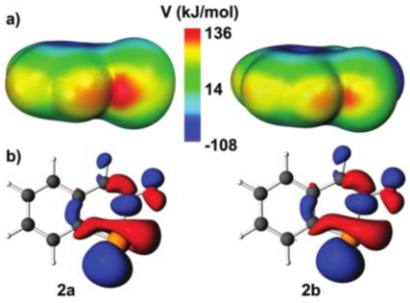

Fig. 13 DFT analysis of the electronic structure of **2a** and **2b**. (a) Electrostatic potential maps plotted on the 0.001 a.u. isodensity surfaces; (b) LUMOs plotted at 0.04 a.u.

repulsion (E_{Pauli}) between the molecules. Combinedly, the electrostatic and Pauli repulsion energies are termed the total steric interaction (E_{Steric}). The second stage consists of the mixing of orbitals of the interacting molecules, here relaxation of the system by polarization gives the orbital interaction ($E_{Orbital}$). Combinations of these contributions and the dispersion correction ($E_{Dispersion}$) give the total $E_{E\cdots O}$. However, there is an energetic cost ($E_{Preparation}$) for the geometric distortion of the molecules from their non-associated structures. The combination with $E_{E\cdots O}$ gives the total electronic bonding energy (E_{Total}, eqn (3)). All contributions are compiled in Table 2.

$$\begin{aligned} E_{Total} &= E_{elstat} + E_{Pauli} + E_{Orbital} + E_{Dispersion} + E_{Preparation} \\ &= E_{Steric} + E_{Orbital} + E_{Dispersion} + E_{Preparation} \\ &= E_{E\cdots O} + E_{Preparation} \end{aligned} \quad (3)$$

Each of the energy terms is larger in magnitude for the tellurium case. The most important stabilising contributions are E_{elstat} and $E_{Orbital}$, the former being slightly larger in magnitude. The difference of E_{elstat} is related to the magnitudes of V_{max} at the σ hole of each molecule (**2a**: 139.62 kJ mol^{-1}, 0.053 e bohr^{-3}; **2b**: 118.15 kJ mol^{-1}, 0.045 e bohr^{-3}, for **2b**). As the energies of the HOMOs (O centred lone pairs) are similar (−5.328 eV for **2a** and −5.410 eV for **2b**), the $E_{Orbital}$ values reflect the LUMO heights (−3.303 eV for **2a** and −2.884 eV for **2b**) and different overlapping abilities of the Te and Se orbitals with those of oxygen. The electrostatic potential maps and LUMOs are displayed in Fig. 13.

Vibrational calculations were carried out to demonstrate that each optimized geometry is an actual minimum on the respective potential energy surface and to derive the corresponding standard thermodynamic parameters in the gas-phase. The results in Table 2 show that while the autoassociation of **2a** is a spontaneous process, the Se···O interaction is too weak to compensate for the entropic cost of the dimerization of **2b** at ambient temperature. As calculated, the differences in the stability of the aggregates of these molecules are consistent with the behaviour of their NMR spectra in solution as a function of temperature.

Experimental

Materials and methods

Air sensitive materials were handled using an atmosphere of nitrogen. Organic solvents were purified either by distillation over appropriate dehydrating agents under nitrogen or using an Innovative Technologies purification system. The following chemicals were used as received from commercial suppliers: dichloromethane-d$_2$ (Aldrich), DMSO-d$_6$ (Aldrich), 2-bromobenzaldehyde (Aldrich), 2.5 M *n*-butyllithium solution in hexanes (Aldrich), hydroxylamine hydrochloride (Fisher), sodium hydroxide (EMD), ethylene glycol (Fisher), sodium bicarbonate (Sigma), sodium sulphate (EMD), silica gel (EM, 230–400 mesh), elemental tellurium (CERAC), iodine (AnalaR), and *p*-toluenesulfonic acid (Eastern).

Nuclear magnetic resonance. All spectra were measured in solution with a deuterated solvent. The spectra were obtained using Bruker Avance 500 MHz (Bruker 5 mm Broad Band Inverse probe) or Bruker Avance 600 MHz (Bruker 5 mm Broad Band Observe probe) spectrometers at 287.5 K unless otherwise noted. The ^{1}H, ^{13}C and ^{125}Te spectra were processed using Bruker TopSpin 2.1 or 3.2 software packages. The ^{1}H and ^{13}C spectra were referenced to tetramethylsilane using the deuterated solvent signal as a secondary reference. The ^{125}Te and ^{77}Se chemical shifts are reported with respect to the room-temperature resonance of $TeMe_2$ and $SeMe_2$ (δ = 0.00 ppm) but were measured using secondary references of diphenyl ditelluride (δ = 420.36 ppm) and diphenyldiselenide (δ = 462.99 ppm) in CD_2Cl_2.

Electrospray ionization mass spectrometry. Mass spectra were acquired in positive ion mode on a Waters/Micromass Quattro Ultima Global TOF mass spectrometer functioning in W mode. Pure samples were dissolved in dichloromethane followed by dilution with methanol. High resolution mass spectra were obtained in a Waters Global Ultima (ES Q-TOF)

mass spectrometer (capillary = 3.20 V, cone = 100 V, source temp. = 80 °C and resolving power = 10 000).

Single-crystal X-ray diffraction. All crystals were mounted on nylon loops (Hampton, California) or MiTeGen micromounts (Ithaca, New York) with Paratone-N oil. Data were collected at 100 K or 173.15 K using Mo-Kα radiation (λ = 0.71073 Å) with a Bruker APEX2 diffractometer. The CCD area detector was equipped with a low-temperature accessory (Oxford cryostream). A minimum of 50 frames from three different orientations were used for the determination of the precursory unit cell parameters and final cell advancement after integration in SAINT.[23] The absorption was corrected for each data set in SADABS.[24] Direct methods were used to solve all structures and then refined by the full-matrix least-squares techniques on F^2 using SHELXL.[25] All non-hydrogen atoms were assigned anisotropic thermal parameters. Appropriate riding models were used to place hydrogen atoms in idealized positions.

Other instrumental methods. Infrared vibrational spectra were measured in a Bio-Rad FTS-40 FT-IR spectrometer or a Thermo Scientific Nicolet 6700 FT-IR spectrometer. Melting points were measured with Uni-Melt Thomas Hoover capillary melting point apparatus and are reported uncorrected. Combustion elemental analyses were carried out by the London Metropolitan University elemental analysis service (London, United Kingdom).

Syntheses

2-(2-Bromophenyl)-1,3-dioxolane. Ethylene glycol (6 g, 96.7 mmol) and *p*-toluenesulfonic acid (0.616 g, 3.24 mmol) were added to 2-bromobenzaldehyde (12 g, 64.9 mmol) in 150 mL of toluene. The solution was heated to reflux with a Dean-Stark trap for 19 hours. The slightly cloudy yellow solution was cooled and then washed with a $NaHCO_3$ solution (1 M) until the organic phase was no longer acidic. This treatment was followed by washings, first with distilled water and later with brine. The organic layer was dehydrated with Na_2SO_4 and concentrated. The crude product, a yellow liquid, was purified by chromatography on a silica gel column with a hexane/EtOAc 95 : 5 mixture. The product was obtained as a clear colourless liquid after solvent evaporation. Yield 90%. ^{1}H NMR (600 MHz, CD_2Cl_2) δ 7.60–7.56 (m, 2H), 7.37–7.34 (m, 1H), 7.26–7.23 (m, 1H), 6.05 (s, 1H), 4.16–4.01 (m, 4H). ^{13}C NMR (600 MHz, CD_2Cl_2) δ 133, 131, 128, 128, 123, 103, 66. HRMS-ESI+: m/z $[M + H]^+$ calcd for $C_9H_9O_2BrH$: 228.9864; found: 228.9863.

2,2′-(Ditellurodi-2,1-phenylene)bis-1,3-dioxolane. A 2.5 M solution *n*-butyllithium in hexanes (11.7 mL, 29.2 mmol) was added dropwise to 2-(2-bromophenyl)-1,3-dioxolane (6.08 g, 26.5 mmol) in anhydrous diethyl ether (80 mL) at 0 °C; the solution developed a brown colour and a pale pink solid precipitated. The mixture was stirred for 1 h at room temperature; the precipitate was filtered under argon and washed with anhydrous diethyl ether. The precipitate was dissolved under argon with freshly-distilled anhydrous THF (80 mL) and tellurium powder (26.5 mmol) was added all at once while maintaining a temperature of 0 °C. The mixture was stirred at room temperature for 2 h. The reaction mixture was quenched with distilled water (60 mL) at 0 °C and stirred for 30 min. The product was extracted with dichloromethane, washed with distilled water, dehydrated over anhydrous Na_2SO_4 and concentrated under vacuum to yield a dark yellow crystalline material. No further purification was necessary before the next step, but it can be achieved by chromatography on a silica gel column with a hexane–EtOAc gradient from 95 : 5 to 80 : 20. Yield 75%. Mp 118–120 °C. ^{1}H NMR (600 MHz, CD_2Cl_2) δ 7.98–7.96 (m, 2H), 7.37–7.36 (m, 2H), 7.26–7.23 (m, 2H), 7.16–7.13 (m, 2H), 5.83 (s, 2H), 4.21–4.15 (m, 4H), 4.08–4.03 (m, 4H). ^{13}C NMR (600 MHz, CD_2Cl_2) δ 140.2, 139.2, 130.8, 127.8, 126.3, 108.0, 105.7, 65.6. ^{125}Te NMR (600 MHz, CD_2Cl_2) δ 318.3. IR (KBr, $\tilde{\nu}$): 3052, 2971, 2885, 1582, 1565, 1462, 1446, 1390, 1285, 1213, 1119, 1083, 1043, 1016, 966, 942, 874, 754, 734, 654, 440. HRMS-ESI+: m/z $[M + H]^+$ calcd for $C_{18}H_{18}O_4{}^{129}Te_2H$: 558.9408; found: 558.9426.

Bis(2-formylphenyl)ditelluride. 2,2′-(Ditellurodi-2,1-phenylene)bis-1,3-dioxolane (1 g, 1.8 mmol) and *p*-toluenesulfonic acid (0.190 g, 1.1 mmol) were dissolved in a mixture of distilled water/acetone/distilled THF (60 : 60 : 30 mL) and then refluxed for 2 h. After cooling to room temperature, distilled water (300 mL) was added to the yellow solution; the product was extracted with CH_2Cl_2, and washed with distilled water and then with brine. The yellow solution was dehydrated over anhydrous Na_2SO_4 and concentrated under vacuum to yield a dark yellow crystalline material. No further purification was necessary before the next step, but it can be achieved by precipitation in hexanes from a concentrated solution of CH_2Cl_2 (93%). Mp 141–143 °C. ^{1}H NMR (600 MHz, CD_2Cl_2) δ 10.14 (s, 2H), 8.02 (d, 2H), 7.85–7.84 (m, 2H), 7.48–7.45 (m, 2H), 7.34–7.31 (m, 2H). ^{13}C NMR (600 MHz, CD_2Cl_2) δ 193.7, 140.8, 137.3, 137.2, 134.8, 127.5, 112.8. ^{125}Te NMR (600 MHz, CD_2Cl_2) δ 414.4. IR (KBr, $\tilde{\nu}$): 2835, 2742, 1654, 1577, 1551, 1447, 1436, 1386, 1298, 1255, 1205, 1163, 1112, 1019, 840, 760, 745, 700, 657, 435. HRMS-ESI+: m/z $[M + H]$+ calcd for $C_{18}H_{18}O_4{}^{129}Te_2H$: 470.8884; found: 470.8889.

2,2′-Ditellurobis-benzaldehyde dioxime (3a). A solution of hydroxylamine hydrochloride (0.063 g, 0.9 mmol) and sodium hydroxide (0.036 g, 0.9 mmol) in distilled water (1.6 mL) was added dropwise into bis(2-formylphenyl) ditelluride (0.093 g, 0.2 mmol) dissolved in pyridine (1.6 mL) at 0 °C under a nitrogen atmosphere. The solution was stirred at room temperature for 2 h, diluted with 10 mL of CH_2Cl_2, and then washed with distilled water. The yellow solution was dehydrated over anhydrous Na_2SO_4 and concentrated under vacuum to yield a yellow solid. The moist crude product was suspended in $CHCl_3$ (freshly-filtered through activated neutral alumina) and filtered to yield a light-yellow crystalline powder. Yield 73%. Mp 166 °C (d). ^{1}H NMR (600 MHz, DMSO-d_6) δ 11.83 (s, 2H), 8.45 (s, 2H), 7.90 (d, 2H), 7.49–7.47 (m, 2H), 7.32–7.29 (m, 2H), 7.17–7.14 (m, 2H). ^{13}C and ^{125}Te NMR could not be recorded due to the low solubility of this compound. IR (KBr, $\tilde{\nu}$): 3356, 3250, 1581, 1523, 1458, 1432, 1342, 1301, 1254, 1204, 1161, 1122, 1042, 1034, 1020, 970, 943, 904, 880, 750, 730, 713, 663,

652, 562, 527, 453, 432. HRMS-ESI+: m/z $[M + H]^+$ calcd for $C_{14}H_{12}N_2O_2{}^{129}Te_2H$: 500.9142; found: 500.9144. Elemental anal. % calcd $C_{14}H_{12}N_2O_2Te_2$: C 33.94, H 2.44, N 5.65; found: C 34.07, H 2.52, N 5.54.

Benzo-1,2-tellurazole 2-oxide (2a). 2,2′-Ditellurobis-benzaldehyde dioxime (0.1 g, 0.2 mmol) was suspended in methanol (5 mL). The solid that was consumed as I_2 (0.051 g, 0.2 mmol) was added. The red solution was stirred at room temperature for a period of 2 h, after which 0.1 M $NaHCO_3$ (5 mL) was added and a light yellow solid precipitated. The crude product was re-dissolved and extracted with CH_2Cl_2. The organic layer was washed with distilled water, dehydrated over anhydrous Na_2SO_4 and concentrated under reduced pressure yielding a light-yellow precipitate. Yield 95%. Mp 221–222 °C (d). ^{1}H NMR (600 MHz, DMSO-d_6) δ 9.28 (s, 1H), 7.98 (d, 1H), 7.91 (d, 1H), 7.52 (t, 1H), 7.45 (t, 1H). ^{13}C and ^{125}Te NMR could not be recorded due to the low solubility of this compound. HRMS-ESI+: m/z $[M + H]^+$ calcd for $C_7H_5NO^{129}TeH$: 249.9512; found: 249.9505. IR (KBr, $\tilde{\nu}$): 1582, 1568, 1523, 1454, 1432, 1341, 1256, 1204, 1122, 1060, 1049, 1020, 899, 880, 750, 713, 682, 664, 652, 559, 530, 453, 430. Elemental anal. % calcd C_7H_5NOTe: C 34.08, H 2.04, N 5.68; found: C 33.92, H 1.95, N 5.76. Single crystals of the polymorphs of **2a** were grown as follows. (**2a**$_6$)·(CH_2Cl_2)·(H_2O): slow evaporation from a 0.043 M dichloromethane solution with pyridine (15% v/v). Elemental anal. % calcd $C_{42}H_{30}N_6O_6Te_6$·1.78(CH_2Cl_2)·0.22(H_2O): C 32.15, H 2.10, N 5.14; found: C 32.36, H 2.11, N 5.31. (**2a**$_4$): slow evaporation from a 0.043 M dichloromethane solution with an equal volume of pyridine. Elemental anal. % calcd C_7H_5NOTe: C 34.08, H 2.04, N 5.68; found: C 33.90, H 2.03, N 5.55. (**2a**$_4$)·(C_6H_6): slow evaporation from a benzene solution. Elemental anal. % calcd $C_{34}H_{26}N_4O_4Te_4$: C 38.34, H 2.46, N 5.26; found: C 38.21, H 2.40, N 5.33.

2,2′-(Diselenadi-2,1-phenylene)bis-1,3-dioxolane. Similarly to the 2,2′-(ditellurodi-2,1-phenylene)bis-1,3-dioxolane synthesis, a 2.5 M solution *n*-butyllithium in hexanes (6.28 mL, 15.7 mmol) was added dropwise to 2-(2-bromophenyl)-1,3-dioxolane (3.27 g, 14.3 mmol) in anhydrous diethyl ether (40 mL) at 0 °C; the solution developed a brown colour and a pale pink solid precipitated. The mixture was stirred for 1 h at room temperature; the precipitate was filtered under argon and washed with anhydrous diethyl ether. The precipitate was dissolved under argon with freshly-distilled anhydrous THF (40 mL) and selenium powder (1.13 g, 14.3 mmol) was added all at once while maintaining a temperature of 0 °C. The mixture was stirred at room temperature for 2 h. The reaction mixture was quenched with distilled water (30 mL) at 0 °C and stirred for 30 min. The product was extracted with dichloromethane, washed with distilled water, dehydrated over anhydrous Na_2SO_4 and concentrated under vacuum to yield a dark yellow crystalline material. No further purification was necessary before the next step, but it can be achieved by chromatography on a silica gel column with a hexane–EtOAc gradient from 95 : 5 to 90 : 10. Yield 70%. ^{1}H NMR (600 MHz, $CDCl_3$) δ 7.79–7.77 (m, 2H), 7.48–7.46 (m, 2H), 7.25–7.24 (m, 4H), 6.01 (s, 2H), 4.18–4.15 (m, 4H), 4.06–4.04 (m, 4H). ^{13}C NMR (600 MHz, $CDCl_3$) δ 136.8, 132.5, 130.3, 130.1, 127.2, 127.1, 103.6, 65.4. ^{77}Se NMR (600 MHz, $CDCl_3$) δ 411.3. HRMS-TOFEI+: m/z $[M]^+$ calcd for $C_{18}H_{18}O_4{}^{80}Se_2$: 457.9535; found: 457.9557. All data were in agreement with literature values.[22]

Bis(2-formylphenyl)diselenide. Similarly to the bis(2-formylphenyl)ditelluride synthesis, 2,2′-(diselenadi-2,1-phenylene)bis-1,3-dioxolane (1.60 g, 3.5 mmol) and *p*-toluenesulfonic acid (0.41 g, 2.13 mmol) were dissolved in a mixture of distilled water/acetone/distilled THF (120 : 120 : 60 mL) and then refluxed for 2 h. After cooling to room temperature, distilled water (600 mL) was added to the yellow solution; the product was extracted with CH_2Cl_2, and washed with distilled water and then with brine. The yellow solution was dehydrated over anhydrous Na_2SO_4 and concentrated under vacuum to yield a dark yellow crystalline material. No further purification was necessary before the next step, but it can be achieved by precipitation in hexanes from a concentrated solution of CH_2Cl_2 (90%). Mp = 171.2–172.3 °C (d). ^{1}H NMR (600 MHz, $CDCl_3$) δ 10.17 (s, 2H), 7.86–7.84 (m, 2H), 7.83–7.82 (m, 2H), 7.42–7.40 (m, 4H). ^{13}C NMR (600 MHz, $CDCl_3$) δ 193.1, 136.0, 135.0, 134.8, 134.5, 131.2, 126.5. ^{77}Se NMR (600 MHz, $CDCl_3$) δ 456.4. HRMS-TOFEI+: m/z $[M]^+$ calcd for $C_{14}H_{10}O_2{}^{80}Se_2$: 369.9014; found: 369.8999. All data were in agreement with literature values.[23]

2,2′-Diselenabis-benzaldehyde dioxime (3b). A solution of hydroxylamine hydrochloride (0.968 g, 13.9 mmol) and sodium hydroxide (0.58 g, 13.9 mmol) in distilled water (25 mL) was added dropwise into bis(2-formylphenyl)diselenide (1.14 g, 3.10 mmol) dissolved in pyridine (25 mL) at 0 °C under a nitrogen atmosphere. The mixture was stirred at room temperature for 2 h, diluted with 10 mL of CH_2Cl_2 and then washed with distilled water. The yellow organic layer was dehydrated with anhydrous Na_2SO_4 and concentrated under vacuum to yield an oily yellow crude product that can be crystallized at room temperature from dichloromethane by slow addition of hexanes. Yield 86%. Mp 138.5–139.0 °C (d). ^{1}H NMR (600 MHz, DMSO-d_6) δ 11.74 (s, 2H), 8.44 (s, 2H), 7.69 (d, 2H), 7.56 (d, 2H), 7.32–7.27 (m, 4H). ^{13}C NMR (600 MHz, $CDCl_3$) δ 149.0, 131.7, 130.7, 130.3, 129.5, 128.9, 126.6. ^{77}Se NMR (600 MHz, DMSO-d_6) δ 446.3. IR (KBr, $\tilde{\nu}$): 3317, 3039, 2836, 2729, 1584, 1556, 1471, 1436, 1300, 1256, 1208, 1025, 964, 942, 931, 876, 866, 745, 711, 661, 642, 488, 443. Elemental anal. % calcd $C_{14}H_{12}N_2O_2Se_2$: C 42.23, H 3.04, N 7.04; found: C 42.38, H 2.96, N 7.06.

Benzo-1,2-selenazole 2-oxide (2b). 2,2′-Diselenabis-benzaldehyde dioxime (1.23 g, 3.11 mmol) was suspended in methanol (80 mL). The solid that was consumed as I_2 (0.79 g, 3.11 mmol) was added. The red mixture was stirred at room temperature for a period of 2 h, after which 0.1 M $NaHCO_3$ (80 mL) was added and a light yellow solid precipitated. The crude product was re-dissolved and extracted with CH_2Cl_2. The organic layer was washed with distilled water, dehydrated over anhydrous Na_2SO_4 and concentrated under reduced pressure yielding a light-yellow precipitate. Yield 95%. Mp

108.0–112.0 °C (d). ^{1}H NMR (600 MHz, DMSO-d_6) δ 8.33 (s, 1H), 7.83–7.81 (m, 1H), 7.66–7.64 (m, 1H), 7.40–7.34 (m, 2H). ^{13}C NMR (600 MHz, DMSO-d_6) δ 139.5, 134.6, 132.6, 127.0, 126.2, 124.8, 123.4. ^{77}Se NMR (600 MHz, DMSO-d_6) δ 1175.0. HRMS-TOFEI+: m/z $[M]^+$ calcd for $C_7H_5NO^{80}Se$: 198.9536; found: 198.9536. IR (KBr, $\tilde{\nu}$): 3055, 3038, 2964, 2923, 2225, 1585, 1560, 1492, 1428, 1414, 1335, 1308, 1259, 1251, 1199, 1153, 1131, 1094, 1040, 1016, 877, 859, 756, 716. Elemental anal. % calcd C_7H_5NOSe: C 42.44, H 2.54, N 7.07; found: C 42.59, H 2.42, N 6.92.

DFT calculations. All calculations were performed using the ADF DFT package (Version 2013.01).[26,27] Models for **2a**, **2b** and their respective dimers were optimized using the exchange–correlation functionals of Perdew, Burke, and Ernzerhof[28] and corrected for dispersion[29] with a triple-ζ all-electron basis set with two polarization functions each and applying the Zeroth Order Regular Approximation[30–33] formalism with specially adapted basis sets. All frequency calculations were performed to ensure that each geometry was at an actual minimum in the potential energy surface and to derive the corresponding thermodynamic parameters.[34,35]

Conclusions

The procedures here described provide a more convenient entry point to the supramolecular chemistry of iso-chalcogenazole *N*-oxides. Compared to other methods for the preparation of such heterocycles, the synthesis of benzoannulated derivatives is simpler because it only requires two inert-atmosphere steps that can be carried out in sequence without isolation and purification of sensitive intermediates. The crystal structures confirm that these species retain the ability of the parent heterocycles to undergo autoassociation. While self-assembled macrocyclic tetra- and hexamers were obtained from the tellurium compound, a supramolecular polymer was obtained from the selenium heterocycle. DFT-D3 calculations indicate that the chalcogen bonds formed by the selenium compound are much weaker; however, VT NMR spectroscopy provides evidence of its aggregation in solution at low temperature.

Acknowledgements

We gratefully acknowledge funding from the NSERC, OGS and MITACS (Canada) as well as CAPES (Brazil).

Notes and references

1 G. R. Desiraju, P. S. Ho, L. Kloo, A. C. Legon, R. Marquardt, P. Metrangolo, P. Politzer, G. Resnati and K. Rissanen, *Pure Appl. Chem.*, 2013, **85**, 1711–1713.
2 V. R. Pedireddi, D. S. Reddy, B. S. Goud, D. C. Craig, A. D. Rae and G. R. Desiraju, *J. Chem. Soc., Perkin Trans. 2*, 1994, 2353–2360.
3 N. W. Alcock, *Adv. Inorg. Chem. Radiochem.*, 1972, **15**, 1–58.
4 D. B. Werz, T. H. Staeb, C. Benisch, B. J. Rausch, A. Frank Rominger and R. Gleiter, *Org. Lett.*, 2002, **4**, 339–342.
5 R. Gleiter and D. B. Werz, *Chem. Lett.*, 2005, **34**, 126–131.
6 A. Lari, R. Gleiter and F. Rominger, *Eur. J. Org. Chem.*, 2009, 2267–2274.
7 A. F. Cozzolino, P. S. Whitfield and I. Vargas-Baca, *J. Am. Chem. Soc.*, 2010, **132**, 17265–17270.
8 E. A. Suturina, N. A. Semenov, A. V. Lonchakov, I. Y. Bagryanskaya, Y. V. Gatilov, I. G. Irtegova, N. V. Vasilieva, E. Lork, R. Mews, N. P. Gritsan and A. V. Zibarev, *J. Phys. Chem. A*, 2011, **115**, 4851–4860.
9 A. F. Cozzolino, P. J. W. Elder, L. M. Lee and I. Vargas-Baca, *Can. J. Chem.*, 2013, **91**, 338–347.
10 N. A. Semenov, A. V. Lonchakov, N. A. Pushkarevsky, E. A. Suturina, V. V. Korolev, E. Lork, V. G. Vasiliev, S. N. Konchenko, J. Beckmann, N. P. Gritsan and A. V. Zibarev, *Organometallics*, 2014, **33**, 4302–4314.
11 G. E. Garrett, G. L. Gibson, R. N. Straus, D. S. Seferos and M. S. Taylor, *J. Am. Chem. Soc.*, 2015, **137**, 4126–4133.
12 A. F. Cozzolino and I. Vargas-Baca, *J. Organomet. Chem.*, 2007, **692**, 2654–2657.
13 A. Kremer, A. Fermi, N. Biot, J. Wouters and D. Bonifazi, *Chem. – Eur. J.*, 2016, **22**, 5665–5675.
14 G. E. Garrett, E. I. Carrera, D. S. Seferos and M. S. Taylor, *Chem. Commun.*, 2016, **52**, 9881–9884.
15 S. Benz, J. López Andarias, J. Mareda, N. Sakai and S. Matile, *Angew. Chem., Int. Ed.*, 2017, **56**, 812–815.
16 P. C. Ho, P. Szydlowski, J. Sinclair, P. J. W. Elder, J. Kübel, C. Gendy, L. M. Lee, H. Jenkins, J. F. Britten, D. R. Morim and I. Vargas-Baca, *Nat. Commun.*, 2016, **7**, 11299.
17 P. C. Ho, L. M. Lee, H. Jenkins, J. F. Britten and I. Vargas-Baca, *Can. J. Chem.*, 2016, **94**, 453–457.
18 J. Kübel, P. J. W. Elder, H. A. Jenkins and I. Vargas-Baca, *Dalton Trans.*, 2010, **39**, 11126–11128.
19 M. M. J. Smulders, M. M. L. Nieuwenhuizen, T. F. A. de Greef, P. van der Schoot, A. P. H. J. Schenning and E. W. Meijer, *Chem. – Eur. J.*, 2010, **16**, 362–367.
20 T. Ziegler and A. Rauk, *Theor. Chim. Acta*, 1977, **46**, 1–10.
21 T. Ziegler and A. Rauk, *Inorg. Chem.*, 1979, **18**, 1755–1759.
22 T. Ziegler and A. Rauk, *Inorg. Chem.*, 1979, **18**, 1558–1565.
23 Bruker, *SAINT*, Bruker AXS Inc., Madison, Wisconsin, USA, 2012.
24 Bruker, *SADABS*, Bruker AXS Inc., Madison, Wisconsin, USA, 2001.
25 G. M. Sheldrick, *Acta Crystallogr., Sect. C: Cryst. Struct. Commun.*, 2015, **71**, 3–8.
26 G. te Velde, F. M. Bickelhaupt, E. J. Baerends, C. Fonseca Guerra, S. J. A. van Gisbergen, J. G. Snijders and T. Ziegler, *J. Comput. Chem.*, 2001, **22**, 931–967.
27 C. F. Guerra, J. G. Snijders, G. te Velde and E. J. Baerends, *Theor. Chem. Acc.*, 1998, **99**, 391–403.
28 J. P. Perdew, K. Burke and M. Ernzerhof, *Phys. Rev. Lett.*, 1996, **77**, 3865–3868.
29 S. Grimme, *J. Comput. Chem.*, 2006, **27**, 1787–1799.

30 E. van Lenthe, A. Ehlers and E.-J. Baerends, *J. Chem. Phys.*, 1999, **110**, 8943–8953.
31 E. Van Lenthe, R. Van Leeuwen, E. J. Baerends and J. G. Snijders, *Int. J. Quantum Chem.*, 1996, **57**, 281–293.
32 E. Van Lenthe, E. J. Baerends and J. G. Snijders, *J. Chem. Phys.*, 1994, **101**, 9783–9792.
33 E. Van Lenthe, E. J. Baerends and J. G. Snijders, *J. Chem. Phys.*, 1993, **99**, 4597–4610.
34 A. Bérces, R. M. Dickson, L. Fan, H. Jacobsen, D. Swerhone and T. Ziegler, *Comput. Phys. Commun.*, 1997, **100**, 247–262.
35 S. K. Wolff, *Int. J. Quantum Chem.*, 2005, **104**, 645–659.

Chapter 4. Building New Discrete Supramolecular Assemblies through the Interaction of Iso-Tellurazole *N*-Oxides with Lewis Acids and Bases

Original citation: Ho, P. C.; Jenkins, H. A.; Britten, J. F.; Vargas-Baca, I. Building New Discrete Supramolecular Assemblies through the Interaction of Iso-Tellurazole N-Oxides with Lewis Acids and Bases. *Faraday Discuss.* **2017**, *203*, 187–199.

4.1 Preamble

In the most general sense, a ChB is as a type of Lewis acid-base interaction. When these interactions have a significant degree of covalency, ChB acceptors act as Lewis bases and the ChB donors as acids. Therefore, reactions with Lewis acids or bases could compete with formation of the Te···O ChBs from iso-tellurazole N-oxides. However, it is also conceivable that such reagents could be used to build new supramolecular assemblies. Those ideas are investigated in this chapter.

Faraday Discussions

Cite this: *Faraday Discuss.*, 2017, **203**, 187

PAPER View Article Online
View Journal | View Issue

Building new discrete supramolecular assemblies through the interaction of iso-tellurazole N-oxides with Lewis acids and bases†

Peter C. Ho, Hilary A. Jenkins, James F. Britten and Ignacio Vargas-Baca *

Received 21st February 2017, Accepted 7th April 2017
DOI: 10.1039/c7fd00075h

The supramolecular macrocycles spontaneously assembled by iso-tellurazole N-oxides are stable towards Lewis bases as strong as N-heterocyclic carbenes (NHC) but readily react with Lewis acids such as BR_3 (R = Ph, F). The electron acceptor ability of the tellurium atom is greatly enhanced in the resulting O-bonded adducts, which consequently enables binding to a variety of Lewis bases that includes acetonitrile, 4-dimethylaminopyridine, 4,4′-bipyridine, triphenyl phosphine, a N-heterocyclic carbene and a second molecule of iso-tellurazole N-oxide.

Introduction

The ability of σ–hole interactions – most prominently halogen bonding – to influence molecular organization and the properties of crystalline solids is now well established.[1–4] This phenomenon has been successfully applied in other macroscopic assemblies such as liquid crystals.[5] Attention is now turning to the other extreme of size , *i.e.* discrete assemblies of a few molecules with well-defined structures, properties and function. Significant recent developments in this area include the demonstration of anion recognition by rotaxanes,[6,7] bis-tellurophenes,[8] and chelating antimony(III) receptors;[9] the creation of organocatalysts based on halogen[10] and chalcogen bonding;[11] the construction of halogen-bonded molecular capsules[12] and functional macrocycles self-assembled by chalcogen bonding.[13] In the last example, molecules of iso-tellurazole N-oxides such as **1** (Scheme 1), undergo reversible autoassociation through Te···O interactions into annular structures ($\mathbf{1}_4$, $\mathbf{1}_6$, Scheme 2) that are persistent in solution and function

Department of Chemistry and Chemical Biology, McMaster University, 1280 Main Street West, Hamilton, Ontario, Canada L8S 4M1. E-mail: vargas@chemistry.mcmaster.ca

† Electronic supplementary information (ESI) available: DFT-optimised structures. CCDC 1532977, 1532984, 1532985, 1532987, 1532988, 1532989, 1532990, 1532991 and 1532996. For ESI and crystallographic data in CIF or other electronic format see DOI: 10.1039/c7fd00075h

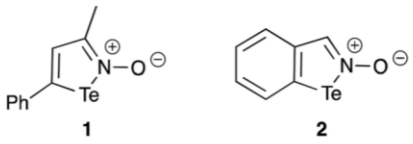

1 2

Scheme 1 Iso-tellurazole N-oxides in this study.

as actual macrocycles able to complex transition metal ions, form adducts with fullerenes, and host small molecules.

Remarkably for molecules with Te–N bonds, these heterocycles and their aggregates are stable in ambient conditions and are tolerant of water. Mineral acids such as HX (X = Cl, Br) protonate the oxygen atom while the halide binds the chalcogen atom yielding X–**1**–H.[14] The process is reversible and is applicable to switching on and off the self-assembly of macrocycles. One of the limitations of these systems is their laborious syntheses which require several steps under an inert atmosphere. In this regard, the benzoannulated derivative **2** (ref. 15) is more convenient because its synthesis is simpler while it displays the same ability to assemble macrocyclic tetramers and hexamers.

Sigma-hole bonding is a particular case of the Lewis acid–base concept. Halogen-bonding acceptors are Lewis bases, and halogen-bonding donors are Lewis acids. Ambiphilic molecules like **1** and **2** that undergo autoassociation are in effect Lewis pairs. Compounds such as 1,2,5-chalcogenadiazoles are so strongly associated in the solid state that coordinating solvents such as pyridine or dimethlylsulfoxide are required to dissolve them and, in some instances, it is possible to isolate the corresponding adducts.[16] Several reports have examined in detail the binding of such heterocycles to neutral and anionic Lewis bases in the solid state[17–19] and in solution.[20]

In this report we examine the interaction of Lewis acids and bases with **1** and **2** to establish in which conditions the Te···O chalcogen bonds are disrupted and whether that process can be exploited in the construction of new discrete supramolecular assemblies. As the end goal is preparative, here we only present products that could be isolated as crystalline solids and thus structurally characterised by X-ray diffraction. The Lewis acids in this case are the boranes BPh_3

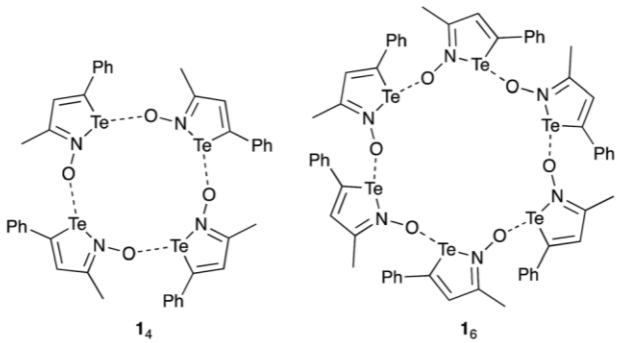

1_4 1_6

Scheme 2 Macrocyclic aggregates of **1**.

and BF_3. The bases include acetonitrile, 4-dimethylamino-pyridine (DMAP), 4,4′-bipyridine (4,4′-bipy), triphenyl-phosphine, and the N-heterocyclic carbene 1,3-bis(2,6-diisopropylphenyl)-1,3-dihydro-2*H*-imidazol-2-ylidene (**3**).

Results and discussion

Spectroscopic and synthetic investigations

In room-temperature experiments, the resonances in the ^{1}H NMR spectra of **1** and **2** exhibited only small changes of position ($<3 \times 10^{-4}$ ppm) upon mixing with a stoichiometric amount of each Lewis base (Fig. S1†). Frequency shifts of comparable magnitude were observed when the solution NMR spectrum of pure iso-tellurazole N-oxides was measured in solvent mixtures of variable composition as the tetramer–hexamer equilibrium is likely influenced by differential solvation of the macrocyclic aggregates. Moreover, the resonances of the Lewis bases were indistinguishable from those in their spectra acquired from the pure compounds. These observations suggest that the integrity of the macrocyclic aggregates of iso-tellurazole N-oxides is not compromised by the Lewis bases, including the N-heterocyclic carbene **3**.

On the other hand, the addition of BR_3 (R = Ph or F) to a solution of **1** immediately caused a colour change from pale yellow to pale orange and the corresponding products could be isolated in crystalline form. Their ^{1}H NMR resonances are shifted to higher frequency (Fig. S2†); mass spectrometry, and single-crystal X-ray diffraction confirmed the identity of the products as the O-bonded borane adducts **1**-BR_3.

In sharp contrast to **1**, **1**-BR_3 (R = Ph, F) readily reacted with Lewis bases. Upon mixing, an immediate colour change from orange to pale yellow was accompanied by marked changes in the ^{1}H NMR spectra. For example, the methyl resonances of **1**-BR_3 shift to lower frequency after the addition of DMAP (Fig. S3†). However, pure products could not be isolated from **1**-BPh_3. From **1**-BF_3, it was possible to isolate DMAP-**1**-BF_3 and BF_3-**1**-4,4′-bipy-**1**-BF_3 as crystalline solids, the latter as an example of a 1 : 2 adduct with a bidentate base. It was also possible to obtain an adduct by the addition of one equivalent of **1** to **1**-BF_3, the product **1**-**1**-BF_3 is effectively a borane capped version of the dimer of an iso-tellurazole N-oxide.

The annulated iso-tellurazole N-oxide **2** also reacts with BF_3 but pure **2**-BF_3 could not be crystallised, instead crystals of CH_3CN-**2**-BF_3 were obtained from acetonitrile solutions. This adduct of acetonitrile with **2**-BF_3 is more soluble than pure **2** and the acetonitrile molecule was readily displaced by other bases. These properties permitted the preparation of Ph_3P-**2**-BF_3, and **3**-**2**-BF_3. The latter is very sensitive to moisture; attempts to isolate the analogue from **1** yielded a solid that quickly transformed into an adduct of O^{2-} and crystallised as $[\mathbf{3}\text{-H}]_2^+[BF_3\text{-}\mathbf{1}\text{-}O\text{-}\mathbf{1}\text{-}BF_3]^{2-}$ and is also very moisture sensitive.

X-ray diffraction structures

Details of the crystallographic determination of the structures of **1**-BR_3 (R = Ph, F) are provided in the ESI.† The most relevant molecular dimensions are compiled in Table 1. There are no structurally characterised examples in literature of non-aggregated iso-tellurazole oxides other than protonated products such as X–**1**–H (X = Cl, Br),[14] even in that case the tellurium atom is bound to the halide anion. In

Table 1 Selected bond distances and angles, and torsion angles of **1**-BR_3 (R = Ph, F)

	1-BPh_3	**1**-BF_3
Bond distances (Å)		
Te1–C1	2.081(2)	2.076(4)
Te1–N1	2.063(2)	2.072(3)
N1–O1	1.355(2)	1.372(4)
O1–B1	1.571(3)	1.480(5)
C1–C2	1.364(3)	1.354(5)
C2–C3	1.425(3)	1.430(6)
C3–N1	1.320(3)	1.313(5)
Bond angles (°)		
N1–Te1–C1	79.63(8)	79.2(1)
O1–N1–Te1	124.2(1)	123.9(2)
Torsion angles (°)		
Te1–N1–O1–B1	72.5(2)	46.0(4)
C1–Te1–N1–O1	175.6(2)	173.1(3)

this regard, the borane adducts **1**-BPh_3, and **1**-BF_3 display inter- and intramolecular contacts to C_{BPh} and F atoms (Fig. 1) shorter than the sums of van der Waals radii. The B–O bond is longer **1**-BPh_3 (1.571(3) Å) than in **1**-BF_3 (1.480(5) Å). Compared to previous measurements for the heterocycles,[13,15] the Te–C distances, 2.081(2) and 2.076(4) Å, are unchanged but the Te–N distances, 2.063(2) and 2.072(3) Å, are longer by more than 0.1 Å and the C–Te–N angles, 79.63(8)° and 79.2(1)°, are wider by more than 2°.

The crystallographic analyses confirmed that in the other compounds the bases do form Te···LB chalcogen bonds with the iso-tellurazole heterocycle. All crystallographic details are included in the ESI;† selected molecular dimensions are compiled in Table 2 and ORTEPs are presented in Fig. 2.

The geometry around the chalcogen atoms is approximately T-shaped but the N–Te···LB ranges only from 162.44(5)° in CH_3CN-**2**-BF_3 to just 168.48(6)° in Ph_3P-**2**-BF_3. Scaled to the sum of van der Waals radii, the length of the chalcogen bonds varies from 58% in **3**-**2**-BF_3 to 68% in CH_3CN-**2**-BF_3 and Ph_3P-**2**-BF_3. In most cases there is an inverse correlation between the distance from Te to N and LB. In **3**-**2**-BF_3 and especially in $[BF_3$-**1**-*O*-**1**-$BF_3]^{2-}$ the Te1···LB distance is nearly equal to the sum of covalent radii and the Te–N1 distance is so long (>2.4 Å) that the roles of N

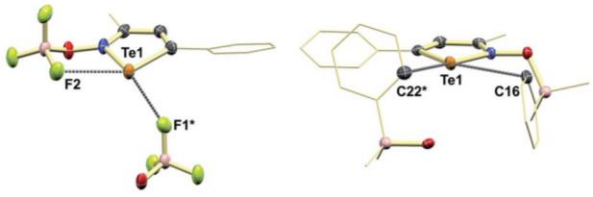

Fig. 1 ORTEP (75%) detail of the crystal structures of **1**-BR_3 (R = Ph, F). Te1···C16 3.253 Å, Te1···C22* 3.445 Å, *cf.* $\Sigma r_{vdW} = 3.76$ Å. Te1···F2 3.253 Å, Te1···F1* 3.445 Å, *cf.* $\Sigma r_{vdW} = 3.53$ Å. All hydrogens are omitted and portions of the structure are simplified for clarity.

Table 2 Selected bond distances and angles from the adducts formed by **1**-BF_3 and **2**-BF_3 with Lewis bases

	CH_3CN-**2**-BF_3	DMAP-**1**-BF_3	BF_3-**1**-4,4′-bipy-**1**-BF_3	Ph_3P-**2**-BF_3	**3**-**2**-BF_3	**1**-**1**-BF_3	$[BF_3$-**1**-*O*-**1**-$BF_3]^{2-}$
Bond distances (Å)							
Te1···LB[a]	2.463(2)	2.251(3), 2.262(3)	2.332(2)	2.6072(9)	2.179(9)	2.194(6)	2.014(3)
% Σr_{cov}	118%	108%, 108%	112%	106%	103%	108%	99%
% Σr_{vdW}	68%	62%, 63%	65%	68%	58%	61%	56%
Te1–C1	2.097(1)	2.101(3), 2.105(3)	2.109(3)	2.126(3)	2.15(1)	2.112(9)	2.099(4), 2.106(6)
Te1–N1	2.156(2)	2.266(3), 2.267(3)	2.219(2)	2.409(2)	2.489(8)	2.221(5)	2.409(3), 2.488(4)
N1–O1	1.378(2)	1.376(3), 1.379(4)	1.378(2)	1.367(3)	1.34(1)	1.374(9)	1.386(5), 1.397(5)
O1–B1	1.494(2)	1.482(5), 1.490(5)	1.498(3)	1.485(5)	1.44(2)	1.50(1)	1.484(8), 1.489(6)
C1–C2	1.414(2)	1.348(4), 1.356(4)	1.350(3)	1.411(4)	1.46(2)	1.35(1)	1.338(6), 1.354(6)
C2–C3	1.436(2)	1.449(4), 1.456(4)	1.441(3)	1.458(4)	1.39(2)	1.43(1)	1.448(7), 1.450(6)
C3–N1	1.293(2)	1.298(4), 1.299(4)	1.302(3)	1.280(4)	1.29(2)	1.29(1)	1.285(7), 1.297(6)
$Te2^b$–$C11^b$						2.089(9)	
$Te2^b$–$N2^b$						2.082(6)	
$N2^b$–$O2^b$						1.346(9)	
$C11^b$–$C12^b$						1.36(1)	
$C12^b$–$C13^b$						1.43(1)	
$C13^b$–$N2^b$						1.32(1)	
Bond angles (°)							
N1–Te1–LB[a]	162.44(5)	164.0(1), 165.2(1)	163.37(8)	168.48(6)	167.7(3)	165.8(2)	166.0(1), 165.3(1)
N1–Te1–C1	77.70(5)	75.6(1)	76.10(8)	74.3(1)	74.7(3)	76.2(3)	72.3(1), 72.7(2)
C1–Te1–LB[a]	85.34(6)	88.7(1)	87.29(8)	94.78(8)	93.0(4)	90.4(3)	92.6(2), 93.9(1)
O1–N1–Te1	125.7(1)	129.2(2), 129.4(2)	129.0(1)	130.4(2)	133.1(6)	128.0(5)	131.8(3), 133.9(2)
$N2^b$–$Te2^b$–$C11^b$						79.0(3)	
$O2^b$–$N2^b$–$Te2^b$						124.2(5)	

Table 2 (*Contd.*)

	CH_3CN-**2**-BF_3	DMAP-**1**-BF_3	BF_3-**1**-4,4′-bipy-**1**-BF_3	Ph_3P-**2**-BF_3	**3**-**2**-BF_3	**1**-**1**-BF_3	$[BF_3$-**1**-*O*-**1**-$BF_3]^{2-}$
Torsion angles (°)							
Te1–N1–O1–LB[a]	51.9(2)	10.6(4), 30.2(4)	24.6(3)	25.1(3)	15(1)	14.9(9)	13.7(5), 34.8(5)
LB[a]–Te1–N1–O1	157.8(2)	168.8(3), 177.6(3)	177.8(2)	156.8(2)	179(1)	158.4(7)	164.6(4), 173.9(4)
C1–Te1–N1–O1	173.2(1)	174.4(3), 179.0(3)	174.9(2)	176.6(2)	179(1)	177.5(7)	170.6(4), 176.7(4)
C11[b]–Te2[b]–N2[b]–O2[b]						179.7(6)	

[a] LB denotes the atom of the chalcogen-bond acceptor atom, *i.e.* the atom of the Lewis base linked to tellurium. [b] Denotes atoms in the molecule of **1** acting as a Lewis base in **1**-**1**-BF_3.

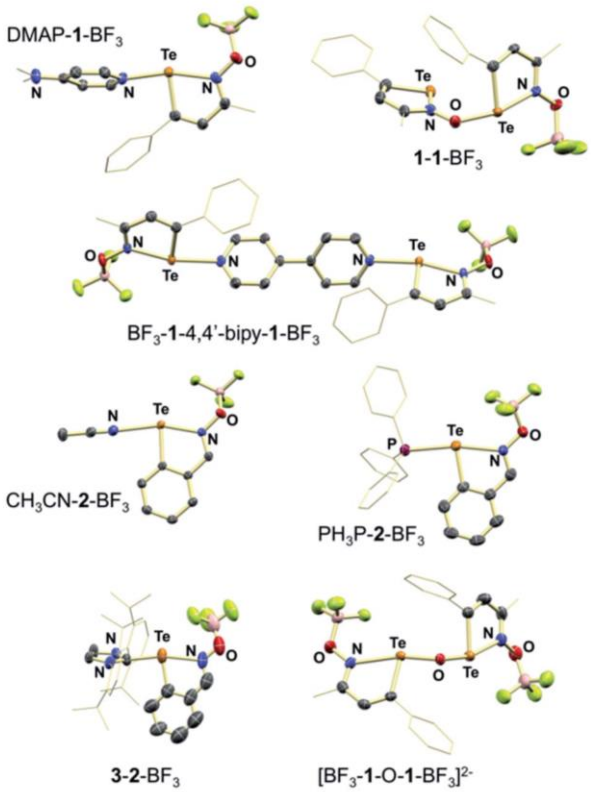

Fig. 2 ORTEP (75%) representation of the compounds structurally characterised. All hydrogens are omitted and portions of the structure are simplified for clarity.

and LB are practically swapped, N1 can be regarded as the chalcogen bond acceptor atom. However, Ph_3P-**2**-BF_3 stands out having one of the longest Te–N1 distances with a Te–P distance about 68% of the sum of van der Waals radii.

The case of **1**-**1**-BF_3 is particularly interesting as it features two iso-tellurazole-oxide moieties in two different roles, one as chalcogen-bond acceptor and the other as the donor; alternatively, they could be identified as the Lewis base and the Lewis acid. Indeed, the bond distances and angles around tellurium in the terminal heterocycle are comparable to those observed in **1**-BR_3 (R = Ph, F) and in the middle ring the structural parameters are similar to the measurements from the other Lewis base adducts.

Table 3 Maximum electrostatic potential on the 10^{-3} a.u. isodensity surface and frontier orbital energies of **1** and **2** and their borane adducts

	1	**1**-BPh_3	**1**-BF_3	**2**	**2**-BF_3
V_{max} (a.u.) × 10^{-2}	3.4	4.7	4.7	5.3	8.6
V_{max} (kJ mol^{-1})	89.3	94.5	147.0	139.6	225.8
E_{LUMO} (eV)	−3.03	−3.03	−3.31	−3.30	−3.55

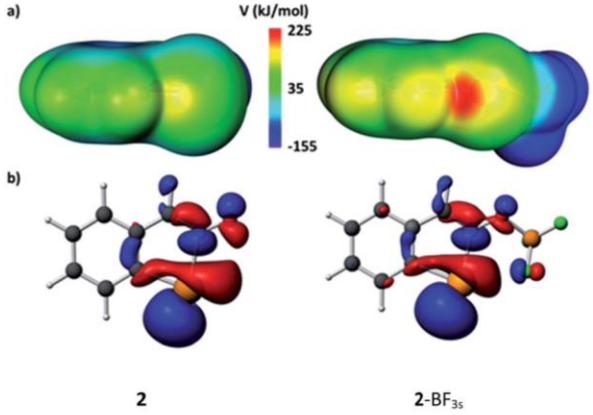

Fig. 3 (a) Maps of electrostatic potential on the isosurface of 10^{-3} a.u. electron density for **2** and **2**-BF_3. (b) LUMO of **2** and **2**-BF_3 plotted at 0.04 a.u.

Computational analysis

DFT calculations (PBE-D3, ZORA, TZ2P) were carried out to assess the strength of the interactions of the Lewis bases with the borane adducts of iso-tellurazole N-oxides. In the first instance, the impact of borane binding on the electron acceptor abilities of **1** and **2** was evaluated by its effect on the σ holes and the LUMO energies of these molecules; the results are compiled in Table 3 and are depicted graphically for **2** and **2**-BF_3 in Fig. 3. The maps of electrostatic potential and the composition of the LUMO both indicate that the preferred point of

Table 4 Energy decomposition analysis, degree of charge transfer (Hirschfeld), and the Te···LB bcp densities for the interaction of Lewis bases with **1**-BF_3 and **2**-BF_3. All energy values are in kJ mol^{-1} unless otherwise stated

	CH_3CN-**2**-BF_3	DMAP-**1**-BF_3	BF_3-**1**-4,4′-bipy-**1**-BF_3	Ph_3P-**2**-BF_3	**3**-**2**-BF_3	**1**-**1**-BF_3	[BF_3-**1**-*O*-**1**-BF_3]$^{2-}$
E_{elstat}	−81.59	−233.26	−163.20	−266.91	−463.09	−290.06	−344.98
E_{Pauli}	96.48	304.16	224.45	398.71	644.48	448.61	635.65
E_{steric}	14.89	70.90	61.25	131.8	181.39	158.55	290.68
$E_{orbital}$	−50.67	−147.51	−105.28	−229.94	−351.08	−246.67	−1072.72
$E_{dispersion}$	−6.06	−22.38	−28.15	−30.11	−55.34	−27.47	−29.37
$E_{Te\cdots LB}$	−41.84	−98.99	−72.18	−128.25	−225.03	−115.59	−811.41
$E_{preparation}$	2.81	19.57	22.31	37.76	54.64	28.39	477.49
E_{total}	−39.03	−79.42	−49.87	−90.49	−170.39	−87.20	−333.92
ΔZPE × 10^{-2} [eV]	2.54	4.80	3.10	2.80	4.20	2.66	4.24
ΔH	−36.24	−77.16	−49.26	−89.35	−165.29	−86.94	−334.35
ΔS [J mol^{-1} K^{-1}]	−130.59	−215.84	−244.94	−213.26	−205.39	−223.61	−246.43
$\Delta G_{273.15\ K}$	2.69	−12.81	23.77	−25.74	−104.05	−20.26	−260.88
Δq (a.u.)	0.07	0.20	0.14	0.24	0.27	0.07	0.69
ρ_{BCP} (Te···LB) (a.u.) × 10^{-2}	2.72	5.44	4.38	5.69	7.77	6.72	10.9

attachment of a base is not collinear with the Te–N bond, in agreement with the observations. According to the calculations, binding of BF_3 increases the maximum of potential at the σ holes by more than 60% and stabilizes the LUMO by at least 0.25 eV. The effect of BPh_3 on **1** is smaller but not negligible.

The energetic contributions to the interaction of Lewis bases with **1**-BF_3 and **2**-BF_3 were analysed under the Ziegler–Rauk transition-state approach,[21–23] the details of which are discussed elsewhere.[15] Under this scheme the total interaction (E_{total}) is the combination (eqn (1)) of the electrostatic interaction (E_{elstat}), Pauli repulsion (E_{Pauli}) and orbital interaction ($E_{orbital}$) supplemented by ($E_{dispersion}$) and geometric distortion ($E_{preparation}$) contributions. The sum of electrostatic and Pauli repulsion is called the total steric interaction (E_{steric}) and quantifies the electronic interaction without polarization or covalency. All calculated contributions are compiled in Table 4. For the 1 : 2 adducts, the analyses refer to the interactions between BF_3-**1**-4,4′-bipy and **1**-BF_3, and between $[BF_3$-**1**-$O]^{2-}$ and **1**-BF_3.

$$\begin{aligned} E_{total} &= E_{elstat} + E_{Pauli} + E_{orbital} + E_{dispersion} + E_{preparation} \\ &= E_{steric} + E_{orbital} + E_{dispersion} + E_{preparation} \\ &= E_{Te\cdots LB} + E_{preparation} \end{aligned} \quad (1)$$

In general, a weak long Te···LB chalcogen bond would be predominantly controlled by the electrostatic interaction between the LB electrons and the σ hole on the chalcogen. As the attractive interaction becomes stronger, the distance decreases and the molecules become increasingly polarized until orbital mixing (covalency) ensues, further strengthening the Te···LB link. Therefore, it is reasonable to regard the lengthening of the bond opposite to the σ–hole interaction as an indicator of strength. The total energies of interaction, degrees of electron transfer and Atoms-In-Molecules (AIM) electron densities at the bond critical point (ρ_{bcp}) seem to agree with such qualitative arguments. Being the stronger bases, the carbene **3** and $[BF_3$-**1**-$O]^{2-}$ give the largest energies of interaction and bcp densities. However, in spite of the similarities in all the energetic contributions to the Te···LB interactions in Ph_3P-**2**-BF_3 and **1**-**1**-BF_3 the effect of the phosphine and the iso-tellurazole N-oxide on the Te–N1 distance is very different.

Experimental

Materials and methods

Organic solvents were purified either by distillation over the appropriate dehydrating agents under nitrogen or using an Innovative Technology purification system. Compounds **1** (ref. 13) and **2** (ref. 15) were prepared as previously described. The following chemicals were used as received from the commercial suppliers: *N*,*N*′-bis(2,6 diisopropyl-phenyl)imidazol-2-ylidene (Strem), DMSO-d_6 (Aldrich), triphenylborane (Strem). 4-Dimethylaminopyridine (Aldrich), triphenylphosphine (Aldrich), and 4.4′-bipyridine (Aldrich) were recrystallized from anhydrous toluene and sublimed under vacuum. Combustion elemental analyses were carried out by the London Metropolitan University elemental analysis service (London, United Kingdom).

Syntheses

All compounds were prepared by mixing the reagents at room temperature under an atmosphere of nitrogen. Proportions, work up and characterization are

described below. The ^{125}Te NMR resonance could not be observed in many cases due to limited solubility of the samples.

1-BF_3

3-Methyl-5-phenyl-1,2-tellurazole N-oxide (**1**, 100 mg, 0.35 mmol), 0.81 M $BF_3 \cdot Et_2O$ (0.43 mL, 0.35 mmol), chloroform (1.15 g). The product was recrystallized from chloroform, centrifuged and dried under vacuum. Yield 92%. ^{1}H NMR (600 MHz, CD_2Cl_2, δ ppm): 7.58 (s, 1H); 7.56–7.49 (m, 3H); 7.45–7.42 (m, 2H); 2.73 (s, 3H). ^{13}C NMR (600 MHz, CD_2Cl_2, δ ppm): 169.76 (s, 1C); 169.25 (s, 1C); 135.53 (s, 1C); 132.03 (s, 1C); 130.30 (s, 2C); 127.64 (s, 2C); 123.01 (s, 1C); 18.63 (s, 1C). ^{125}Te NMR (600 MHz, CD_2Cl_2, δ ppm): 2116.47. Mp: 175.5–178.2 °C. Elemental anal. calcd $C_{10}H_9BF_3NOTe$: C 33.87, H 2.56, N 3.95; found: C 33.70, H 2.38, N 3.98.

1-BPh_3

3-Methyl-5-phenyl-1,2-tellurazole N-oxide (**1**, 100 mg, 0.35 mmol), BPh_3 (84.7 mg, 0.35 mmol), chloroform (1.15 g). The product was recrystallized in a mixture of chloroform : hexanes (1 : 2 v/v), centrifuged and dried under vacuum. Yield 79%. ^{1}H NMR (600 MHz, 19.2 mg in 0.8 mL CD_2Cl_2, δ ppm): 7.54–7.52 (m, 6H); 7.43–7.32 (m, 4H); 7.26–7.22 (m, 8H); 7.19–7.17 (m, 3H); 2.65 (s, 3H). ^{13}C NMR (600 MHz, 19.2 mg in 0.8 mL CD_2Cl_2, δ ppm): 166.47 (s, 1C); 164.95 (s, 1C); 136.88 (s, 3C); 134.99 (s, 6C); 134.59 (s, 1C); 130.53 (s, 3C); 129.58 (s, 2C); 128.14 (s, 1C); 127.92 (s, 6C); 126.18 (s, 2C); 122.50 (s, 1C); 19.13 (s, 1C). Mp: 115.2–118.2 °C.

CH_3CN-2-BF_3

Benzo-1,2-tellurazole 2-oxide (**2**, 100 mg, 0.405 mmol) in acetonitrile (2 mL), 0.81 M $BF_3 \cdot Et_2O$ (0.5 mL, 0.405 mmol) in chloroform (1 mL). The mixture was stirred for 1 h and the product was centrifuged and dried under vacuum. Yield 94%. ^{1}H NMR (600 MHz, CD_2Cl_2, δ ppm): 9.09 (s, 1H); 8.11 (d, 1H); 8.01 (d, 1H); 7.60 (dt, 1H); 7.54 (dt, 1H); 2.13 (s, 3H). ^{13}C NMR (600 MHz, CD_2Cl_2, δ ppm): 155.5 (s, 1C); 139.8 (s, 1C); 132.3 (s, 1C); 131.8 (s, 1C); 131.4 (s, 1C); 131.4 (s, 1C); 128.2 (s, 1C); 117.2 (s, 1C); 2.2 (s, 1C). Mp: 134.1–136.2 °C. Elemental anal. calcd $C_9H_8BF_3N_2OTe$: C 30.40, H 2.27, N 7.88; found: C 30.52, H 2.19, N 8.02.

DMAP-1-BF_3

1-BF_3 (38.4 mg, 0.11 mmol) in dichloromethane (1.66 g), 4-dimethylaminopyridine (20.2 mg, 0.16 mmol) in dichloromethane (0.50 g). The product was precipitated with hexanes, centrifuged and dried under vacuum. Yield 98%. ^{1}H NMR (600 MHz, 10.2 mg in 0.8 mL CD_2Cl_2, δ ppm): 7.77 (s, 2H); 7.14 (s, 1H); 7.10 (s, 5H); 6.21 (s, 2H); 3.01 (s, 6H); 2.37 (s, 3H). ^{13}C NMR (600 MHz, 10.2 mg in 0.8 mL CD_2Cl_2, δ ppm): 161.31 (s); 155.29 (bs); 148.52 (bs); 140.19 (s); 129.12 (s); 128.06 (s); 127.19 (s); 107.40 (s), 39.70 (bs), 17.00 (s). Mp: 152.4–155.0 °C. Elemental anal. calcd $C_{17}H_{19}BF_3N_3OTe$: C 42.83, H 4.02, N 8.81; found: C 42.94, H 3.85, N 8.89.

BF_3-1-4,4′-bipy-1-BF_3

1-BF_3 (45.4 mg, 0.13 mmol) in dichloromethane (1.8 g), 4,4′-bipyridine (10 mg, 0.064 mmol). The product was precipitated with hexanes, centrifuged and dried

under vacuum. Yield 98%. ^{1}H NMR (600 MHz, CD_2Cl_2, δ ppm): 8.53 (d, 4H); 7.43 (d, 4H); 7.39 (s, 2H); 7.29–7.27 (m, 10H); 2.60 (s, 6H). ^{13}C could not be measured due to low solubility. Mp: 233.6–235.0 °C. Elemental anal. calcd $C_{30}H_{26}B_2F_6N_4O_2Te_2$: C 41.64, H 3.03, N 6.47; found: C 41.46, H 3.15, N 6.39.

2[3-*H*]·[BF_3-1-*O*-1-BF_3]

1-BF_3 (10 mg, 0.028 mmol) in benzene-d_6 (2 g), 1,3-bis(2,6-diisopropylphenyl)-1,3-dihydro-2*H*-imidazol-2-ylidene (**3**, 10.8 mg, 0.028 mmol). The product was centrifuged and dried under vacuum. Yield 80%. ^{1}H NMR (600 MHz, CD_2Cl_2, δ ppm): 8.65 (s, 2H); 7.73 (s, 4H); 7.64 (t, 4H); 7.42 (d, 8H); 7.33–7.12 (bm, 10H); 6.81 (bs, 1H), 6.59 (bs, 1H), 2.39 (sept, 8H); 2.04 (bs, 3H); 1.91 (bs, 3H); 1.29 (d, 24); 1.21 (d, 24H). ^{13}C NMR (700 MHz, CD_2Cl_2, δ ppm): 145.4 (s); 137.8 (s); 132.9 (s); 129.9 (s) 129.4 (bs); 128.0 (bs); 127.6 (bs); 127.4 (bs); 126.6 (s); 125.4 (s); 125.2 (bs); 29.6 (s); 24.7 (s); 24.0 (s); 16.2 (bs). Mp: 122.5–125.6 °C. Despite the crystallographic determination, repeated attempts failed to provide a satisfactory elemental analysis due to moisture sensitivity.

Ph_3P-2-BF_3

2-BF_3 (29.8 mg, 0.084 mmol) in toluene (6.3 g), triphenylphosphine (34.2 mg, 0.130 mmol) in dichloromethane (7.3 g). The product was precipitated upon evaporation, centrifuged and dried under vacuum. Yield 95%. Note: Ph_3P-**2**-BF_3 appears to be partly dissociated in solution; an excess of phosphine is required for isolation. Consequently, small amounts of phosphine contaminate the product, as made evident by combustion analyses. Recrystallization attempts mostly yield the reactants. Crude yield 82%. ^{1}H NMR (600 MHz, 21.4 mg in 0.8 mL CD_2Cl_2, δ ppm): 8.688 (d, 1H); 7.67–7.57 (m, 16H); 7.33 (t, 1H); 7.15 (d, 1H), 6.90 (t, 1H). ^{13}C NMR (700 MHz, CD_2Cl_2, δ ppm): 149.7 (s, 1C); 135.1 (s, 1C); 134.7 (s, 1C); 134.2 (s, 6C); 134.1 (s, 6C); 133.7 (s, 3C); 131.4 (s, 1C); 130.6 (s, 3C); 130.2 (s, 1C); 128.0 (s, 1C); 123.9 (s, 1C). Mp: 152.1–154.2 °C.

3-2-BF_3

2-BF_3 (28.7 mg, 0.081 mmol) in dichloromethane (7.5 g), **3** (31.4 mg, 0.081 mmol) in benzene (7.5 mL). The product was precipitated by evaporation of the dichloromethane under vacuum, it was centrifuged and dried under vacuum. Yield 85%. ^{1}H NMR (600 MHz, 40 : 60 v/v CD_2Cl_2 : C_6D_6, δ ppm): 8.57 (s, 1H); 7.85 (t, 2H); 7.70 (d, 1H), 7.66–7.65 (m, 5H); 7.62 (d, 1H); 7.52–7.50 (m, 3H); 2.94 (hept, 4H), 1.72 (d, 12H), 1.58 (d 12H). Mp: 260 °C (d). ^{13}C could not be observed due to low solubility. Despite the crystallographic determination, repeated attempts failed to provide a satisfactory elemental analysis due to moisture sensitivity.

1-1-BF_3

1-BF_3 (10 mg, 0.028 mmol) in benzene (2 g), **1** (8.1 mg, 0.028 mmol). The product crystalized slowly after mixing, it was centrifuged and dried under vacuum. Yield 75%. ^{1}H NMR (700 MHz, CD_2Cl_2, δ ppm): 7.55 (s, 1H); 7.41–7.32 (m, 10H); 7.21 (s, 1H); 2.45 (s, 3H); 1.88 (s, 3H). ^{13}C NMR (700 MHz, CD_2Cl_2, δ ppm): 163.4 (s, 1C); 160.2 (s, 1C); 158.1 (s, 1C); 138.0 (s, 1C); 136.9 (s, 1C); 129.9 (s, 1C); 129.2 (s, 2C); 129.1 (s, 2C); 128.8 (s, 1C); 128.3 (s, 1C); 127.9 (s, 2C), 127.3 (s, 2C), 126.9 (s, 1C),

125.0 (s, 1C); 17.0 (s, 1C), 16.4 (s, 1C). Mp: 180.1–182.0 °C. Elemental anal. calcd $C_{20}H_{18}BF_3N_2O_2Te_2$: C 37.45, H 2.83, N 4.37; found: C 37.48, H 2.74, N 4.41.

DFT calculations

All calculations were performed using the ADF DFT package (Version 2013.01).[24,25] All models were optimized using the exchange–correlation functionals of Perdew, Burke, and Ernzerhof[26] and corrected for dispersion[27] with a triple-ζ all-electron basis set with two polarization functions each and applying the Zeroth Order Regular Approximation[28–31] formalism with specially adapted basis sets. Frequency calculations were performed to ensure that each geometry was at an actual minimum in the potential energy surface and to derive the corresponding thermodynamic parameters.[32,33]

Conclusions

The supramolecular macrocycles assembled by iso-tellurazole oxides appear to be remarkably impervious to bases as strong as N-heterocyclic carbenes. This is puzzling considering the fast equilibrium that takes place in solution between tetramers and hexamers in solution. In contrast, BR_3 (R = Ph, F) boranes yielded 1 : 1 O-bonded adducts that readily form strong chalcogen bonds with Lewis bases. In this way, it is possible to obtain new adducts and even stabilize an unusual chalcogen-bonded dimer of iso-tellurazole N-oxide. These reactions will be particularly useful in guiding the combination of iso-tellurazole N-oxides with other building blocks to build supramolecular structures beyond halogen bonding.

Acknowledgements

We gratefully acknowledge funding from the Natural Science and Engineering Research Council of Canada and the Ontario Graduate Scholarship program.

Notes and references

1 K. Rissanen, *CrystEngComm*, 2008, **10**, 1107–1113.
2 P. Metrangolo, F. Meyer, T. Pilati, G. Resnati and G. Terraneo, *Angew. Chem., Int. Ed.*, 2008, **47**, 6114–6127.
3 P. Metrangolo and G. Resnati, *Science*, 2008, **321**, 918–919.
4 K. Raatikainen and K. Rissanen, *Chem. Sci.*, 2012, **3**, 1235–1239.
5 A. Priimagi, M. Saccone, G. Cavallo, A. Shishido, T. Pilati, P. Metrangolo and G. Resnati, *Adv. Mater.*, 2012, **24**, OP345–OP352.
6 M. J. Langton, S. W. Robinson, I. Marques, V. Félix and P. D. Beer, *Nat. Chem.*, 2014, **6**, 1039–1043.
7 T. A. Barendt, A. Docker, I. Marques, V. Félix and P. D. Beer, *Angew. Chem., Int. Ed.*, 2016, **55**, 11069–11076.
8 G. E. Garrett, E. I. Carrera, D. S. Seferos and M. S. Taylor, *Chem. Commun.*, 2016, **52**, 9881–9884.
9 J. Qiu, D. K. Unruh and A. F. Cozzolino, *J. Phys. Chem. A*, 2016, **120**, 9257–9269.

10 F. Kniep, S. H. Jungbauer, Q. Zhang, S. M. Walter, S. Schindler, I. Schnapperelle, E. Herdtweck and S. M. Huber, *Angew. Chem., Int. Ed.*, 2013, **52**, 7028–7032.
11 S. Benz, J. López Andarias, J. Mareda, N. Sakai and S. Matile, *Angew. Chem., Int. Ed.*, 2017, **56**, 812–815.
12 N. K. Beyeh, F. Pan and K. Rissanen, *Angew. Chem., Int. Ed.*, 2015, **54**, 7303–7307.
13 P. C. Ho, P. Szydlowski, J. Sinclair, P. J. W. Elder, J. Kübel, C. Gendy, L. M. Lee, H. Jenkins, J. F. Britten, D. R. Morim and I. Vargas-Baca, *Nat. Commun.*, 2016, **7**, 11299.
14 P. C. Ho, L. M. Lee, H. Jenkins, J. F. Britten and I. Vargas-Baca, *Can. J. Chem.*, 2016, **94**, 453–457.
15 P. C.-W. Ho, J. Rafique, J. Lee, M. L. Lee, H. A. Jenkins, J. F. Britten, A. L. Braga and I. Vargas-Baca, *Dalton Trans.*, 2017, **46**, 6570.
16 A. F. Cozzolino, P. S. Whitfield and I. Vargas-Baca, *J. Am. Chem. Soc.*, 2010, **132**, 17265–17270.
17 N. A. Semenov, A. V. Lonchakov, N. A. Pushkarevsky, E. A. Suturina, V. V. Korolev, E. Lork, V. G. Vasiliev, S. N. Konchenko, J. Beckmann, N. P. Gritsan and A. V. Zibarev, *Organometallics*, 2014, **33**, 4302–4314.
18 N. A. Semenov, A. V. Lonchakov, N. P. Gritsan and A. V. Zibarev, *Russ. Chem. Bull.*, 2015, **64**, 499–510.
19 J. L. Dutton and P. J. Ragogna, *Inorg. Chem.*, 2009, **48**, 1722–1730.
20 G. E. Garrett, G. L. Gibson, R. N. Straus, D. S. Seferos and M. S. Taylor, *J. Am. Chem. Soc.*, 2015, **137**, 4126–4133.
21 T. Ziegler and A. Rauk, *Theor. Chim. Acta*, 1977, **46**, 1–10.
22 T. Ziegler and A. Rauk, *Inorg. Chem.*, 1979, **18**, 1755–1759.
23 T. Ziegler and A. Rauk, *Inorg. Chem.*, 1979, **18**, 1558–1565.
24 G. te Velde, F. M. Bickelhaupt, E. J. Baerends, C. Fonseca Guerra, S. J. A. van Gisbergen, J. G. Snijders and T. Ziegler, *J. Comput. Chem.*, 2001, **22**, 931–967.
25 C. F. Guerra, J. G. Snijders, G. te Velde and E. J. Baerends, *Theor. Chem. Acc.*, 1998, **99**, 391–403.
26 J. P. Perdew, K. Burke and M. Ernzerhof, *Phys. Rev. Lett.*, 1996, **77**, 3865–3868.
27 S. Grimme, *J. Comput. Chem.*, 2006, **27**, 1787–1799.
28 E. van Lenthe, A. Ehlers and E.-J. Baerends, *J. Chem. Phys.*, 1999, **110**, 8943–8953.
29 E. Van Lenthe, R. Van Leeuwen, E. J. Baerends and J. G. Snijders, *Int. J. Quantum Chem.*, 1996, **57**, 281–293.
30 E. Van Lenthe, E. J. Baerends and J. G. Snijders, *J. Chem. Phys.*, 1994, **101**, 9783–9792.
31 E. Van Lenthe, E. J. Baerends and J. G. Snijders, *J. Chem. Phys.*, 1993, **99**, 4597–4610.
32 A. Bérces, R. M. Dickson, L. Fan, H. Jacobsen, D. Swerhone and T. Ziegler, *Comput. Phys. Commun.*, 1997, **100**, 247–262.
33 S. K. Wolff, *Int. J. Quantum Chem.*, 2005, **104**, 645–659.

Chapter 5. Macrocyclic Complexes of Pt(II) and Rh(III) with Iso-Tellurazole: *N*-Oxides

Original citation: Ho, P. C.; Bui, R.; Cevallos, A.; Sequeira, S.; Britten, J. F.; Vargas-Baca, I. Macrocyclic Complexes of Pt(II) and Rh(III) with Iso-Tellurazole: *N*-Oxides. *Dalton Trans.* **2019**, *48*, 4879–4886.

5.1 Preamble

Coordination complexes of the tellurium analogues of crown ethers and related macrocycles are rare. Synthetic difficulties are one major reason; another is that the Te-C bond is easily cleaved after coordination of a metal ion to the chalcogen. The few published examples have relied on the use of other donor atoms, such as nitrogen, to stabilize the complex. These facts sharply contrast with how readily Pd(II) formed a complex with the tetramer of the iso-tellurazole *N*-oxide **1b**$_4$.[18] However, it was uncertain how stable the [Pd(**1b**$_4$)](BF$_4$)$_2$ metal complex is in solution because it has a very low solubility. Its crystal structure displayed significant metal depletion; single crystals grown by diffusion of the reactants contained a significant proportion of free macrocycle. A platinum analogue was even less soluble and could not be crystallized. The article contained in this chapter presents an iso-tellurazole *N*-oxide, **1c**, functionalized with a di-*tert*-butylphenyl groups to increase the solubility of its aggregates and their complexes. This compound was employed to produce a soluble complex with platinum (II). Multinuclear NMR spectroscopy was then employed to characterize the compound in solution. Similarly, a soluble complex of **1b**$_4$ with rhodium (III) was isolated and studied in solution.

Dalton Transactions

PAPER

View Article Online
View Journal | View Issue

Cite this: *Dalton Trans.*, 2019, **48**, 4879

Macrocyclic complexes of Pt(II) and Rh(III) with iso-tellurazole *N*-oxides†

Peter C. Ho, Robert Bui, Alberto Cevallos, Shanel Sequeira, James F. Britten and Ignacio Vargas-Baca *

Received 1st February 2019,
Accepted 11th March 2019

DOI: 10.1039/c9dt00500e

rsc.li/dalton

Pt(II) and Rh(III) readily form complexes with 3-methyl-5-aryl-1,2-tellurazole 2-oxides (L = (3-Me-5-Ar-1,2-$C_3HTe(NO)$). The aryl group is either phenyl or 3,5-di-*tert*-butylphenyl, the latter case being a new derivative with enhanced solubility. The compound $[Pt(3\text{-}Me\text{-}5\text{-}(3,5\text{-}^tBu_2C_6H_3)\text{-}1,2\text{-}C_3HTe(NO))_4](BF_4)_2$ crystallizes in the $P2_1/C$ space group featuring a square planar complex in the lattice. The crystal of $[RhCl_2(3\text{-}Me\text{-}5\text{-}(C_6H_5)\text{-}1,2\text{-}C_3HTe(NO))_4](BF_4)$ belongs to the $I\bar{4}$ space group and contains an octahedral complex. In both instances, the iso-tellurazole *N*-oxide molecules are linked by Te···O chalcogen bonding interactions confirming an annular tetramer that binds the metal ion as a κ^4Te macrocycle in a boat conformation. Low-frequency shifts of the ^{125}Te magnetic resonance upon coordination and the observation of ^{125}Te–^{195}Pt and ^{125}Te–^{103}Rh ^1J coupling constants indicate that the complexes are stable species in solution. The complex ions were also observed in the electrospray mass spectra.

Introduction

The current surge of interest in chalcogen bonding (ChB),[1–3] *i.e.* the interactions of electron-rich centers with electrophilic sites on molecules containing heavy group-16 elements, has resulted in an impressive set of reports in areas as diverse as the construction of supramolecular structures,[4–7] hydrogen transfer catalysis,[8] anion transport across membranes,[9] anion recognition[10,11] and functional materials.[12]

Amongst the molecular building blocks often employed in ChB, the iso-tellurazole *N*-oxides (**1**, Scheme 1) stand out because of their ability to reversibly assemble cyclic tetramers and hexamers that are persistent in solution and display properties of genuine macrocyclic species.[13–15] While these aggregates are resilient to attack by Lewis bases, they are easily disassembled by the formation of O-bonded adducts with Lewis acids[16] or protonation with Brønsted acids.[17] Metal ions could in principle act in an analogous manner, but the reaction of **1b** with Pd(II) affords the κ^4Te macrocyclic coordination complex $[Pd(\mathbf{1b}_4)]^{2+}$.[14] This species was authenticated by X-ray diffraction of its BF_4^- salt. However, its single crystals display variable degrees of metal depletion as the lattice includes uncoordinated $\mathbf{1b}_4$ tetramers. Nevertheless, analytically pure $[Pd(\mathbf{1b}_4)](BF_4)_2$ was obtained by rapid growth of microcrystalline samples. Given these observations and the very low solubility of the complex salt, the stability of the macrocyclic complex in solution was not unequivocally demonstrated. Conceivably, the metal salt could be incorporated into the lattice as the crystal grew. In order to address this issue, we pursued the synthesis of other coordination complexes of $\mathbf{1}_4$ macrocycles that could be demonstrated to exist in solution. To facilitate these investigations, we performed the synthesis of an iso-tellurazole *N*-oxide with improved solubility. Here we present new κ^4Te complexes of $\mathbf{1}_4$ macrocycles with Rh(III) and Pt(II) and employ spectroscopic means to investigate their nature in solution.

McMaster University, Department of Chemistry and Chemical Biology, 1280 Main Street West, Hamilton, Ontario, Canada L8S 4M1.
E-mail: vargas@chemistry.mcmaster.ca

†CCDC 1891995, 1894245 and 1891996. For crystallographic data in CIF or other electronic format see DOI: 10.1039/c9dt00500e

Experimental

Materials and methods

Air sensitive materials were handled under an atmosphere of argon. Organic solvents were purified either by distillation over

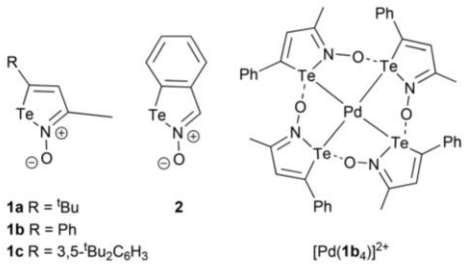

1a R = ^{t}Bu
1b R = Ph
1c R = 3,5-^{t}Bu$_2$C$_6$H$_3$

2

$[Pd(\mathbf{1b}_4)]^{2+}$

Scheme 1 Iso-tellurazole *N*-oxides and $[Pd(\mathbf{1b}_4)]^{2+}$.

appropriate dehydrating agents under nitrogen or using an Innovative Technologies purification system. The following chemicals were used as received from the commercial suppliers: dichloromethane-d_2 (Aldrich), 2.5 M *n*-butyllithium solution in hexanes (Aldrich), 3,5-di-*tert*-butylbromobenzene (Aldrich), sodium sulfate (EMD), silica gel (EM, 230–400 mesh), elemental tellurium (CERAC), and hydroxylamine-*O*-sulfonic acid (Aldrich), $PtCl_2$ (Pressure Chemical), $(PPh_3)_2PdCl_2$, silver tetrafluoroborate, trimethylsilylacetylene (Alfa Aesar), boron trifluoride diethyl etherate (Aldrich), sodium borohydride (Aldrich), and $Rh(CH_3CN)_2(COD)BF_4$ (Alfa Aesar). 3-Methyl-5-phenyl-1,2-tellurazole *N*-oxide was prepared by literature methods.[14]

Nuclear magnetic resonance

All spectra were measured in solution with a deuterated solvent. Spectra were obtained using Bruker AVANCE 500 MHz (Bruker 5 mm Broad Band Inverse probe) or Bruker AVANCE 600 MHz (Bruker 5 mm BROAD BAND OBSERVE probe) Spectrometers at 287.5 K. The ^{1}H, ^{13}C, ^{195}Pt and ^{125}Te spectra were processed using the Bruker TopSpin 3.2 software packages. The ^{1}H and ^{13}C spectra were referenced to tetramethyl silane using the deuterated solvent signal as a secondary reference. The ^{125}Te chemical shifts are reported with respect to the room-temperature resonance of $TeMe_2/C_6D_6$ (9 : 1, δ = 0.00 ppm)[18] but were measured using a secondary reference of diphenyl ditelluride in CD_2Cl_2 (δ = 420.36 ppm). Similarly, the ^{195}Pt chemical shift is reported relative to $Na_2[PtCl_6]$ (δ = 0.00 ppm) and measured with a secondary reference of $K_2[PtCl_4]$ (δ = −1617.4 ppm).

Electrospray ionization mass spectrometry

Mass spectra were acquired in the positive ion mode on an Agilent 1969 TOF mass spectrometer. Pure samples were dissolved in dichloromethane followed by dilution with methanol or dissolved and diluted with anhydrous acetonitrile. High resolution Mass spectra were obtained in a Waters Global and Ultima (ES Q-TOF) Mass Spectrometer (capillary = 3.20 V, cone = 100 V, source temp = 80 °C and resolving power = 10 000).

Other instrumental methods

IR spectra were recorded by using a Thermo Scientific Nicolet 6700 FT-IR spectrometer with a Smart iTX attenuated total reflectance (ATR) sample analyzer attachment. Melting points were measured with Uni-Melt Thomas Hoover capillary melting point apparatus and are reported uncorrected. Combustion elemental analyses were carried out by the London Metropolitan University elemental analysis service (London, United Kingdom). UV-Vis absorption spectra were obtained on a Cary 5000 spectrometer in the dual beam mode obtained using 10 mm quartz cuvettes.

Syntheses

3,5-Di-*tert*-butyl[(trimethylsilyl)ethynyl]benzene. A mixture of 3,5-di-*tert*-butylbromobenzene (1.50 g, 5.57 mmol), $(PPh_3)_2PdCl_2$ (0.280 g, 7% mol., 0.40 mmol), and cupric iodide (0.038 g, 3% mol., 0.2 mmol) in 35 mL of triethylamine was stirred for 1 h under argon. A solution of trimethylsilylacetylene (0.642 g, 6.54 mmol) in 2 mL of triethylamine was then added *via* a cannula. The resulting yellow slurry was refluxed for 4 h. The slurry was filtered through Celite and concentrated to ~5 mL, and the residue was purified by column chromatography on silica gel with hexanes as the eluent. The solvent from the eluate was evaporated and the product was a pale yellow solid. Yield 96%. Mp 134–137 °C. ^{1}H NMR (600 MHz, $CDCl_3$) δ 7.40 (t, ^{4}J = 1.9 Hz, 1H), 7.29 (d, ^{4}J = 1.9 Hz, 2H), 1.30 (s, 18H), 0.24 (s, 9H). *cf.* lit.:[19] Mp 135–137 °C. ^{1}H NMR ($CDCl_3$): δ 7.37 (t, 1H), 7.31 (d, 2H), 1.31 (s, 18H), 0.26 (s, 9H).

(3,5-Di-*tert*-butylphenyl)acetylene. As a modification of the reported method,[17] 3,5-di-tertbutyl[(trimethylsilyl)ethynyl] benzene (1.51 g, 5.27 mmol), potassium carbonate (0.451 g, 0.326 mmol), methanol (30 mL), and CH_2Cl_2 (6 mL) were stirred for 1.5 h under argon. The resulting yellow mixture was concentrated and then poured into water followed by extraction with CH_2Cl_2 as a yellow solution. The extract was washed with aqueous $NaHCO_3$ (3% m/v) and water. After dehydration with Na_2SO_4, the yellow solution was concentrated under reduced pressure to dryness. The crude product was further purified by sublimation at 50 °C/1 mmHg, giving white crystals. Yield 88%. Mp: 84–85 °C. ^{1}H NMR (600 MHz, $CDCl_3$): δ 7.43 (t, ^{4}J = 1.5 Hz, 1H), 7.34 (d, ^{4}J = 1.5 Hz, 2H), 3.07 (s, 1H), 1.30 (s, 18H). *cf.* lit: Mp 85–86 °C, ^{1}H NMR ($CDCl_3$): δ 7.42 (t, 1H), 7.35 (d, 2H), 3.02 (s, 1H), 1.31 (s, 18H).

4-[(3,5-Di-*tert*-butyl)phenyl]but-3-yn-2-one. To a solution of (3,5-di-*tert*-butylphenyl)acetylene (225 mg, 1.05 mmol) in THF (1.2 mL), 2.5 M *n*-BuLi (0.420 mL, 1.05 mmol) was added dropwise at −78 °C followed by stirring for 30 minutes at −78 °C. Ethyl acetate (0.050 mL, 0.51 mmol) in THF (1.5 mL), and boron trifluoride diethyl etherate (0.155 mL, 1.26 mmol) were then added successively at −78 °C. After stirring continuously under argon for 30 min, the reaction was quenched with a saturated solution of NH_4Cl and the mixtures were allowed to warm to room temperature. The product was extracted with diethyl ether, washed with brine and water, and then dehydrated with Na_2SO_4. The solvent was evaporated under reduced pressure and purified by column chromatography on silica gel with 5% ethyl acetate in hexanes as an eluent. The final product was isolated as a light-yellow oil. Yield 54%. Alternatively, the synthesis can be carried out with acetic anhydride instead of ethyl acetate, in which case 1.5 equivalents are required to attain 55% yield. ^{1}H NMR (600 MHz, $CDCl_3$) δ 7.54 (t, ^{4}J = 1.8 Hz, 1H), 7.44 (d, ^{4}J = 1.8 Hz, 2H), 2.47 (s, 3H), 1.32 (s, 18H). ^{13}C NMR (600 MHz, $CDCl_3$) δ 185.0, 151.5, 127.6, 125.5, 119.0, 92.2, 87.7, 35.0, 32.9, 31.4. HR-ESMS (*m*/*z*): 257.1903, calc. for $[MH]^+$ $C_{18}H_{25}O$ 257.1905. IR (ATR, $\tilde{\nu}$, cm^{-1}): 2964, 2871, 2184, 1668, 1589, 1470, 1426, 1362, 1310, 1248, 1204, 1164, 1021, 988, 900, 881, 704, 704, 604, 583, 572.

(*Z*)-4-[(Dimethylamino)carbonyltelluro]-4-[(3,5-di-*tert*-butyl) phenyl]but-3-yn-2-one. A methanolic solution (4 mL) of sodium borohydride (0.03 g, 1.73 mmol) was added to di-(*N*,*N*-dimethylcarbamoyl)-ditelluride (0.158 g, 0.40 mmol) in DMF

(6.26 mL) under an argon atmosphere at −78 °C. The mixture was warmed to 0 °C and kept at this temperature for 30 min, after which a DMF solution (1.56 mL) of 4-[(3,5-di-*tert*-butyl) phenyl]but-3-yn-2-one (0.180 g, 0.70 mmol) was added. The mixture was stirred at room temperature for 12 hours. Brine addition was followed by extraction with toluene. The extract was washed with more brine and distilled water, and then dried with sodium sulfate. The solvent was evaporated under reduced pressure followed by purification by column chromatography on silica gel with 5% ethyl acetate in dichloromethane. The product was isolated as an orange oil after evaporation. Yield 65%. ^{1}H NMR (600 MHz, $CDCl_3$) δ 7.39 (t, ^{4}J = 1.7 Hz, 1H), 7.37 (s, 1H), 7.23 (d, ^{4}J = 1.7 Hz, 2H), 2.68 (s, 3H), 2.52 (s, 3H), 2.35 (s, 3H), 1.33 (s, 18H). ^{13}C NMR (600 MHz, $CDCl_3$) δ 196.8, 161.4, 160.4, 150.6, 142.7, 129.4, 123.3, 123.0, 42.3, 35.1, 33.6, 31.6, 30.0. ^{125}Te NMR (600 MHz, $CDCl_3$) δ 994.2. HR-ESMS (*m*/*z*): 482.1303 calc. for $[NaM]^+$ $C_{21}H_{31}NNaO_2Te$ 482.1315. IR (ATR, $\tilde{\nu}$, cm^{-1}): 2959, 2869, 1618, 1512, 1476, 1425, 1395, 1360, 1317, 1247, 1213, 1182, 1084, 1054, 1029, 1003, 879, 824, 732, 713, 684, 661, 645.

3-Methyl-5-[(3,5-di-*tert*-butyl)phenyl]-1,2-tellurazole 2-oxide (1c). Hydroxylamine-*O*-sulfonic acid (273.7 mg, 2.4 mmol) and (*Z*)-4-[(dimethylamino)carbonyltelluro]-4-[(3,5-di-*tert*-butyl)phenyl] but-3-yn-2-one (251.8 mg, 0.55 mmol) were refluxed in MeOH (8.7 mL) for three hours under an atmosphere of argon. The product was extracted with dichloromethane, washed with brine and water, and dehydrated over sodium sulfate. The crude product was deposited on a silica layer (5 cm thick), impurities were eluted with dichloromethane and the product was then eluted with a 1 : 1 DCM–methanol mixture. After evaporation, the pure product was obtained as a pale yellow solid. Crystals suitable for X-ray diffraction were obtained by cooling a concentrated solution of **1c** in toluene from room temperature to −22 °C and it was maintained at −22 °C. Yield 88%. ^{1}H NMR (600 MHz, CD_2Cl_2) δ 7.36 (t, ^{4}J = 1.7 Hz, 1H), 7.23 (d, ^{4}J = 1.7 Hz, 2H), 7.07 (s, 1H), 1.61 (s, 3H), 1.31 (s, 18H). ^{13}C NMR (600 MHz, CD_2Cl_2): δ 156.9, 154.0, 149.7, 139.8, 126.8, 123.7, 121.9, 34.9, 31.6, 15.4. ^{125}Te NMR (600 MHz, $CDCl_3$) δ 1613. Mp 256–263 °C. HR-ESMS (*m*/*z*): 402.1076 calc. for $[MH]^+$ $C_{18}H_{26}NOTe$ 402.1077. IR (ATR, $\tilde{\nu}$, cm^{-1}): 2961, 2866, 1579, 1475, 1427, 1392, 1361, 1265, 1247, 1205, 1099, 1026, 983, 904, 891, 872, 831, 735, 708, 654, 584.

Tetrakis(acetonitrile)platinum(II) bistetrafluoroborate. Based on a reported procedure,[20] anhydrous acetonitrile (8 mL) was added into platinum dichloride (0.08 g, 0.3 mmol) under an argon atmosphere. The yellow solution was left stirring for 4 hours and then filtered hot. The solution was added into silver tetrafluoroborate (0.06 g, 0.3 mmol) in the absence of light and refluxed for additional 4 hours. The solution was filtered, reduced to a small volume and then precipitated with diethyl ether. The precipitate was recrystallized from acetonitrile–diethyl ether solution and then dried. Yield 92%. ^{1}H NMR (600 MHz, CD_3CN): δ 2.61 (s, 12H), *cf.* lit. 2.6.

$[Pt(1c_4)](BF_4)_2$. $[Pt(CH_3CN)_4](BF_4)_2$ (7.6 mg, 0.014 mmol) and **1c** (22.8 mg, 0.057 mmol) were dissolved in anhydrous dichloromethane (2 mL). The solution was stirred at room temperature for 12 h and the colour changed from yellow to dark red. Crystals suitable for X-ray diffraction were obtained at −35 °C by diffusion of hexanes to a concentrated solution of $[Pt(1c_4)](BF_4)_2$ in DCM until the growth of crystals reached equilibrium. Yield 35%. ^{1}H NMR (500 MHz, CD_2Cl_2) δ 7.46 (t, ^{4}J = 1.7 Hz, 1H), 7.28 (d, ^{4}J = 1.7 Hz, 2H), 6.98 (s, 1H), 2.13 (s, 3H), 1.34 (s, 18H). ^{13}C NMR (500 MHz, CD_2Cl_2) δ 160.7, 150.9, 145.2, 134.7, 132.9, 126.0, 35.3, 31.5, 31.4, 16.1. ^{125}Te NMR (500 MHz, CD_3CN) δ 1371.3. ^{195}Pt NMR (600 MHz, CD_2Cl_2): δ −5066.2. ^{1}J(Te,Pt) = 455 Hz. HR-ESMS (*m*/*z*): 896.1808 calc. for $[M]^{2+}$ $C_{74}H_{100}N_4O_4PtTe_4$ 896.1800. UV-vis absorption (λ_{max}, nm//ε L mol^{-1} cm^{-1}): 316//49 469, 482^{sh}//3355. IR (ATR, $\tilde{\nu}$, cm^{-1}): 2953, 2901, 2868, 1613, 1593, 1476, 1427, 1393, 1362, 1332, 1249, 1204, 1120, 1067, 1047, 1033, 898, 879, 847, 822, 762, 735, 710, 649, 628, 609, 602. Anal. calcd for $C_{72}H_{100}B_2F_8N_4O_4PtTe_4$: C, 44.02; H, 5.13; N, 2.85. Found: C, 44.17; H, 5.28; N, 2.71.

$[RhCl_2(1b_4)]BF_4$. *Method I*: An acetonitrile solution (1.25 mL) of $Rh(CH_3CN)_2(COD)BF_4$ (7 mg, 0.018 mmol) was mixed with a dichloromethane solution (2.8 mL) of **1b**[14] (21 mg, 0.073 mmol) and heated to reflux for one hour. The dark brown solution was allowed to cool down to room temperature and crystals suitable for X-ray diffraction formed after two days. Yield 42%. *Method II*: $RhCl_3$ (5.6 mg, 0.027 mmol), **1b** (30.6 mg, 0.107 mmol), and NH_4BF_4 (2.8 mg, 0.027 mmol) were mixed in anhydrous THF (3 mL). After 3 hours of reflux, the solution turned dark brown. The solution was filtered and the product was precipitated with diethyl ether. Yield 92%. ^{1}H NMR (600 MHz, CD_3CN) δ 7.44–7.42 (m, 3H), 7.41–7.38 (m, 2H), 7.14 (s, 1H), 2.01 (s, 3H). ^{13}C NMR (700 MHz, CD_3CN) δ 162.6, 146.7, 137.5, 134.7, 130.7, 130.5, 129.2, 15.2. ^{125}Te NMR (500 MHz, DMSO-d_6) δ 1550.9. ^{1}J(Te,Rh) = 64 Hz. HR-ESMS (*m*/*z*): 1320.7343 calc. for $[M]^+$ $C_{40}H_{36}Cl_2N_4O_4RhTe_4$ 1320.7347. UV-vis absorption (λ_{max}, nm//ε L mol^{-1} cm^{-1}): 299^{sh}//20 599, 395//10 882, 520//1656. IR (ATR, $\tilde{\nu}$, cm^{-1}): 3002, 2946, 2890, 2836, 2323, 2293, 1491, 1430, 1370, 1308, 1048, 1028, 999, 978, 879, 778. Anal. calcd for $C_{40}H_{36}BN_4O_4F_4Cl_2RhTe_4$: C, 34.13; H, 2.58; N, 3.98. Found: C, 34.03; H, 2.54; N, 3.87.

X-ray crystallography

Crystals were mounted on MiTeGen Micromounts (Ithaca, New York) using Paratone-n oil. A Bruker APEX2 diffractometer was used to collect data at 100 K with Mo-Kα radiation (λ = 0.71073 Å). A CCD area detector was used and equipped with a low temperature accessory (Oxford cryostream). Three different orientations were used with a minimum of 50 frames for the determination of the unit cell parameters and final cell advancement after integration with SAINT.[21] SADABS[22] was used for the absorption correction. All structures were solved by direct methods and then refined using SHELXL[23] by the full-matrix least-squares techniques on F^2. All non-hydrogen atoms were assigned anisotropic thermal parameters. Appropriate riding models were used to place hydrogen atoms in idealized positions.

Results and discussion

Syntheses

Hitherto reported iso-tellurazole *N*-oxides (**1a**, **1b**, Scheme 1) and their benzo-annulated derivative **2** have rather low solubilities in common organic solvents, and the Pd(II) complex [Pd(**1b**$_4$)](BF$_4$)$_2$ is even less soluble. Attempts to prepare an analogous Pt(II) complex invariably resulted in insoluble intractable products. To overcome this issue, the *tert*-butylated derivative **1c** was prepared based on published procedures[14] (Scheme 2). Trimethylsilyl acetylene and 1-bromo-3,5-di-*tert*-butylbenzene were coupled using the palladium-catalyzed Sonogashira reaction. Deprotection gave 1,3-di-*tert*-butyl-5-ethynylbenzene, which was transformed into the methylynone through deprotonation and the reaction with acetic anhydride or ethyl acetate. Trans addition of *in situ*-generated tellurocarbamic acid and condensation with hydroxylamine-*O*-sulfonic acid yielded an intermediate that cyclized upon hydrolysis to **1c**. Single crystal X-ray diffraction confirmed the identity of the product (see below).

The new derivative **1c** readily reacted with transition metal salts. The reaction of [Pt(CH$_3$CN)$_4$](BF$_4$)$_2$ with four equivalents of **1c** in CH$_2$Cl$_2$ slowly produced a dark red solution from which [Pt(**1c**$_4$)](BF$_4$)$_2$ was isolated upon addition of hexanes. Similarly, the reaction of [Rh(CH$_3$CN)$_2$(COD)]BF$_4$ with four equivalents of **1c** produced dark brown solutions; however, attempts to completely remove the solvent under vacuum or induce precipitation yielded glassy residues from which the products could not be identified. Therefore, the reaction of [Rh(CH$_3$CN)$_2$(COD)]BF$_4$ was carried out with the less soluble **1b**; similar color changes were observed and a crystalline material precipitated. Structural determination showed that this product is the Rh(III) complex [RhCl$_2$(**1b**$_4$)]BF$_4$. Because [Rh(CH$_3$CN)$_2$(COD)]BF$_4$ does not react with CH$_2$Cl$_2$,[24] it is likely that an initial product of reaction with **1b** undergoes oxidative addition with CH$_2$Cl$_2$ as other Rh(I) complexes do.[25,26] Alternatively, the iso-tellurazole *N*-oxide **1b** could act as an oxidant forming a Rh(III) species that would subsequently react with CH$_2$Cl$_2$; however, ^{1}H-NMR did not detect any 3-methyl-5-aryl-1,2-tellurazole[27] in the reaction mixture. [RhCl$_2$(**1b**$_4$)]BF$_4$ was more efficiently obtained by the reaction of RhCl$_3$ with 4 equivalents of **1c** and an excess of NH$_4$BF$_4$.

Crystal structures

Compound **1c** crystalized from toluene forming plate-like crystals that belong to the monoclinic $P2_1/c$ space group. Crystallographic refinement data are presented in Table 1; selected distances and angles are compiled in Table 2. The lattice is built from **1c**$_6$ macrocyclic aggregates and toluene molecules. As the hexamers sit at C_i positions, the asymmetric unit consists of three crystallographically independent **1c** units plus two toluene molecules. The hexamers display a typical puckered structure over that observed in **1b**$_6$ (Fig. 1) and **2**$_6$. The Te···O ChB distances (2.180(2), 2.186(2), 2.199(2) Å) are intermediate between the sums of van der Waals (3.58 Å) and covalent (2.08 Å) radii and comparable to those previously observed in the structures of **1a**, **1b** and **2**. Also as in the earlier examples, the N–Te···O angles (164.14(9), 164.58(9), 164.75(9)°) deviate from the linear geometry expected for the interaction of the O lone pairs of electrons with the σ hole; Politzer has noted that such deviations occur when the maximum of potential on the molecule of **1c** is not coincident with the σ hole. Adjacent C$_3$NTe heterocycles are nearly orthogonal to each other, with interplanar angles (79.61, 83.76, 89.78°) comparable to those in other hexamers. The transannular Te–Te distances are 7.1805(7), 7.3206(8) and 7.7383(9) Å, longer than those in **2**$_6$ (7.1297(8), 7.3407(8) and 7.3589(5) Å) and **1b**$_6$·2THF (7.638(2) Å).

The plate-like crystals of [Pt(**1c**$_4$)](BF$_4$)$_2$ belong to the monoclinic $P2_1/c$ space group. Crystallographic refinement data are presented in Table 1; selected distances and angles are com-

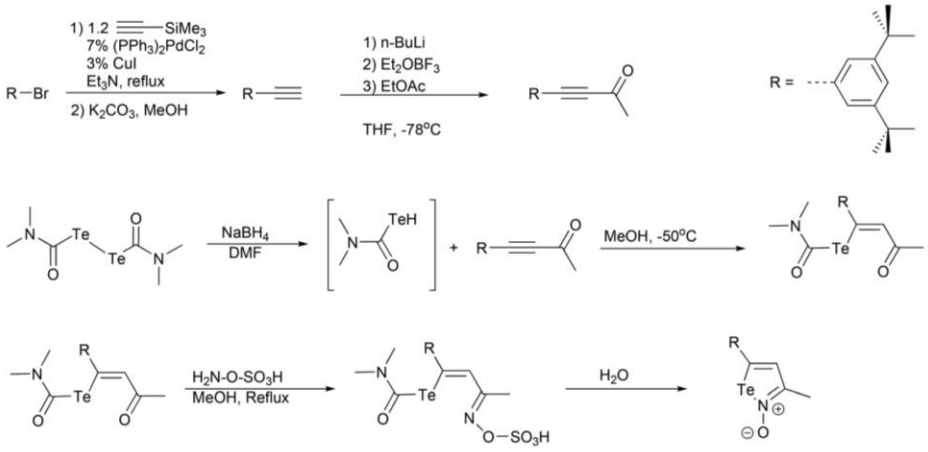

Scheme 2 Synthesis of **1c**.

Table 1 Crystallographic and refinement parameters of $\mathbf{1c}_6{\cdot}4(C_7H_8)$, $[Pt(\mathbf{1c}_4)](BF_4)_2$ and $[RhCl_2(\mathbf{1b}_4)]BF_4$

Crystal composition	$\mathbf{1c}_6{\cdot}4(C_7H_8)$	$[Pt(\mathbf{1c}_4)](BF_4)_2$	$[RhCl_2(\mathbf{1b}_4)]BF_4$
CCDC	1891995	1894245	1891996
Empirical formula	$C_{17}H_{22.75}N_{0.75}O_{0.75}Te_{0.75}$	$C_{72}H_{100}B_2F_8N_4O_4PtTe_4$	$C_{10}H_9B_{0.25}Cl_{0.5}FNORh_{0.25}Te$
Crystal system, space group	Monoclinic, $P21/c$	Monoclinic, $P2_1/c$	Tetragonal, $I\bar{4}$
a [Å]	19.067(2)	13.8287(7)	11.276(1)
b [Å]	20.129(2)	31.411(2)	11.276(1)
c [Å]	16.9559(18)	20.584(1)	24.219(3)
α [°]	90	90	90
β [°]	95.272(3)	90.411(2)	90
γ [°]	90	90	90
V [Å^3]	6480(1)	8941.0(8)	3079.1(7)
Z, ρ(calc.) [g cm^{-3}]	2, 1.416	4, 1.460	2, 1.518
T [K]	100	100	100
μ [mm^{-1}]	1.387	2.906	2.266
2θ range [°]	3.932 to 52.766	2.366 to 54.044	3.364 to 52.892
Limiting indices	$-23 \le h \le 23$	$-17 \le h \le 17$	$-14 \le h \le 14$
	$-25 \le k \le 25$	$-40 \le k \le 39$	$-14 \le k \le 14$
	$-21 \le l \le 21$	$-26 \le l \le 26$	$-30 \le l \le 30$
Refl. collec./unique	190 828/13 244	223 351/19 494	28 399/3161
R(int.)	0.0497	0.1279	0.0886
No. of parameters	748	946	138
R_1 [a]/wR_2 [a] ($I > 2\sigma(I)$)	0.0304/0.0634	0.0499/0.1018	0.0412/0.0991
R_1 [a]/wR_2 [a] for all data	0.0438/0.0697	0.0878/0.1130	0.0504/0.1050
Goodness-of-fit on F^2	1.055	1.030	1.021
Larg. diff. peak/hole [e Å^{-3}]	1.10/−0.42	1.37/−2.15	3.00/−1.26

[a] $R_1 = \sum||F_o| - |F_c||/\sum|F_o|$, $wR_2 = \{\sum[w(F_o^2 - F_c^2)^2]/\sum w(F_o^2)^2\}^{1/2}$.

Table 2 Selected distances and angles in the structures of $\mathbf{1c}_6{\cdot}4(C_7H_8)$, $[Pt(\mathbf{1c}_4)](BF_4)_2$ and $[RhCl_2(\mathbf{1b}_4)]BF_4$

Crystal composition	$\mathbf{1c}_6{\cdot}4(C_7H_8)$	$[Pt(\mathbf{1c}_4)](BF_4)_2$	$[RhCl_2(\mathbf{1b}_4)]BF_4$
Distances (Å)			
Te–C	2.095(3), 2.102(3)	2.136(7), 2.145(6), 2.148(6), 2.150(6)	2.14(1)
Te–N	2.220(2), 2.251(2), 2.253(3)	2.209(6), 2.218(6), 2.226(6), 2.229(6)	2.239(9)
Te···O	2.180(2), 2.186(2), 2.199(2)	2.144(4), 2.171(5), 2.177(4), 2.179(4)	2.172(7)
N–O	1.359(3), 1.365(3), 1.375(3)	1.359(7), 1.369(7), 1.371(7), 1.373(8)	1.34(1)
N–O	4.380(3), 4.391(3), 4.397(3)	4.329(7), 4.342(7), 4.356(7), 4.379(8)	4.37(1)
C–N	1.297(4), 1.301(4), 1.304(4)	1.284(9), 1.294(9), 1.306(8), 1.306(9)	1.26(1)
Te···Te	3.6997(6), 3.7815(6), 3.8036(6)	3.6582(7), 3.6645(7), 3.6897(7), 3.6957(7)	3.7165(8)
Bond angles (°)			
N–Te···O	164.14(9), 164.58(9), 164.74(9)	163.8(2), 164.3(2), 164.7(2), 168.1(2)	164.0(3)
N–Te–C	75.7(1), 76.1(1), 76.4(1)	74.8(2), 75.2(2), 75.3(2), 76.0(2)	76.4(4)
O–N–Te	126.7(2), 127.0(2), 128.4(2)	120.2(4), 122.0(4), 122.3(4), 123.2(4)	123.4(6)
Torsion angles (°)			
Te–N–O···Te	17.8(3), 27.6(3), 31.5(3)	45.8(5), 46.0(5), 50.5(5), 50.7(5)	35.8(8)
N–O···Te–C	80.8(2), 80.8(2), 88.6(2)	104.0(4), 106.8(4), 109.3(4), 111.4(4)	104.8(6)
C–Te–N–O	176.1(2), 176.2(2), 176.4(2)	173.7(5), 174.3(5), 175.3(5)	172.4(8)

piled in Table 2. The complex sits at general positions, and its molecular structure (Fig. 2) is analogous to that of $[Pd(\mathbf{1b}_4)]^{2+}$, featuring the boat conformer of the macrocyclic tetramer of **1c**. The metal ion has full occupancy and is coordinated to the four tellurium atoms with a slightly distorted square-planar geometry as the average trans Te–Pt–Te bond angles are 175.75 (2)°. The average Pt–Te bond distance (2.5983(8) Å) of $[Pt(\mathbf{1c}_4)](BF_4)_2$ is comparable to the values measured for the Pt(II) complexes c-$PtCl_2$\{[18]aneO_4Te_2\} (2.5323(6) and 2.5355(6) Å),[28] 2-formylcyclohexenyltelluride (2.5843(3) Å) and 2,3,5,6,7,8-hexahydro-1*H*-telluroxanthene-4-carbaldehyde (2.538(2), 2.541 (2), 2.542(3), 2.551(3) Å).[29] The BF_4 counter ions are located above and below the coordination plane, and the Pt–F distances (>3.1 Å) are too long for a meaningful interaction.

The rhodium derivative $[RhCl_2(\mathbf{1b}_4)]BF_4$ crystallizes as plates that belong to the $I\bar{4}$ space group. Crystallographic refinement data are presented in Table 1; selected distances and angles are compiled in Table 2. The molecular structure of the complex $[RhCl_2(\mathbf{1b}_4)]^+$ is octahedral with the chlorido ligands trans to each other and the $\mathbf{1b}_4$ tetramer in the boat conformation (Fig. 3). The coordination sphere bears significant resemblance to that of $[RhCl_2(TeRR')_4]^+$ (R = $(CH_2)_2$-(1,2-C_4H_8ON)-4, R′ = C_6H_4-OMe-4). The Rh–Cl bond distances (2.375(4) Å) are equal (*cf.* 2.353(2) and 2.365(2) Å), the Rh–Te

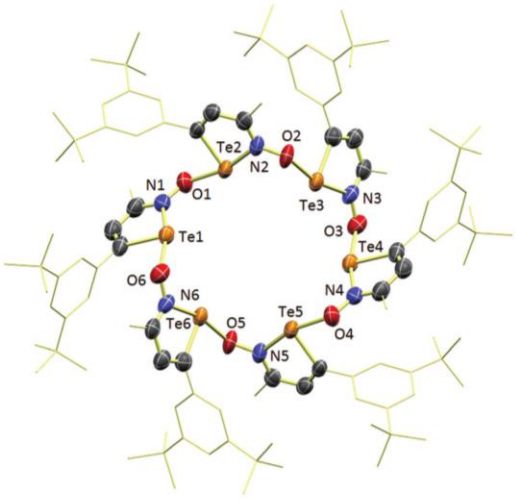

Fig. 1 Macrocyclic structure of the hexamer $\mathbf{1c}_6$. Displacement ellipsoids plotted at 95% probability.

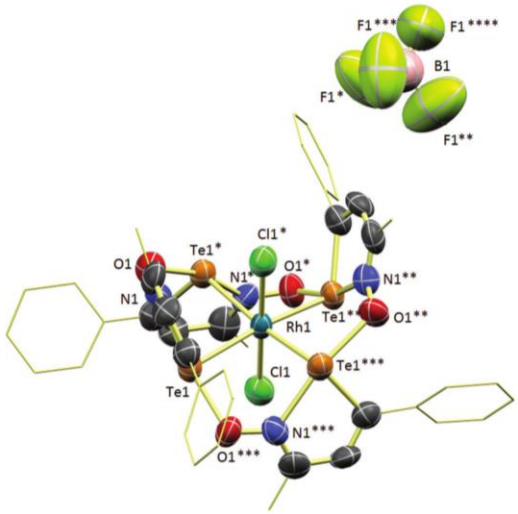

Fig. 3 Molecular ions in the structure of $[RhCl_2(\mathbf{1b}_4)]BF_4$. Displacement ellipsoids plotted at 95% of probability.

bond distances (2.6199(4) Å) are slightly shorter (*cf.* 2.6510(8) to 2.6687(8)), and the $RhTe_4$ fragment displays a larger D_{2d} distortion with Te–Rh–Te trans bond angles (170.96(3)°) smaller (*cf.* 175.85(3) and 176.80(3)°) than those of the complex with the monodentate telluroether.[30] The BF_4^- anions display no interaction with $[RhCl_2(\mathbf{1b}_4)]^+$. Packing creates tubular channels along the *a* and *b* directions of the unit cell. The cavities are filled with solvent molecules that are heavily disordered; satisfactory refinement of the structure required application of the SQUEEZE[31] tool fitting 7.72 CH_2Cl_2 molecules and an electron count of 324.4 per unit cell. However, analytically pure samples of $[RhCl_2(\mathbf{1b}_4)]BF_4$ could be prepared by fast precipitation from solution.

NMR spectroscopy

The good solubility of these compounds facilitated the observation of their $^{125}Te\{^1H\}$ NMR spectra (Fig. 4). A broad but well-defined resonance was observed at 298 K for **1c** in CD_2Cl_2 at 1613.2 ppm (*cf.* 1595.2 ppm for **1b**). In contrast, locating the ^{125}Te resonances of the metal complexes required modest heating to sharpen the bands. For $[Pt(\mathbf{1c}_4)](BF_4)_2$ in CH_2Cl_2 at 323 K, a single peak was centered at 1371.3 ppm; its ^{195}Pt reso-

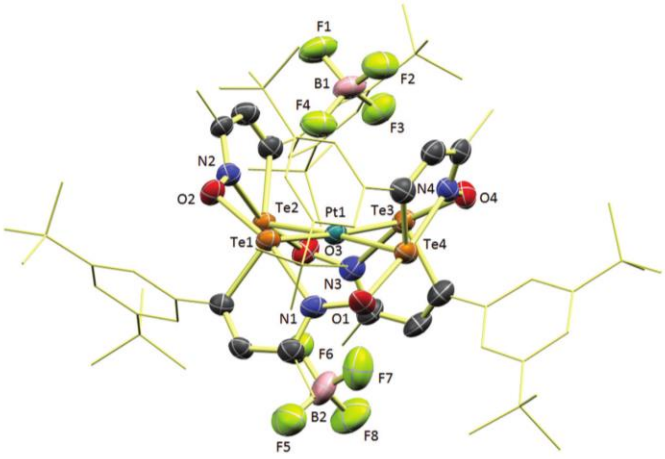

Fig. 2 Molecular ions in the structure of $[Pt(\mathbf{1c}_4)](BF_4)_2$. Displacement ellipsoids plotted at 75% probability.

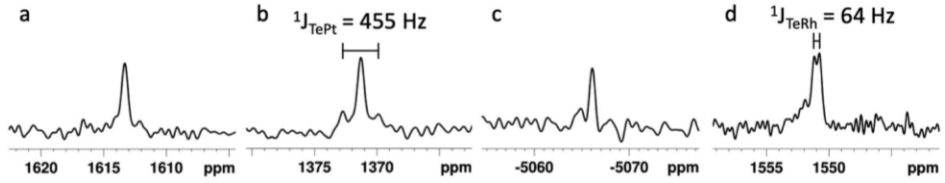

Fig. 4 Selected NMR spectra. (a) ^{125}Te{^{1}H} of **1c**; (b) ^{125}Te{^{1}H} of [Pt(**1c**$_4$)](BF$_4$)$_2$; (c) ^{195}Pt{^{1}H} of [Pt(**1c**$_4$)](BF$_4$)$_2$; (d) ^{125}Te{^{1}H} of [RhCl$_2$(**1b**$_4$)]BF$_4$.

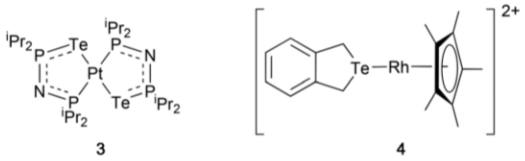

3 4

Scheme 3 Complexes with comparable ^{125}Te or ^{195}Pt NMR parameters to those observed for the Pt(II) and Rh(III) complexes of iso-tellurazole *N*-oxides.

nance appeared as a single peak at −5066.2 ppm in CD_3CN. The latter clearly corresponds to platinum in a complex with very soft donor atoms; it is comparable to −5410 ppm observed for the complex of a monotellurido imidodiphosphinate (**3**, Scheme 3).[32] From the isotopic satellites in the ^{125}Te{^{1}H} NMR spectrum, the ^1J(Te,Pt) coupling constant is 455 Hz. This value is similar to 469 Hz observed for t-[PtCl$_2${Te(CH$_2$SiMe$_3$)$_2$}$_2$].[33] A broad doublet was observed at 1551 ppm in the ^{125}Te{^{1}H} spectrum of [RhCl$_2$(**1b**$_4$)]BF$_4$ in DMSO-d$_6$ at 333 K from which the magnitude of the ^1J(Te,Rh) coupling constant is estimated at 64 Hz, which is comparable to 65.9 Hz reported for the complex of 2-telluraindane **4**.[34] In both complexes, the high frequency shift of the ^{125}Te resonance and the ^1J(Te,M) coupling constant indicate that the metal complexes are stable in solution.

Mass spectrometry

The electrospray mass spectra of the complexes presented in this report displayed patterns that match the isotopic distribution patterns recorded for [Pt(**1c**$_4$)]$^{2+}$ and [RhCl$_2$(**1b**$_4$)]$^+$ (Fig. 5). Moreover, the isotopic patterns of the free iso-tellurazole *N*-oxides (**1c** or **1b**) and their aggregates were absent in the mass spectra. These observations demonstrate that the complexes of these metal ions are a very stable species.

Conclusions

Heavy-chalcogen analogues of crown ethers frequently display unique structures and reactivity patterns with metal ions. However, macrocyclic ligands that contain only tellurium donor atoms have been much less studied than their sulfur and selenium counterparts. Those investigations are often complicated by laborious syntheses and detrimental side-reactions that are facilitated by the large size of the chalcogen atom and the polarity of the Te–C bond. In many instances, tellurium macrocycles include donor heteroatoms such as

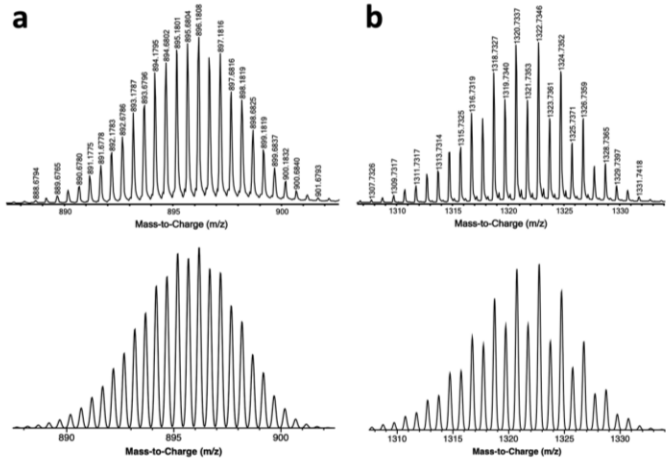

Fig. 5 Experimental (top) and calculated (bottom) high-resolution electrospray mass spectra of (a) [Pt(**1c**$_4$)](BF$_4$)$_2$; (b) [RhCl$_2$(**1b**$_4$)]BF$_4$.

oxygen and nitrogen to facilitate the synthesis and stabilize the ligands. In this report, we have demonstrated that complexes of the macrocyclic aggregates of the iso-tellurazole *N*-oxides are stable species in solution. This property and the facility with which these macrocycles are spontaneously assembled offer remarkable opportunities to study the behaviour of metal ions imbedded in an all-tellurium coordination sphere.

Conflicts of interest

There are no conflicts to declare.

Acknowledgements

We gratefully acknowledge funding from the Natural Science and Engineering Research Council of Canada.

References

1 L. Vogel, P. Wonner and S. M. Huber, *Angew. Chem., Int. Ed.*, 2019, **58**, 1880–1891.
2 R. Gleiter, G. Haberhauer, D. B. Werz, F. Rominger and C. Bleiholder, *Chem. Rev.*, 2018, **118**, 2010–2041.
3 A. F. Cozzolino, P. J. Elder and I. Vargas-Baca, *Coord. Chem. Rev.*, 2011, **255**, 1426–1438.
4 L.-J. Riwar, N. Trapp, K. Root, R. Zenobi and F. Diederich, *Angew. Chem.*, 2018, **115**, 17259–17264.
5 S. Langis-Barsetti, T. Maris and J. D. Wuest, *J. Org. Chem.*, 2017, **82**, 5034–5045.
6 M. S. Pavan, A. Jana, S. Natarajan and T. N. Row, *J. Phys. Chem. B*, 2015, **119**, 11382–11390.
7 N. Biot and D. Bonifazi, *Chem. – Eur. J.*, 2018, **24**, 5439–5443.
8 S. Benz, J. López-Andarias, J. Mareda, N. Sakai and S. Matile, *Angew. Chem., Int. Ed.*, 2017, **56**, 812–815.
9 L. M. Lee, M. Tsemperouli, A. I. Poblador-Bahamonde, S. Benz, N. Sakai, K. Sugihara and S. Matile, *J. Am. Chem. Soc.*, 2019, **141**, 810–814.
10 G. E. Garrett, G. L. Gibson, R. N. Straus, D. S. Seferos and M. S. Taylor, *J. Am. Chem. Soc.*, 2015, **137**, 4126–4133.
11 J. Y. Lim, I. Marques, A. L. Thompson, K. E. Christensen, V. Félix and P. D. Beer, *J. Am. Chem. Soc.*, 2017, **139**, 3122–3133.
12 A. F. Cozzolino, P. S. Whitfield and I. Vargas-Baca, *J. Am. Chem. Soc.*, 2010, **132**, 17265–17270.
13 P. C. Ho, J. Rafique, J. Lee, L. M. Lee, H. A. Jenkins, J. F. Britten, A. L. Braga and I. Vargas-Baca, *Dalton Trans.*, 2017, **46**, 6570–6579.
14 P. C. Ho, P. Szydlowski, J. Sinclair, P. J. Elder, J. Kübel, C. Gendy, L. Lee, H. Jenkins, J. F. Britten, D. R. Morim and I. Vargas-Baca, *Nat. Commun.*, 2016, **7**, 11299.
15 J. Kübel, P. J. Elder, H. A. Jenkins and I. Vargas-Baca, *Dalton Trans.*, 2010, **39**, 11126–11128.
16 P. C. Ho, H. A. Jenkins, J. F. Britten and I. Vargas-Baca, *Faraday Discuss.*, 2017, **203**, 187–199.
17 P. C. Ho, L. Lee, H. Jenkins, J. F. Britten and I. Vargas-Baca, *Can. J. Chem.*, 2016, **94**, 453–457.
18 P. Elder and I. Vargas-Baca, *Phys. Chem. Chem. Phys.*, 2016, **18**, 30740–30747.
19 Y. Miura, M. Matsumoto, Y. Ushitani, Y. Teki, T. Takui and K. Itoh, *Macromolecules*, 1993, **26**, 6673–6675.
20 T. E. Müller, J. C. Green, M. D. Mingos, M. C. McPartlin, C. Whittingham, D. J. Williams and T. M. Woodroffe, *J. Organomet. Chem.*, 1998, **551**, 313–330.
21 *2012 Bruker, SAINT*, Bruker AXS Inc., Madison, Wisconsin, USA, 2012.
22 *2001 Bruker, SADABS*, Bruker AXS Inc., Madison, Wisconsin, USA, 2001.
23 G. Sheldrick, *Acta Crystallogr., Sect. C: Struct. Chem.*, 2015, **71**, 3–8.
24 Y. Bolshan and R. A. Batey, *Org. Lett.*, 2005, **7**, 1481–1484.
25 J. Zeng, M.-H. Hsieh and H. Lee, *J. Organomet. Chem.*, 2005, **690**, 5662–5671.
26 G. E. Ball, W. R. Cullen, M. D. Fryzuk, B. R. James and S. J. Rettig, *Organometallics*, 1991, **10**, 3767–3769.
27 K. Shimada, A. Moro-oka, A. Maruyama, H. Fujisawa, T. Saito, R. Kawamura, H. Kogawa, M. Sakuraba, Y. Takata, S. Aoyagi, Y. Takikawa and C. Kabuto, *Bull. Chem. Soc. Jpn.*, 2007, **80**, 567–577.
28 M. J. Hesford, W. Levason, M. L. Matthews and G. Reid, *Dalton Trans.*, 2003, 2852–2858.
29 P. R. Prasad, H. B. Singh and R. J. Butcher, *J. Organomet. Chem.*, 2016, **814**, 42–56.
30 P. Singh, D. Das, M. Singh and A. K. Singh, *Inorg. Chem. Commun.*, 2010, **13**, 988–991.
31 A. Spek, *Acta Crystallogr., Sect. C: Struct. Chem.*, 2015, **71**, 9–18.
32 S. D. Robertson, J. S. Ritch and T. Chivers, *Dalton Trans.*, 2009, 8582–8592.
33 M. J. Poropudas, L. Vigo, R. Oilunkaniemi and R. S. Laitinen, *Heteroat. Chem.*, 2011, **22**, 348–357.
34 K. Badyal, W. R. McWhinnie, J. Homer and M. C. Perry, *J. Organomet. Chem.*, 1998, **555**, 279–284.

Chapter 6. Competing Effects of Chlorination on the Strength of Te···O Chalcogen Bonds Select the Structure of Mixed Supramolecular Macrocyclic Aggregates of Iso-Tellurazole *N*-Oxides

Original citation: Ho, P. C.; Lomax, J.; Tomassetti, V.; Britten, J. F.; Vargas-Baca, I. Competing Effects of Chlorination on the Strength of Te···O Chalcogen Bonds Select the Structure of Mixed Supramolecular Macrocyclic Aggregates of Iso-Tellurazole N-Oxides. *Chem. Eur. J.* **2021**, *27*, 10849–10853.

6.1 Preamble

An increase in electrophilicity on the chalcogen should strengthen a Te···O ChB. This could be achieved by installing an electron withdrawing group on the iso-tellurazole heterocycle. For example, trifluoromethyl or pentaflurophenyl groups at positions 3 or 5, respectively. However, preparing such compounds would require significant modifications to the established synthetic method. An alternative, faster to implement method would be to attach electron-withdrawing groups on the chalcogen. Divalent tellurium atoms are readily halogenated to λ^3 cationic or λ^4 neutral centres. However, there could also be detrimental effects. For example, increased steric hindrance at the chalcogen, decreased basicity of the oxygen atom and competition with the halogen atom as a ChB acceptor. Research in this chapter examined this concept with the chlorination of iso-tellurazole *N*-oxide **1b**.

Chemistry–A European Journal | Communication
doi.org/10.1002/chem.202101425
Chemistry Europe
European Chemical Societies Publishing

Competing Effects of Chlorination on the Strength of Te···O Chalcogen Bonds Select the Structure of Mixed Supramolecular Macrocyclic Aggregates of Iso-Tellurazole *N*-Oxides

Peter C. Ho,[a] Justin Lomax,[a] Valerie Tomassetti,[a] James F. Britten,[a] and Ignacio Vargas-Baca*[a]

Dedicated to Professor Tristram Chivers on the occasion of his 81st birthday

Abstract: Chlorination of 3-methyl-5-phenyl-1,2-tellurazole-2-oxide yielded the λ^4Te dichloro derivative. Its crystal structure demonstrates that the heterocycle retains its ability to autoassociate by chalcogen bonding (ChB) forming macrocyclic tetramers. The corresponding Te···O ChB distances are 2.062 Å, the shortest observed to date in aggregates of this type. DFT–D3 calculations indicate that while the halogenated molecule is stronger as a ChB donor it also is a weaker ChB acceptor; the overall effect is that the ChBs in the chlorinated homotetramer are not significantly stronger. However, partial halogenation or scrambling selectively yield the 2:2 heterotetramer with alternating λ^4Te and λ^2Te centers, which calculations identified as the thermodynamically preferred arrangement.

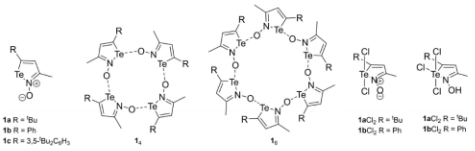

Scheme 1. Iso-tellurazole *N*-oxides, their macrocyclic aggregates and chlorinated derivatives.

Chalcogen bonding (ChB),[1–7] i.e. the attractive supramolecular interaction of electrophilic sites on atoms of heavy group 16-elements (S, Se, Te) with electron-rich centers, has unveiled an array of fascinating chemistry in fields as diverse as Lewis-acid catalysis,[8–15] optical probes,[14,16,17] functional materials,[5,18–24] crystal engineering,[25–30] ion recognition and transport,[22,31–36] and protein folding.[37]

Amongst the many molecules capable of forming ChBs, iso-tellurazole *N*-oxides (**1**, Scheme 1) stand apart because of their ability to spontaneously assemble cyclic tetramers ($\mathbf{1}_4$) and hexamers ($\mathbf{1}_6$) that exist in equilibrium in solution.[38–40] There are two electrophilic regions on the tellurium atom of **1**, antipodal to each the N–Te and the C–Te bonds. The former has a larger V_{max} and, consequently, the Te···O ChB interaction in all known cases is formed trans to the N atom (e.g. $\mathbf{1}_{4,6}$ in Scheme 1). The Te···O ChBs are reversible, scrambling is observed when **1a** and **1b** are mixed in solution. However, the annular aggregates behave in many respects as genuine macrocycles that host small molecules, form adducts with C_{60} and coordinate a variety of transition metal ions. Macrocyclic κ^4Te complexes of the tetramer have been isolated with Cu(I), Pd(II), Pt(II), and Rh(III); while Au(I) forms a binuclear complex in which the metals ions are bound to only one tellurium atom each.[41,42] Complexes of the hexamers have only been reported with Ag(I), with two endocyclic κ^2Te metal ions (also are bridged by two $CF_3SO_3^-$ anions) and two κ^1Te, κ^1C, κ^1O exocyclic silver ions.[42] The metal-free macrocycles are stable towards Lewis bases as strong as N-heterocyclic carbenes.[43] In contrast, their Te···O ChBs are readily cleaved by Brønsted and Lewis acids.[43,44] Protonation of the oxygen atom of **1** by HCl or HBr is reversible, which offers a means to switch the self-assembly on and off.[44] Boranes also bind the oxygen atom and break apart the macrocycles; the resulting adducts leave the tellurium atom readily available for bonding to ChB acceptors.[43]

Molecules with divalent chalcogens readily react with halogens, most commonly yielding λ^4 neutral or λ^3 cationic chalcogen centers. In the case of the possible products of halogenation of **1**, the increase of oxidation state should enhance the electrophilicity of the chalcogen and the stability of the Te···O ChBs.[45] However, steric hindrance between oxygen and the halogen atoms is likely to counter that effect. Competition between these factors makes it difficult to predict the overall effect that halogenation would have on the stability of the supramolecular macrocycles $\mathbf{1}_{4,6}$.[46] Furthermore, alternative structures could be assembled from $\mathbf{1}X_2$ (X=Cl, Br, I, Scheme 2). Dimers formed by Ch···O ChBs trans to C are known

[a] P. C. Ho, J. Lomax, V. Tomassetti, Dr. J. F. Britten, Dr. I. Vargas-Baca
Department of Chemistry and Chemical Biology
McMaster University
1280 Main Street West, L8S 4 M1 Hamilton, Ontario (Canada)
E-mail: vargas@chemistry.mcmaster.ca

Supporting information for this article is available on the WWW under https://doi.org/10.1002/chem.202101425Part of a Special Collection on Noncovalent Interactions.

Chemistry–A European Journal | Communication doi.org/10.1002/chem.202101425 | Chemistry Europe European Chemical Societies Publishing

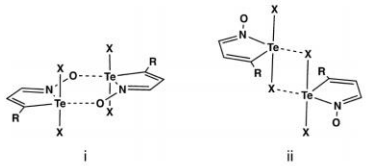

Scheme 2. Possible structures of the supramolecular dimers $(1X_2)_2$.

for the selenium analogue of **1 b**,[47] the corresponding arrangement for $(1X_2)_2$ would be structure i. Structure ii would be assembled by two antiparallel Te···X ChBs, which are common in the crystals of organotellurium trihalides, R–TeX.[48,49,58–62,50–57] We used a combined experimental and computational approach to investigate the nature of the products of chlorination of **1 b** and examine those issues.

Compound **1 b** readily reacts with chlorinating agents. An excess of freshly-purified SO_2Cl_2 yielded crystalline λ^4 dichloro iso-telurazole *N*-oxide (**1b**Cl_2) after a few hours. The crystal structure confirmed chlorination of the chalcogen with the Cl atoms at the axial positions of the disphenoidal center and show that the **1b**Cl_2 molecules retain their ability to form Te···O ChBs (Figure 1). The lattice contains macrocyclic tetramers, however, none of the molecular building blocks of $(\mathbf{1b}Cl_2)_4$ are related by symmetry. The four tellurium atoms are nearly coplanar (maximum deviation: 0.140 Å). The Te···O ChB lengths, are significantly shorter than in any known structures of $\mathbf{1}_{4r6r\infty}$ (2.171(3) to 2.242(1) Å).[38] In fact, they are comparable to the sum of covalent radii (2.10 Å). Conversely, the Te–N distances are longer than in $\mathbf{1}_{4r6r\infty}$ (2.197(2) to 2.258(3) Å). There is small expansion of the tetramer's cavity but one of the trans-annular Te–Te distances (5.581(1) and 5.712(1) Å) is comparable to one of the corresponding distances in $\mathbf{1b}_4$ (5.5895(2) and 5.3043(2) Å). The planes of all the iso-tellurazole heterocycles are oriented at distinct angles (12.0, 18.1, 33.6 and 49.7°) from the average Te_4 plane; the corresponding Cl–(Te)–Cl axes are nearly perpendicular (85.7, 86.6, 88.2, 89.0°) to each $TeNC_3$ ring. The Cl3–(Te2)–Cl4 axis is tilted from the Te_4 plane by just 36.4°, placing the Cl3 atom in close proximity to Te1 and Te3 (3.478(2) and 3.515(2) Å, respectively; Cf. $\Sigma r_{vdW} = 3.81$ Å). The Cl3–Te1–C1 angle (177.1(2)°) is optimal for interaction of a Cl lone pair with the Te electrophilic region that is antipodal to C1. The Cl3–Te3–C21 angle (138.6(2)°) is less favorable. These are additional Te···Cl ChBs that likely contribute to the unusual conformation of $(\mathbf{1b}Cl_2)_4$.

The reaction of **1 b** with half an equivalent of SO_2Cl_2 yielded a solid of composition **1b**Cl (by combustion analysis). Crystals grown from $CHCl_3$ feature a unit cell with solvent molecules and $\mathbf{1b}_2(\mathbf{1b}Cl_2)_2$ heterotetramers. The macrocycles display a chair conformation (Figure 2), similar to the structure of $\mathbf{1b}_4$, in which the four tellurium atoms are contained in the same plane.[38] The Te···O ChB distances are shorter for the λ^4 atoms than for the λ^2 Te atoms. Te–N bond lengths show the opposite trend. In each tetramer, the chlorinated λ^4 tellurium atoms occupy trans-annular positions. The Te- -Te distances (5.3451(4) and 5.3816(5), 5.4865(4) and 5.5792(3) Å) are comparable to those in $\mathbf{1b}_4$ and $(\mathbf{1b}Cl_2)_4$. The Cl–(Te)–Cl axes are tilted towards the Te_4 plane by 45.9 and 61.5°. However, the shortest Te- -Cl distance (3.90 Å) is longer than the sum of van der Waals radii. The specimen used for X-ray diffraction displayed a 92% chlorine occupancy about one Te atom, suggesting that the lattice contains a small proportion of $\mathbf{1b}_3(\mathbf{1b}Cl_2)$. Consequently, the positions of other atoms in the corresponding macrocycle are disordered as well.

Traces of moisture during chlorination led to the formation of crystalline **1b**HCl_3, i.e. the HCl adduct of **1b**Cl_2. As in the case of **1b**HCl,[44] protonation of the oxygen atom prevents formation of the Te···O ChBs. However, instead of a polymer, dimers are formed by a pair of antiparallel Te1···Cl2* chalcogen bonds, as in Scheme 2i, and a pair of O1–H···Cl2 hydrogen bonds (Figure 3). This structure provides useful points of comparison to the chlorinated macrocycles. The intermolecular Te1···Cl2* ChB distance and C1–Te1···Cl2* bond angles are similar to those that pertain the Te3···Cl3 ChB in $(\mathbf{1b}Cl_2)_4$. The Cl2 and Cl3 atoms occupy the axial positions on Te but the distance from Te1 to

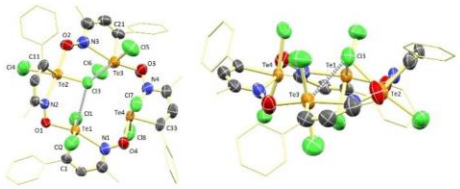

Figure 1. Two perspectives of the molecular structure in the crystal of $(\mathbf{1b}Cl_2)_4$. Hydrogen atoms are omitted for clarity; 90% ellipsoids. Selected distances (Å) and angles (°): Te1···O1 2.072(5), Te2···O2 2.088(6), Te3···O3 2.045(5), Te4···O4 2.043(5), Te1-N1 2.391(7), Te2-N2 2.363(7), Te3-N3 2.535(7), Te4-N4 2.439(7), Te1–C1 2.127(8), Te2–C11 2.152(9), Te3–C21 2.146(8), Te4–C33 2.121(9), Te1–Cl1 2.499(2), Te1–Cl2 2.487(2), Te2–Cl3 2.503(2), Te2–Cl4 2.513(3), Te3–Cl5 2.489(3), Te3–Cl6 2.481(2), Te4–Cl7 2.503(2), Te4–Cl8 2.471(2), N1–Te1···O1 162.3(2), N2–Te2···O2 159.2(2), N3–Te3···O3 162.4(2), N4–Te4···O4 162.6(2).

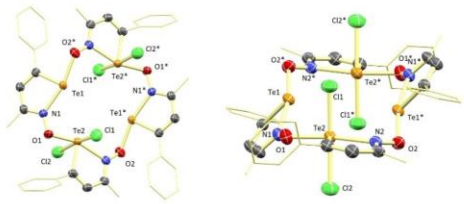

Figure 2. Two perspectives of the molecular structure in the crystal of $\mathbf{1b}_3(\mathbf{1b}Cl_2)_2$. Hydrogen atoms and solvent molecules are omitted for clarity; 70% displacement ellipsoids. Selected distances (Å) and angles (°) for two crystallographically independent molecules: Te1···O2* 2.204(1), 2.200(1), Te2···O1 2.098(1), 2.092(1), Te1-N1 2.205(1), 2.200(1), Te2-N2 2.307(1), 2.304(1), Te1–C1 2.085(1), 2.082(1), Te2–C11 2.123(1), 2.119(1), Te2–Cl1 2.4952(5), 2.4776(6), Te2–Cl2 2.5035(6), 2.5023(5), N1–Te1···O2* 165.62(5), 164.91(4), N2–Te2···O1 162.05(4), 161.03(5).

Chemistry–A European Journal | Communication
doi.org/10.1002/chem.202101425
Chemistry Europe
European Chemical Societies Publishing

Table 1. Calculated thermodynamic parameters (ADF, GGA DFT, PBE–D3, ZORA, all-electron TZ2P, gas phase) for the formation of aggregates, i.e. macrocyclic tetramers in chair conformation or dimers, from individual molecules of **1b**, **1b**Cl_2, or **1b**HCl_3. The position of the distinct Te atoms is identified in the isomers of **1b**$_2$(**1b**Cl_2)$_2$. All values are given in kJ per mole of aggregate unless otherwise noted.

Model[a]	**1b**$_4$	**1b**$_2$(**1b**Cl_2)$_2$ $\lambda^4_{eq}\lambda^2_{ax}\lambda^4_{eq}\lambda^2_{ax}$	**1b**$_2$(**1b**Cl_2)$_2$ $\lambda^4_{eq}\lambda^4_{ax}\lambda^2_{eq}\lambda^2_{ax}$	**1b**$_2$(**1b**Cl_2)$_2$ $\lambda^2_{eq}\lambda^4_{ax}\lambda^4_{eq}\lambda^2_{ax}$	(**1b**Cl_2)$_4$	(**1b**Cl_2)$_2$ i	(**1b**Cl_2)$_2$ ii	(**1b**Cl_3H)$_2$
ΔZPE [$\times 10^{-2}$ eV]	0.10	0.11	0.10	0.09	0.08	0.02	0.02	0.03
ΔH	−261.6	−297.9	−282.1	−283.4	−271.8	−43.1	−47.8	−109.6
ΔS [J mol^{-1}K^{-1}]	−676.4	−669.2	−688.6	−681.7	−737.7	−213.9	−220.6	−227.5
$\Delta G_{298.15K}$	−59.8	−98.4	−76.8	−80.1	−51.8	20.7	17.9	−41.8

[a] The sequence of tellurium atoms follows the ChB donor to ChB acceptor direction of the Te···O ChB interactions.

Cl2 is longer than to Cl3. Cl1 lays 0.340 Å from the average plane of the iso-tellurazole ring and has a bond to tellurium significantly shorter than in **1b**HCl (2.6605(5), 2.6816(5) Å). Conversely, the Te–N bond is longer than in **1b**HCl (2.173(2), 2.177(2) Å). Other bond lengths and angles within the iso-tellurazole heterocycles fall within the published ranges for the structures of **1b**HCl and **1b**HBr.

Relativistic GGA DFT–D3 calculations satisfactorily reproduced the experimental structures of (**1b**Cl_2)$_4$, **1b**$_2$(**1b**Cl_2)$_2$, and (**1b**HCl_3)$_2$ and were expanded to include the isomers of **1b**$_2$(**1b**Cl_2)$_2$, **1b**$_4$ in its chair conformation, and the hypothetical dimers (**1b**Cl_2)$_2$ in order to examine the thermodynamics of assembly from the respective molecular building blocks. The results are summarized in Table 1. Four isomers are possible for the heterotetramer **1b**$_2$(**1b**Cl_2)$_2$ in the chair conformation (Scheme 3), considering whether the two λ^4 Te atoms are in neighboring $TeNC_3$ heterocycles, the two possible orientations of the heterocycles and the direction of the Te···O ChB interaction. Geometry optimizations for a model in which the two λ^4 Te atoms were in the axial heterocycles converged to the conformation that contains them in the equatorial rings.

The calculation results indicate that neither (**1b**Cl_2)$_2$ dimer could significantly compete with formation of the (**1b**Cl_2)$_4$ tetramer. Also, the dimer of the protonated species, (**1b**Cl_3H)$_2$, significantly stabilized by the formation of a pair of N–O···H hydrogen bonds.

Amongst all the tetramers considered here, the mixed structures **1b**$_2$(**1b**Cl_2)$_2$ are thermodynamically more stable than **1b**$_4$. However, based on ΔH, the fully halogenated (**1b**Cl_2)$_4$ is only marginally more stable than **1b**$_4$; and the $\Delta G_{298.15K}$ is less favorable. The energy decomposition analysis (EDA) based on the Ziegler–Rauk transition-state formalism[63–65] was performed to reconcile such contrasting observations (Table 2). The energy contributions to one Te···O ChB were evaluated from two interacting molecules, using coordinates extracted from the most stable structures of the tetramers without further geometry optimization. In a tetramer, the total aggregation energy is the result of four ChBs. The results in Table 2 for **1b**Cl_2**1b**Cl_2 correspond to the average of all four ChBs in **1b**$_2$(**1b**Cl_2)$_2$; the entry for **1b**$_4$ belongs to the shortest ChB in the chair conformer of and is used as the base line against which the other calculations are compared.

As anticipated, chlorination does increase the electrophilicity of tellurium. The magnitude of the stabilizing electrostatic contribution (E_{elstat}) increases by more than 70 kJ mol^{-1} when **1b**Cl_2 is the ChB donor instead of **1b**. Congruently, V_{max} on the 10^{-3} a.u. iso-surface (Figure 4a) increases from 94.5 kJ mol^{-1} on

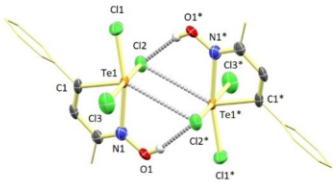

Figure 3. Molecular structure in the crystal of $C_{10}H_{10}Cl_3NOTe$. Hydrogen atoms are omitted for clarity; 75% displacement ellipsoids. Selected distances (Å) and angles (°): Te1-N1 2.407(7), Te1–C1 2.158(9), Te1–Cl1 2.394(2), Te1–Cl2 2.627(2), Te1–Cl3 2.410(3), Te···Cl2* 3.538(2), Cl2–Te1–Cl3 173.84(9), C1–Te···Cl2* 144.2(2).

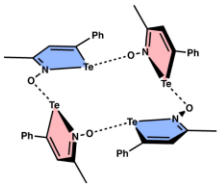

Scheme 3. Axial (red) and equatorial (blue) orientations of the building blocks in the chair conformation of **1b**$_4$.

Table 2. EDA, Te···O distance, bcp electron density and thermodynamic parameters (gas-phase) for the formation of Te···O ChBs in the macrocyclic tetramers (most stable structures) of **1b**$_4$, (**1b**)$_2$(**1b**Cl_2)$_2$, and (**1b**Cl_2)$_4$. Te and O superscripts identify the atom participating in the intermolecular interaction and thus the role of the corresponding building block as ChB donor or acceptor. All values in kJ mol^{-1} unless otherwise noted.

	1b^{Te}···**1b**^{O}	**1b**^{Te}···**1b**$Cl_2{}^{O}$	**1b**$Cl_2{}^{Te}$···**1b**^{O}	**1b**$Cl_2{}^{Te}$···**1b**$Cl_2{}^{O}$
E_{elstat}	−254.7	−227.8	−326.2	−303.00
E_{Pauli}	396.1	382.0	539.0	529.9
$E_{Orbital}$	−209.3	−206.0	−267.2	−265.1
$E_{Dispersion}$	−14.0	−25.8	−26.6	−27.6
E_{Te-O} [a]	−81.8	−77.6	−81.1	−65.8
d_{Te-O} [Å]	2.275	2.279	2.188	2.194
$r_{bcp,Te-O}$ (a.u.)	0.068	0.067	0.085	0.083

[a] $E_{Te-O} = E_{elstat} + E_{Pauli} + E_{Orbital} + E_{Dispersion}$.

Chemistry–A European Journal | Communication doi.org/10.1002/chem.202101425 | Chemistry Europe European Chemical Societies Publishing

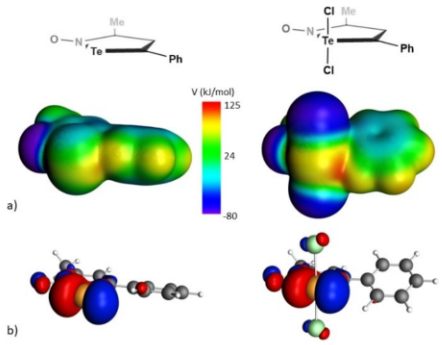

Figure 4. DFT analysis of electronic structure of **1 b** and **1b**Cl_2. (a) Electrostatic potential maps plotted on the 0.001 a.u. isodensity surfaces; (b) LUMOs plotted at 0.045 a.u.

1 b to 105.0 kJ mol^{-1} in **1b**Cl_2. However, chlorination of tellurium also impacts the nucleophilicity of the oxygen atom decreasing the magnitude of E_{elstat} by ca. 23 kJ mol^{-1} when **1b**Cl_2 is the ChB acceptor. The values of the Pauli repulsion (E_{Pauli}) reflect the effect of steric crowding on the tellurium atom. It imposes a 140 kJ mol^{-1} penalty when **1b**Cl_2 is the ChB donor; but there is little effect when **1b**Cl_2 is the ChB acceptor. In the Ziegler-Rauk scheme, the balance of electrostatic and Pauli contributions quantifies the interaction between the two molecular units with frozen electron clouds and would be destabilizing in all four cases were it not for orbital mixing and electron transfer. The calculated magnitude of the orbital interaction ($E_{orbital}$) is determined by the nature of the ChB donor, being ca. 58 kJ mol^{-1} more for **1b**Cl_2 than for **1 b**. In simplistic terms, this is related to the energy descent of the LUMO (predominantly the σ*Te–N orbital, Figure 4b) from −3.11 in **1 b** to −4.05 eV in **1b**Cl_2. Calculations for the interaction energy of ChBs formed by 1,2,5-chalcogenadiazoles[66] have shown correlation with the electron density at the bond critical point (bcp, QTAIM[67]); however no such correlation is apparent in this case, the Te···O distance appears to have a more important effect on the bcp density. In these calculations, dispersion is accounted for with Grimme's D^3 corrections and has an overall small contribution to the stability of the model ChB dimers.

The combination of all contributions to the Te···O ChB energy in these systems has important consequences. The ChB distance does not correlate with the magnitude of the energy of ChB interaction ($E_{Te\cdots O}$). Chlorination makes **1b**Cl_2 better than **1 b** as ChB donor, but worse as ChB acceptor. The ChB between two molecules of **1b**Cl_2 is not stronger than between **1 b** molecules. The interaction energies of individual ChBs in this case are not strictly additive, and the most stable assembly is the mixed **1b**$_2$(**1b**$Cl_2)_2$ macrocyclic structure in which **1 b** and **1b**Cl_2 alternate positions.

While low solubility precluded observing the resonances of the ^{13}C and ^{125}Te nuclei, the ^1H NMR spectra of the chlorinated products established the identity of the iso-tellurazole aggregates in CD_2Cl_2 solution. Two distinct iso-tellurazole patterns are discernible for **1b**$_2$(**1b**$Cl_2)_2$ while (**1b**$Cl_2)_4$ displays the pattern of one single iso-tellurazole oxide, albeit broadened and shifted to higher frequency than the spectrum of **1 b**. Different to the well-defined changes in the variable-temperature spectrum of **1 b** due to the tetramer-hexamer equilibrium,[38] the spectra of (**1b**$Cl_2)_4$ and **1b**$_2$(**1b**$Cl_2)_2$ in CD_2Cl_2 remained invariant between 189.4 and 298.0 K, aside from a thermal drift $< 2.5 \times 10^{-4}$ ppm K^{-1}. Most significantly, an equimolar mixture of **1b**$_4$ and (**1b**$Cl_2)_4$ produced the same NMR spectrum as pure **1b**$_2$(**1b**$Cl_2)_2$ (Figure S1). This observation indicates that the Te···O ChBs remain reversible and scrambling predominantly leads to the alternating structure, which is the thermodynamically preferred arrangement of the mixed aggregate. Such selectivity sharply contrasts with the observation of all possible homo- and heterotetramers in the equimolar mixture of **1 a** and **1 b**.[38]

Whereas complete chlorination of tellurium has conflicting effects on the ability of **1** to form ChBs, the spontaneous selection of an alternating sequence upon partial halogenation offers a unique strategy for the design of supramolecular macrocyclic architectures based on these ChB building blocks.

Supplementary Information

Experimental procedures, DFT optimized coordinates, and crystallographic parameters are reported in the Supporting Information. Deposition numbers 2073477 (for **1b**$_2$(**1b**$Cl_2)_2$), 2073475 (for (**1b**$Cl_2)_4$) and 2073476 (for (**1b**$Cl_3H)_2$) contain the supplementary crystallographic data for this paper. These data are provided free of charge by the joint Cambridge Crystallographic Data Centre and Fachinformationszentrum Karlsruhe Access Structures service.

Acknowledgements

The support of the Natural Sciences and Engineering Research Council (NSERC) of Canada (PCH PGSD; IVB DGI RGPIN-2016-06452) is gratefully acknowledged. This research was enabled in part by support provided by Compute Ontario (www.computeontario.ca) and Compute Canada (www.computecanada.ca).

Conflict of Interest

The authors declare no conflict of interest.

Keywords: chalcogen bonding · intermolecular interactions · macrocycles · supramolecular chemistry · tellurium

[1] C. B. Aakeroy, D. L. Bryce, G. R. Desiraju, A. Frontera, A. C. Legon, F. Nicotra, K. Rissanen, S. Scheiner, G. Terraneo, P. Metrangolo, G. Resnati, *Pure Appl. Chem.* **2019**, *91*, 1889–1892.
[2] L. Vogel, P. Wonner, S. M. Huber, *Angew. Chem. Int. Ed.* **2019**, *58*, 1880–1891; *Angew. Chem.* **2019**, *131*, 1896–1907.

Chemistry–A European Journal | Communication doi.org/10.1002/chem.202101425 | Chemistry Europe European Chemical Societies Publishing

[3] D. J. Pascoe, K. B. Ling, S. L. Cockroft, *J. Am. Chem. Soc.* **2017**, *139*, 15160–15167.
[4] J. S. Murray, P. Lane, T. Clark, P. Politzer, *J. Mol. Model.* **2007**, *13*, 1033–1038.
[5] K. T. Mahmudov, M. N. Kopylovich, M. F. C. Guedes Da Silva, A. J. L. Pombeiro, *Dalton Trans.* **2017**, *46*, 10121–10138.
[6] R. Gleiter, G. Haberhauer, D. B. Werz, F. Rominger, C. Bleiholder, *Chem. Rev.* **2018**, *118*, 2010–2041.
[7] I. Vargas-Baca, T. Chivers, *Phosphorus Sulfur Silicon Relat. Elem.* **2000**, *164*, 207–227.
[8] P. Wonner, L. Vogel, F. Kniep, S. M. Huber, *Chem. Eur. J.* **2017**, *23*, 16972–16975.
[9] S. Benz, A. I. Poblador-Bahamonde, N. Low-Ders, S. Matile, *Angew. Chem. Int. Ed.* **2018**, *57*, 5408–5412; *Angew. Chem.* **2018**, *130*, 5506–5510.
[10] L. Lu, Y. Lu, Z. Zhu, H. Liu, *J. Mol. Model.* **2020**, *26*, 1–12.
[11] P. Wonner, T. Steinke, L. Vogel, S. M. Huber, *Chem. Eur. J.* **2020**, *26*, 1258–1262.
[12] C. M. Young, A. Elmi, D. J. Pascoe, R. K. Morris, C. McLaughlin, A. M. Woods, A. B. Frost, A. Houpliere, K. B. Ling, T. K. Smith, A. M. Z. Slawin, P. H. Willoughby, S. L. Cockroft, A. D. Smith, *Angew. Chem. Int. Ed.* **2020**, *59*, 3705–3710; *Angew. Chem.* **2020**, *132*, 3734–3793.
[13] J. Bamberger, F. Ostler, O. G. Mancheño, *ChemCatChem* **2019**, *11*, 5198–5211.
[14] K. Strakova, L. Assies, A. Goujon, F. Piazzolla, H. V. Humeniuk, S. Matile, *Chem. Rev.* **2019**, *119*, 10977–11005.
[15] W. Wang, H. Zhu, L. Feng, Q. Yu, J. Hao, R. Zhu, Y. Wang, *J. Am. Chem. Soc.* **2020**, *142*, 3117–3124.
[16] X. Zhang, N. Sakai, S. Matile, *ChemistryOpen* **2020**, *9*, 18–22.
[17] A. Goujon, A. Colom, K. Straková, V. Mercier, D. Mahecic, S. Manley, N. Sakai, A. Roux, S. Matile, *J. Am. Chem. Soc.* **2019**, *141*, 3380–3384.
[18] A. F. Cozzolino, P. S. Whitfield, I. Vargas-Baca, *J. Am. Chem. Soc.* **2010**, *132*, 17265–17270.
[19] N. A. Pushkarevsky, A. V. Lonchakov, N. A. Semenov, E. Lork, L. I. Buravov, L. S. Konstantinova, G. T. Silber, N. Robertson, N. P. Gritsan, O. A. Rakitin, J. D. Woollins, E. B. Yagubskii, J. Beckmann, A. V. Zibarev, *Synth. Met.* **2012**, *162*, 2267–2276.
[20] M. Bai, S. P. Thomas, R. Kottokkaran, S. K. Nayak, P. C. Ramamurthy, T. N. Guru Row, *Cryst. Growth Des.* **2014**, *14*, 459–466.
[21] T. Dong, L. Lv, L. Feng, Y. Xia, W. Deng, P. Ye, B. Yang, S. Ding, A. Facchetti, H. Dong, H. Huang, *Adv. Mater.* **2017**, *29*, 1606025.
[22] G. E. Garrett, G. L. Gibson, R. N. Straus, D. S. Seferos, M. S. Taylor, *J. Am. Chem. Soc.* **2015**, *137*, 4126–4133.
[23] P. C. Ho, J. Z. Wang, F. Meloni, I. Vargas-Baca, *Coord. Chem. Rev.* **2020**, *422*, 213464.
[24] M. Fourmigué, A. Dhaka, *Coord. Chem. Rev.* **2020**, *403*, 213084.
[25] L. J. Riwar, N. Trapp, K. Root, R. Zenobi, F. Diederich, *Angew. Chem. Int. Ed.* **2018**, *57*, 17259–17264; *Angew. Chem.* **2018**, *130*, 17506–17512.
[26] N. Biot, D. Bonifazi, *Chem. Eur. J.* **2018**, *24*, 5439–5443.
[27] S. Langis-Barsetti, T. Maris, J. D. Wuest, *J. Org. Chem.* **2017**, *82*, 5034–5045.
[28] M. S. Pavan, A. K. Jana, S. Natarajan, T. N. Guru Row, *J. Phys. Chem. B* **2015**, *119*, 11382–11390.
[29] V. Kumar, Y. Xu, D. L. Bryce, *Chem. Eur. J.* **2020**, *26*, 3275–3286.
[30] P. Scilabra, G. Terraneo, G. Resnati, *Acc. Chem. Res.* **2019**, *52*, 1313.
[31] J. Y. C. Lim, P. D. Beer, *Chem* **2018**, *4*, 731–783.
[32] L. M. Lee, M. Tsemperouli, A. I. Poblador-Bahamonde, S. Benz, N. Sakai, K. Sugihara, S. Matile, *J. Am. Chem. Soc.* **2019**, *141*, 810–814.
[33] J. Y. C. Lim, I. Marques, A. L. Thompson, K. E. Christensen, V. Félix, P. D. Beer, *J. Am. Chem. Soc.* **2017**, *139*, 3122–3133.
[34] N. Biot, D. Bonifazi, *Coord. Chem. Rev.* **2020**, *413*, 213243.
[35] M. S. Taylor, *Coord. Chem. Rev.* **2020**, *413*, 213270.
[36] L. M. Lee, V. Corless, H. Luu, A. He, H. Jenkins, J. F. Britten, F. Adam Pani, I. Vargas-Baca, *Dalton Trans.* **2019**, *48*, 12541–12548.
[37] R. W. Newberry, R. T. Raines, *ACS Chem. Biol.* **2019**, *14*, 1677–1686.
[38] P. C. Ho, P. Szydlowski, J. Sinclair, P. J. W. Elder, J. Kübel, C. Gendy, L. M. Lee, H. Jenkins, J. F. Britten, D. R. Morim, I. Vargas-Baca, *Nat. Commun.* **2016**, *7*, 11299.
[39] P. C. Ho, J. Rafique, J. Lee, L. M. Lee, H. A. Jenkins, J. F. Britten, A. L. Braga, I. Vargas-Baca, *Dalton Trans.* **2017**, *46*, 6570–6579.
[40] J. Kübel, P. J. W. Elder, H. A. Jenkins, I. Vargas-Baca, *Dalton Trans.* **2010**, *39*, 11126–11128.
[41] P. C. Ho, R. Bui, A. Cevallos, S. Sequeira, J. F. Britten, I. Vargas-Baca, *Dalton Trans.* **2019**, *48*, 4879–4886.
[42] J. Wang, P. C. Ho, J. F. Britten, V. Tomassetti, I. Vargas-Baca, *New J. Chem.* **2019**, *43*, 12601–12608.
[43] P. C. Ho, H. A. Jenkins, J. F. Britten, I. Vargas-Baca, *Faraday Discuss.* **2017**, *203*, 187–199.
[44] P. C. Ho, L. M. Lee, H. Jenkins, J. F. Britten, I. Vargas-Baca, *Can. J. Chem.* **2016**, *94*, 453–457.
[45] A. Franconetti, D. Quiñonero, A. Frontera, G. Resnati, *Phys. Chem. Chem. Phys.* **2019**, *21*, 11313–11319.
[46] S. Scheiner, J. Lu, *Chem. Eur. J.* **2018**, *24*, 8167–8177.
[47] K. Shimada, A. Moro-oka, A. Maruyama, H. Fujisawa, T. Saito, R. Kawamura, H. Kogawa, M. Sakuraba, Y. Takata, S. Aoyagi, Y. Takikawa, C. Kabuto, *Bull. Chem. Soc. Jpn.* **2007**, *80*, 567–577.
[48] R. K. Chadha, J. E. Drake, *J. Organomet. Chem.* **1985**, *293*, 37–43.
[49] B. Krebs, F. P. Ahlers, *Adv. Inorg. Chem.* **1990**, *35*, 235–317.
[50] J. Pietikäinen, R. S. Laitinen, J. Konu, J. Valkonen, *Zeitschrift fur Naturforsch. – Sect. B J. Chem. Sci.* **2001**, *56*, 1369–1372.
[51] J. Bergman, J. Sidén, K. Maartmann-Moe, *Tetrahedron* **1984**, *40*, 1607–1610.
[52] L. D. Jason, D. M. Caleb, J. S. Michael, D. J. Nathan, P. J. Ragogna, *Inorg. Chem.* **2009**, *48*, 3239–3247.
[53] R. K. Askerov, J. M. Lukiyanova, Z. V. Matsulevich, A. V. Borisov, V. N. Khrustalev, *Acta Crystallogr. Sect. E Crystallogr. Commun.* **2015**, *71*, o598–o599.
[54] J. Bergman, L. Engman, *J. Organomet. Chem.* **1979**, *181*, 335–347.
[55] J. Bergman, T. Laitalainen, M. R. Sundberg, R. Uggla, R. Kivekäs, *Polyhedron* **1998**, *17*, 2153–2159.
[56] P. Singh, A. K. S. Chauhan, R. J. Butcher, A. Duthie, *J. Organomet. Chem.* **2013**, *731*, 49–54.
[57] D. Dakternieks, J. O'Connell, E. R. T. Tiekink, *J. Organomet. Chem.* **2000**, *598*, 49–54.
[58] R. L. O. R. Cunha, J. Zukerman-Schpector, I. Caracelli, J. V. Comasseto, *J. Organomet. Chem.* **2006**, *691*, 4807–4815.
[59] T. M. Klapötke, B. Krumm, P. Mayer, H. Piotrowski, O. P. Ruscitti, *Zeitschrift für Anorg. und Allg. Chemie* **2002**, *628*, 229–234.
[60] J. Beckmann, J. Bolsinger, A. Duthie, *Chem. Eur. J.* **2011**, *17*, 930–940.
[61] A. A. P. Y. V. Torubaev, A. V. Pavlova, *Koord. khimiia* **2012**, *38*, 229.
[62] F. Einstein, J. Trotter, C. Williston, *J. Chem. Soc. A Inorganic, Phys. Theor. Chem.* **1967**, 2018–2023.
[63] T. Ziegler, A. Rauk, *Theor. Chim. Acta* **1977**, *46*, 1–10.
[64] T. Ziegler, A. Rauk, *Inorg. Chem.* **1979**, *18*, 1558–1565.
[65] T. Ziegler, A. Rauk, *Inorg. Chem.* **1979**, *18*, 1755–1759.
[66] A. F. Cozzolino, P. J. W. Elder, L. M. Lee, I. Vargas-Baca, *Can. J. Chem.* **2013**, *91*, 338–347.
[67] R. F. W. Bader, *Chem. Rev.* **1991**, *91*, 893–928.

Manuscript received: April 21, 2021
Accepted manuscript online: May 20, 2021
Version of record online: June 9, 2021

Chapter 7. Iso-Tellurazolium-*N*-Phenoxides: a Family of Te···O Chalcogen-Bonding Supramolecular Building Blocks

Original citation: P.C. Ho, V. Tomassetti, J.F. Britten, I. Vargas-Baca,* "Iso-Tellurazolium-N-Phenoxides: a Family of Te···O Chalcogen-Bonding Supramolecular Building Blocks", *Inorg. Chem.*, **2021**, *60*, 16726–16733.

This scholarly work is printed with permission.

7.1 Preamble

The preceding chapters 2 to 6 illustrate the diversity of the supramolecular chemistry of iso-tellurazole *N*-oxides. However, cavities of their macrocyclic aggregates are rather small. Measured transannular Te---Te distances, range from 5.21 Å in the tetramer **2a**$_4$ to 7.64 Å in the hexamer **1b**$_6$. The host ability of these rings is therefore limited to small guests. This chapter explores the creation of larger macrocycles by increasing the distance between the nitrogen and oxygen atoms with a spacer group. Formal substitution of the oxygen atom on the nitrogen atom of the iso-tellurazole heterocycle with a phenoxide group could yield a molecule that retains the ability for form Te···O ChBs leading to the assembly of larger cavities. Three isomers, based on the substitution of the aromatic bridge, were prepared and investigated as crystalline solids and in solution.

Inorganic Chemistry

pubs.acs.org/IC Article

Iso-Tellurazolium-*N*-Phenoxides: A Family of Te···O Chalcogen-Bonding Supramolecular Building Blocks

Peter C. Ho, Valerie Tomassetti, James F. Britten, and Ignacio Vargas-Baca*

Cite This: *Inorg. Chem.* 2021, 60, 16726−16733 Read Online

ACCESS | Metrics & More | Article Recommendations | Supporting Information

ABSTRACT: Formal substitution of the oxygen atom of an iso-tellurazole *N*-oxide with deprotonated (*ortho*, *meta*, and *para*)-hydroxyphenyl groups generated molecules that readily aggregate through Te···O chalcogen bonding (ChB) interactions. The molecules undergo autoassociation in solution, as shown by variable temperature (VT) ^{1}H NMR experiments and paralleling the behavior of iso-tellurazole *N*-oxides. Judicious adjustment of crystallization conditions enabled the isolation of either polymeric or macrocyclic aggregates. Among the latter, the *ortho* compound assembled a calixarene-like trimer, while the *para* isomer built a macrocyclic tetramer akin to a molecular square. The Te···O ChB distances in these structures range from 2.13 to 2.17 Å, comparable to those in the structures of iso-tellurazole *N*-oxides. DFT calculations estimate that the corresponding Te···O ChB energies are between −122 and −195 kJ mol^{-1} in model dimers and suggest that macrocyclic aggregation enhances these interactions.

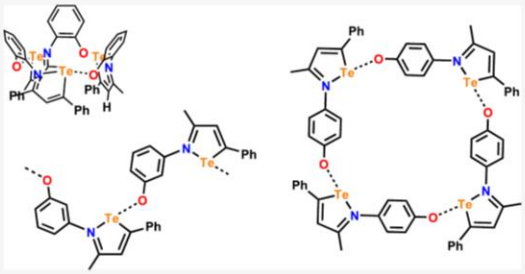

INTRODUCTION

The electrostatic potential at the surface of an atom in a molecule is not homogeneous. Covalent bonds polarize the electron density creating regions of nonzero potential,[1] even in homodiatomic molecules.[2] In the electron-depleted region antipodal to a bond, the σ-hole, the potential can be high enough to enable directional attractive interactions with nucleophilic sites.[3−6] This concept has enabled new understanding of the supramolecular interactions of electron-rich centers with molecules that contain heavy main-group elements[7] and sparked a surge of interest. Well-defined instances of these interactions have been identified across the p-block, and specific names are customarily used according to the family of the electrophilic element.[8] Halogen (XB)[9] and chalcogen bonding (ChB)[10,11] are IUPAC-endorsed terms. Vigorous research currently pursues the manipulation and application of ChB interactions to influence structure and function. While a significant portion of that research focuses on the solid state,[12−19] solution and dispersed-phase examples have been demonstrated in catalysis[20−23] as well as anion recognition[24,25] and transport.[26]

Less frequent in the literature are discrete aggregates of a few molecular units self-assembled by this type of interactions. Supramolecular macrocycles have been observed in the crystal structures of triiodo-1-methyl-imidazole,[27] dichalcogena alkynes,[28−30] 2-(iodoethynyl)pyridines,[31,32] and 1,2-tellurazole 2-oxides (**1** and **2** in Chart 1).[33−35] However, the latter are the only systems whose aggregates have been demonstrated to persist in solution. Because Te···O ChB interactions are reversible, the tetramers $\mathbf{1}_4$ and hexamers $\mathbf{1}_6$ coexist in equilibrium in solution, and the crystallization conditions permit selective isolation of either macrocycle or alternative polymeric phases. The self-assembly of **1** and **2** can be reversibly switched off by protonation or formation of O-adducts with boranes.[36,37] In the **1**-BR_3 (R = F, Ph) adducts, the electrophilic sites of tellurium are available for binding to

Chart 1. Iso-Tellurazole *N*-Oxides and *N*-Phenoxides

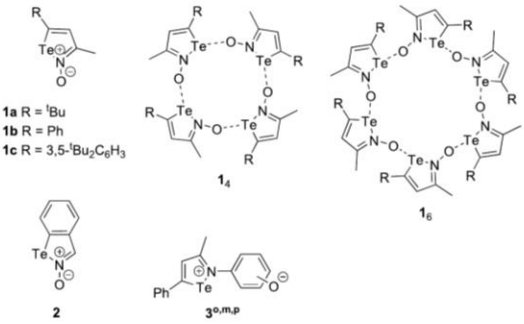

Received: August 23, 2021
Published: October 21, 2021

https://doi.org/10.1021/acs.inorgchem.1c02585
Inorg. Chem. 2021, 60, 16726−16733

Lewis bases.[37] Molecules of $\mathbf{1}Cl_2$ are stronger ChB donors but weaker ChB acceptors than **1**. The balance of competing effects selectively assembles 2:2 heterotetramers with alternating Te(II) and Te(IV) centers when **1b** is partially chlorinated or combined with an equimolar amount of $\mathbf{1b}Cl_2$.[38]

Despite the reversible nature of ChBs, the annular aggregates of **1** and **2** behave as veritable macrocycles capable of coordinating transition metal ions,[33,39,40] forming adducts with C_{60} and hosting small molecules.[33] Nevertheless, the cavities of $\mathbf{1}_4$ and $\mathbf{1}_6$ are small, transannular Te−Te distances range from 5.5 Å in $\mathbf{2a}_4$ to 7.6 Å in $\mathbf{1b}_6$. In pursuit of larger macrocyclic rings, we modified the structure of **1** by installing deprotonated hydroxyphenyl groups on nitrogen, in place of the oxygen atom. Three isomers ($\mathbf{3}^{o,m,p}$) are possible. While the *para* compound $\mathbf{3}^p\mathbf{1}$ the closest, the *meta* $\mathbf{3}^m$ and ortho **3***o* impose different geometric constraints and consequently should lead to new supramolecular arrangements.

■ EXPERIMENTAL SECTION

Materials and Methods. Air sensitive materials were handled under an atmosphere of argon. Organic solvents were purified either by distillation over the appropriate dehydrating agents under nitrogen or using an Innovative Technologies purification system. The following chemicals were used as received from the commercial suppliers: alumina (Fischer Chemical), dichloromethane-d_2 (Caledon), sulfuryl chloride (Aldrich). (*o*-, *m*-, *p*-) aminophenol hydrochlorides (Aldrich) were sublimed before use. (*Z*)-4-[(Dimethylamino)carbonyltelluro]-4-phenyl-3-buten-2-one was prepared as described elsewhere.[33]

Nuclear Magnetic Resonance. All spectra were measured in solution with a deuterated solvent. Spectra were obtained using Bruker AVANCE 500 MHz (Bruker 5 mm broadband inverse probe) or Bruker AVANCE 600 MHz (Bruker 5 mm broadband observe probe) spectrometers at 287.5 K. The ^{1}H, ^{13}C, and ^{125}Te spectra were processed using the Bruker TopSpin 3.2 software packages. The ^{1}H and ^{13}C spectra were referenced to tetramethyl silane using the deuterated solvent signal as a secondary reference. The ^{125}Te chemical shifts are reported with respect to the room-temperature resonance of $TeMe_2/C_6D_6$ (9:1, δ = 0.00 ppm)[41] but were measured using a secondary reference of diphenyl ditelluride in CD_2Cl_2 (3.73×10^{-4} M, δ = 420.36 ppm).

Electrospray Ionization Mass Spectrometry. Mass spectra were acquired in positive ion mode on an Agilent 1969 TOF mass spectrometer. Pure samples were dissolved in dichloromethane followed by dilution with methanol or dissolved and diluted with anhydrous acetonitrile. High-resolution mass spectra were obtained in a Waters Global and Ultima (ES Q-TOF) mass spectrometer (capillary = 3000−4000 V, cone = 60 V, source temperature = 300 °C, and resolving power = 6000−8000).

Other Instrumental Methods. IR spectra were measured by a Thermo Scientific Nicolet 6700 FT-IR spectrometer with a Smart iTX attenuated total reflectance (ATR) sample analyzer attachment. Combustion elemental analyses were carried out by the London Metropolitan University elemental analysis service (London, United Kingdom).

General Procedure for the Synthesis of Cl-3-H. In preliminary experiments, iso-tellurazole *N*-oxide **1b** was unreactive toward primary amines even in conditions that normally favor exchange with Schiff bases. The syntheses of $\mathbf{3}^{o,m,p}$ was instead carried out from (*Z*)-4-[(dimethylamino)carbonyltelluro]-4-phenyl-3-buten-2-one (**4**).

To (*Z*)-4-[(dimethylamino)carbonyltelluro]-4-phenyl-3-buten-2-one (**4**, 100 mg, 0.29 mmol), aminophenol hydrochloride (380 mg, 2.61 mmol, 9 equiv) and anhydrous ethanol (13 mL) were added. The mixture was refluxed through a dehydrating column under an argon atmosphere during 6 h. Crude products were isolated by reducing the reaction mixture and purified by recrystallization. All three hydrochlorides were sparingly soluble in common solvents at room temperature and their ^{125}Te NMR resonances could not be observed.

Cl-3°-H. 61% yield, brown solid. ^{1}H NMR (500 MHz, CD_3OD) δ 7.86 (s, 1H), 7.47−7.46 (m, 2H), 7.43−7.37 (m, 3H), 7.31 (dt, *J* = 7.9, 1.6 Hz, 1H), 7.19 (dd, *J* = 7.9, 1.6 Hz, 1H), 7.02 (dd, *J* = 8.3, 1.1 Hz, 1H), 6.99 (dt, *J* = 7.9, 1.1 Hz, 1H), 2.32 (s, 3H). ^{13}C NMR (500 MHz, CD_3OD) δ 178.2, 173.3, 151.9, 140.4, 132.5, 131.2, 130.5, 130.2,129.2, 128.9, 127.5, 120.9, 117.7, 20.5. IR: 3244, 3055, 3025, 1597, 1573, 1503, 1452, 1414, 1370, 1343, 1292, 1273, 1249, 1219, 1209, 1186, 1154, 1104, 1071, 1039, 1031, 1001, 938, 884, 866, 846, 806, 752, 727 cm^{-1}. HRMS (ESI-MS): *m*/*z* calcd for $[C_{16}H_{14}NO(^{130}Te)]^+$: *m*/*z* 366.0132, found 366.0137.

Cl-3^m-H. 80% yield, dark yellow solid. ^{1}H NMR (500 MHz, CD_3OD) δ 7.86 (s, 1H), 7.46−7.39 (m, 5H), 7.35 (t, *J* = 8.1 Hz, 1H), 6.91−6.89 (m, 1H), 6.77−6.75 (m, 1H), 6.72 (t, *J* = 2.1 Hz, 1H), 2.40 (s, 3H). ^{13}C NMR (500 MHz, CD_3OD) δ 177.2, 171.4, 159.8, 143.1, 140.5, 132.9, 131.5, 130.6, 130.2, 128.9, 116.7, 116.6, 112.8, 20.4. IR: 3230, 1597, 1559, 1498, 1454, 1422, 1373, 1352, 1315, 1285, 1205, 1178, 1161, 1154, 1086, 1074, 1030, 1019, 999, 962, 923, 914, 871, 859, 842, 816, 788, 758 cm^{-1}. HRMS (ESI-MS): *m*/*z* calcd for $[C_{16}H_{14}NO(^{130}Te)]^+$: *m*/*z* 366.0132, found 366.0135.

Cl-3^p-H. 77% yield, dark yellow solid. ^{1}H NMR (500 MHz, CD_3OD) δ 7.88 (s, 1H), 7.47−7.40 (m, 5H), 7.18−7.15 (m, 2H), 6.95−6.92 (m, 2H), 2.40 (s, 3H). ^{13}C NMR (500 MHz, CD_3OD) δ 176.8, 171.9, 159.3, 140.4, 133.6, 132.8, 130.5, 130.2, 128.9, 126.9, 117.0, 20.4. IR: 3265, 2920, 2850, 1608, 1592, 1560, 1507, 1492, 1458, 1441, 1374, 1346, 1278, 1218, 1206, 1158, 1100, 1014, 998, 857, 830, 798, 758, 712, 695, 606, 548 cm^{-1}. HRMS (ESI-MS): *m*/*z* calcd for $[C_{16}H_{14}NO(^{130}Te)]^+$: *m*/*z* 366.0132, found 366.0139.

General Procedure for the Synthesis of 3. A concentrated solution of Cl-3-H in MeOH was added to 10 volume amounts of $NaHCO_3$ (aq, 0.07 M) solution. Product was extracted with CH_2Cl_2 and washed with $NaHCO_3$ (aq) and distilled water. The solubility was reduced in cyclohexane and the product was isolated as yellow.

3°. 94% yield, dark yellow powder. ^{1}H NMR (500 MHz, $CDCl_3$) δ 8.28 (s, 1H), 7.98 (d, *J* = 8.5 Hz, 1H), 7.57−7.55 (m, 2H), 7.49−7.41 (m, 3H), 7.26 (d, *J* = 7.4 Hz, 1H), 7.22−7.19 (m, 1H), 6.74−6.71 (m, 1H), 3.15 (s, 3H). ^{13}C NMR (500 MHz, $CDCl_3$) δ 183.8, 159.8, 157.2, 137.7, 129.6, 128.9, 128.5, 128.4, 127.8, 127.6, 126.8, 117.2, 114.1, 26.4. ^{125}Te NMR (500 MHz, $CDCl_3$) δ 1779.8. IR: 3052, 3018, 2919, 2845, 1586, 1498, 1473, 1461, 1445, 1369, 1345, 1323, 1260, 1218, 1205, 1177, 1149, 1104, 1071, 1035, 1000, 986, 904, 887, 869, 847, 834, 808, 755, 732 cm^{-1}. HRMS (ESI-MS): *m*/*z* calcd for $C_{16}H_{14}NO[^{130}Te]$ $[M + H]^+$: *m*/*z* 366.0132, found 366.0133. Elemental analysis % calcd $C_{16}H_{13}NOTe{\cdot}C_6H_{12}$: C 59.11, H 5.64, N 3.13; found: C 59.37, H 5.79, N 3.05.

3^m. 95% yield, light yellow powder. ^{1}H NMR (500 MHz, $CDCl_3$) δ 7.57 (s, 1H), 7.49−7.47 (m, 2H), 7.37−7.30 (m, 3H), 6.91 (t, 1H), 6.27−6.26 (m, 2H), 5.94 (d, 1H), 2.14 (s, 3H). ^{13}C NMR (500 MHz, $CDCl_3$) δ 174.6, 167.4, 165.7, 142.0, 139.7, 129.6, 129.2, 129.0, 128.5, 127.7, 119.6, 115.1, 112.9, 20.4. ^{125}Te NMR (500 MHz, $CDCl_3$) δ 1545.6. IR: 3053, 3002, 2912, 2590, 1775, 1593, 1503, 1468, 1372, 1338, 1252, 1221, 1168, 1142, 1108, 1042, 1002, 988, 860, 848, 834, 805, 762, 735 cm^{-1}. HRMS (ESI-MS): *m*/*z* calcd for $C_{16}H_{14}NO[^{130}Te]$ $[M + H]^+$: *m*/*z* 366.0132, found 366.0126. Elemental analysis % calcd $C_{49}H_{41}Cl_2N_3O_3Te_3$ ($\mathbf{3}^m_3{\cdot}CH_2Cl_2$)*: C 50.15, H 3.52, N 3.58; found: C 49.90, H 3.68, N 3.33. *The pure compound cocrystallizes with CH_2Cl_2, which cannot be completely removed under high vacuum at 60 °C.

3^p. 90% yield, light yellow powder. ^{1}H NMR (500 MHz, CD_3OD) δ 7.59 (s, 1H), 7.47−7.48 (m, 2H), 7.35−7.41 (m, 3H), 6.98 (d, 2H), 6.88 (d, 2H), 2.28 (s, 3H). ^{13}C NMR (700 MHz, CD_3OD) δ 170.1, 168.8, 157.7, 141.1, 135.4, 130.3, 131.1, 129.3, 128.8, 125.9, 116.7, 20.5. ^{125}Te NMR (500 MHz, CD_3OD) δ1547.3. IR: 3050, 2977, 2596, 2484, 1770, 1607, 1589, 1507, 1488, 1466, 1374, 1344, 1254, 1224, 1162, 1100, 1073, 1031, 858, 835, 801, 759, 731, 695, 660, 624, 612, 588 cm^{-1}; HRMS (ESI-MS): *m*/*z*) calcd for $C_{16}H_{14}NO[^{130}Te]$ $[M + H]^+$: *m*/*z* 366.0132, found 366.0134. Elemental analysis % calcd $C_{16}H_{13}NOTe$: C 52.96, H 3.61, N 3.86; found: C 52.72, H 3.53, N 3.64.

https://doi.org/10.1021/acs.inorgchem.1c02585
Inorg. Chem. 2021, 60, 16726−16733

DFT Calculations. All calculations were performed using the ADF DFT package (versions 2017.01 to 2019.305).[42,43] Models for Cl-**3**-H, **3**, and their respective macrocyclic trimers and tetramers were optimized using the exchange-and-correlation functional of Perdew, Burke, and Ernzerhof[44] and corrected for dispersion.[45] The relativistic zeroth order regular approximation[46−49] was applied using specially adapted all-electron basis sets of triple-ζ quality with two polarization functions. Analytical frequency calculations were performed to demonstrate that each structure was at an actual minimum in the potential energy surface and to derive the corresponding thermodynamic parameters.[50,51] Supplemental analysis employed localization of orbitals by the Boys−Foster[52] and NBO[53] methods and the ETS-NOCV[54] charge and energy decomposition scheme.

Comparisons of the total bonding energy between molecules and aggregates were employed to evaluate the relative strengths of the Te···O chalcogen bonds formed by $\mathbf{3}^{o,m,p}$. The models are based on individual molecules of **1a**−**1c** and their dimers. All energetically minimized dimers are not planar, and the interplanar angles are 36.54, 74.12, and 70.59° in $\mathbf{3}^{o}_{2}$, $\mathbf{3}^{m}_{2}$, and $\mathbf{3}^{p}_{2}$, respectively. The interplanar angles of $\mathbf{3}^{m}_{2}$ and $\mathbf{3}^{p}_{2}$ deviate slightly from $\mathbf{3}^{m}_{\infty}$ (71.67°) and $\mathbf{3}^{p}_{\infty}$ (70.56°); the angles from $\mathbf{3}^{m}_{4}$ (57.26°) deviate much more. The optimized intramolecular distances in the dimers differ by less than 0.11 Å with respect to the crystallographic determinations and by less than 0.06 Å from the optimized individual molecules. The deviations in the Te···O distances are 0.062(3) and 0.080(2) Å for $\mathbf{3}^{m}_{2}$ and $\mathbf{3}^{p}_{2}$, respectively.

RESULTS AND DISCUSSION

Based on the synthesis of **1**,[33] the three isomers were prepared from a carbamotellurenyl vinyl ketone (**4**, Chart 2) by condensation with aminophenols, followed by deprotonation of the Cl-$\mathbf{3}^{o,m,p}$-H intermediates.

Chart 2. Synthetic Precursor of iso-Tellurazole *N*-Oxides and *N*-Phenoxides

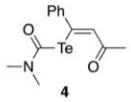

4

Crystal Structures. The Cl-**3**-H intermediates were isolated and authenticated by crystallographic structural determination. All three compounds have monoclinic $P2_1/c$ crystal lattices in which the oxygen atoms are protonated and no Te···O ChBs are observed (Figure 1). Instead, the halides form NTe···Cl ChBs, similar to the structures of H-**1b**-Cl/Br.[36] The Te···Cl distance is longest in Cl-$\mathbf{3}^{p}$-H and shortest in Cl-$\mathbf{3}^{o}$-H (Table 1); they are comparable to those in Cl-**1b**-H (2.6816(5), 2.6605(5) Å), much longer than in sterically protected aryltellurenyl chlorides (2.3484(1) Å,[55] Cf. Σr_{vdW} = 3.81 Å). Each Cl-$\mathbf{3}^{o,m,p}$-H molecule is connected to a neighbor by OH···Cl hydrogen bonds, forming infinite chains in Cl-$\mathbf{3}^{o,p}$-H and cyclic dimers in Cl-$\mathbf{3}^{m}$-H. The structure of Cl-$\mathbf{3}^{p}$-H also features interchain CTe···Cl ChBs.

As in the case of **1** and **2**, the crystal structures of $\mathbf{3}^{o,m,p}$ feature molecules associated through NTe···O ChBs (2.13−2.17 Å, Cf. Σr_{vdW} = 3.58 Å) organized in either infinite chains or macrocyclic aggregates. Te···O ChB distances and N−Te···O angles (Table 1) are comparable to those in the structures of **1** and **2**. Infinite chains are formed by the meta and para derivatives (Figure 2). Both crystallize in the $P2_1/n$ space group, and the chains are built by the glide planes with the C_3NTe heterocycles alternating in two orientations that subtend interplanar angles of 71.6° and 70.6° in $\mathbf{3}^{m}_{\infty}$ and

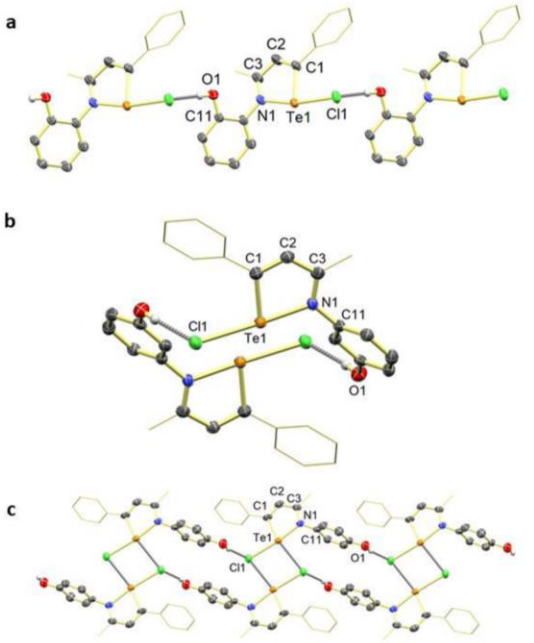

Figure 1. Arrangement of molecules in the crystals of Cl-$\mathbf{3}^{o}$-H (a), Cl-$\mathbf{3}^{m}$-H (b), Cl-$\mathbf{3}^{p}$-H (c). 75% displacement ellipsoids; hydrogen atoms are omitted; methyl and phenyl groups are shown as a wire frame for clarity.

$\mathbf{3}^{p}_{\infty}$, respectively. This arrangement is similar to that of $\mathbf{1a}_{\infty}$;[36] and contrasts with the helical chains of $(\mathbf{1a}_3{\cdot}C_6H_6)_{\infty}$.[33] The $\mathbf{3}^{m}_{\infty}$ chains feature additional CTe···Cl ChBs (3.632 Å, Cf. Σr_{vdW} = 3.81 Å) to CH_2Cl_2.

Compound $\mathbf{3}^{o}$ formed *P*-1 crystals featuring a cyclic trimer (Figure 3). Adjacent C_3NTe heterocycles subtend interplanar angles of 61.09, 61.26, and 64.18°. The pendant phenyl groups and the C_6H_4 bridges are located on opposite sides of the macrocycle backbone, resembling the structure of a calixarene. The cavity of $\mathbf{3}^{o}_{3}$ is smaller than that of an actual resorcinarene but large enough for a molecule of cyclohexane to dock onto. The $\mathbf{3}^{o}_{3}{\cdot}C_6H_{12}$ pairs stack in columns along *a*. Large pores between columns are occupied by cyclohexane molecules, the loss of which slowly degrades the crystals in ambient pressure and temperature. The structure suggests the possibility of creating open frameworks with ChBs. An actual supramolecular framework has been assembled with Te···O ChBs formed between carbonyl and tellurazole groups connecting macrocyclic peptides.[56]

A second polymorph of $\mathbf{3}^{p}$, also *P*-1, features macrocyclic tetramers (Figure 4). By the relative orientation of the C_3NTe heterocycles (57.26° interplanar angles), the structure is similar to the chair conformers of $\mathbf{1b}_4$ and $\mathbf{2a}_4$,[33,35] but all the tellurium atoms are contained in the same plane. These macrocycles are comparable in size to the $[M_4(4,4'bipy)_4]^{8+}$ (M = Pd, Pt) molecular squares,[57,58] as shown by the two trans-annular Te−Te distances: 11.2289(6) and 11.3623(6) Å. In the crystal, the cavity is occupied by a molecule of CH_2Cl_2 disordered in two orientations as the macrocycle sits on an inversion center. Consequently, two of the O−C_6H_4−N bridges also are rotationally disordered.

https://doi.org/10.1021/acs.inorgchem.1c02585
Inorg. Chem. 2021, 60, 16726−16733

Table 1. Selected Distances (Å) and Angles in the Crystal Structures of Cl-$3^{o,m,p}$-H and $3^{o,m,p}$[a]

crystal composition	Cl-3^o-H	Cl-3^m-H	Cl-3^p-H	$3^o{}_3$	$3^m{}_\infty$	$3^p{}_\infty$	$3^p{}_4$
				Distance (Å)			
Te1−C1	2.088(2)	2.100(4)	2.098(5)	2.078(3), 2.077(2), 2.076(3)	2.087(4)	2.088(5)	2.082(5), 2.098(4)
Te1−N1	2.168(1)	2.154(2)	2.153(5)	2.184(2), 2.187(2), 2.202(2)	2.233(3)	2.203(4)	2.229(5), 2.231(4)
C1−C2	1.357(2)	1.368(4)	1.357(8)	1.359(4), 1.363(4), 1.366(3)	1.357(6)	1.356(7)	1.354(6), 1.370(9)
C2−C3	1.436(2)	1.430(5)	1.422(9)	1.428(4), 1.432(4), 1.435(4)	1.440(6)	1.452(6)	1.438(7), 1.443(9)
C3−N1	1.315(2)	1.324(5)	1.328(7)	1.312(3), 1.313(4), 1.316(5)	1.307(5)	1.306(6)	1.295(6), 1.302(7)
Te−Cl1	2.6165(5)	2.6942(9)	2.696(2)				
Te···O†				2.164(2), 2.167(2), 2.181(2)	2.145(3)	2.147(2)	2.129(4), 2.134(5)
Te1···Te1†				4.7511(5), 4.8239(5), 4.8817(5)	7.0616(4)	8.596(1)	7.8093(5), 8.1615(6)
				Bond Angles (deg)			
Te1−N1−C11	120.8(1)	119.8(2)	121.3(3)	120.3(2), 120.7(2), 121.4(2)	121.4(2)	118.7(3)	119.6(3), 123.0(5)
N1−Te1−C1	77.53(6)	78.1(1)	77.6(2)	76.6(1), 76.7(1), 76.8(1)	75.9(1)	76.8(2)	76.1(2), 76.2(2)
N1−Te1−Cl1	168.04(4)	172.86(7)	171.7(1)				
N1−Te1−O†				163.94(8), 164.04(8), 164.30(8)	165.7(1)	169.0(1)	164.1(1), 164.6(1)
				Torsion Angles (deg)			
C1−Te1−N1−C11	174.7(1)	177.5(2)	179.5(4)	174.1(2), 178.3(2), 179.3(2)	179.7(3)	179.5(4)	179.5(4), 179.9(7)
C3−N1−C11−C12	61.8(2)	55.9(4)	79.2(7)	63.0(4), 63.7(4), 67.0(4)	77.0(5)	62.9(7)	50(2), 57.6(7), 140.0(8)
Cl1−Te1−N1−C11	175.3(1)	129.7(5)	167.5(6)				
O1*−Te1−N1−C11				174.3(2), 176.2(2), 177.9(2)	173.6(4)	176.4(5)	160.3(4), 168.9(7)
N1−Te1−O1*−C 12/13/14*				170.6(3), 173.1(3), 173.3(3)	69.3(5)	109.1(7)	83(1), 154.8(5)

[a]* and † denote chemically equivalent atoms in a neighboring molecule.

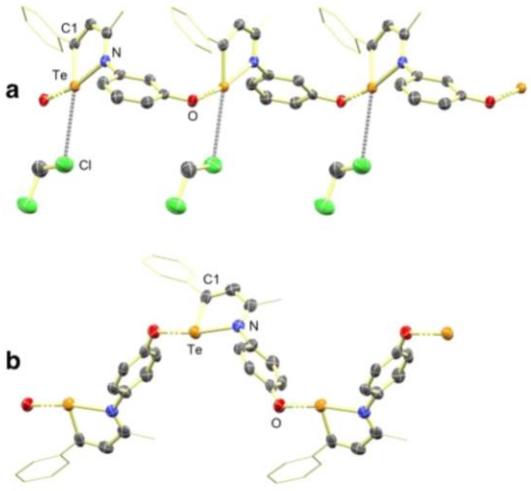

Figure 2. Detail of the arrangement of molecules in the crystals of (a) $(\mathbf{3^m}{\cdot}CH_2Cl_2)_\infty$ grown from CH_2Cl_2/CH_3OH and (b) $\mathbf{3^p}_\infty$ grown from CH_2Cl_2. Displacement ellipsoids at 75%. For clarity, selected hydrogen atoms are omitted, and phenyl and methyl groups are shown as wire frames.

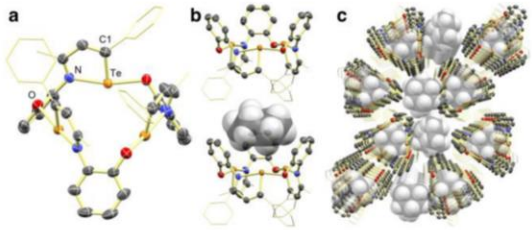

Figure 3. Details of the crystal structure of $\mathbf{3^o}_3{\cdot}3C_6H_{12}$ obtained from CH_2Cl_2/C_6H_{12}: (a) macrocyclic aggregate and (b) columnar stack of molecules along *a* and (c) lattice viewed along *a*. Displacement ellipsoids at 75%. For clarity, selected hydrogen atoms are omitted, phenyl and methyl groups are shown as a wire frame, and cyclohexane are shown as space-filling models.

Spectroscopy. Electrospray mass spectrometry (ESMS) suggested the NTe···O ChBs between molecules of $\mathbf{3^{o,m,p}}$ exist beyond the solid state. The isotopic patterns of consecutive $[\mathbf{3}_n\text{-H}]^+$ aggregates up to $n = 2$ were detected for $\mathbf{3^o}$, $n = 4$ for $\mathbf{3^p}$ and $n = 5$ for $\mathbf{3^m}$. These results resemble the observation of $[\mathbf{1b}_n\text{-H}]^+$ ($n = 1-7$) ions.[33]

In the case of **1**, NMR spectroscopy provided evidence of aggregation in solution.[33] Measurable NOE between the Me and the ^{t}Bu/Ph groups established that the molecules are connected by NTe···O ChBs, spectral changes in a **1a−1b** continuous variations experiment was consistent with tetramers in solution and the dependence of the spectrum on concentration revealed the equilibrium with the hexamer. As NSe···O ChBs are weaker, the temperature dependence of

https://doi.org/10.1021/acs.inorgchem.1c02585
Inorg. Chem. 2021, 60, 16726−16733

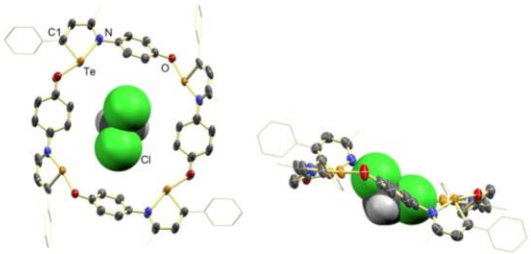

Figure 4. Two views of the macrocyclic arrangement of molecules in the crystal of $\mathbf{3}^{\mathbf{p}}_4$, grown from C_6H_6/CH_2Cl_2 (20% w/w). Displacement ellipsoids at 75%. For clarity, selected hydrogen atoms are omitted, phenyl and methyl groups are visualized as wire frames, and the disorder of the aromatic bridges is not shown.

the molecules-aggregates equilibrium was observed for the selenium analogue of **2**.[35]

Similarly, the variable temperature (VT) ^{1}H NMR spectra of $\mathbf{3}^{\mathbf{o,m,p}}$ point to aggregation in solution. NOE between protons that are too distant in the individual molecules was observed for the three compounds. At 190 K in CD_2Cl_2, the spectra of $\mathbf{3}^{\mathbf{m,p}}$ displayed significant broadening and intricate patterns that could not be completely resolved with our 500 MHz instrument. The spectra did simplify at higher temperatures; broadening disappeared at 280 K for $\mathbf{3}^{\mathbf{m}}$ but persisted beyond 320 K for $\mathbf{3}^{\mathbf{p}}$ in $CDCl_2$−$CDCl_2$. Such dynamic processes could originate in exchange between aggregates of different size or conformers but not individual molecules.

In contrast, the ^{1}H NMR spectrum of $\mathbf{3}^{\mathbf{o}}$ (Figure 5b) displayed no significant broadening upon cooling but a new set of resonances grew at the expense of the first. The change was nearly complete at 190 K, the new pattern still corresponding to $\mathbf{3}^{\mathbf{o}}$. The resonances of the heterocyclic hydrogen and the methyl protons underwent large shifts. At 298 K, these nuclei resonated at 8.33 and 3.14 ppm (Figure S2a), unusually high frequencies not observed in any spectrum of $\mathbf{3}^{\mathbf{m,p}}$ or **1b**. At 190 K, the corresponding singlets appeared at the more typical 7.70 and 1.86 ppm. The unusual high frequencies at 280 K likely resulted from the structure of the trimer. The affected nuclei are in close proximity to the phenyl ring (Figure 5a) and thus are subject to the effect of the phenyl ring current. The ratio of intensities of the low and high temperature resonances was dependent on the total concentration (Figure 5c). The trimer was more abundant in dilute solution and high temperature, suggesting that the second species has a larger aggregation number. The situation is reminiscent of the equilibrium between $\mathbf{1b}_4$ and $\mathbf{1b}_6$, but the stochiometric coefficient of ∼1.6 suggests that the aggregate is predominant at low temperature and high concentration is $\mathbf{3}^{\mathbf{o}}_5$. The decrease of entropy (Figure 5d) is consistent with autoassociation. However, attempts to crystallize and structurally authenticate the larger oligomer have been unsuccessful.

Computational Modeling. Gas-phase calculations for models of $\mathbf{3}^{\mathbf{o,m,p}}_2$, $\mathbf{3}^{\mathbf{o}}_3$, and $\mathbf{3}^{\mathbf{p}}_4$ gave electronic aggregation energies (ΔE_{total}, Table 2) ranging from −122 to −195 kJ mol^{-1} (Cf. −60 to −80 kJ/mol for aggregates of **1** and **2**). The energy decomposition analysis (EDA) showed that the Pauli (steric repulsion) is considerably smaller in the aggregates of $\mathbf{3}^{\mathbf{o,m,p}}$. There is a strong electrostatic contribution (ΔE_{elstat}), as expected, from the V_{max} of the electrophilic region on tellurium (Figure 6, $\mathbf{3}^{\mathbf{o}}$ 110, $\mathbf{3}^{\mathbf{m}}$ 118, $\mathbf{3}^{\mathbf{p}}$ 87 kJ mol^{-1}; Cf. **1b** 150,[33] **2** 140[35] kJ mol^{-1}). The electrostatic contributions, however, are not enough to counter the Pauli repulsion. Strong polarization or covalency ($\Delta E_{orbital}$) from the interaction of the LUMO (predominantly σ^*_{Te-N}) with an oxygen lone pair is necessary to form Te···O ChBs. NBO and Boys−Foster localized orbitals are consistent with this model. ETS-NOCV calculations for the dimers estimate that this energetic contribution is between −90 and −160 kJ/mol. While stabilizing, dispersion is a modest contribution in this case. Comparison of the calculations for the dimers $\mathbf{3}^{\mathbf{o,p}}_2$ (bearing only one Te···O ChB) with those of $\mathbf{3}^{\mathbf{o}}_3$ and $\mathbf{3}^{\mathbf{p}}_4$ show that the effect of the ChBs is not additive, i.e., formation of the macrocycles

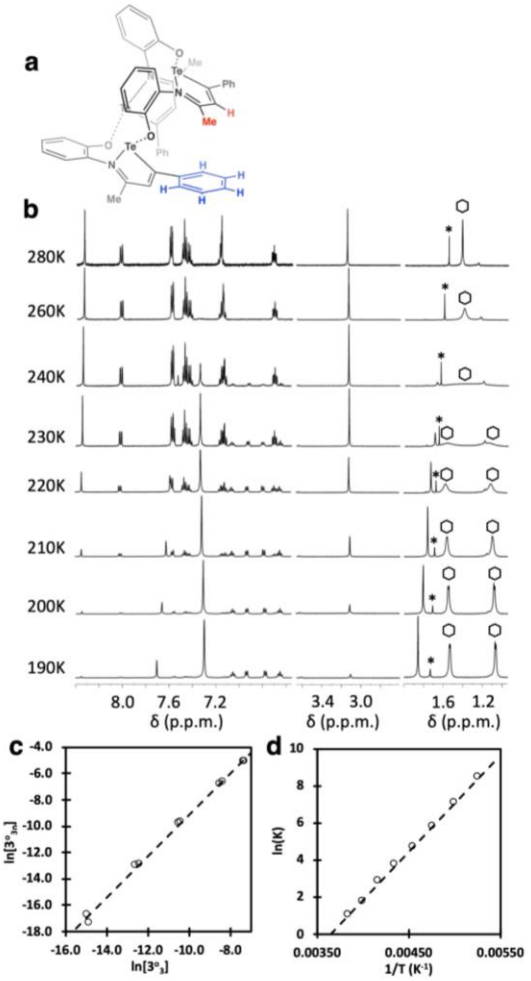

Figure 5. NMR investigation of $\mathbf{3}^{\mathbf{o}}$. (a) Orientation of the phenyl and methyl groups and the heterocyclic proton in the trimer $\mathbf{3}^{\mathbf{o}}_3$. (b) VT ^{1}H spectra acquired between 190 and 280 K; * and ⬡ denote the resonances of residual H_2O and cyclohexane, respectively. (c) Determination of stoichiometric coefficient (n = 1.57 ± 0.03) and equilibrium constant ($K = |\mathbf{3}^{\mathbf{o}}_n|/|\mathbf{3}^{\mathbf{o}}_3|^n$; ln K = 6.1 ± 0.4) from the integrations of the resonances of the methyl and heterocyclic ^{1}H nuclei as a function of concentration at 220 K. (d) Van't Hoff plot (ΔH = −43.3 ± 0.5 kJ mol^{-1}, ΔS = −158 ± 3 J mol^{-1} K^{-1}).

https://doi.org/10.1021/acs.inorgchem.1c02585
Inorg. Chem. 2021, 60, 16726−16733

Table 2. ChB Distances and Energy[a] Decomposition Analysis (AMS DFT: PBE-D3, ZORA, TZ2P All-Electron) For Model Aggregates of $3^{o,m,p}$

model	$3^o{}_2$	$3^o{}_3$	$3^m{}_2$	$3^p{}_2$	$3^p{}_4$
$d(\text{Te}\cdots\text{O})_{calc}$ (Å)	2.316	2.212	2.207	2.227	2.172, 2.177
ΔE_{elstat}	−261.1	−310.3	−357.7	−331.4	−376.7
ΔE_{Pauli}	397.8	495.7	546.5	518.2	601.7
$\Delta E_{orbital}$[c] $\{LP_O{-}\sigma^*_{TeN}\}$[d]	−218.6 {-79.0}	−323.9	−356.8 {-159.3}	−300.6 {-92.0}	−390.4
ΔE_{disp}	−39.7	−33.7	−26.7	−26.6	−16.8
ΔE_{total}[b]	−121.7	−172.2	−194.7	−140.3	−182.2
ΔH	−93.0	−131.8	−145.5	−105.8	−142.2
ΔS (J mol^{-1} K^{-1})	−230.0	−162.0	−222.8	−273.2	−212.4
$\Delta G_{298\ K}$	−24.2	−83.50	−79.1	−24.3	−78.9

[a]All values are scaled to one Te···O ChB and given in kJ mol^{-1}, unless otherwise noted. [b]$\Delta E_{total} = \Delta E_{elstat} + \Delta E_{Pauli} + \Delta E_{orbital} + \Delta E_{disp}$ by the transition state method.[59−61] [c]$\Delta E_{orbital}$ includes intramolecular (polarization) and intermolecular contributions. [d]ETS-NOCV calculation

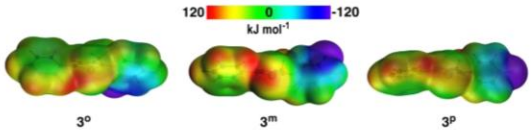

Figure 6. DFT-calculated electrostatic potential maps of $3^{o,m,p}$ plotted on the 0.001 au isodensity surfaces. Negative values are truncated at −120 kJ mol^{-1} for clarity.

enhances the stability of the Te···O links. The effect is also observed in the Te···O ChB distances as well as the enthalpy and free energy of aggregation from the corresponding vibrational calculations. These thermodynamic parameters are taken with caution as they do not account for solvation changes.

CONCLUSION

Macrocyclic species are fundamental pillars of supramolecular chemistry.[62] There are natural examples, but most macrocycles are synthetic; their preparation and purification often are laborious processes. Such limitations are in sharp contrast to the ease with which NTe···O interactions can build annular structures from one molecular building block. Even in the case of metallamacrocycles, assembly requires steps of ligand substitution that are fairly complex in comparison to the formation and dissociation of ChBs. In this article, we demonstrated that the self-assembling abilities of the isotellurazole *N*-oxides survive modifications to the ChB acceptor center. While reversibility can hinder some applications of ChB-assembled macrocycles, it also offers the possibility of combining different building blocks with distinct geometric preferences and invites investigating the adaptive self-assembly of host structures around templating guests.

ASSOCIATED CONTENT

Supporting Information

The Supporting Information is available free of charge at https://pubs.acs.org/doi/10.1021/acs.inorgchem.1c02585.

Crystallographic details, spectroscopic characterization data, and optimized Cartesian coordinates of the computational models (PDF)

Accession Codes

CCDC 2091360−2091365 and 2096539 contain the supplementary crystallographic data for this paper. These data can be obtained free of charge via www.ccdc.cam.ac.uk/data_request/cif, or by emailing data_request@ccdc.cam.ac.uk, or by contacting The Cambridge Crystallographic Data Centre, 12 Union Road, Cambridge CB2 1EZ, UK; fax: +44 1223 336033.

AUTHOR INFORMATION

Corresponding Author

Ignacio Vargas-Baca − *Department of Chemistry and Chemical Biology, McMaster University, Hamilton, Ontario, Canada L8S 4M1*; orcid.org/0000-0002-3074-2051; Email: vargas@chemistry.mcmaster.ca

Authors

Peter C. Ho − *Department of Chemistry and Chemical Biology, McMaster University, Hamilton, Ontario, Canada L8S 4M1*

Valerie Tomassetti − *Department of Chemistry and Chemical Biology, McMaster University, Hamilton, Ontario, Canada L8S 4M1*

James F. Britten − *Department of Chemistry and Chemical Biology, McMaster University, Hamilton, Ontario, Canada L8S 4M1*

Complete contact information is available at: https://pubs.acs.org/10.1021/acs.inorgchem.1c02585

Author Contributions

P.C.H. and V.T. performed all the experiments. J.F.B. oversaw the crystallographic characterization. P.C.H. and I.V.-B. designed the experiments, interpreted the results, and wrote manuscript.

Notes

The authors declare no competing financial interest.

ACKNOWLEDGMENTS

We gratefully acknowledge the support of the Natural Sciences and Engineering Research Council (NSERC) of Canada (I.V.-B., DG; P.C.H., PGSD). This research was enabled in part by support provided by the Shared Hierarchical Academic Research Computing Network (SHARCNET, www.sharcnet.ca) and Compute Canada (www.computecanada.ca).

REFERENCES

(1) Politzer, P.; Murray, J. S.; Concha, M. C. Halogen Bonding and the Design of New Materials: Organic Bromides, Chlorides and Perhaps Even Fluorides as Donors. *J. Mol. Model.* **2007**, *13*, 643−650.

(2) Walbaum, C.; Richter, M.; Sachs, U.; Pantenburg, I.; Riedel, S.; Mudring, A.-V.; Meyer, G. Iodine−Iodine Bonding Makes Tetra(Diiodine)Chloride, [Cl(I2)4]−, Planar. *Angew. Chem., Int. Ed.* **2013**, *52*, 12732−12735.

(3) Murray, J. S.; Lane, P.; Clark, T.; Politzer, P. σ-Hole Bonding: Molecules Containing Group VI Atoms. *J. Mol. Model.* **2007**, *13*, 1033−1038.

(4) Clark, T.; Hennemann, M.; Murray, J. S.; Politzer, P. Halogen Bonding: The σ-Hole: Proceedings of "Modeling Interactions in Biomolecules II", Prague, September 5th-9th, 2005. *J. Mol. Model.* **2007**, *13*, 291−296.

(5) Riley, K. E.; Murray, J. S.; Politzer, P.; Concha, M. C.; Hobza, P. Br···O Complexes as Probes of Factors Affecting Halogen Bonding: Interactions of Bromobenzenes and Bromopyrimidines with Acetone. *J. Chem. Theory Comput.* **2009**, *5*, 155−163.
(6) Shields, Z. P.; Murray, J. S.; Politzer, P. Directional Tendencies of Halogen and Hydrogen Bonds. *Int. J. Quantum Chem.* **2010**, *110*, 2823−2832.
(7) Alcock, N. W. Secondary Bonding to Nonmetallic Elements. *Adv. Inorg. Chem. Radiochem.* **1972**, *15*, 1−58.
(8) Cavallo, G.; Metrangolo, P.; Pilati, T.; Resnati, G.; Terraneo, G. Naming Interactions from the Electrophilic Site. *Cryst. Growth Des.* **2014**, *14*, 2697−2702.
(9) Cavallo, G.; Metrangolo, P.; Milani, R.; Pilati, T.; Priimagi, A.; Resnati, G.; Terraneo, G. The Halogen Bond. *Chem. Rev.* **2016**, *116*, 2478−2601.
(10) Pascoe, D. J.; Ling, K. B.; Cockroft, S. L. The Origin of Chalcogen-Bonding Interactions. *J. Am. Chem. Soc.* **2017**, *139*, 15160−15167.
(11) Vogel, L.; Wonner, P.; Huber, S. M. Chalcogen Bonding: An Overview. *Angew. Chem., Int. Ed.* **2019**, *58*, 1880−1891.
(12) Mahmudov, K. T.; Kopylovich, M. N.; Guedes Da Silva, M. F. C.; Pombeiro, A. J. L. Chalcogen Bonding in Synthesis, Catalysis and Design of Materials. *Dalton Trans.* **2017**, *46*, 10121−10138.
(13) Ho, P. C.; Wang, J. Z.; Meloni, F.; Vargas-Baca, I. Chalcogen Bonding in Materials Chemistry. *Coord. Chem. Rev.* **2020**, *422*, 213464.
(14) Pushkarevsky, N. A.; Lonchakov, A. V.; Semenov, N. A.; Lork, E.; Buravov, L. I.; Konstantinova, L. S.; Silber, G. T.; Robertson, N.; Gritsan, N. P.; Rakitin, O. A.; Woollins, J. D.; Yagubskii, E. B.; Beckmann, J.; Zibarev, A. V. First Charge-Transfer Complexes between Tetrathiafulvalene and 1,2,5-Chalcogenadiazole Derivatives: Design, Synthesis, Crystal Structures, Electronic and Electrical Properties. *Synth. Met.* **2012**, *162*, 2267−2276.
(15) Dong, T.; Lv, L.; Feng, L.; Xia, Y.; Deng, W.; Ye, P.; Yang, B.; Ding, S.; Facchetti, A.; Dong, H.; Huang, H. Noncovalent Se···O Conformational Locks for Constructing High-Performing Optoelectronic Conjugated Polymers. *Adv. Mater.* **2017**, *29*, 1606025.
(16) Garrett, G. E.; Gibson, G. L.; Straus, R. N.; Seferos, D. S.; Taylor, M. S. Chalcogen Bonding in Solution: Interactions of Benzotelluradiazoles with Anionic and Uncharged Lewis Bases. *J. Am. Chem. Soc.* **2015**, *137*, 4126−4133.
(17) Fourmigué, M.; Dhaka, A. Chalcogen Bonding in Crystalline Diselenides and Selenocyanates: From Molecules of Pharmaceutical Interest to Conducting Materials. *Coord. Chem. Rev.* **2020**, *403*, 213084.
(18) Kumar, V.; Xu, Y.; Bryce, D. L. Double Chalcogen Bonds: Crystal Engineering Stratagems via Diffraction and Multinuclear Solid-State Magnetic Resonance Spectroscopy. *Chem. Eur. J.* **2020**, *26*, 3275−3286.
(19) Scilabra, P.; Terraneo, G.; Resnati, G. The Chalcogen Bond in Crystalline Solids: A World Parallel to Halogen Bond. *Acc. Chem. Res.* **2019**, *52*, 1313.
(20) Benz, S.; López-Andarias, J.; Mareda, J.; Sakai, N.; Matile, S. Catalysis with Chalcogen Bonds. *Angew. Chem., Int. Ed.* **2017**, *56*, 812−815.
(21) Wang, W.; Zhu, H.; Feng, L.; Yu, Q.; Hao, J.; Zhu, R.; Wang, Y. Dual Chalcogen-Chalcogen Bonding Catalysis. *J. Am. Chem. Soc.* **2020**, *142*, 3117−3124.
(22) Wang, W.; Zhu, H.; Liu, S.; Zhao, Z.; Zhang, L.; Hao, J.; Wang, Y. Chalcogen-Chalcogen Bonding Catalysis Enables Assembly of Discrete Molecules. *J. Am. Chem. Soc.* **2019**, *141*, 9175−9179.
(23) Wonner, P.; Steinke, T.; Vogel, L.; Huber, S. M. Carbonyl Activation by Selenium- and Tellurium-Based Chalcogen Bonding in a Michael Addition Reaction. *Chem. Eur. J.* **2020**, *26*, 1258−1262.
(24) Lim, J. Y. C.; Marques, I.; Thompson, A. L.; Christensen, K. E.; Félix, V.; Beer, P. D. Chalcogen Bonding Macrocycles and [2]Rotaxanes for Anion Recognition. *J. Am. Chem. Soc.* **2017**, *139*, 3122−3133.
(25) Taylor, M. S. Anion Recognition Based on Halogen, Chalcogen, Pnictogen and Tetrel Bonding. *Coord. Chem. Rev.* **2020**, *413*, 213270.
(26) Lee, L. M.; Tsemperouli, M.; Poblador-Bahamonde, A. I.; Benz, S.; Sakai, N.; Sugihara, K.; Matile, S. Anion Transport with Pnictogen Bonds in Direct Comparison with Chalcogen and Halogen Bonds. *J. Am. Chem. Soc.* **2019**, *141*, 810−814.
(27) Mukai, T.; Nishikawa, K. Crystal Structure of 1-Methyl-2,4,5-Triiodoimidazole: Formation of a Triangular Trimer through Halogen Bonding. *X-Ray Struct. Anal. Online* **2013**, *29*, 13−14.
(28) Werz, D. B.; Staeb, T. H.; Benisch, C.; Rausch, B. J.; Rominger, F.; Gleiter, R. Self-Organization of Chalcogen-Containing Cyclic Alkynes and Alkenes to Yield Columnar Structures. *Org. Lett.* **2002**, *4*, 339−342.
(29) Gleiter, R.; Werz, D. B. Elastic Cycles as Flexible Hosts: How Tubes Built by Cyclic Chalcogenaalkynes Individually Host Their Guests. *Chem. Lett.* **2005**, *34*, 126−131.
(30) Lari, A.; Gleiter, R.; Rominger, F. Supramolecular Organization Based on van Der Waals Forces: Syntheses and Solid State Structures of Isomeric [6.6] Cyclophanes with 2,5-Diselenahex-3-Yne Bridges. *Eur. J. Org. Chem.* **2009**, *2009*, 2267−2274.
(31) Ng, C.-F.; Chow, H.-F.; Mak, T. C. W. Halogen-Bond-Mediated Assembly of a Single-Component Supramolecular Triangle and an Enantiomeric Pair of Double Helices from 2-(Iodoethynyl)-Pyridine Derivatives. *Angew. Chem., Int. Ed.* **2018**, *57*, 4986−4990.
(32) Szell, P. M. J.; Siiskonen, A.; Catalano, L.; Cavallo, G.; Terraneo, G.; Priimagi, A.; Bryce, D. L.; Metrangolo, P. Halogen-Bond Driven Self-Assembly of Triangular Macrocycles. *New J. Chem.* **2018**, *42*, 10467−10471.
(33) Ho, P. C.; Szydlowski, P.; Sinclair, J.; Elder, P. J. W.; Kübel, J.; Gendy, C.; Lee, L. M.; Jenkins, H.; Britten, J. F.; Morim, D. R.; Vargas-Baca, I. Supramolecular Macrocycles Reversibly Assembled by Te ··· O Chalcogen Bonding. *Nat. Commun.* **2016**, *7*, 11299.
(34) Kübel, J.; Elder, P. J. W.; Jenkins, H. A.; Vargas-Baca, I. Structure and Formation of the First (-O-Te-N-)4 Ring. *Dalton Trans.* **2010**, *39*, 11126−11128.
(35) Ho, P. C.; Rafique, J.; Lee, J.; Lee, L. M.; Jenkins, H. A.; Britten, J. F.; Braga, A. L.; Vargas-Baca, I. Synthesis and Structural Characterisation of the Aggregates of Benzo-1,2-Chalcogenazole 2-Oxides. *Dalton Trans.* **2017**, *46*, 6570−6579.
(36) Ho, P. C.; Lee, L. M.; Jenkins, H.; Britten, J. F.; Vargas-Baca, I. Influence of Acidic Media on the Supramolecular Aggregation of Iso-Tellurazole N -Oxides. *Can. J. Chem.* **2016**, *94*, 453−457.
(37) Ho, P. C.; Jenkins, H. A.; Britten, J. F.; Vargas-Baca, I. Building New Discrete Supramolecular Assemblies through the Interaction of Iso-Tellurazole N-Oxides with Lewis Acids and Bases. *Faraday Discuss.* **2017**, *203*, 187−199.
(38) Ho, P. C.; Lomax, J.; Tomassetti, V.; Britten, J. F.; Vargas-Baca, I. Competing Effects of Chlorination on the Strength of Te···O Chalcogen Bonds Select the Structure of Mixed Supramolecular Macrocyclic Aggregates of Iso-Tellurazole N-Oxides. *Chem. Eur. J.* **2021**, *27*, 10849−10853.
(39) Ho, P. C.; Bui, R.; Cevallos, A.; Sequeira, S.; Britten, J. F.; Vargas-Baca, I. Macrocyclic Complexes of Pt(II) and Rh(III) with Iso-Tellurazole: N -Oxides. *Dalton Trans.* **2019**, *48*, 4879−4886.
(40) Wang, J.; Ho, P. C.; Britten, J. F.; Tomassetti, V.; Vargas-Baca, I. Structural Diversity of the Complexes of Monovalent Metal d^{10} Ions with Macrocyclic Aggregates of Iso-Tellurazole: N -Oxides. *New J. Chem.* **2019**, *43*, 12601−12608.
(41) Elder, P. J. W.; Vargas-Baca, I. 125Te NMR Provides Evidence of Autoassociation of Organo-Ditellurides in Solution. *Phys. Chem. Chem. Phys.* **2016**, *18*, 30740−30747.
(42) Fonseca Guerra, C.; Snijders, J. G.; Te Velde, G.; Baerends, E. J. Towards an Order-N DFT Method. *Theor. Chem. Acc.* **1998**, *99*, 391−403.
(43) te Velde, G.; Bickelhaupt, F. M.; Baerends, E. J.; Fonseca Guerra, C.; van Gisbergen, S. J. A.; Snijders, J. G.; Ziegler, T. Chemistry with ADF. *J. Comput. Chem.* **2001**, *22*, 931−967.

https://doi.org/10.1021/acs.inorgchem.1c02585
Inorg. Chem. 2021, 60, 16726−16733

(44) Perdew, J. P.; Burke, K.; Ernzerhof, M. Generalized Gradient Approximation Made Simple. *Phys. Rev. Lett.* **1996**, *77*, 3865−3868.
(45) Grimme, S. Semiempirical GGA-Type Density Functional Constructed with a Long-Range Dispersion Correction. *J. Comput. Chem.* **2006**, *27*, 1787−1799.
(46) van Lenthe, E.; Ehlers, A.; Baerends, E.-J. Geometry Optimizations in the Zero Order Regular Approximation for Relativistic Effects. *J. Chem. Phys.* **1999**, *110*, 8943−8953.
(47) Van Lenthe, E.; Van Leeuwen, R.; Baerends, E. J.; Snijders, J. G. Relativistic Regular Two-Component Hamiltonians. *Int. J. Quantum Chem.* **1996**, *57*, 281−293.
(48) Van Lenthe, E.; Baerends, E. J.; Snijders, J. G. Relativistic Total Energy Using Regular Approximations. *J. Chem. Phys.* **1994**, *101*, 9783−9792.
(49) van Lenthe, E.; Baerends, E. J.; Snijders, J. G. Relativistic Regular Two-component Hamiltonians. *J. Chem. Phys.* **1993**, *99*, 4597−4610.
(50) Bérces, A.; Dickson, R. M.; Fan, L.; Jacobsen, H.; Swerhone, D.; Ziegler, T. An Implementation of the Coupled Perturbed Kohn-Sham Equations: Perturbation Due to Nuclear Displacements. *Comput. Phys. Commun.* **1997**, *100*, 247−262.
(51) Wolff, S. K. Analytical Second Derivatives in the Amsterdam Density Functional Package. *Int. J. Quantum Chem.* **2005**, *104*, 645−659.
(52) Autschbach, J.; King, H. F. Analyzing Molecular Static Linear Response Properties with Perturbed Localized Orbitals. *J. Chem. Phys.* **2010**, *133*, 044109.
(53) Weinhold, F.; Landis, C. R.; Glendening, E. D. What Is NBO Analysis and How Is It Useful? *Int. Rev. Phys. Chem.* **2016**, *35*, 399−440.
(54) Mitoraj, M. P.; Michalak, A.; Ziegler, T. A Combined Charge and Energy Decomposition Scheme for Bond Analysis. *J. Chem. Theory Comput.* **2009**, *5*, 962−975.
(55) Beckmann, J.; Heitz, S.; Hesse, M. Four Distinctively Different Decomposition Pathways of Metastable Supermesityltellurium(IV) Trichloride. *Inorg. Chem.* **2007**, *46*, 3275−3282.
(56) Mehrparvar, S.; Wölper, C.; Gleiter, R.; Haberhauer, G. The Carbonyl···Tellurazole Chalcogen Bond as a Molecular Recognition Unit: From Model Studies to Supramolecular Organic Frameworks. *Angew. Chem., Int. Ed.* **2020**, *59*, 17154−17161.
(57) Fujita, M.; Yazaki, J.; Ogura, K. Preparation of a Macrocyclic Polynuclear Complex, $[(En)Pd(4,4'\text{-}Bpy)]_4(NO_3)_8$ (En = Ethylenediamine, Bpy = Bipyridine), Which Recognizes an Organic Molecule in Aqueous Media. *J. Am. Chem. Soc.* **1990**, *112*, 5645−5647.
(58) Fujita, M.; Sasaki, O.; Mitsuhashi, T.; Fujita, T.; Yazaki, J.; Yamaguchi, K.; Ogura, K. On the Structure of Transition-Metal-Linked Molecular Squares. *Chem. Commun.* **1996**, No. 13, 1535−1536.
(59) Ziegler, T.; Rauk, A. On the Calculation of Bonding Energies by the Hartree Fock Slater Method - I. The Transition State Method. *Theor. Chim. Acta* **1977**, *46*, 1−10.
(60) Ziegler, T.; Rauk, A. A Theoretical Study of the Ethylene-Metal Bond in Complexes between Cu^+, Ag^+, Au^+, Pt^0, or Pt^{2+} and Ethylene, Based on the Hartree-Fock-Slater Transition-State Method. *Inorg. Chem.* **1979**, *18*, 1558−1565.
(61) Ziegler, T.; Rauk, A. Carbon Monoxide, Carbon Monosulfide, Molecular Nitrogen, Phosphorus Trifluoride, and Methyl Isocyanide as.Sigma. Donors and.Pi. Acceptors. A Theoretical Study by the Hartree-Fock-Slater Transition-State Method. *Inorg. Chem.* **1979**, *18*, 1755−1759.
(62) Wang, Y.; Wu, H.; Stoddart, J. F. Molecular Triangles: A New Class of Macrocycles. *Acc. Chem. Res.* **2021**, *54*, 2027−2039.

https://doi.org/10.1021/acs.inorgchem.1c02585
Inorg. Chem. 2021, 60, 16726−16733

Chapter 8. Conclusions and Outlook

8.1 Conclusions

The research described in the thesis demonstrates the versatility of iso-tellurazole *N*-oxides (**1**) as supramolecular building blocks that self-assemble through Te···O chalcogen bonds (ChBs) (Scheme 8.1). Key properties of these molecules are the strength and reversibility of their ChBs and their stability, being tolerant of air and moisture.

The supramolecular macrocyclic tetramers and hexamers that coexist in equilibrium in solution dissociate upon protonation with mineral acids. The protonated products are stable. Measurements of the Hammett acidity function showed that **1a,b** are as basic as dialkyl ethers. On deprotonation, the macrocycles are readily reconstituted. The reversibility of protonation constitutes a means to switch on and off the self-assembly of **1**. Earlier work with telluradiazoles showed that aggregation through strong ChBs causes low solubility, complicating purification and characterization of some compounds.[20] In the case of **1**, protonation will likely be useful to control aggregation, facilitating the use of these building blocks.

Similarly, the reaction of $\mathbf{1}_{4,6}$ with boranes readily dissociates the macrocycles forming oxygen-bonded adducts. These products are crystallize as individual **1**-BR_3 (R = F, Ph) molecules in which the electrophilic regions on tellurium atoms are readily available to form ChBs with a wide variety of ChB acceptors, even **1** itself. This reactivity can be used to generate new supramolecular structures.

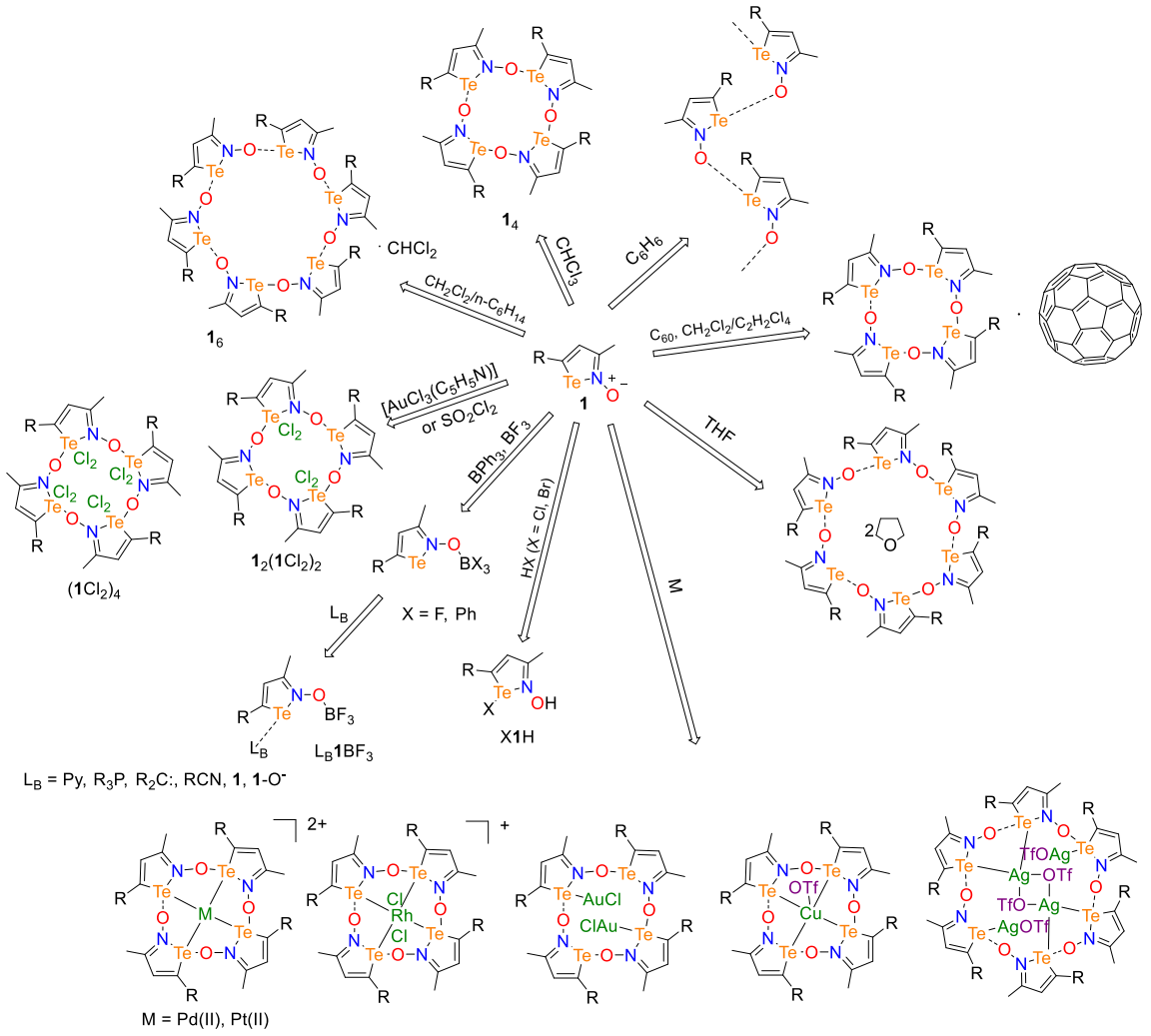

Scheme 8.1. Graphical summary of the supramolecular chemistry of iso-tellurazole *N*-oxides **1a** (R = ^{t}Bu), **1b** (R = Ph). **1c** (R = 3,5-^{t}Bu$_2$C$_6$H$_3$).[18,21–25]

In contrast to the reactivity of **1**$_{4,6}$ towards Brønsted and Lewis acids, the macrocycles do not react with bases, even a carbene. The difference appears to be rooted in the structure of the macrocycles, which hinders access to the nucleophilic sites on Te atoms but allows access to the oxygen atoms lone pairs.

One of the challenges in developing the chemistry of compounds **1**, has been their laborious preparation. The synthesis of benzo-tellurazole *N*-oxide (**2a**) was developed to as a simpler alternative. Only one step in the method requires anaerobic conditions but not as rigorous as those provided by a Schlenk double manifold. Also, the method is readily adaptable to the selenium analogue (**2b**). The chemistry of **2a** parallels in many respects that of **1** (Scheme 8.2),[26] including reversible protonation, formation of macrocyclic tetramers and heaxamers, coordination of Pd(II) and affinity for fullerenes (to be published) .

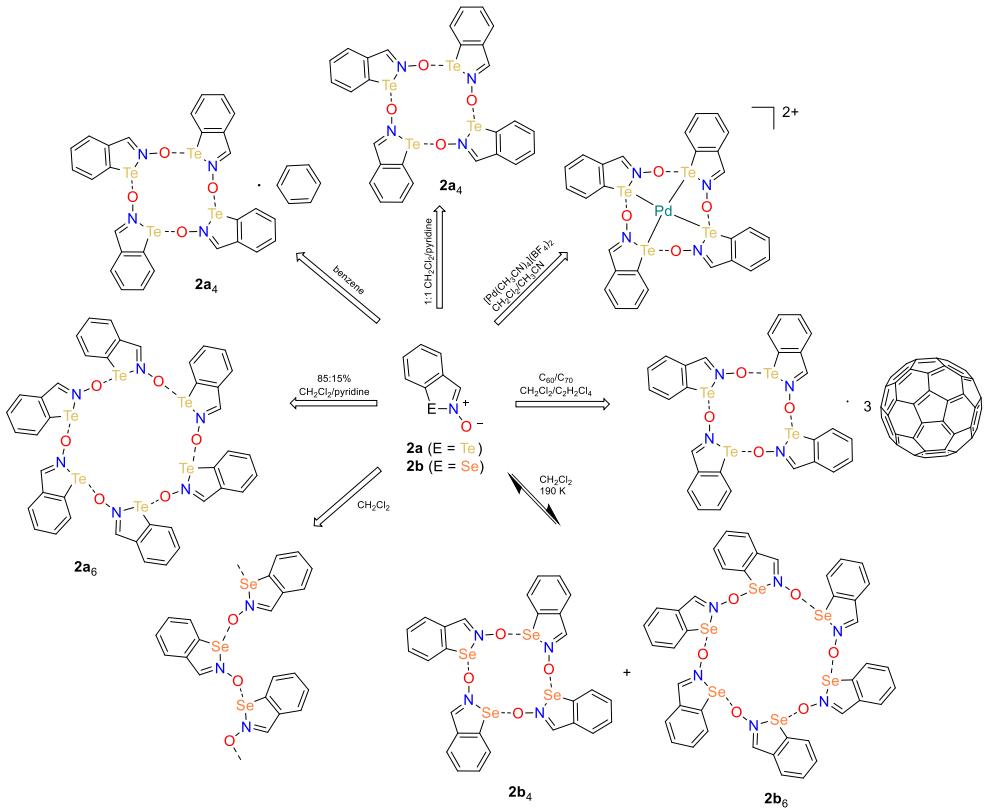

Scheme 8.2. Summary of the supramolecular aggregates and chemistry of benzo-annulated iso-chalcogenazole *N*-oxide **2a** (E = Te) and **2b** (E = Se).

On the other hand, with weaker Se···O ChBs, compound **2b** does not form macrocycles in solution at ambient temperature. However, VT NMR experiments allowed observation of its aggregation into tetramers and hexamers at low temperature.[26]

Investigations of the coordination chemistry of compounds **1** were facilitated by the synthesis of the derivative **1c**, which has improved solubility in non-polar organic solvents. The Pt(II) complex of $\mathbf{1c}_4$ tetramer was soluble enough to permit characterization by multinuclear NMR, including the measurement of the $^1J(^{195}Pt\text{-}^{125}Te)$ coupling constant. Similarly, the $^1J(^{103}Rh\text{-}^{125}Te)$ was obtained for the $[RhCl_2(\mathbf{1b}_4)]^+$ demonstrating that the macrocyclic complexes of the tetramer are stable species in solution. While in both cases strong ligand field effects help stabilize the complexes, further investigations showed that the macrocycles also form complexes with d^{10} metal ions such as Cu(I), Ag(I) and Au(I), coordinating the metal ions by tellurium in all cases.[24]

Chlorination of **1b** yielded the λ^4Te dichloro derivative $\mathbf{1b}Cl_2$. Its crystal structure demonstrated that it does assemble macrocyclic tetramers by Te···O ChBs, although the conformation is irregular due to the formation of additional Te···Cl ChBs. The Te···O distances observed in $(\mathbf{1b}Cl_2)_4$ are by far the shortest in any aggregate of iso-tellurazole *N*-oxides. DFT-D3 calculations showed that chlorination enhances the ChB donor ability of the molecule but weakens the basicity of the oxygen atom. Steric hindrance further weakens the ChBs. The balance of interactions renders the strength of ChBs in $(\mathbf{1b}Cl_2)_4$ about the same as in $(\mathbf{1b})_4$. However, an equimolar mixture of the two tetramers selectively yields $(\mathbf{1b})_2(\mathbf{1b}Cl_2)_2$, with a structure alternating chlorinated and non-chlorinated chalcogens.

Modification of the structure of the iso-tellurazole *N*-oxide with phenoxide groups in place of the oxygen atom produced a family of new building blocks (**3^{o,m,p}**). These molecules do form Te···O ChBs (Scheme) as demonstrated by their crystal structures and solution VT ^{1}H-NMR. While **3^{m}** only crystalized in infinite chains, macrocyclic trimers and tetramers were isolated for **3^{o}** and **3^{p}**, respectively, with structures that resemble a calixarene and molecular square. DFT-D3 calculations indicate that the Te···O dimerization energies in these compounds are stronger than in the aggregates of **1** and **2.**

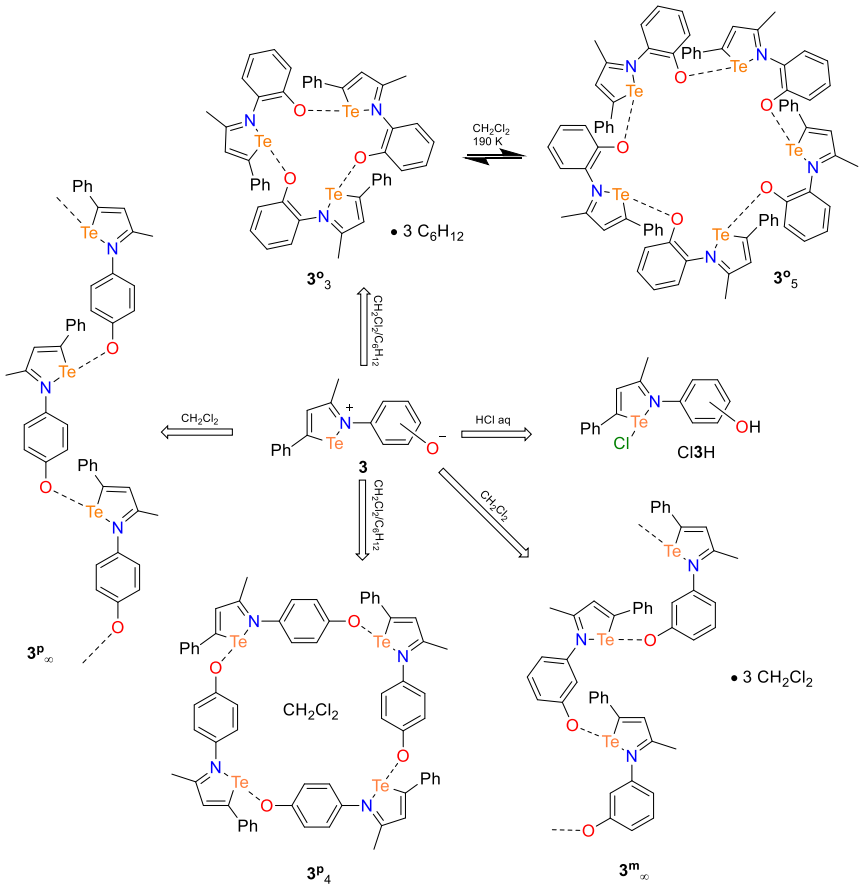

Scheme 8.3. Summary of the supramolecular aggregates and chemistry of iso-tellurazonium-*N*-phenoxides **3^{o,m,p}**.[27]

8.2 Suggestions of Future Work

A significant portion of current research in ChB is devoted to supramolecular assembly,[28,29] anion recognition,[13,16,30,31] anion transport,[32,33] and catalysis.[34–36] Most of that work has been done in non-protic organic solvents[37] as ChB donors usually are hydrophobic. Very few studies have investigated the formation of ChBs in aqueous medium.[38,39] Such research would facilitate using ChBs in biological and environmental applications. The synthesis of iso-tellurazole *N*-oxide can be modified to prepare water-soluble derivatives by grafting the heterocycles with hydrophilic groups such alcohol, sulfonate or tertra-alkyl ammonium. The corresponding macrocycles should be stable in aqueous medium as long as the pH is not strongly acidic. If such water-soluble macrocycles are able coordinate transition metal ions in aqueous medium, they could also be applied in the extraction of heavy metal ions by precipitation as the metal complex.

As noted in chapter 4, the tellurium electrophilic sites of the iso-tellurazole *N*-oxide macrocyclic aggregates are not accessible to Lewis bases. The tetramers cavities are small and can only accommodate metal ions. However, the large cavity $\mathbf{3^p}_4$ is big enough to accommodate a molecule of CH_2Cl_2. It is desirable to investigate of the molecular recognition ability of $\mathbf{3^p}_4$. The bowl shape of $\mathbf{3^o}_3$ might also be suitable for molecular recognition. It is also possible that members of this new family of macrocycles could be applied in anion recognition and transport. For example, two of the tellurium atoms in the tetramer of $\mathbf{3^p}$ have their trans-carbon sigma holes pointing towards the centre of the cavity and thus could host anions withing the cavity.

This thesis has been mostly with the heterocycles that contain tellurium because of the strength of the Te···O ChB. As the study of compound **2b** showed, the selenium analogues can display distinct behaviour because of their weaker ChBs. It would be important to establish and examine such differences as well as to identify efficient strategies to strengthen the Se···O ChBs. Given the reversibility of the Ch···O ChBs it should be possible to combine the different building blocks described in this thesis to form new supramolecular structures.

References cited in the foreword section of chapter 1 to 7 and chapter 8

(1) Desiraju, G. R.; Shing Ho, P.; Kloo, L.; Legon, A. C.; Marquardt, R.; Metrangolo, P.; Politzer, P.; Resnati, G.; Rissanen, K. Definition of the Halogen Bond (IUPAC Recommendations 2013). *Pure Appl. Chem.* **2013**, *85*, 1711–1713.

(2) Aakeroy, C. B.; Bryce, D. L.; Desiraju, G. R.; Frontera, A.; Legon, A. C.; Nicotra, F.; Rissanen, K.; Scheiner, S.; Terraneo, G.; Metrangolo, P.; Resnati, G. Definition of the Chalcogen Bond (IUPAC Recommendations 2019). *Pure Appl. Chem.* **2019**, *91*, 1889–1892.

(3) Kumar, V.; Xu, Y.; Bryce, D. L. Double Chalcogen Bonds: Crystal Engineering Stratagems via Diffraction and Multinuclear Solid-State Magnetic Resonance Spectroscopy. *Chem. Eur. J.* **2020**, *26*, 3275–3286.

(4) Scilabra, P.; Terraneo, G.; Resnati, G. The Chalcogen Bond in Crystalline Solids: A World Parallel to Halogen Bond. *Acc. Chem. Res.* **2019**, *52*, 1313.

(5) Benz, S.; López-Andarias, J.; Mareda, J.; Sakai, N.; Matile, S. Catalysis with Chalcogen Bonds. *Angew. Chem., Int. Ed.* **2017**, *56*, 812–815.

(6) Wang, W.; Zhu, H.; Feng, L.; Yu, Q.; Hao, J.; Zhu, R.; Wang, Y. Dual Chalcogen-Chalcogen Bonding Catalysis. *J. Am. Chem. Soc.* **2020**, *142*, 3117–3124.

(7) Wang, W.; Zhu, H.; Liu, S.; Zhao, Z.; Zhang, L.; Hao, J.; Wang, Y. Chalcogen-Chalcogen Bonding Catalysis Enables Assembly of Discrete Molecules. *J. Am. Chem. Soc.* **2019**, *141*, 9175–9179.

(8) Wonner, P.; Steinke, T.; Vogel, L.; Huber, S. M. Carbonyl Activation by Selenium- and Tellurium-Based Chalcogen Bonding in a Michael Addition Reaction. *Chem. Eur. J.* **2020**, *26*, 1258–1262.

(9) Mahmudov, K. T.; Kopylovich, M. N.; Guedes Da Silva, M. F. C.; Pombeiro, A. J. L. Chalcogen Bonding in Synthesis, Catalysis and Design of Materials. *Dalton Trans.* **2017**, *46*, 10121–10138.

(10) Ho, P. C.; Wang, J. Z.; Meloni, F.; Vargas-Baca, I. Chalcogen Bonding in Materials Chemistry. *Coord. Chem. Rev.* **2020**, *422*, 213464.

(11) Pushkarevsky, N. A.; Lonchakov, A. V.; Semenov, N. A.; Lork, E.; Buravov, L. I.; Konstantinova, L. S.; Silber, G. T.; Robertson, N.; Gritsan, N. P.; Rakitin, O. A.; Woollins, J. D.; Yagubskii, E. B.; Beckmann, J.; Zibarev, A. V. First Charge-Transfer Complexes between Tetrathiafulvalene and 1,2,5-Chalcogenadiazole Derivatives: Design, Synthesis, Crystal Structures, Electronic and Electrical Properties. *Synth. Met.* **2012**, *162*, 2267–2276.

(12) Dong, T.; Lv, L.; Feng, L.; Xia, Y.; Deng, W.; Ye, P.; Yang, B.; Ding, S.; Facchetti, A.; Dong, H.; Huang, H. Noncovalent Se⋯O Conformational Locks for Constructing High-Performing Optoelectronic Conjugated Polymers. *Adv. Mater.* **2017**, *29*, 1606025.

(13) Garrett, G. E.; Gibson, G. L.; Straus, R. N.; Seferos, D. S.; Taylor, M. S. Chalcogen Bonding in Solution: Interactions of Benzotelluradiazoles with Anionic and Uncharged Lewis Bases. *J. Am. Chem. Soc.* **2015**, *137*, 4126–4133.

(14) Fourmigué, M.; Dhaka, A. Chalcogen Bonding in Crystalline Diselenides and Selenocyanates: From Molecules of Pharmaceutical Interest to Conducting Materials. *Coord. Chem. Rev.* **2020**, *403*, 213084.

(15) Lee, L. M.; Tsemperouli, M.; Poblador-Bahamonde, A. I.; Benz, S.; Sakai, N.; Sugihara, K.; Matile, S. Anion Transport with Pnictogen Bonds in Direct Comparison with Chalcogen and Halogen Bonds. *J. Am. Chem. Soc.* **2019**, *141*, 810–814.

(16) Taylor, M. S. Anion Recognition Based on Halogen, Chalcogen, Pnictogen and Tetrel Bonding. *Coord. Chem. Rev.* **2020**, *413*, 213270.

(17) Lim, J. Y. C.; Marques, I.; Thompson, A. L.; Christensen, K. E.; Félix, V.; Beer, P. D. Chalcogen Bonding Macrocycles and [2]Rotaxanes for Anion Recognition. *J. Am. Chem. Soc.* **2017**, *139*, 3122–3133.

(18) Ho, P. C.; Szydlowski, P.; Sinclair, J.; Elder, P. J. W.; Kübel, J.; Gendy, C.; Lee, L. M.; Jenkins, H.; Britten, J. F.; Morim, D. R.; Vargas-Baca, I. Supramolecular Macrocycles Reversibly Assembled by Te ⋯ O Chalcogen Bonding. *Nat. Commun.* **2016**, *7*, 11299.

(19) Ho, P. C. A Study of Iso-Tellurazole N-Oxides: Synthesis, Supramolecular and Coordination Chemistry, McMaster University, 2014.

(20) Anthony F. Cozzolino. Synthesis, Structural Characterization, Spectroscopic Studies and Computational Investigations of 1,2,5-Telluradiazoles and Their

Supramolecular Assemblies., McMaster University, 2009.

(21) Ho, P. C.; Lee, L. M.; Jenkins, H.; Britten, J. F.; Vargas-Baca, I. Influence of Acidic Media on the Supramolecular Aggregation of Iso-Tellurazole N -Oxides. *Can. J. Chem.* **2016**, *94*, 453–457.

(22) Ho, P. C.; Jenkins, H. A.; Britten, J. F.; Vargas-Baca, I. Building New Discrete Supramolecular Assemblies through the Interaction of Iso-Tellurazole N-Oxides with Lewis Acids and Bases. *Faraday Discuss.* **2017**, *203*, 187–199.

(23) Ho, P. C.; Bui, R.; Cevallos, A.; Sequeira, S.; Britten, J. F.; Vargas-Baca, I. Macrocyclic Complexes of Pt(II) and Rh(III) with Iso-Tellurazole: N -Oxides. *Dalton Trans.* **2019**, *48*, 4879–4886.

(24) Wang, J.; Ho, P. C.; Britten, J. F.; Tomassetti, V.; Vargas-Baca, I. Structural Diversity of the Complexes of Monovalent Metal D10 Ions with Macrocyclic Aggregates of Iso-Tellurazole: N -Oxides. *New J. Chem.* **2019**, *43*, 12601–12608.

(25) Ho, P. C.; Lomax, J.; Tomassetti, V.; Britten, J. F.; Vargas-Baca, I. Competing Effects of Chlorination on the Strength of Te···O Chalcogen Bonds Select the Structure of Mixed Supramolecular Macrocyclic Aggregates of Iso-Tellurazole N-Oxides. *Chem. Eur. J.* **2021**, *27*, 10849–10853.

(26) Ho, P. C.; Rafique, J.; Lee, J.; Lee, L. M.; Jenkins, H. A.; Britten, J. F.; Braga, A. L.; Vargas-Baca, I. Synthesis and Structural Characterisation of the Aggregates of Benzo-1,2-Chalcogenazole 2-Oxides. *Dalton Trans.* **2017**, *46*, 6570–6579.

(27) Peter C. Ho, Valerie Tomassetti, J.F. Britten, I. V.-B. A Family of Te…O Chalcogen-Bonding Supramolecular Building Blocks. *Inorg. Chem.* ic-2021–02, in press.

(28) Riwar, L.-J.; Trapp, N.; Root, K.; Zenobi, R.; Diederich, F. Supramolecular Capsules: Strong versus Weak Chalcogen Bonding. *Angew. Chem., Int. Ed.* **2018**, *57*, 17259–17264.

(29) Rahman, F.-U.; Tzeli, D.; Petsalakis, I. D.; Theodorakopoulos, G.; Ballester, P.; Julius Rebek, J.; Yu, Y. Chalcogen Bonding and Hydrophobic Effects Force Molecules into Small Spaces. *J. Am. Chem. Soc.* **2020**, *142*, 5876–5883.

(30) Lim, J. Y. C.; Liew, J. Y.; Beer, P. D. Thermodynamics of Anion Binding by Chalcogen Bonding Receptors. *Chem. Eur. J.* **2018**, *24*, 14560–14566.

(31) Lim, J. Y. C.; Beer, P. D. Sigma-Hole Interactions in Anion Recognition. *Chem* **2018**, *4*, 731–783.

(32) Benz, S.; Macchione, M.; Verolet, Q.; Mareda, J.; Sakai, N.; Matile, S. Anion Transport with Chalcogen Bonds. *J. Am. Chem. Soc.* **2016**, *138*, 9093–9096.

(33) Macchione, M.; Tsemperouli, M.; Goujon, A.; Mallia, A. R.; Sakai, N.; Sugihara, K.; Matile, S. Mechanosensitive Oligodithienothiophenes: Transmembrane Anion Transport Along Chalcogen-Bonding Cascades. *Helv. Chim. Acta* **2018**, *101*, e1800014.

(34) Vogel, L.; Wonner, P.; Huber, S. M. Chalcogen Bonding: An Overview. *Angew.*

Chem., Int. Ed. **2019**, *58*, 1880–1891.

(35) Benz, S.; López-Andarias, J.; Mareda, J.; Sakai, N.; Matile, S. Catalysis with Chalcogen Bonds. *Angew. Chem., Int. Ed.* **2017**, *56*, 812–815.

(36) Benz, S.; Mareda, J.; Besnard, C.; Sakai, N.; Matile, S. Catalysis with Chalcogen Bonds: Neutral Benzodiselenazole Scaffolds with High-Precision Selenium Donors of Variable Strength. *Chem. Sci.* **2017**, *8*, 8164–8169.

(37) Mahmudov, K. T.; Aliyeva, V. A.; Silva, M. F. C. G. da; Pombeiro, A. J. L. The Chalcogen Bond in Solution: Synthesis, Catalysis and Molecular Recognition. *Halogen Bond. Solut.* **2021**, 363–382.

(38) Borissov, A.; Marques, I.; Lim, J. Y. C.; Félix, V.; Smith, M. D.; Beer, P. D. Anion Recognition in Water by Charge-Neutral Halogen and Chalcogen Bonding Foldamer Receptors. *J. Am. Chem. Soc.* **2019**, *141*, 4119–4129.

(39) Lim, J. Y. C.; Marques, I.; Thompson, A. L.; Christensen, K. E.; Félix, V.; Beer, P. D. Chalcogen Bonding Macrocycles and [2]Rotaxanes for Anion Recognition. *J. Am. Chem. Soc.* **2017**, *139*, 3122–3133.